

Techniques for asteroid spectroscopy

Marcel Popescu

► To cite this version:

Marcel Popescu. Techniques for asteroid spectroscopy. Earth and Planetary Astrophysics [astro-ph.EP]. Observatoire de Paris; Universitatea Politehnica din Bucuresti, Facultatea de Științe Aplicate, 2012. English. tel-00785991

HAL Id: tel-00785991

<https://tel.archives-ouvertes.fr/tel-00785991>

Submitted on 7 Feb 2013

HAL is a multi-disciplinary open access archive for the deposit and dissemination of scientific research documents, whether they are published or not. The documents may come from teaching and research institutions in France or abroad, or from public or private research centers.

L'archive ouverte pluridisciplinaire **HAL**, est destinée au dépôt et à la diffusion de documents scientifiques de niveau recherche, publiés ou non, émanant des établissements d'enseignement et de recherche français ou étrangers, des laboratoires publics ou privés.

**OBSERVATOIRE DE PARIS
ÉCOLE DOCTORALE D'ASTRONOMIE ET D'ASTROPHYSIQUE
D'ÎLE-DE-FRANCE**

*

**UNIVERSITATEA POLITHENICA BUCUREȘTI
FACULTATEA DE ȘTIINȚE APLICATE**

DOCTORAL THESIS

by

Marcel Popescu

TECHNIQUES FOR ASTEROID SPECTROSCOPY

Defended the 23 Octobre 2012 before the jury:

Vasile IFTODE	(Universitatea Politehnica București)	President
Olivier GROUSSIN	(Laboratoire d'Astrophysique de Marseille)	Reviewer
Petre POPESCU	(Institutul Astronomic al Academiei Române)	Reviewer
Dan DUMITRAȘ	(INFLPR, România)	Reviewer
Jean SOUCHAY	(SYRTE - Observatoire de Paris)	Examiner
Mirel BIRLAN	(IMCCE - Observatoire de Paris)	Co-Advisor
Constantin P. CRISTESCU	(Universitatea Politehnica, București)	Co-Advisor

mpopescu@imcce.fr

**OBSERVATOIRE DE PARIS
ÉCOLE DOCTORALE D'ASTRONOMIE ET D'ASTROPHYSIQUE
D'ÎLE-DE-FRANCE**

*

**UNIVERSITATEA POLITHENICA BUCUREȘTI
FACULTATEA DE ȘTIINȚE APLICATE**

THÈSE DE DOCTORAT

**par
Marcel Popescu**

TECHNIQUES D'OBSERVATION SPECTROSCOPIQUE D'ASTÉROÏDES

Soutenue le 23 Octobre 2012 devant un jury composé de :

Vasile IFTODE	(Universitatea Politehnica, București)	Présidente
Olivier GROUSSIN	(Laboratoire d'Astrophysique de Marseille)	Rapporteur
Petre POPESCU	(Institutul Astronomic al Academiei Române)	Rapporteur
Dan DUMITRAȘ	(INFLPR, România)	Rapporteur
Jean SOUCHAY	(SYRTE - Observatoire de Paris)	Examineur
Mirel BIRLAN	(IMCCE - Observatoire de Paris)	Co-Directeur de thèse
Constantin P. CRISTESCU	(Universitatea Politehnica, București)	Co-Directeur de thèse

mpopescu@imcce.fr

**OBSERVATOIRE DE PARIS
ÉCOLE DOCTORALE D'ASTRONOMIE ET D'ASTROPHYSIQUE
D'ÎLE-DE-FRANCE**

*

**UNIVERSITATEA POLITHENICA BUCUREȘTI
FACULTATEA DE ȘTIINȚE APLICATE**

TEZĂ DOCTORAT

autor

Marcel Popescu

TEHNICI DE OBSERVAȚIE SPECTROSCOPICĂ PENTRU ASTEROIZI

Susținută în 23 Octombrie 2012 în fața juriului:

Vasile IFTODE	(Universitatea Politehnica București)	President
Olivier GROUSSIN	(Laboratoire d'Astrophysique de Marseille)	Reviewer
Petre POPESCU	(Institutul Astronomic al Academiei Române)	Reviewer
Dan DUMITRAȘ	(INFLPR, România)	Reviewer
Jean SOUCHAY	(SYRTE - Observatoire de Paris)	Examiner
Mirel BIRLAN	(IMCCE - Observatoire de Paris)	Co-Advisor
Constantin P. CRISTESCU	(Universitatea Politehnica, București)	Co-Advisor

mpopescu@imcce.fr

Abstract: The fundamental goal of the planetary sciences is to understand the formation and evolution of the Solar System. For achieving this goal, the asteroids are of a special interest to the astronomical community as a possible window back to the beginning of the planetary formation. Being the only remnants of the early stages of planetary history they recorded the complex chemical and physical evolution that occurred in the solar nebula. Thus, the knowledge of both dynamical and physical properties of the current asteroid population brings valuable information for understanding the Solar System and more generally other planetary systems.

In this thesis I present the project Modeling for Asteroids (acronym M4AST). M4AST is an on-line service that I developed for modeling surfaces of asteroids using several theoretical approaches. M4AST consists into a database containing more than 2,500 spectra of asteroids together with a library of routines which can model and extract several mineralogical parameters. The database M4AST could be accessed via its own webpage interface as well as via the Virtual Observatory (VO-Paris) protocols. This service is available to the web address <http://cardamine.imcce.fr/m4ast>. It allows several routines for modeling spectra: taxonomic classification, space weathering effects modeling, comparison to laboratory spectra of meteorites and minerals, band centers and band area computing.

I have participated to more than 10 observational campaigns for observing both physical and orbital parameters of asteroids. The objective of spectral runs was to characterize the mineralogical properties of these bodies based on their reflectance spectra. Astrometry was mainly devoted to the confirmation and secures orbits of new discovered asteroid.

During the thesis I observed and characterized near-infrared spectra of eight Near Earth Asteroids namely 1917, 8567, 16960, 164400, 188452, 2010 TD54, 5620, and 2001 SG286. These observations were obtained using the NASA telescope IRTF equipped with the spectro-imager SpeX, and the CODAM-Paris observatory facilities. Based on these spectra mineralogical solutions were proposed for each asteroid. The taxonomic classification of five of these objects was reviewed and a corresponding type was assigned to the other three asteroids that were not classified before. Four of the observed objects have delta - V lower than 7 km/sec, which make them suitable targets in terms of propulsion for a future spacecraft mission. The asteroid (5620) Jasonwheeler exhibits spectral behaviors similar to the carbonaceous chondrite meteorites.

I observed and modeled six Main Belt Asteroids. (9147) Kourakuen, (854) Frostia, (10484) Hecht and (31569) 1999 FL18 show the characteristics of V-type objects, while (1333) Cevenola, (3623) Chaplin belong to S-complex. Some of them have some peculiar properties: (854) Frostia is a binary asteroid, (10484) Hecht and (31569) 1999 FL18 have pairs, (1333) Cevenola, (3623) Chaplin show large amplitude lightcurves. The taxonomic classification, the comparisons to the meteorite spectra from the Relab database and the mineralogical analysis converged to the same solutions for each of these objects, allowing to find important details for the chemical compositions and resemblances to the Howardite-Eucrite-Diogenite class of meteorites.

Résumé: L'objectif fondamental des sciences planétaires est la compréhension de la formation et de l'évolution du Système Solaire. Pour atteindre cet objectif les astéroïdes présentent un intérêt tout particulier pour la communauté scientifique. En effet, nous pouvons regarder la population astéroïdale comme une fenêtre vers le passé, par laquelle nous regardons les débuts de la formation du système planétaire. Ils sont les témoins des premiers moments de la formation des planètes gardant dans leur structure la complexité chimique de la nébuleuse primordiale. Pour cette raison, les études physiques et dynamiques de ces corps nous apportent des informations essentielles sur l'histoire et l'évolution de notre Système Solaire et plus généralement sur la formation des systèmes planétaires.

Pendant ma thèse j'ai développé l'application Modelling for Asteroids (acronyme M4AST). M4AST est un service en libre service sur internet permettant la modélisation des surfaces d'astéroïdes en utilisant plusieurs approches théoriques. M4AST est composé d'une base de données contenant quelques 2500 spectres d'astéroïdes et d'une bibliothèque de routines permettant la modélisation et l'obtention de plusieurs paramètres minéralogiques. La base de données est accessible aussi bien par les biais des protocoles de l'Observatoire Virtuel (OV-Paris) que par sa propre interface. Le service est accessible depuis l'adresse <http://cardamine.imcce.fr/m4ast>. M4AST permet plusieurs types d'analyses : classification taxonomique, modélisation de l'altération spatiale, comparaison avec les spectres des météorites et des minéraux terrestres, calculs des centres et des surfaces des bandes.

J'ai participé à plus de 10 campagnes d'observations pour la caractérisation physique et dynamique des astéroïdes. Les observations spectroscopiques ont servi à la caractérisation minéralogique des surfaces d'astéroïdes. L'astrométrie a plutôt servi à la confirmation et la sécurisation de nouvelles découvertes d'astéroïdes. Pendant la thèse, j'ai observé et caractérisé les spectres en infrarouge proche de huit astéroïdes géocroiseurs : 1917, 8567, 16960, 164400, 188452, 2010 TD54, 5620, and 2001 SG286. Ces observations ont été obtenues avec le télescope IRTF et du spectrographe SpeX, en employant l'infrastructure CODAM de l'Observatoire de Paris. Pour chaque astéroïde j'ai proposé des solutions minéralogiques. Une révision de leur taxonomie a aussi été effectuée pour cinq astéroïdes de mon échantillon. Quatre des objets sont des objets à faible delta-V, qui sont des cibles souhaitables/possibles pour des missions spatiales. L'astéroïde (5620) Jasonwheeler montre un spectre similaire à ceux des météorites chondritiques.

J'ai observé et modélisé six astéroïdes de la ceinture principale. (9147) Kourakuen, (854) Frostia, (10484) Hecht and (31569) 1999 FL18 montrent des caractéristiques des astéroïdes du type V; (1333) Cevenola, (3623) Chaplin sont du type taxonomique S. Quelques astéroïdes de cet échantillon sont particuliers : (854) Frostia est un astéroïde binaire, (10484) Hecht et (31569) 1999 FL18 ont des gémeaux dynamiques, (1333) Cevenola et (3623) Chaplin sont des objets avec des courbes de lumières à grandes amplitudes. La classification taxonomique, la comparaison avec les météorites, permettent l'établissement des solutions minéralogiques

intéressantes et des ressemblances avec les météorites de la classe des howardites, eucrites et diogenites.

Rezumat: Obiectivul fundamental al științelor planetare este înțelegerea formării și evoluției Sistemului Solar. În atingerea acestui obiectiv asteroizii prezintă un interes special pentru comunitatea științifică. Populația de asteroizi poate fi privită ca o fereastră spre trecut, prin care se pot cunoaște originile Sistemului Solar. Astfel, asteroizii sunt mărturiile primelor momente ale formării planetelor, păstrând în structura lor complexitatea chimică a nebuloasei primordiale. Din acest motiv, studiile fizice și dinamice ale acestor corpuri aduc informații esențiale despre istoria și evoluția sistemului nostru solar și generalizând despre formarea altor sisteme planetare.

Pentru realizarea acestei teze am dezvoltat aplicația Modelling for Asteroids (M4AST). M4AST este un serviciu gratuit, care poate fi accesat online. Acesta permite modelarea proprietăților fizice ale suprafețelor de asteroizi utilizând mai multe abordări teoretice. M4AST este compus dintr-o bază de date care conține peste 2 500 de spectre de asteroizi și un set de rutine care permit modelarea și obținerea mai multor parametri mineralogici. Baza de date este accesibilă și indirect folosind protocolul Observatorului Virtual (OV - Paris). Serviciul este accesibil la adresa <http://cardamine.imcce.fr/m4ast>. M4AST permite mai multe tipuri de analize: clasificarea taxonomică, modelarea alterării spațiale, comparația spectrală cu meteoriții și mineralele terestre, calculele centrelor de bandă și ariilor benzilor.

Am participat la mai mult de 10 campanii de observații pentru caracterizarea fizică și dinamică a asteroizilor. Observațiile spectroscopice au servit la caracterizarea mineralogică a suprafețelor asteroizilor. În perioada tezei am obținut și analizat spectrele în infraroșu a opt asteroizi geointersectori (asteroizi ce se apropie sau intersectează orbita Pământului): 1917, 8567, 16960, 164400, 188452, 2010 TD54, 5620 și 2001 SG286. Aceste observații au fost obținute cu ajutorul telescopului IRTF și al spectografului SpeX, utilizând infrastructura CODAM a Observatorului din Paris. Pentru fiecare asteroid am propus soluții mineralogice. O revizuire a taxonomiei lor a fost efectuată pentru cinci asteroizi din acest eșantion. Patru dintre obiecte sunt obiecte cu delta - V mic, acestea fiind ținte posibile pentru misiunile spațiale. Asteroidul (5620) Jasonwheelr prezintă un spectru similar cu cel al meteoriților condritici.

Am observat și modelat spectrele a șase asteroizi din centura principală. (9147) Kourakuen, (854) Frostia, (10484) Hecht și (31569) 1999 FL18 prezintă caracteristici ale asteroizilor de tipul V. (1333) Cevenola, (3623) Chaplin sunt de tipul taxonomic S. Aceste șase obiecte au câteva proprietăți remarcabile: (854) Frostia este un asteroid binar, (10484) Hecht și (31569) 1999 FL18 au perechi dinamice, (1333) Cevenola și (3623) Chaplin sunt obiecte care au curbe de lumină cu amplitudini mari. Clasificarea taxonomică, comparația cu meteoriții, permit stabilirea de soluții mineralogice interesante.

Acknowledgements

Foremost, I would like to express my sincere gratitude to my advisors Mirel Birlan and Constantin P. Cristescu for their continuous support of my Ph.D study and research, for their patience, motivation, enthusiasm, and immense knowledge. I am grateful to Mirel also for the observational data, the telescope time and the scholarships. He also took care of all the administrative staff and ensured me with a very pleasant stay in Paris (thanks also to Mariana, Mirela, Daniel and Florian).

I would like to thank my thesis committee: Vasile Iftode - the jury president, Olivier Groussin, Petre Popescu, Dan Dumitraş - the reviewers, and Jean Souchay the examiner, for evaluating my work, and for their constructive and helpful suggestions.

I am grateful to the colleagues from IMCCE - Observatoire de Paris, for the chance to visit and to be a part of the institute. Thank you for welcoming me as a friend and helping to develop the ideas in this thesis.

I thank to Dan Alin Nedelcu for the encouragement, for insightful comments, and for all the help during the period I wrote my thesis at Astronomical Institute of Romanian Academy. I am also grateful for getting me in your team at AIRA.

I thank to Ovidiu Vaduvescu for the opportunity to become astronomer. Our collaborations were very fruitful for me, and I will always appreciate the help you gave me at the beginning of my career.

I also want to thank to all of my friends from Admiral V. Urseanu Observatory and from Astroclubul Bucureşti. In particular, I want to thank to Adrian Şonka, Oana Sandu, Radu Gherase and Marian Naiman for all the evenings full of astronomy, for all the discussions we had and for all star parties.

Last but not the least, I would like to thank my future wife - Andreea, for her love and support over the past two years. To my Mom and Dad, to my brother Bogdan, and to my aunt Silvia, I am grateful for their support and encouragement.

Vă mulţumesc tuturor!

*Dedicated to my grandfather,
Iosif Popescu*

Contents

Tables	22
Figures	27
 I INTRODUCTION	 29
1 Why asteroids?	31
1.1 The place of asteroids in the structure of the Solar System	31
1.2 The Discovery Of Asteroids	33
1.3 Distribution and diversity of asteroids	35
1.4 Asteroid brightness and albedo	38
1.5 My contribution to asteroids discovery	38
 2 Why spectroscopy?	 43
2.1 Diffraction gratings and prisms	44
2.2 Spectroscopy and atmospheric transparency	46
2.3 A simple application	47
2.4 Spectroscopy for asteroids	50
2.4.1 Reflectance versus emission	50
2.4.2 Spectral features	52
 II TECHNIQUES FOR ASTEROID SPECTROSCOPY	 55
3 Observing techniques	57
3.1 IRTF Telescope and the SpeX instrument	57
3.2 Planning the observations	58
3.3 Data reduction procedures	59
 4 Spectral analysis techniques	 65
4.1 Interpretation	65
4.1.1 Taxonomy	65
4.1.2 Spectral comparison - Comparative planetology	68
4.1.3 Space weathering effects	70
4.1.4 Band parameters	71
4.2 Algorithms	72
4.2.1 Taxonomic classification	72
4.2.2 Curve matching	73

4.2.3	Computing the space weathering effects	74
4.2.4	Application of the Cloutis model	75

5 M4AST - Modeling of Asteroids Spectra 77

5.1	Spectral database	78
5.1.1	Structure of M4AST database	78
5.1.2	The content	79
5.1.3	M4AST database via the Virtual Observatory	80
5.2	The interface	81
5.2.1	Database interface	81
5.2.2	Modeling tool interface	82
5.2.3	Updating the database	84
5.3	Testing of M4AST	84
5.3.1	Results	85
5.3.2	Discussions regarding misinterpretations of spectra	88

III OBSERVATIONS AND RESULTS 91

6 Spectral properties of near-Earth asteroids 93

6.1	Log of observations	94
6.2	S-type Near-Earth Asteroids	95
6.2.1	(1917) Cuyo	96
6.2.2	(8567) 1996 HW1	97
6.2.3	(16960) 1998 QS52	100
6.2.4	(188452) 2004 HE62	101
6.2.5	2010 TD54	103
6.2.6	(164400) 2005 GN59	104
6.3	Spectral properties of two primitive NEAs	105
6.3.1	(5620) Jasonwheeler	106
6.3.2	2001 SG286	108
6.4	Discussion	109

7 Spectral properties of Main Belt Asteroids 113

7.1	Log of observations	113
7.2	(9147) Kourakuen - a V-type asteroid outside Vesta family	115
7.3	A binary asteroid: (854) Frostia	119
7.4	1333 and 3623 - two asteroids with large amplitude lightcurves	123
7.4.1	(1333) Cevenola	123

7.4.2	(3623) Chaplin	126
7.5	Asteroid pairs: (10484) Hecht, (31569)1999 FL18	129
IV	CONCLUSIONS AND PERSPECTIVES	131
8	Conclusions and perspectives	133
A	The GuideDog and the BigDog interfaces	135
B	List of publications	137
B.1	First Author	137
B.2	Co-Author	137
B.3	Conferences and Workshops	138

List of Tables

2.1	The emission lines identification in spectrum of PG1634 +706. The line labels, their corresponding laboratory wavelengths, these wavelengths shifted with $z = 1.34$, and the wavelengths observed in the spectrum are presented.	50
5.1	Summary of the results obtained by matching the asteroids spectra with spectra from the Relab database. For each asteroid, I show the best two matches, obtained by measuring the standard deviation (std. dev.) and the correlation coefficient (corr. coef.).	85
6.1	Some characteristics of the observed NEAs: orbit type, semi-major axis, eccentricity, inclination, absolute magnitude (H), and the delta-V.	94
6.2	Log of NEAs observations. Their designations, date of observation with the fraction of the day for the mid time of the observation, the apparent magnitude, the phase angle, the heliocentric distance, the airmass at the mean UT of each observation, the integration time for each spectrum (ITime), and the number of cycles are shown.	95
6.3	The solar analogs used for data reduction in the case of the NEAs spectra. The airmass at the moment of observations and relative distance to the asteroid are presented.	95
6.4	Summary of results obtained by matching the asteroid spectra and de-reddened asteroid spectra with spectra from the Relab database. The comparison was made using a χ^2 method and a selection of the obtained results was done based on spectral features (band, band-gap, concavity) positions, and albedo values. For (5620) Jasonwheeler, a de-reddening model was not applied	99
6.5	Slope and C_s parameter for the S-type objects studied in this article. The calculation was made by normalization of spectra to $0.55 \mu\text{m}$. Objects marked with (*) are normalized to $1.25 \mu\text{m}$ (only for NIR part).	110
6.6	Computed parameters from the Cloutis <i>et al.</i> [1986a] model applied to the V+NIR spectra of (1917) Cuyo, (8567) 1996 HW1, and (16960) 1998 QS52. The estimation error for band centers (BI, BII) is ± 0.005	111
7.1	Some characteristics of our observed MBAs: semi-major axis, eccentricity, inclination, absolute magnitude (H), and orbital period.	114
7.2	Log of asteroids observations. Asteroid designation, date of observation with the fraction of the day for the mid time of the observation, apparent magnitude, phase angle, heliocentric distance, the airmass at the mean UT of each observation, the integration time for each spectrum (ITime), and the number of cycles are presented.	114

7.3	Solar analogs used for data reduction, their airmass at the moment of observations and their relative distance to the object.	115
7.4	Summary of results obtained by matching the main belt asteroids spectra with spectra from Relab database. The most relevant matches are presented. The comparison coefficients are given together with some details related to the laboratory samples.	119

List of Figures

1.1	A field obtained with INT-WFC on February 28, 2012. Ten asteroids were identified (marked with pink), from which only three were known at the moment of the observation. The size of the field is (15 arcmin x 15 arcmin)	34
1.2	a) The position of asteroids in the inner part of the Solar System (Source: http://en.wikipedia.org/). b) The distribution of asteroids in a representation (a,e)- bottom and ($a,sini$) - top, a is the semi-major axis and i the inclination [Nedelcu, 2010].	36
1.3	The flowchart of Mega-Precovery [Vaduvescu <i>et al.</i> , 2012].	39
1.4	The first part of the Minor Planet Electronic Circular issued for the orbit recovery of the asteroid 2007 ES.	41
2.1	The diffraction pattern produced by a diffraction grating having $b = d = 5\mu m$ and $N=1000$. Different wavelengths are considered.	45
2.2	The atmospheric transmission above Mauna Kea for the wavelength ranges 0.9 - 2.7 μm with a water vapor column of 1.6 mm and an air mass of 1 (Source: http://www.gemini.edu/?q=node/10789).	46
2.3	The field of quasar PG1634+706 (north is at bottom of the figure). The object and its spectrum are surrounded by a rectangle. In this image it can be distinguish the zero order (objects are dots) and the first order (light is dispersed) - Popescu et al. [2012a].	48
2.4	a) PG1634 + 706 spectrum obtained after data reduction and continuum subtraction; b) the correlation coefficient between quasar spectrum and the template spectrum shifted with different z [Popescu et al. , 2012a].	49
2.5	The components of the radiation received from 1km square lunar mare area (dark basaltic plain on Moon formed by ancient volcanic eruptions) having an albedo of 006, considering the average Earth-Moon distance, phase angle 0, $T = 395K$. The flux is measured in Watts per square meter per micron. Source McCord & Adams [1977]	51
2.6	Reflectance spectra of several meteoritic important minerals: a) Spinel, b) Pyroxene, c) Olivine, d) Iron-Nickel alloy.	52
3.1	a) The 3m NASA InfraRed Telescope Facility at the Mauna Kea Observatory on Hawaii. b) SpeX instrument mounted to IRTF telescope. As scale, SpeX is 1.4m tall and weighs 478kg.	58
3.2	The data reduction procedure for NIR spectra obtained with IRTF/SpeX [Nedelcu, 2010].	60

3.3	The raw spectra of an asteroid and standard star. The two spectra are modulated by the absorption bands of the Earth atmosphere (essentially telluric water bands).	62
4.1	Bus-DeMeo taxonomy key figures. Source : http://smass.mit.edu/busdemeoclass.html	68
4.2	a) The photomicrograph of a thin section of the carbonaceous chondrite Allende, which was seen to fall in Chihuahua, Mexico on the night of February 8, 1969. Numerous round silicate chondrules together with irregular inclusions can be observed . b) Comparison of solar-system abundances (relative to silicon) determined by solar spectroscopy and by analysis of carbonaceous chondrites [Ringwood, 1979].	70
4.3	Different ways in which space weathering affects the visible and near-infrared spectra of soil. Space weathering processes alters the properties of the soil that covers the surface of all bodies which are not protected by an atmosphere (Source http://en.wikipedia.org/).	71
5.1	M4AST logo and the aims of this project.	78
5.2	Block diagram and work flow of M4AST [Popescu et al. , 2012b].	79
5.3	The database interface of M4AST. Here is illustrated the search of a spectrum for (1917) Cuyo and the result of this search displayed at the bottom of the interface.	80
5.4	M4AST web application tool : modelling tool interface	82
5.5	M4AST web tool application: screen-shoot from the table containing the list of the closest fifty best matches which are ordered upon the comparison coefficient (column two of the table).	83
5.6	Classification in Bus-DeMeo taxonomical system for: a) (99942) Apophis, and b) (175706) 1996 FG3. All the spectra are normalized to 1.25 μm .	84
5.7	Classification in the G-mode taxonomical system for: a) (99942) Apophis using G13 taxonomy, b) (175706) 1996 FG3 using G13 taxonomy, and c) (175706) 1996 FG3 using G9 taxonomy. All the spectra are normalized either to 1.25 μm (left and central panel), or to 0.55 μm (c).	86

5.8	Asteroid spectra and the best two matches derived from a comparison with laboratory spectra:(a) spectrum of Apophis and the spectrum of a simulant Lunar soil, (b) spectrum of Apophis and the spectrum of a particulate sample from the Hamlet meteorite, (c) de-reddened spectrum of Apophis and the spectrum of a particulate sample from the Cherokee Springs meteorite, (d) de-reddened spectrum of Apophis and the spectrum of a particulate sample from the Cat Mountain meteorite, (e) spectrum of 1996 FG3 and the spectrum of a sample from the meteorite Sete Lagoas, and (f) spectrum of 1996 FG3 and the spectrum of a sample from the Murchison meteorite heated to 1000 °C.	87
6.1	a) The visible [Binzel <i>et al.</i> , 2004b] and the NIR spectrum of (1917) Cuyo; b) a polynomial fit of the V+NIR spectrum of (1917) Cuyo compared with the theoretical spectra of R and Sr types; c) reflectance spectrum of (1917) Cuyo and the closest match resulting from meteorite comparison - H3-4 ordinary chondrite Dhajala; d) De-reddened spectrum of (1917) Cuyo and the closest match resulting from meteorite comparison, H6 ordinary chondrite Lancon. . .	96
6.2	a) The visible [Vernazza, 2006] and the NIR spectra of (8567) 1996 HW1; b) a polynomial fit of the V+NIR spectrum of (8567) 1996 HW1 compared with the theoretical spectra of S and Sq types; c) reflectance spectrum of (8567) 1996 and the closest match resulting from the meteorite comparison - the LL4 ordinary chondrite Hamlet; d) de-reddened spectrum of (8567) 1996 HW1 and the closest match resulting from meteorite comparison -the LL6 ordinary chondrite Cherokee Springs.	98
6.3	a) The visible [Binzel <i>et al.</i> , 2004b] and the NIR spectra of (16960) 1998 QS52; b) a polynomial fit of the V+NIR spectrum of (16960) 1998 QS52 compared with the theoretical spectra of Sr, Sq and Q types; c) the reflectance spectrum of (16960) 1998 QS52 and the closest fit resulting from spectral comparison - the L4 ordinary chondrite Saratov; d) the de-reddened spectrum of (16960) 1998 QS52 and the closest fit resulting from meteorite comparison - the LL4 ordinary chondrite Hamlet.	100
6.4	a) The NIR spectrum of (188452) 2004 HE62 normalized to 1.25 μm ; b) a polynomial fit for the spectrum of (188452) 2004 HE62 compared with the theoretical spectra of Sr and Sv types; c) the reflectance spectrum of (188452) 2004 HE62 and the closest fit resulting from meteorite spectra comparison - the L6 ordinary chondrite La Criolla; d) the de-reddened spectrum of (188452) 2004 HE62 and the closest matches resulting from meteorite comparison - the H6 ordinary chondrite Nanjemoy.	102

6.5	a) The NIR spectrum of 2010 TD54; b) a polynomial fit for the spectrum of 2010 TD54 compared with the theoretical spectra of Sv, Sr and S types; c) the reflectance spectrum of 2010 TD54 and the closest match resulting from meteorite comparison - the L4 ordinary chondrite Saratov; d) the de-reddened spectrum of 2010 TD54 and the closest match resulting from meteorite comparison - the H4 ordinary chondrite Gruneberg.	103
6.6	NIR spectrum of (164400) 2005 GN59 and its taxonomic classification.	105
6.7	The NIR spectrum of (5620) Jasonwheeler; b) a polynomial fit for the spectrum of (5620) Jasonwheeler compared with the theoretical spectra of D and T types; c) estimation of thermal flux in the spectrum of (5620) Jasonwheeler - the dashed line indicates where a linearly extrapolated continuum would fall, the solid line shows the presence of thermal flux; d), e), f) the reflectance spectrum of (5620) Jasonwheeler and the closest three matches resulting from meteorite comparison: the CM2 carbonaceous chondrite Mighei/Meghei, the CM2 carbonaceous chondrite Cold Bokkeveld, and the CM2 carbonaceous chondrite ALH84029 [Popescu <i>et al.</i> , 2011].	107
6.8	Visible [Binzel <i>et al.</i> , 2004a] and NIR spectrum of 2001 SG286. A linear fit and the D-type theoretical spectrum are plotted for comparison.	108
6.9	a) Wavelength position of the centers of the two absorption bands computed using Cloutis <i>et al.</i> [1986a]. The regions enclosed correspond to the band centers computed for the H, L, and LL chondrites, respectively [de León <i>et al.</i> , 2010]; b) BAR versus band I centers. The regions enclosed by continuous lines correspond to the values computed for basaltic achondrites, ordinary chondrites(OC), and olivine-rich meteorites(OI) [Gaffey <i>et al.</i> , 1993b].	109
7.1	a) Spectrum of (9147) Kourakuen normalized to 1.25 μm ; b) a polynomial fit of the spectrum of (9147) Kourakuen compared with the theoretical spectra of V, Sv, and Sr types; c) the comparison between the spectrum of (9147) Kourakuen and the spectrum of a sample from Pavlovka, d) the comparison between the spectrum of (9147) Kourakuen and the spectrum of a mixture of Pyroxene-Hypersthene-Plagioclase-Bytownite-Ilmenite.	116
7.2	a) The visible and NIR spectrum of (854) Frostia; b) A polynomial fit for the spectrum of (854) Frostia compared with the theoretical spectra of V, Sv and Sr types; c) the comparison between the spectrum of (854) Frostia and the spectrum of a sample from "ALHA76005,85" meteorite; d) the comparison between the spectrum of (854) Frostia and the spectrum of a sample from Y – 793591,90 meteorite.	120

7.3	The NIR spectra with the error-bars for (1333) Cevenola; a) obtained in March 12, 2007; b) obtained in March 13, 2007. The spectra are normalized to 1.25 μm .	124
7.4	a) The visible and the averaged NIR spectrum of (1333) Cevenola; b) A polynomial fit for the V+NIR spectrum of (1333) Cevenola compared with the theoretical spectra of Sq, Q and K taxonomic types; c) the comparison between the spectrum of (1333) Cevenola and the spectrum of a sample from <i>Saratov</i> meteorite; d) the comparison between the spectrum of (1333) Cevenola and the spectrum of a sample from <i>Hamlet#1</i> meteorite.	125
7.5	The NIR spectra of (3623) Chaplin; a) obtained in March 12, 2007; b) obtained in March 13, 2007. The spectra are normalized to 1.25 μm	126
7.6	a) The NIR averaged spectrum of (3623) Chaplin; b) A polynomial fit for (3623) Chaplin compared with the theoretical spectra of S, Sv and Sq taxonomic types;; c) the comparison between the spectrum of (3623) Chaplin and the spectrum of a sample from igneous plutonic rock; d) the comparison between the spectrum of spectrum of (3623) Chaplin and the spectrum of a sample from low-calcium impact melt breccia rock.	127
7.7	The NIR spectra of a) (10484) Hecht and b) (31569) 1999 FL18. Both spectra are normalized to 1.25 μm . Taxonomic classification of c) (10484) Hecht and d) (31569) 1999 FL18.	128
A.1	The GuideDog interface is used to control the guider system of the telescope. Source: Rayner <i>et al.</i> [2004].	135
A.2	The BigDog interface is used to control the spectrograph set-up and spectra acquisition. Source: Rayner <i>et al.</i> [2004].	136

Part I

INTRODUCTION

1

Why asteroids?

Even if the total mass of the asteroids is insignificant in rapport with the total mass of the planets, their large number, wide distribution throughout the Solar System and extremely divers composition makes them a valuable resource for Solar System studies. This introductory chapter provides a general overview of this population. The asteroids place in the diversity of the Solar System objects is described based on the scientific literature. Some briefly notes about asteroids discovery, following an historical line are given. The main physical properties of these objects are outlined. At the end of the chapter is made a short summary regarding my contribution in the discovery of the asteroids are outlined.

1.1 The place of asteroids in the structure of the Solar System

Asteroids are well-preserved samples from the first phase of the Solar System formation which started $4.57 \cdot 10^9$ years ago. In order to discuss their physical properties it is useful to trace back the events that took place at the beginning of the Solar System. According to the Solar Nebula Disk Model, the Solar System emerged from a large molecular gas and dust cloud which accumulated sufficient mass and density for gravitational collapse to occur. When the gravitational collapse was triggered (typically by random turbulence which locally increase the density within the cloud), the gas and dust cloud condensed until it formed a central mass and a protoplanetary disk that surrounded it.

As a consequence of the angular momentum conservation, the rate of rotation of the disk and central mass increased as it collapsed. The central mass continued to grow until it formed a protosun. When enough mass was accumulated for fusion to occur it became the Sun. At this stage a strong temperature gradient across the disk was present. The gradient of the temperature into the protoplanetary disk determines the distance where the different components started to condense. The inner disk was too hot for the condensation of volatiles, so it was dominated by rocky material, while the outer disk had a mixture of volatiles and ices. Within the disk, micron-size dust grains collided at velocities forming bodies up to a kilometer in size. Many of these large bodies collided and merged or ejected other bodies and eventually grew to planetary sizes [DeMeo, 2010].

This part of the planetary formation process occurred over a period of less than 10 millions

of years [Yin *et al.*, 2002]. After this period strong solar winds begin to clear dust from the Solar System, leaving the minor bodies and planets with a paucity of new material to accumulate.

The asteroids are remnants of the planetesimal population that once formed the planets. Even if some of the asteroids were affected by thermal and dynamical evolution and by collisions, most of them did not suffer a significant geological evolution preserving the physical evidences related to the first 200 million years of the Solar System history .

Currently, there is a wide diversity of bodies in the Solar System, thus in order to facilitate their studies and the discussions some definitions are required for different categories. The definitions of a planet, dwarf planet, and of a small body given below were assigned in Resolution 5 and 6 of the IAU (International Astronomical Union) 2006 General Assembly¹.

According to this resolution, **a planet** is a celestial body that: *a*) is in orbit around the Sun, *b*) has sufficient mass for its self-gravity to overcome rigid body forces so that it assumes a hydrostatic equilibrium - nearly round shape, and *c*) has cleared the neighborhood around its orbit.

A dwarf planet is a celestial body that *a*) is in orbit around the Sun, *b*) has sufficient mass for its self-gravity to overcome rigid body forces so that it assumes a hydrostatic equilibrium - nearly round shape, *c*) has not cleared the neighborhood around its orbit, and *d*) is not a satellite of a planet. Plutoids are dwarf planets with a semi-major axis greater than that of Neptune. All other objects except satellites orbiting the planets shall be referred collectively as **small bodies of Solar System** (are also called minor planets).

Following these definitions, there are eight planets in our Solar System: Mercury, Venus, Earth, Mars, Jupiter, Saturn, Uranus, and Neptune. Pluto is a dwarf planet, also as Ceres, Haumea, Makemake, and Eris. Ceres is located in the asteroid belt, while all others have semimajor axes greater than that of Neptune.

The categories of small bodies of Solar System include asteroids, trans-neptunian objects (denoted TNOs), comets and other small bodies. The size of the objects ranges from dust grains and small coherent rocks up to hundreds of kilometers size boulders. These categories are briefly presented below. The statistic data is taken from Minor Planet Center (MPC) website (<http://www.minorplanetcenter.org/iau/mpc.html>).

Asteroids are referred to being rocky minor planets that orbit the Sun at distances ranging from interior to Earth's orbit up to Jupiter's orbit [de Pater & Lissauer, 2010].

Comets are ice-rich bodies for which the volatile constituents sublime during close approaches to the Sun. They are characterized by a nucleus - the inner part of the body, the coma - the spherical halo of sublimated material surrounding the nucleus, and two tails: a dust tail trailing opposite the comet's trajectory and an ion tail in the anti-Sun direction.

Centaurs are icy bodies orbiting between (and in some cases also cross) the orbits of Jupiter and Neptune. There are 64 known Centaurs as of August 12, 2012. Centaurs are on chaotic

¹<http://www.iau.org/>

orbits with high eccentricities and/or inclinations. Dynamical calculations show that they are transitioning from the trans-neptunian region [de Pater & Lissauer, 2010].

TNOs are small bodies of the Solar System whose orbits lie partly or entirely beyond the orbit of Neptune. There are 1,044 known TNOs as of August 12, 2012. The existence of a disk of numerous small bodies exterior to the major planets was postulated by K. E. Edgeworth and by G. P. Kuiper. Therefore, this ensemble is referred as the Edgeworth-Kuiper belt.

All small bodies (excepting the comets) with well-determined orbits are designated by a number (in a chronological order of the discoveries) and additionally can receive a name, e.g., (1) Ceres, (7986) Romania, (99942) Apophis, (134340) Pluto. After an object is discovered, but the orbit is not well determined, it receives a provisional designation. This designation is related to the date of discovery of the object: the first four characters indicate the year, followed by a space, then a letter to show the half of the month (A for January 1-15, K for May 16-31, I is omitted), followed by another letter to show the order of discovery within the half month (A for 1st, Z for 25). If a large number of the asteroids are discovered in certain half month, an additional number completes the designation, e.g: 2012 AA, 2001 SG286, 2005 UJ516.

The next sections of this chapter discuss the discovery of the asteroids and the diversity of these small bodies, while this thesis concerns their composition using spectroscopy.

1.2 The Discovery Of Asteroids

The roots of asteroid studies can be found at the end of the 16th century when the German mathematician and astronomer, Johannes Kepler realized that the distance between Mars and Jupiter was not proportional to the distances between other planets. He concluded that it must be another planet, undiscovered yet, occupying this part of the Solar System: "Inter Jovem et Martem interposui planetam" (Kepler 1596).

Further studies of the relative distances of the planets from the Sun were made 170 years later when Johan Daniel Titius noted that the sequence of the distances from the Sun of the known planets could be fitted by a geometric progression. The relation was published by Johan Elert Bode in 1772, and today the modern formulation of the Titius-Bode empirical law is:

$$r_n = 0.4 + 0.3 * 2^n \quad (1.1)$$

where r_n is the semi-major axis of the n-th planet. Here, the units are considered such that the Earth's semi-major axis is equal to 1.

It can be identified Mercury for $n = -1$, Venus for $n = 0$, Earth for $n = 1$, Mars for $n = 2$, Jupiter for $n = 4$, and Saturn for $n = 5$. After the discovery of the planet Uranus (made by Sir William Herschel in 1781) at a solar distance close to the solution $n = 6$, the regularity in the planetary location was considered a primary feature of the Solar System. At that moment the searching for the "missing planet" with $n = 3$ began.

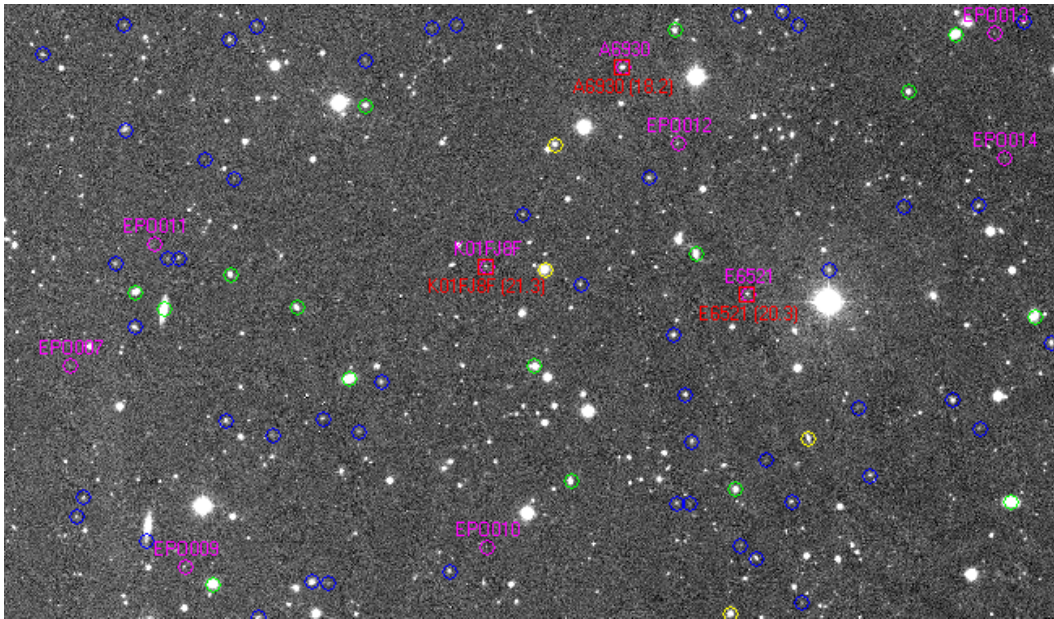


Figure 1.1: A field obtained with INT-WFC on February 28, 2012. Ten asteroids were identified (marked with pink), from which only three were known at the moment of the observation. The size of the field is (15 arcmin x 15 arcmin)

In January 1801, the abbot Giuseppe Piazzi discovered Ceres, a small body at just the right distance. In 1802 Heinrich Olbers discovered Pallas at the same orbital distance. In the following years, Juno (1804) and Vesta (1807) were discovered also at similar orbital distances with Ceres and Pallas. These bodies were too small to be classified as planets, but the gap was filled.

At the beginning of the XIX century, only comets were known to be small objects orbiting the Sun, but they appear like diffuse objects. Herschel, one of the most known astronomers at that time called these objects (Ceres, Palas, Juno, Vesta) asteroids (from Greek "asteroeides"). In this way it was underlined their different appearance - point sources ("star-like") unresolved by the telescopes, compared with the comets which show extended comas.

The first theory of the origin of asteroids, was developed by Olbers in 1803, who suggested that they are fragments of a planet that had been broken to pieces and additional fragments will be found. This prediction became popular, while other asteroids were discovered orbiting at the same solar distance. With the increasing number of these new findings the hypothesis that they could be fragments of an exploded planet became very popular.

In the middle of the 20th century Otto Johannes Schmidt proposed that asteroids represented an arrested stage of planet formation and have never been assembled into a large body. This is now the most plausible hypothesis.

The apparition of photography, offered new means for finding new asteroids. The method consists in comparison of photographic films of the same region of the sky taken at different time intervals. The vast majority of the objects recorded on films were stars and galaxies and

their images were located in the same relative positions on all photographic films. Because a moving asteroid would be in a slightly different position on each picture exposure and the background stars and galaxies were not, it could be identified.

Nowadays the charge coupled devices (CCD) are used instead of photography. While, the CCD technology is more sensitive and accurate than the older photographic methods, the modern discovery technique itself is rather similar. Separated by several minutes, three or more CCD images are taken of the same region of the sky. These images are then compared to see if any asteroid has systematically moved to different positions on each of the separate images (Fig. 1.1).

For a newly discovered object, the separation of the asteroid location from one image to another, the direction it appears to be traveling, and its brightness allow to estimate its orbital characteristics and roughly its size. For example, an object that appears to be moving very rapidly from one image to the next one, is almost certainly very close to the Earth. Computer-aided analyses of the CCD images have replaced the older, manual techniques for all the current asteroid search programs.

Fig. 1.1 shows a field obtained with INT-WFC (Isaac Newton Telescope, Wide Field Camera) on the night of February 28, 2012. Ten asteroids could be identified in this field by taking consecutive images at an interval of five minutes. At the moment of the observation only three of the identified asteroids were known.

Thanks to this technological development, during the last decades the total numbers of the asteroids discovered had grown exponentially. Among the most important surveys dedicated to asteroid detection (particularly to Near Earth Asteroids) are those leaded by the United States (CSS, LINEAR, Spacewatch, LONEOS and NEAT) which have been using large field, mostly 1m class telescopes. In the Europe the most important programs were: ASIAGO/ADAS in Italy and Germany, CINEOS in Italy, KLENOT in the Czech Republic, NEON in Finland.

An example of successfully observing run is the one performed by [Boattini *et al.*, 2004]. During two short runs at ESO (European Southern Observatory) LaSilla, they employed the MPG (Max Planck Gesellschaft) 2.2m telescope as a search facility, and the NTT (New Technology Telescope) 3.5m as a follow-up telescope to survey faint asteroids beyond 22 magnitude, for three observing nights. The authors observed about 700 Main Belt asteroids as faint as V 22 magnitude. They exposed between 60s and 150s in the R(red) band.

To conclude this section, as of August 13, 2012 there are 588,219 observed asteroids from which 333,841 have the orbits well determined (as a consequence they were numbered) ².

1.3 Distribution and diversity of asteroids

Asteroids are often grouped according to their orbital parameters. Fig. 1.2 shows the distribution of the asteroids as a function of their heliocentric distance. The majority of asteroids are

²<http://www.naic.edu/~nolan/astorb.html>

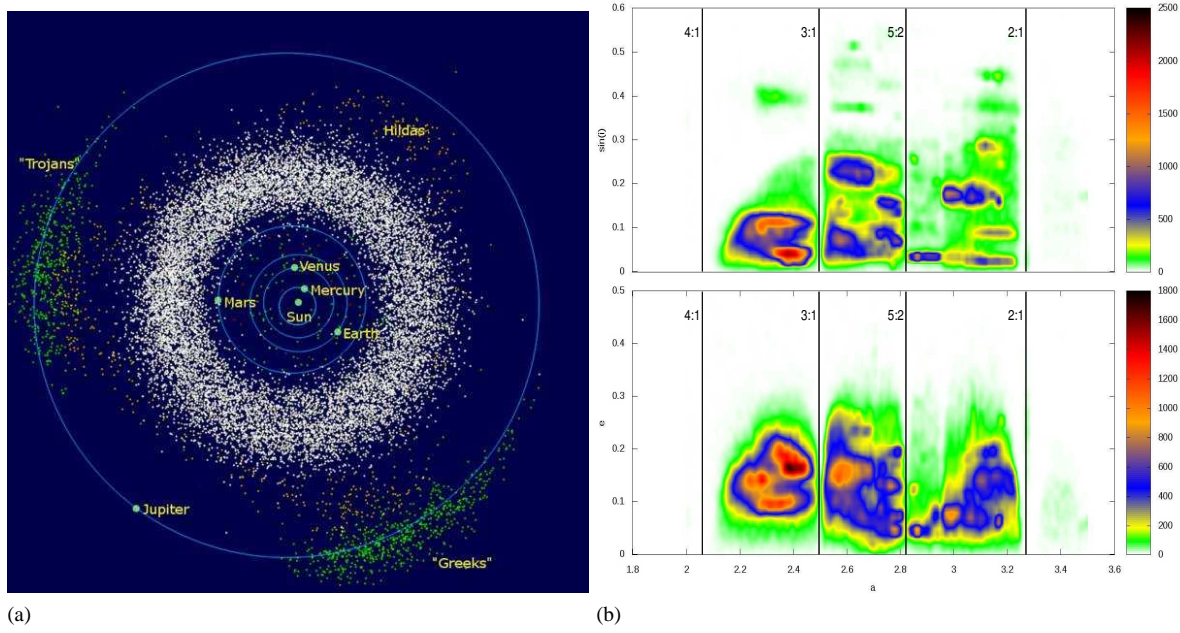


Figure 1.2: a) The position of asteroids in the inner part of the Solar System (Source: <http://en.wikipedia.org/>). b) The distribution of asteroids in a representation (a, e) - bottom and $(a, \sin i)$ - top, a is the semi-major axis and i the inclination [Nedelcu, 2010].

located in the Main Belt, at heliocentric distances between 2.1 and 3.3 AU³ (these are called Main Belt Asteroids - MBAs). Several gaps and concentrations can be distinguished by plotting the distribution versus semi-major axis (Fig. 1.2b). These gaps are called Kirkwood gaps and correspond to the locations of resonances with Jupiter (in the Fig. 1.2 there are marked 4:1, 3:1, 5:2, 2:1 resonances). The 3:1 and 5:2 resonances located at 2.5 and 2.82 AU, respectively define the boundaries between the inner (2.0 - 2.5 AU), middle (2.5 - 2.82 AU), and outer (2.82-3.3 AU) regions of asteroid belt.

The MBAs have diameters up to ≈ 500 km (Pallas, Vesta). Ceres, the largest body from the Main Belt, which has a diameter of ≈ 1000 km is classified as a dwarf planet.

Inside the Main Belt, several clusters of asteroids could be identified [Birlan & Nedelcu, 2010]. These are called asteroid families and are defined by Zappala *et al.* [1995] as a group of bodies that are genetically and dynamically linked as a result of a catastrophic event: collision of two bodies followed by the destruction of both target and impactor. Usually, they are identified as groups in the space of orbital proper elements [Milani & Knezevic, 1990].

According to Minor Planet Center (as of August 2012), a total of 5,188 asteroids were discovered near Jupiter's Lagrangian points L_4 (3404 objects) and L_5 (1784 objects) - Fig. 1.2a. These objects are called **Trojan asteroids**. They are characterized by low albedo. The largest body is (624) Hektor with a mean radius ≈ 100 km [de Pater & Lissauer, 2010]. Several Mars and Neptune Trojans have also been discovered.

³AU is an astronomical unit of distances, $1\text{AU} = 149,597,870,700$ m (\approx the average Earth - Sun distance.)

Owing to some mechanisms some of the Main Belt Asteroids have migrated into the inner part of the Solar System [Morbidelli *et al.*, 2002]. These are **Near-Earth Asteroids** (denoted NEAs), small bodies of the Solar System with perihelion distances $q \leq 1.3$ AU and aphelion distances $Q \geq 0.983$ AU, whose orbits approach or intersect Earth orbit. Dynamical studies confirmed the main belt origin for the majority of NEAs population. The transition of a main belt asteroid to NEA class is due to the dynamical perturbations associated with the main belt resonances. The most active of these regions acting as escape hatches are the ν_6 secular resonance and the orbital resonances 3:1, 5:2 and 2:1 with Jupiter situated at 2.5, 2.8 et 3.2 astronomical units. Long term numerical integrations have revealed the source regions of the current NEAs population: 61% originated in the inner region of main belt, 24% in the central and 8% in the outer main belt. Only 6% of NEAs are considered to have a cometary origin. The steady-state model of NEA will require a constant flux of objects with $H \leq 18$ of 800/Myr.

Depending on their orbital parameters, NEAs are subdivided into Amors ($1.016 < q < 1.3$ AU), Apollos ($a \geq 1.0$ AU; $q \leq 1.016$ AU), Athens (semi-major axe $a < 1.0$ AU; $Q \geq 0.983$ AU), and Atiras ($Q < 0.983$ AU).

Potentially Hazardous Asteroids (PHAs) are currently defined based on parameters that measure the asteroid's potential to make threatening close approaches to the Earth. All asteroids with an Earth minimum orbit intersection distance (MOID) smaller than 0.05 AU and an absolute magnitude (H) of 22.0 or brighter are considered PHAs [Milani *et al.*, 2000]. A sub-category of these asteroids are virtual impactors (VIs), objects for which the future Earth impact probability is non-zero according to the actual orbital uncertainty [Milani & Gronchi, 2010].

One of the most important aspects related to the NEAs is their accessibility to be investigated by the spacecrafts. Some of them require less propulsion in order to be encountered by spacecraft than that for the Moon, making them ideal mission targets. This enables their scientific study and the detailed assessment of their future use as space resources.

In the last fifty years different observing programs dedicated to asteroids have shown a large diversity in their properties. Several physical properties like diameter, albedo, shape could be deduced from light-curve analysis, radar observations, and polarimetry. The asteroid composition could be inferred through spectroscopic observations. Based on this type of observations, different taxonomic categories were defined with the purpose to roughly correlate the surface compositions of different objects. The first identified types were S (stony - based on the resemblance with stony meteorites), C (resemblances with carbonaceous chondrite meteorites), M (metallic), and E (enstatite achondrite). As a consequence of this taxonomic classification it was discovered the correlation between taxonomic classes and heliocentric distances. The more thermally processed, metamorphic and igneous asteroids classes (E, S, M) are usually found in the central and inner regions of the main belt while the outer regions are dominated by the primitive, relatively unaltered asteroids types. This correlation is rooted in the original

heterogeneity of the protoplanetary disk at the time when the accretion of asteroids started.

These taxonomic classes emerged as more and more asteroids observations were available, such that the modern taxonomies (e.g. Bus-DeMeo [DeMeo *et al.*, 2009]) contain more than 20 classes.

From the point of view of their geological evolution, asteroids could be described by three broad categories: primitive, partially melted, and differentiated. Primitive objects are mainly made of silicates, carbon, and organics and some are similar to CI and CM meteorites. Olivine, pyroxene and metal are the main constituents of asteroids partially melted, or at least thermally altered. Remnants of disrupted differentiated bodies include basaltic types, nearly-pure olivine, and metallic bodies, that represent pieces of the crust, mantle, and core [DeMeo, 2010].

1.4 Asteroid brightness and albedo

The apparent magnitude of asteroids depends on geometric parameters (Earth-object distance, Sun-object distance and phase angle) and on the physical and optical properties of the body (size and albedo). The absolute magnitude takes into account only the body intrinsic properties. For asteroids it is defined as being the apparent magnitude if the body were at 1 AU from both the observer and the Sun as seen at phase angle $\phi = 0$. This is an analytical definition because no geometrical point can satisfy the three conditions at the same time. It can be computed from astrometric and photometric observations with the formula:

$$H = m_v + 2.5 \cdot \log \frac{\Phi}{r \cdot \Delta} \quad (1.2)$$

where H is the absolute magnitude, m_v is apparent magnitude, Φ is the phase integral (integration of reflected light; a number in the 0 to 1 range), r is the heliocentric distance (measured in AU), and Δ is Earth-object distance (measured in AU) [Magrin, 2006].

The relation between the absolute magnitude and the body physical properties is:

$$\log(p_v \cdot D^2) = 6.259 - 0.4 \cdot H \quad (1.3)$$

where D is the diameter of the body expressed in km and p_v is the geometrical albedo [Magrin, 2006].

The geometric albedo can be thought of as the amount of radiation reflected from a body relative to that of a flat diffuse surface which is a perfect reflector at all wavelengths (called Lambertian surface) [de Pater & Lissauer, 2010].

1.5 My contribution to asteroids discovery

My contribution to asteroids discovery can be divided in two parts: 1) the observing campaigns in which I was involved and 2) the data-mining of archives for asteroids randomly appearing in

the fields.

Together with my colleagues, I participated to the following observing campaigns for discovery, follow-up and recovery of asteroids (in particular for NEAs):

- March, 03 2010; Isaac Newton Telescope (INT) 2.5m, Roque de Los Muchachos Observatory (ORM) in La Palma (Canary); Data reduction and measurements;
- April 19, 2010; Telescope - T120 Obsv. de Haute Provence (France); Data reduction and measurements of NEAs;
- November 15-19, 2010; Telescope - T120 Obsv. de Haute Provence (France); On site mission (observer, data reduction and measurements);
- March 01-04, 2011; T1m, Pic du Midi (France); On site mission (observer, data reduction and measurements);
- June 03-04, 2011; Blanco 4m - Cerro Tololo, Chile; Data reduction and measurements;
- November 16-24, 2011; T1m, Pic du Midi (France); On site mission (observer, data reduction and measurements);
- February 25 - 28, 2012; Isaac Newton Telescope (INT) 2.5m, Roque de Los Muchachos Observatory (ORM) in La Palma (Canary); On site mission (observer, data reduction and measurements);

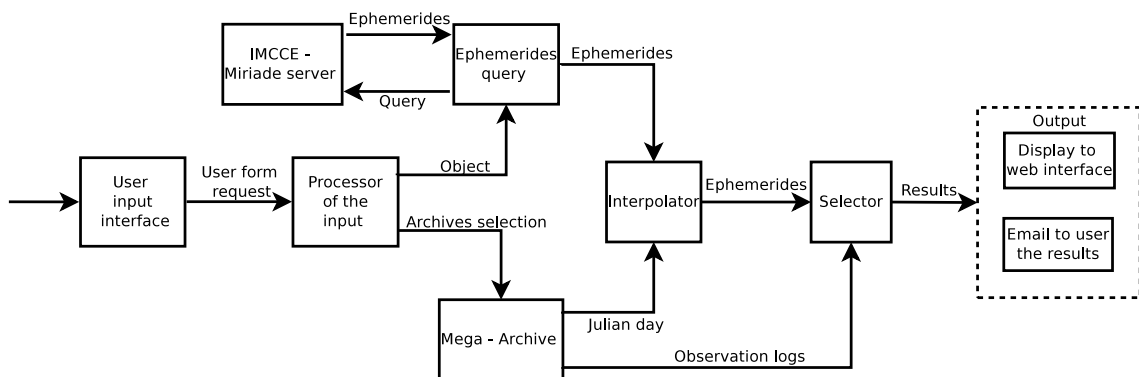


Figure 1.3: The flowchart of Mega-Preccovery [Vaduvescu *et al.*, 2012].

Despite some recent data mining efforts, the vast collection of CCD images and photographic plate archives still remains insufficiently exploited. Considering this point, I was involved in the design of a software project for data mining worldwide image archives for poorly known asteroids called MegaPreccovery.

We designed Mega-Preccovery [Vaduvescu *et al.*, 2012], with the aim to fasten and target the search of one or some few important objects, such as PHAs or VIs. Given this, we propose to search very large collections of archives for images which include one or few selected known asteroids in their field. There are two components of this project:

Mega-Archive - the database which includes the individual instrument archives, namely the observing logs for their science CCD images or plates available from a collection of instruments and telescope around the globe. The Mega-Archive is an open project allowing other instrument archives to be added later for exploration by anybody who would like to contribute. As of March 2012, the Mega-Archive counts about two million images from 20 instrument archives available for search via Mega-Precovery. This include all ESO imaging instruments, the INT WFC, CFHTLS, Subaru Suprime-Cam, Blanco Mosaic-2 and AAT WFI archives;

Mega-Precovery software ⁴ for data mining the Mega-Archive for the images containing one or a more desired catalogued object (NEAs, PHAs or other asteroids) included in a local daily updated MPC database. The Mega-Precovery software is written in PHP, being embedded on the EURONEAR website as a public access application under the Observing Tools section. The flowchart of the project is given in Fig. 1.3.

The output of Mega-Precovery consists in a list including the images and the corresponding CCD number predicted to contain the queried object(s). The results are displayed both in the web interface (visible only at the end of the run) and sent via e-mail to the user (in case this option was selected). The user can search the images in the online instrumental archive, then download, inspect and measure the data related to this asteroid according to his/her own scientific interest (astrometry, photometry, etc).

Inside EURONEAR team [Vaduvescu *et al.*, 2012], I searched for randomly appearances of known Near Earth Asteroids (NEAs) and Potentially Hazardous Asteroids (PHAs) in ESO/MPG WFI(Wide Field Imager) and INT WFC archives (these are two wide field 2m class telescope). A total of 152 asteroids (108 NEAs and 44 PHAs) were identified and measured on 761 images and their astrometry was reported to Minor Planet Center (MPC). Both recoveries and precoveries (apparitions of the object in the images before official discovery) were reported, including prolonged orbital arcs for 18 precovered asteroids and 10 recoveries, plus other 124 recoveries.

All the astrometric measurements were submitted to Minor Planet Center <http://www.minorplanetcenter.org/iau/mpc.html>. These measurements appear in 12 Minor Planet Circulars and 21 Minor Planet Electronic Circulars: (79530, 1 (2012); 78894, 9 (2012); 78437, 11 (2012); 77699, 2 (2012); 77266, 11 (2011); 77265, 3 (2011); 77173, 6 (2011); 75198, 5 (2011); 74036, 3 (2011); 72456, 4 (2010); 70198, 9 (2010); 69303, 1 (2010)); (2012-E19 (2012); 2012-D102 (2012); 2012-D82 (2012); 2011-W52 (2011); 2011-W45 (2011); 2011-W44 (2011); 2011-W33 (2011); 2011-W29 (2011); 2011-W28 (2011); 2011-W27 (2011); 2011-W25 (2011); 2011-W22 (2011); 2011-W12 (2011); 2011-E19 (2011); 2011-E14 (2011); 2011-E13 (2011); 2011-E12 (2011); 2011-E11 (2011); 2010-W13 (2010); 2010-W12 (2010); 2010-W11 (2010)). An example of such circular is given in Fig. 1.4.

⁴<http://euronear.imcce.fr/tiki-index.php?page=MegaPrecovery>

The Minor Planet Electronic Circulars contain information on unusual minor planets and routine data on comets. They are published on behalf of Commission 20 of the International Astronomical Union by the Minor Planet Center, Smithsonian Astrophysical Observatory, Cambridge, MA 02138, U.S.A.

Prepared using the [Tamkin Foundation Computer Network](#)

MPC@CFA.HARVARD.EDU
 URL <http://www.minorplanetcenter.net/> ISSN 1523-6714

2007 ES

Revision to [MPEC 2007-E43](#)

Additional Observations:

K07E00S	C2011	03	02.23925	09	39	50.07	+20	25	09.6	21.1	VrEE011G96
K07E00S	C2011	03	02.24505	09	39	49.28	+20	25	07.9	20.9	VrEE011G96
K07E00S	C2011	03	02.25080	09	39	48.56	+20	25	05.9	21.8	VrEE011G96
K07E00S	C2011	03	02.25661	09	39	47.88	+20	25	03.8	21.5	VrEE011G96
K07E00S	C2011	03	02.43234	09	39	25.77	+20	24	07.4	21.8	VrEE011G96
K07E00S	C2011	03	02.43338	09	39	25.74	+20	24	06.9	21.6	VrEE011G96
K07E00S	C2011	03	02.43441	09	39	25.63	+20	24	06.2	21.9	VrEE011G96
K07E00S	C2011	03	02.43546	09	39	25.48	+20	24	05.7	21.6	VrEE011G96
K07E00S	C2011	03	03.01288	09	38	15.46	+20	20	58.8	20.9	RvEE011586
K07E00S	C2011	03	03.01516	09	38	15.09	+20	20	57.9	21.0	RvEE011586
K07E00S	C2011	03	03.01756	09	38	14.84	+20	20	57.1	21.1	RvEE011586
K07E00S	C2011	03	03.02221	09	38	14.29	+20	20	55.3	21.4	RvEE011586
K07E00S	C2011	03	03.02432	09	38	14.04	+20	20	54.8	20.9	RvEE011586
K07E00S	C2011	03	03.02642	09	38	13.79	+20	20	54.0	20.5	RvEE011586
K07E00S	C2011	03	03.02853	09	38	13.41	+20	20	53.0	21.3	RvEE011586
K07E00S	C2011	03	03.03348	09	38	12.90	+20	20	51.6	20.7	RvEE011586
K07E00S	C2011	03	03.03559	09	38	12.66	+20	20	51.0	20.7	RvEE011586
K07E00S	C2011	03	03.03770	09	38	12.42	+20	20	50.7	20.5	RvEE011586

Observer details:

[586 Pic du Midi.](#) Observers M. Birlan, F. Colas, M. Popescu. Measurer M. Popescu. 1.05-m f/12.7 reflector + CCD.
[G96 Mt. Lemmon Survey.](#) Observer A. D. Grauer. Measurers J. D. Ahern, E. C. Beshore, A. Boattini, G. J. Garradd, A. R. Gibbs, A. D. Grauer, R. E. Hill, R. A. Kowalski, S. M. Larson, R. H. McNaught. 1.5-m reflector + CCD.

Figure 1.4: The first part of the Minor Planet Electronic Circular issued for the orbit recovery of the asteroid 2007 ES.

2

Why spectroscopy?

Much of the knowledge about the Univers came from the study of electromagnetic radiation received from the cosmic bodies. The most important method to study the electromagnetic radiation is spectroscopy. This chapter introduces the theory behind the application of spectroscopy in astronomy. A short description of the basic components of a spectrometer (the prism and gratings) is made. The transparency of the Earth atmosphere as a function of wavelength is presented. A simple example of the way in which the properties of celestial bodies could be studied using spectroscopy is shown. The chapter ends by outlining the principles for applying spectroscopy in asteroid studies.

Spectroscopy is one of the most powerful scientific tools for studying the nature. The study of celestial bodies using spectroscopy connects astronomy with fundamental physics at atomic and molecular levels.

The beginning of spectroscopy applied to celestial bodies could be traced back to early nineteenth century with the discovery of dark lines in the solar spectrum by W. H. Wollaston in 1802 and J. von Fraunhofer in 1815. Fraunhofer did not know what is the cause for the dark lines he observed besides the well known characteristic colors of the rainbow. However, he catalogued the exact wavelength of each dark line and today these are still known as *Fraunhofer lines*.

On the contrary, in the same period the positivist French philosopher Auguste Comte noted referring to celestial bodies: "We will never know how to study by any means the chemical composition, or their mineralogical structure".

Performing similar observations using light from brightest stars, Fraunhofer concluded that most of the spectral features are somehow related to the composition of the object he observed [Tennyson, 2005]. The physical explanation came later, with the development of quantum mechanics: the dark lines at discrete wavelengths arise from the absorption of energy by the atoms or the ions in the star atmosphere.

Nowadays, the laboratory spectroscopic studies of different chemical components provide the basis for interpreting astronomical spectra. There is a direct connection between the physical parameters of a celestial body and the information that can be obtained by observing its spectrum. By carefully analyzing the spectra it is possible to obtain information about the com-

position of the object being observed, its temperature and its internal pressure or density, its motion relative to the Earth, and the presence of a magnetic field.

2.1 Diffraction gratings and prisms

There are several methods that can be used to separate the light into its component wavelengths. The simplest way is to use broad band filters before the detector in order to isolate different spectral regions. This method is called photometry and is considered as a separate subject from the spectroscopy.

Spectral resolution (or resolving power) is defined as the fraction of the wavelength - $\Delta\lambda$, that can be resolved relative to that of the operating wavelength - λ (Eq. 2.1). in general, the spectroscopy is considered to involve spectral resolutions higher than 50.

$$R = \frac{\lambda}{\Delta\lambda} \quad (2.1)$$

The astronomical spectrometers are devices that measure the amount of radiation coming from the celestial bodies at different wavelengths. To split the light into its component wavelength, astronomers can use diffraction gratings, prisms, Fabry-Pérot etalons and Fourier transform spectroscopes. Bellow are summarized the main characteristics of diffraction gratings and prisms which were used during different observations that I performed.

The diffraction grating generally consists of a large number N , of parallel slits separated by opaque spaces of comparable dimensions. Producing the spectra with the diffraction gratings involves the interference of N waves and the diffraction on slit phenomena [Cristescu, 2004]. The distribution of intensity of the radiation in the diffraction pattern is described by the formula Eq. 2.2.

$$I = I_0 \cdot \left[\frac{\sin \frac{\pi b \sin \theta}{\lambda}}{\frac{\pi b \sin \theta}{\lambda}} \right]^2 \cdot \left[\frac{\sin \frac{N \pi (b+d) \sin \theta}{\lambda}}{\sin \frac{\pi (b+d) \sin \theta}{\lambda}} \right]^2 \quad (2.2)$$

where d is the size of opaque spaces, b is the size of the slit, θ is the angle between a certain direction and the normal to the grating and I_0 is the total intensity passing through a slit [Cristescu, 2004]. The minima and the maxima position depend on the wavelength and on the diffraction grating parameters (b and d).

By increasing the number N of slits, the interference fringes become sharpest. Two wavelengths (λ and $\lambda + \Delta\lambda$) could be barely separated, if the minimum of the diffraction pattern corresponding to λ is in the same position as the bright fringe corresponding to $\lambda + \Delta\lambda$ for the same diffraction order m . From this condition it can be computed the spectral resolution $R = N \cdot m$. Thus the chromatic resolving power is proportional to the total number of slits and it is higher in the higher orders. In Fig. 2.1 are shown the diffraction patterns obtained using a diffraction grating having $b = d = 5\mu m$ and $N = 1000$.

The dispersion of a spectrum is the rate of change of wavelength with the angular position.

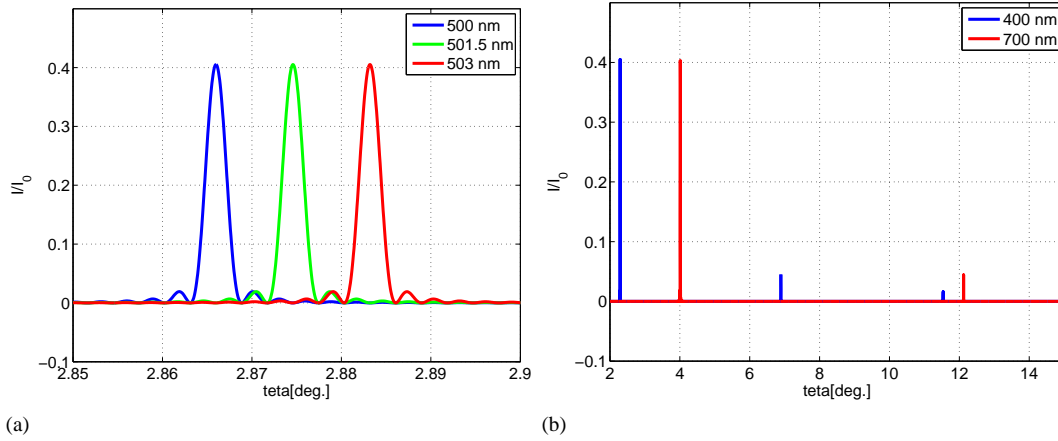


Figure 2.1: The diffraction pattern produced by a diffraction grating having $b = d = 5\mu m$ and $N = 1000$. Different wavelengths are considered.

It can be computed by deriving Eq. 2.3.

$$\lambda = \frac{d \cdot \sin \theta}{m} \quad (2.3)$$

In practice most gratings use mirrors in place of the slits. On a well-polished surface of a metal, very thin, parallel grooves are drawn. The waves reflected from these grooves behave exactly as the transmitted waves in the case of the transmission gratings. They can be designed such that the main part of the incoming radiation is diffracted selectively on a given order. Because a blaze of light is seen when the grating is viewed at the correct angle, this is called blazed grating [Cristescu, 2004].

The prism acts as a disperser through the effect of differential refraction. This follows from the fact that the refractive index of a material depends on the wavelength. This dependence can be described by the empirical Hartmann formula - Eq. 2.4.

$$n_\lambda \approx A + \frac{B}{\lambda - C} \quad (2.4)$$

where A, B, C are the Hartmann constants for a particular material [Kitchin, 1995].

The spectral resolution of a prism is given by:

$$R \approx \frac{ABL \sqrt{1 - 0.25n_\lambda^2}}{(\lambda - C)^2} \quad (2.5)$$

where L is the length of the face of the prism. For a typical prism used in astronomy made of a dense flint and a side length of 10 cm, the spectral resolution could be up to 15,000 [Kitchin, 1995]. Compared to the diffraction gratings which can have higher spectral resolution, this is one of the disadvantages of prisms.

In order to produce a reliable spectrum, the dispersive element should be combined with

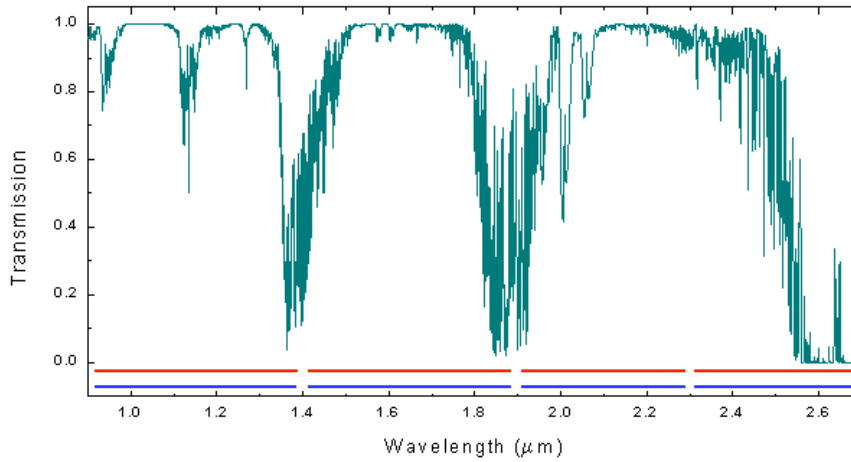


Figure 2.2: The atmospheric transmission above Mauna Kea for the wavelength ranges 0.9 - 2.7 μm with a water vapor column of 1.6 mm and an air mass of 1 (Source: <http://www.gemini.edu/?q=node/10789>).

several other components into the instrument called spectrometer. Usually, the designs of spectrometers incorporate the following basic components: an entrance slit to reduce the overlap between adjacent wavelengths and to reduce the background noise, collimators to produce parallel beams of light, a dispersive element, a focusing element to produce focused images of the slit for different wavelengths of the spectrum, and a detector.

2.2 Spectroscopy and atmospheric transparency

The observation of celestial bodies using different types of ground-based telescopes is possible in the regions of electromagnetic spectrum for which the atmosphere is transparent. There are two spectral windows which allow the observation: the optical (V) up to the mid-infrared (the near-infrared 0.8 - 2.5 μm interval is denoted as NIR) and the radio one. The X-rays and ultraviolet wavelengths are blocked due to absorption by ozone and oxygen, while the far infrared radiation is blocked mainly due to absorption by water and carbon dioxide.

While in the optical wavelength region the atmosphere is almost completely transparent, in the near-infrared there are absorption bands of water vapors making some regions like 1.4-1.5 μm and 1.8-2.0 μm poorly transparent (Fig. 2.2). Because of the effects of the atmosphere, observations with space telescopes, such as the Hubble and Spitzer telescopes, are very valuable.

Another important difference between the V and NIR spectral intervals is the fact that the sky is brighter in the NIR region. For example in the J, H, K filters¹ the estimated sky background has 15.7, 13.6, respectively 13 mag/arcsec². Additional, important variations of the sky background could be observed in the intervals of tens of arc minutes of the sky.

¹Wide band filters centered on 1.25 μm (J), 1.65 μm (H), 2.2 μm (K)

These issues in the NIR part require additional observing techniques and processing methods (described in Chapter 4) comparing to observation in the V part of the spectrum.

2.3 A simple application

Bellow is described a simple application to exemplify the basic method for obtaining spectra of celestial bodies. It concerns an emission spectrum studied in the V region using a small telescope. Additional details regarding this spectral observation can be found in **Popescu et al.** [2012a].

An easy way to obtain spectra of celestial bodies is to use a prism or a transmission grating in front of a telescope objective. Depending on the equipment used, the sky quality on the observing moment and data reduction procedures, the limiting magnitude could be pushed up to $V = 15$ in low resolution mode, with a small telescope (principal mirror diameter below 50 cm).

Together with my colleagues, I carried out observations with telescopes having the diameter of principal mirror between 200-300 mm and a diffraction grating having 100 lines/mm [**Popescu et al.**, 2012a]. Since promising results were obtained both for stars and for the quasar 3C273 we took the challenge to observe the quasar PG1634+706 that has and apparent magnitude $V=14.7$. The purpose was to identify the emission lines in its spectrum and to calculate their redshift. For this run we used a Celestron C8-NGT telescope, which is a Newtonian type having the primary mirror of 200 mm and a focal length of 1,000 mm, which means a focal ratio $f/5$. It is used on a AS-GT (CG-5 GoTo) equatorial mount allowing automated tracking of the object. For image recording we used An ATIK 314L+ CCD (charge coupled device) camera having 1.45 Megapixels (a matrix of 1391x1039 pixels), each pixel being a square - $6.45 \times 6.45 \mu\text{m}$ (chip size - $8.98 \times 6.71\text{mm}$). This camera has a resolution of 16 bits.

The spectrum of PG1634+706 was obtained using a Star Analyser 100 - a high efficiency 100 lines/mm transmission diffraction grating, blazed in the first order. It was mounted in a standard 1.25 inch diameter threaded cell which is compatible with the telescope and CCD camera. A rough calibration of the system can be estimated according to the designer formula adapted to our system (Eq. 2.6):

$$Dispersion_{estim}[\frac{nm}{pixel}] = \frac{6.45}{d[cm]} \quad (2.6)$$

where d is the distance between grating and CCD. The optical design allowed a resolution around 1.5nm. A precise calibration was made using known lines identified in the spectrum of a bright star. The software used for data acquisition was Artemis Capture.

The observations were carried out at 2011-08-05.089 (UT) in a low light pollution area (Vălenii de Munte - România). The object has the equatorial coordinates $RA = 16^h34^m29^s$ and $DEC = +70^\circ31'32''$. At the observing moment the object had an air mass of 1.17. The final

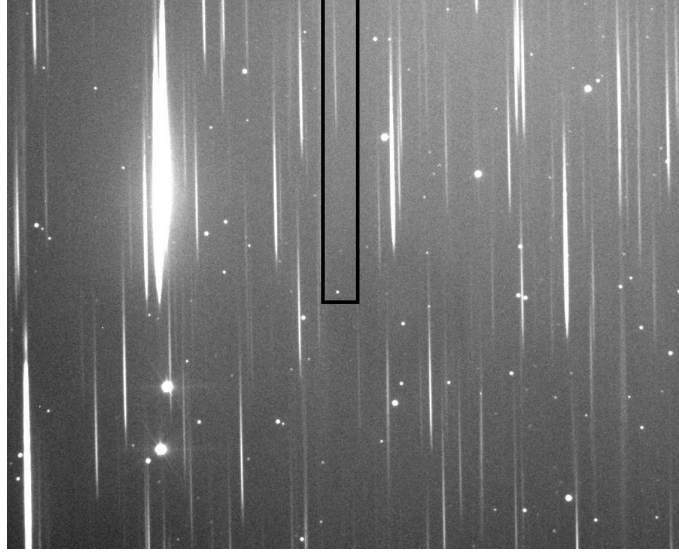


Figure 2.3: The field of quasar PG1634+706 (north is at bottom of the figure). The object and its spectrum are surrounded by a rectangle. In this image it can be distinguish the zero order (objects are dots) and the first order (light is dispersed) - **Popescu et al.** [2012a].

image (Fig. 2.3) consists of a stack of 18 individual images with 90 seconds exposure time each and 3 images with 60 seconds exposure time each, thus a 30 minutes total exposure time. Bias and flat field corrections were made using corresponding images taken at the beginning of the night.

The wavelength calibration was done by identifying the position of the known lines in the star spectra. In general, stellar spectra have two dominant features: the continuum - emission at all wavelengths across their spectrum, and discrete absorption lines corresponding to elements which are present in the stellar atmosphere. Hydrogen is the most common gas in the atmosphere of stars, and thus its well known absorption lines from visible ($H_\alpha, H_\beta, H_\gamma$) can be used for wavelength calibration. Since the image (Fig. 2.3) contains also the spectra of some stars an accurate calibration can be made using this procedure. The value of the resolution found is given in Eq. 2.7:

$$Dispersion[\frac{nm}{pixel}] = 1.480 \pm 0.008 \quad (2.7)$$

The preprocessing of this spectrum consists in noise reduction which was made by applying on the image a Gaussian filter with $\sigma = 2$ pixels. This filter replaces each pixel with a pixel of value proportional to a normal distribution computed over the current pixel and its nearest neighbors [West & Cameron, 2006].

The spectral profile contains a continuum part, which is the continuum emission part of the quasar modulated by the transfer function of the acquisition system (telescope, diffraction grating and CCD camera transfer functions). Continuum subtraction reduces the smoothly

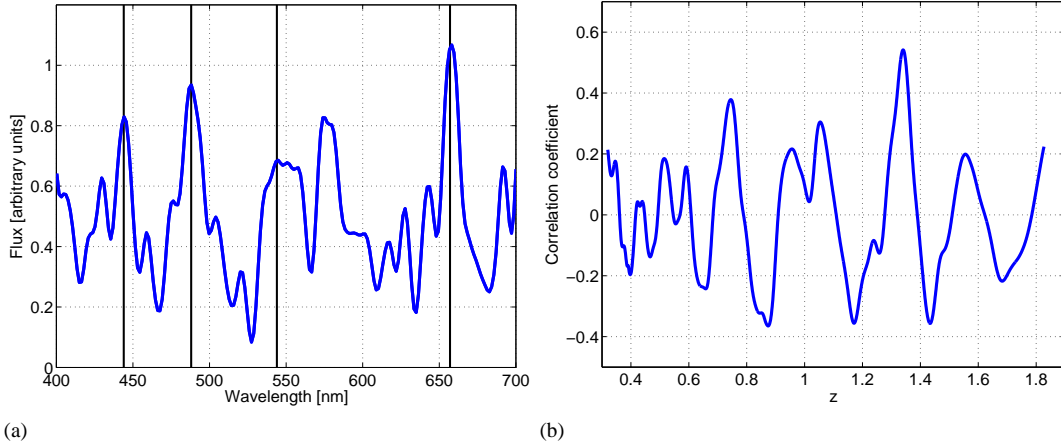


Figure 2.4: a) PG1634 + 706 spectrum obtained after data reduction and continuum subtraction; b) the correlation coefficient between quasar spectrum and the template spectrum shifted with different z [Popescu *et al.*, 2012a].

varying background to zero and essentially has the same effect as filtering out the long-period Fourier components of the spectra. Without continuum subtraction, the intensities of spectral lines are not clearly detectable. The continuum was removed by dividing the spectrum with a fifth order polynomial curve fitting. The obtained result after data reduction and continuum subtraction is given in Fig. 2.4.

The redshift is defined as the ratio of the change in wavelength ($\Delta\lambda = \lambda_{obs} - \lambda_0$) to the non-shifted wavelength (λ_0) from a stationary source:

$$z = \frac{\lambda_{obs} - \lambda_0}{\lambda_0} = \sqrt{\frac{c + v}{c - v}} - 1 \quad (2.8)$$

where c is the speed of light in free space and v is the recession speed of the object. The analysis of the obtained spectrum of PG1634+706 consists in redshift determination and application of Hubble law to determine its distance.

The most common technique [Tonry & Davis, 1979] to determine the redshift is the cross-correlation of the observed spectrum with a template spectrum. The redshift is determined by the location of the largest peak in the cross-correlation functions. Several rest frame composite quasar spectra exists for the optical region like the one from the article of [Francis *et al.*, 1991] obtained using data from Large Bright Quasar Survey (LBQS). Thus for determining the redshift of our spectrum the following steps were taken:

- Shift the template spectrum with a z varying from 0.4 to 1.8 using the step of 0.001. This is a reasonable assumption made after visual inspection of our data.
- At each step, the correlation coefficient between the quasar spectrum and the shifted template spectrum is computed (Fig. 2.4).
- Choose the redshift corresponding to the best correlation coefficient found.

In this way, it was obtained $z = 1.340$ corresponding to the peak value of the correlation

Table 2.1: The emission lines identification in spectrum of PG1634 +706. The line labels, their corresponding laboratory wavelengths, these wavelengths shifted with $z = 1.34$, and the wavelengths observed in the spectrum are presented.

Line	λ_0 [nm]	λ [nm]	λ_{obs} [nm]
C III]	190.6	446.0	444
Fe III	207.7	485.8	488
Fe II + CII]	232.6	544.3	544
Mg II	280.0	655.2	655

coefficient equal to 0.5416. The determination is at 3σ compared with the level of noise (where $\sigma = 0.1987$ is the standard deviation of the correlation coefficient values plotted in Fig. 2.4).

Considering the value found for the redshift - $z = 1.340$, the emission lines of known chemical elements could be identified in the spectrum of PG1634+706 (Table 2). Based on the emission line identification the accuracy of z determination can be ascertained: $z = 1.340 \pm 0.008$.

Because PG1634+706 is a bright quasar with high redshift of spectral lines, it has been studied in some papers like [Schmidt & Green, 1983, Trevese *et al.*, 2007]. Our observation for this object was at the limited magnitude for the type of equipment used. With a robust method, we succeed to extract the signal from noise and compute the redshift. Our determination of redshift $z = 1.340 \pm 0.008$, with a small telescope agrees with the value found from observation with large telescopes.

The result obtained allow to assert that even using a small telescope and the simplest spectrograph valuable results can be obtained. The developed methods for observations and data reduction can be used as a starting point for spectroscopy of celestial bodies with small telescopes.

2.4 Spectroscopy for asteroids

The knowledge of the surface mineralogy of individual asteroids and groups of asteroids can be inferred through the spectroscopy. The solar light reflected from the asteroids contains essential information regarding the optical properties of the materials found at the asteroids surface. The spectral interval $0.8 - 2.5 \mu\text{m}$ is very important to discriminate between different mineralogy of silicate-based compounds. Silicate minerals identification is based on the presence of broad bands of absorption around 1 and $2 \mu\text{m}$. These bands are due essentially to the presence of olivine and pyroxene (or mixtures) on the surface of the asteroid.

2.4.1 Reflectance versus emission

The incident flux arriving from an asteroid surface is splitted in two contributions (Fig. 2.5): the solar radiation passively reflected by the surface material, and the solar radiation which has been absorbed, converted to heat, and re-emitted as thermal radiation [McCord & Adams, 1977].

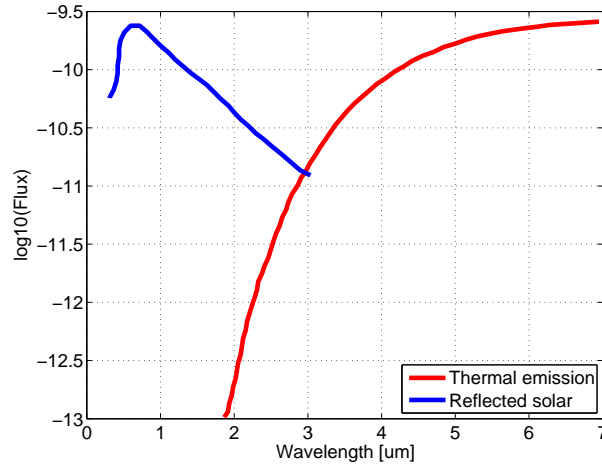


Figure 2.5: The components of the radiation received from 1km square lunar mare area (dark basaltic plain on Moon formed by ancient volcanic eruptions) having an albedo of 006, considering the average Earth-Moon distance, phase angle 0, $T = 395\text{K}$. The flux is measured in Watts per square meter per micron. Source McCord & Adams [1977]

The following relation can be written to describe the spectrum recorded by a detector on a ground base observatory:

$$Y(\lambda) = [X(\lambda) \cdot HA(\lambda) + T(\lambda)] \cdot HT(\lambda) \quad (2.9)$$

where $Y(\lambda)$ is the radiation flux recorded by the spectrometer, $X(\lambda)$ is the radiation flux from the Sun, $HA(\lambda)$ is the transfer function of the asteroid, $HT(\lambda)$ include the transfer function of the Earth atmosphere and of optical instrument and $T(\lambda)$ is the thermal infrared emission of the asteroid

In the VNIR spectral region (0.40, 2.50) μm the thermal emission of the asteroids can be neglected compared to the reflected radiation for the majority of asteroids. Thus in this spectral region, the reflection spectra are studied.

In some particular cases, some asteroids become warm enough such that the thermal flux can not be ignored. These are low-albedo NEAs that become warm enough to emit detectable thermal flux at 2.5 μm when they are located near perihelion. In this case the thermal radiation can account for 33% of the total flux for an object with an albedo 0.04 at 1.0 AU. Rivkin *et al.* [2005] defined a quantity called "thermal excess" to describe this phenomenon:

$$\gamma = \frac{R_{2.5} + T_{2.5}}{R_{2.5}} - 1 \quad (2.10)$$

where $R_{2.5}$ is the reflected flux at 2.5 μm and $T_{2.5}$ is the thermal flux at 2.5 μm . Usually $R_{2.5}$ is determined by extrapolating a linear continuum from shorter wavelengths up to 2.5 μm . It was shown that the lower albedo give larger values of γ as also do smaller solar distances. Beyond 1.9 AU, the expected thermal excess is close to zero for all modeled albedo [Rivkin *et al.*,

2005].

2.4.2 Spectral features

Because minerals are characterized by unique compositions in specific crystallographic structures, each mineral has a characteristic reflectance spectrum with different spectral features. These features come from electronic and vibrational transitions within crystals or molecules. The wavelengths at which the features are located in the spectrum depends upon the ionic (e.g, Fe^{2+} , Fe^{3+} etc.) or molecular (e.g, H_2O , OH , CO_3) species involved and the mineral structure [Gaffey *et al.*, 1993a]. As a general rule, crystal field theory is used to explain absorption bands in asteroid spectra.

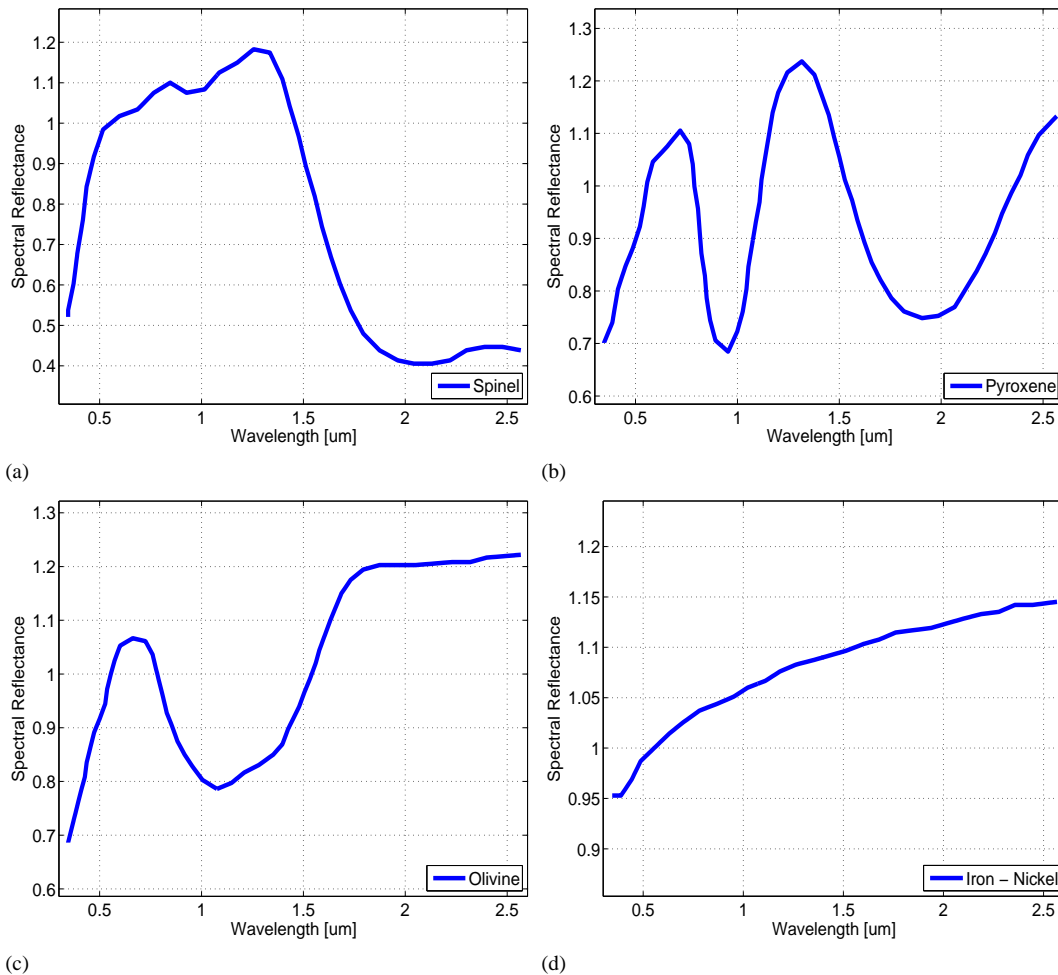


Figure 2.6: Reflectance spectra of several meteoritic important minerals: a) Spinel, b) Pyroxene, c) Olivine, d) Iron-Nickel alloy.

Considering the meteoritic minerals spectra as a starting point for analyzing asteroid spectra it can be found that several features are detectable in the range of (0.35 - 2.50) μm . The most abundant mineral species composing the meteorites are: olivine (Fig 2.6c), pyroxene

(Fig. 2.6b), Iron-Nickel alloy (Fig. 2.6d), spinel (Fig. 2.6a) and feldspar.

Most asteroids are composed by a mixture of these minerals. Since the spectral parameters of different absorption features (i.e. band position and the ratio between band areas) are related to the specific composition of the individual mineral, spectral analysis of the asteroid surface is able in most cases to detect mineralogical signatures characteristic of a particular species. So it is possible to establish the presence of specific mineral phases such as those listed above.

The possibility of revealing a feature depends on the abundance of the particular species so that the strength of the feature can be detected over the spectrum noise. In some high quality spectra of simple mineral mixtures the average composition and relative abundances can be also determined. Several empirical methods have been developed to accomplish this task: Gaffey [1976] defined a procedure for determining the relative abundance of pyroxene and plagioclase in basaltic achondritic assemblages, Cloutis *et al.* [1986b] developed a method for determining the relative abundances of olivine-orthopyroxene mixtures.

However, it cannot be ignored the possibility to obtain the same spectral trend by adding various end-members of minerals. In this case, the degeneracy of mineralogical solutions must be emphasized when the analysis of the asteroid spectra is performed.

Part II

**TECHNIQUES FOR ASTEROID
SPECTROSCOPY**

3

Observing techniques

Observations from Earth remain the most accessible way to study the small bodies of the Solar System. In this chapter are overviewed the observing techniques used to obtain asteroid spectra. First, the NASA IRTF telescope and the SpeX instrument are briefly described. These instruments were used to obtain the spectra presented in this thesis. The planning of the observations on which I was involved is shown. The second part of the chapter present the data reduction procedure. The calibration files used for data reduction are defined. In the end the description of the steps followed for obtaining the spectrum in its final analyzable form is given.

While several programs (like Marco-Polo-R, Osiris-REx, Hayabusa2) are under development for space exploration of asteroids and several others are in service (e.g. Rosetta, Dawn), the choice of their targets is made based on strong groundbased science. However, space-probes can only visit a very limited number of objects. For a picture of the whole asteroid population, the study of their global properties and their diversity is required and this can be achieved by using groundbased telescopes.

3.1 IRTF Telescope and the SpeX instrument

Several large telescopes are equipped with a spectrograph. Some examples among those supporting research programs for planetary sciences are: the NASA InfraRed Telescope Facility (IRTF), the European Southern Observatory (ESO) Very Large Telescope (VLT), the ESO New Technology Telescope (NTT) and Telescopio Nazionale Galileo (TNG).

The NIR spectra presented in this thesis are obtained with NASA IRTF (Fig. 3.1a), a 3.0-meter telescope located on the top of Mauna Kea - Hawaii. It was built initially to support the Voyager missions, but today at least 50% of the observing time is devoted to planetary sciences. The IRTF hosts 6 facility instruments:, SpeX (Fig. 3.1b), NSFCAM2, CSHELL, MIRSI, Apogee, Moris. These instruments allow imaging, polarimetry, low and high resolution spectroscopy in the near to mid infrared (0.8 - 30) μm .

SpeX - the most used instrument by planetologists from NASA IRTF telescope, is a low to medium resolution spectrograph and imager in the (0.8-5.5) μm . It provides spectral resolutions of $R \approx 1000 - 2000$ across 0.8 - 2.4 μm , 2.0 - 4.1 μm , and 2.3 - 5.5 μm , using prism

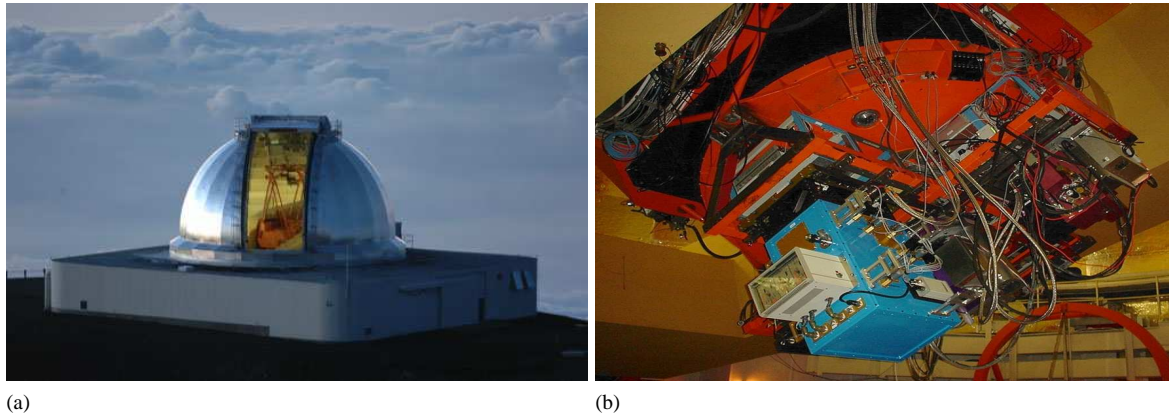


Figure 3.1: a) The 3m NASA InfraRed Telescope Facility at the Mauna Kea Observatory on Hawaii. b) SpeX instrument mounted to IRTF telescope. As scale, SpeX is 1.4m tall and weighs 478kg.

cross-disperser [Rayner *et al.*, 2003]. Single order long slit modes are also available. A high throughput prism mode is provided for $0.8 - 2.5 \mu\text{m}$ spectroscopy at $R \approx 100$.

SpeX employs a 1024×1024 Aladdin3 InSb CCD array for acquiring the spectra, while image acquisition could be made with a 512×512 Alladin2 CCD InSb array.

Two interfaces are used to manage the instrument and the spectrograph, GuideDog interface (Fig. A.1) is dedicated to pointing and tracking the object and BigDog (Fig. A.2) interface is used for spectrograph setup and spectra acquisition.

Observations on IRTF can be performed from anywhere in the world using an internet connection via VNC (Virtual Network Connection) protocol. The observing runs for this work were conducted remotely from Meudon-Paris (France), more than 12 000 Km away from Hawaii [Birlan *et al.*, 2004b, Bus *et al.*, 2002]. Due to different time zones, for the observers in Meudon, the observing time occurred during daylight hours: a full hawaiian night session started at 5 a.m. and ended at 5 p.m. - Paris local time.

Using the equipment provided at Centre d'Observation à Distance en Astronomie à Meudon (CODAM), team had the control remotely of both the instrument/guider system and the spectrograph set-up and spectra acquisition [Birlan *et al.*, 2004a, 2006]. A permanent and constant audio/video link with the telescope operator was essential in order to administrate possible service interruptions, thus another interface was used to keep the audio-video link open (via Polycom ViewStation video-conference system both on Meudon and Mauna Kea). All software was re-initialized at the beginning of each night.

3.2 Planning the observations

The typical cycle of astronomical observations on world-class telescopes imply the following steps: 1) issue received with the call of proposal for observers; 2) targets selection; 3) proposal submission and evaluation; 4) observations; 5) data reductions and analysis; 6) publications

and dissemination of the results.

Generally, the targets are selected based on a desired scientific criterion, which in general reduce their number up to few tens. Observational time is obtained after a severe selection of the best proposals made by the IRTF time allocation committee.

Scheduling the observing time for asteroids requires an ephemerides (the position of astronomical objects on the sky) calculator, such as: <http://ssd.jpl.nasa.gov/horizons.cgi> or <http://www.imcce.fr>. However, for the large observing programs that targets many objects an additional scheduler is required. It is the case of the program *Physical properties of low delta-V Near-Earth Asteroids* for which I designed a planning software, available online at: <http://m4ast.imcce.fr/lowdv.php>.

The tool selects targets based on the following criteria:

- "delta-V" - the available propulsion required remains an engineering design constrain; typically "delta-V" should be lower than 7 km/sec for the initial rendezvous and should have additional 1 km/sec for return;
- H - the absolute magnitude, determines the diameter of the target and should be restricted to consider the kilometers size objects;
- the apparent magnitude and proper motion of the object should be selected in agreement with the telescope capabilities;
- the altitude at the moment of the observing time should correspond to a low airmass.

For example, among the objects accessible for observation with IRTF telescope on May 18-19, 2008 were: (5620) Jasonwheeler, (1943) Anteros, (143651) 2003 QO104, and (433) Eros.

3.3 Data reduction procedures

The data reduction procedures for the observational data consist in obtaining the flux as a function of wavelength from the CCD images. Usually these images are in *.fits*¹ format. Additional information regarding the CCD images for astronomy can be found in the book "Electronic Imaging in Astronomy Detectors and Instrumentation" [McLean, 2008].

The calibration files are:

Bias - in the "no-signal" condition, the CCD electronics system will always produce a small positive readout signal for each pixel. This electronic signature is therefore known as the bias level. This can be easily measured by taking a zero second exposure time. Multiple bias frames can be averaged to reduce the random readout noise by averaging them.

Dark - Dark-current levels, due to thermal noise, are determined by long exposures with the CCD shutter closed. To minimize this effect CCDs are generally cooled to low temper-

¹FITS is the acronym of Flexible Image Transport System

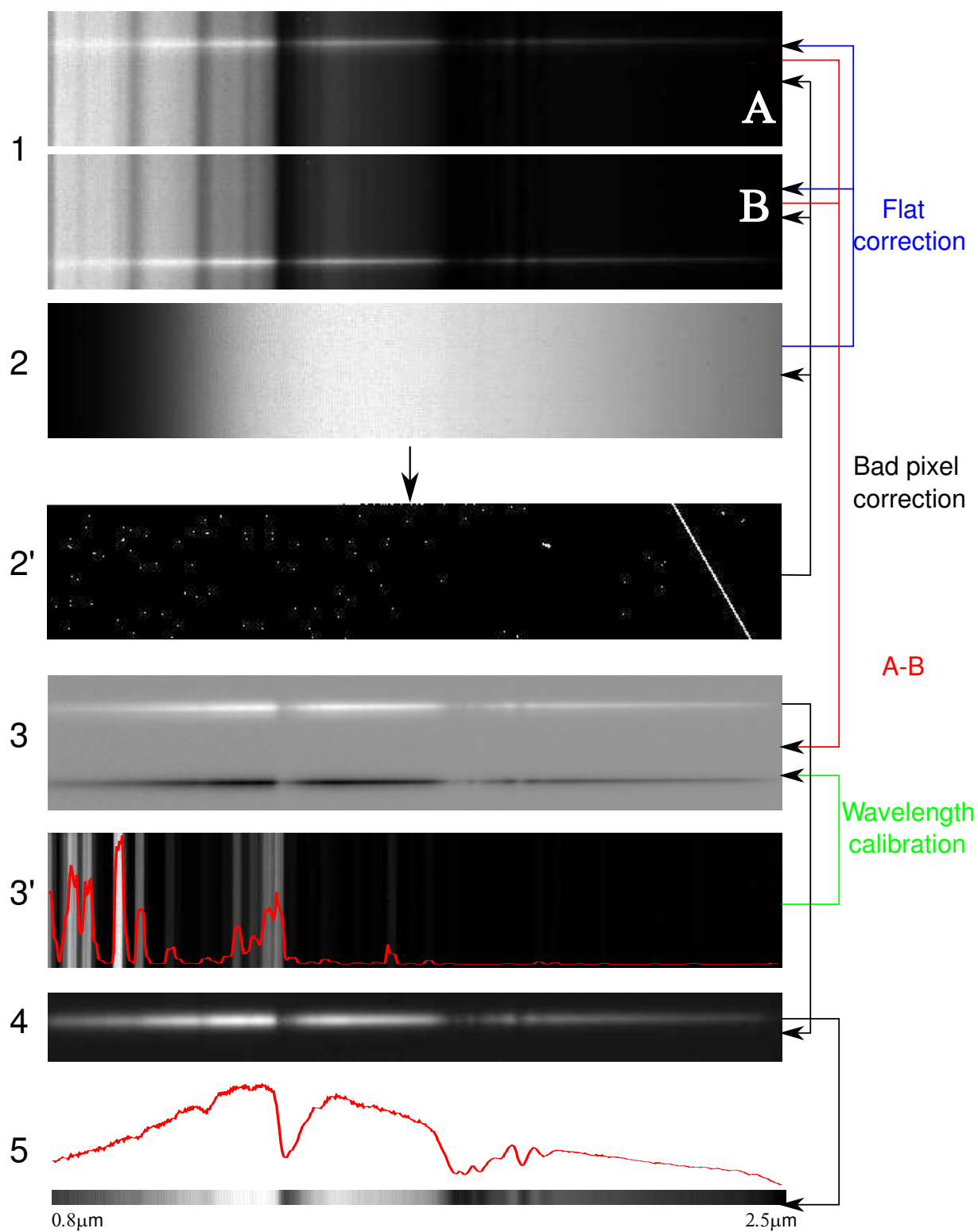


Figure 3.2: The data reduction procedure for NIR spectra obtained with IRTF/SpEx [Nedelcu, 2010].

atures. To remove this noise, an exposure is taken of similar length as the useful images, with the dome and shutter closed. These dark images can also be used to find dead or hot pixels. If dark frames are used, the CCD bias is contained within them and separate bias corrections are not necessary. Similarly, multiple dark exposures can be averaged to reduce the random readout noise by averaging them. This is called a "master dark file". Dark current is more significant in infrared arrays, and it may not be linear and scalable from different exposures [McLean, 2008].

Flat - Sensitivity variations from pixel to pixel arise as the result of fabrication processes and also due to optical attenuation effects such as microscopic dust particles on the surface of the CCD. A flat field image to correct for this effect is usually obtained by observing inside of the telescope dome (if it is matt or white) or place a huge white card on the dome. The dome is illuminated with a projector lamp. In this case the telescope is completely out of focus which ensures that the field is uniformly illuminated. For faint objects it is the light of the sky that dominates, and so it is better to try to use the sky itself as a flat-field. In other cases, as in photometry for instance, the flat field could be done using a sky region in the day light time (at the beginning and end of the night).

Arc lamp - "arc" images are used to determine the pixel to wavelength correspondence, more exactly to make the wavelength calibration. Typically, the lamps used contain helium, neon, xenon, argon or a combination thereof. The emission lines from the spectrum of the arc lamp are at known wavelengths and can be identified. For the IRTF/Spex a lamp with argon is available (Fig. 3.2).

Standard star - A solar-like standard star spectrum taken at similar airmass is required to correct the atmospheric effects and to remove the signature of the Sun's spectrum in order to have only the signature of the asteroid surface. The G2 stars are used with magnitudes (usually between 5 to 12) that allow to obtain a high SNR (signal to noise ratio) spectrum with a short integration time (a few seconds). If the star is too bright it will saturate the CCD, while a fainter star will require an unacceptably long integration time.

The steps required for data reduction are figured in Fig. 3.2. These steps are described below:

Acquisition of the images containing the spectra. The most important aspect that should be taken into account is the variation of the sky background. This effect is caused in principal by the chemical reaction of combination/recombination in ionosphere². There are two techniques used to avoid this unwanted effect. First, the images are taken with an exposure time less than 120 sec. It is known that the variation of the sky background in an interval lower than 120 sec. could be neglected. Images with longer exposure time can be obtained by combining individual images with shorter exposure time. Second, the spectra are obtained alternatively

²the most common name of these phenomena is airglow

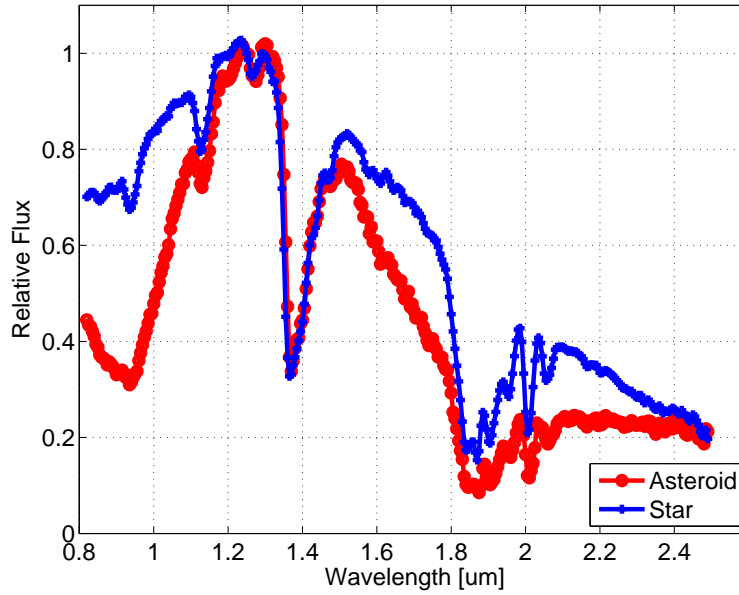


Figure 3.3: The raw spectra of an asteroid and standard star. The two spectra are modulated by the absorption bands of the Earth atmosphere (essentially telluric water bands).

at two separate locations along the slit (close to top - "A" and close to bottom - "B"). This is called the nodding procedure [Nedelcu, 2010]. In the low resolution mode of SpeX, spectra are acquired only in a band of 512x100 pixels of the CCD.

Flat field corrections. The flat field images are made using a lamp based on Quartz-Tungsten-Halogen ($T=3200$ K). This procedure is applied at the beginning and at the end of the observing session, by taking 10 images each time. If a pixel value is greater than 10% of the neighboring pixels, it is considered as a bad pixel. Such pixels are replaced in all images (object images, flat fields and arc images and standard star images) with a value obtained from interpolation of neighboring pixel values. A "master flat" is obtained by combining and averaging all flat field images. The master flat field is subtracted from all images.

Removing the sky background. The consecutive images A and B are subtracted (A-B and B-A) resulting new images containing two spectra: one with positive pixel values and another with negative pixel values (Fig. 3.2.3).

Wavelength calibration. The wavelength calibration is made by identifying the emission lines of an Argon lamp. Thus, it results a correspondence between the pixel position on the x -axis and the wavelength (Fig. 3.2.3).

Combining the images. The two spectra (corresponding to both positive and negative pixel values) are identified in each image. The images are cut, only the positive spectrum being kept. A final spectral image (Fig. 3.2.4) is obtained for each object by gathering all its corresponding images (before summing all images they are aligned by the brightest trace).

Extraction of the raw spectrum. The final point of this stage consists in summing the value

of the pixels from y axis corresponding to the spectrum of an object and extraction of these values in a file containing the wavelengths (in accord with the correspondence pixel position on x axis - wavelength) and the pixel values (Fig. 3.2.3). An example of such a raw spectrum is given in Fig. 4.1.

The next part of the data reduction procedures consists in removing the influence of Earth atmosphere. This task is accomplished using some IDL routines that implements the atmospheric transmission (Atmospheric Transmission Model (ATRAN)) model by Lord [1992].

The final step consists in dividing the asteroid spectrum by the solar analog. In this way we obtain the relative reflectance spectrum of the asteroid. The NIR spectra presented in this thesis are normalized to $1.25 \mu\text{m}$.

4

Spectral analysis techniques

VNIR reflectance spectroscopy is currently the best remote technique for characterizing the surface compositions of asteroids. In the last fifty years it has been used extensively to determine the surface mineralogy of asteroids.

The analysis of reflectance spectra can be done using several methods, such as taxonomic classification, comparison with laboratory spectra, band parameter determination, and modeling of the space weathering effects. This chapter presents those methods which I used for spectral analysis and implemented in a software package.

"Asteroids" actually means "star-like" because viewed through a telescope, these planetesimals are merely point sources of light. A panoply of new observational techniques (e.g. spectroscopy, photometry, polarimetry, adaptive optics, radar, etc.) has transformed these star-like objects into individual little worlds.

4.1 Interpretation

Olivine, pyroxene (clino- and ortho-pyroxene), iron-nickel (Fe-Ni) metal, spinel, and feldspar are some of the most important minerals that can be identified by carefully analyzing the reflection spectra of the asteroid [McSween, 1999]. If these minerals are combined to form a rock the resulting spectrum is a messy composite of the individual spectra for the constituent minerals.

4.1.1 Taxonomy

Taxonomy is the classification of asteroids into categories (classes, taxons) using some parameters and no *a priori* rules. The main goal is to identify groups of asteroids that have similar surface compositions. The classification into taxons is the first step for further studies of comparative planetology. In the case of asteroids, a precise taxonomic system gives an approach to a specific mineralogy for each of the defined classes.

Taxonomic systems of asteroids were initially [Chapman *et al.*, 1971] based on asteroid broadband colors, which allowed us to distinguish between two separate types of objects, denoted "S" (stony) and "C" (carbonaceous). Based on the increasing amount of information from

different types of observations, new taxonomic classes were defined. Historically, the most widely used taxonomies are the following: Tholen [1984] and Barucci *et al.* [1987], which used data from the Eight-Color Asteroid Survey [Zellner *et al.*, 1985] together with thermal albedo; Bus & Binzel [2002a], which used data from the SMASS2 survey; and DeMeo *et al.* [2009], which is an extension of a previous taxonomy scheme into the near-infrared.

Statistical methods are used for defining taxonomic systems of asteroids. We point out two of them, namely principal component analysis (PCA) and the G-mode clustering method.

Principal component analysis (PCA) is a method for reducing the dimensionality of a data set of M variables, involving linear coordinate transformations to minimize the variance. The first transformation rotates the data to maximize the variance along the first axis, known as the principal component 1 (PC1), then along the second axis - the second principal component, and so on. Overall, the new coordinates are ordered decreasingly in terms of the dispersion in the principal components.

Bellow is the summary of Bus-DeMeo taxonomy in conformity with [DeMeo *et al.*, 2009]. The prototype asteroids (specified by their number) of each class and a short description is given.

- A** : 246, 289, 863 - Deep and extremely broad absorption band, first minimum near $1\ \mu\text{m}$; may or may not have a shallow $2\ \mu\text{m}$ absorption band; very highly sloped.
- B** : 2, 3200 - Linear, negatively sloping often with a slight round bump around $0.6\ \mu\text{m}$ and/or a slightly concave up curvature in the 1 to $2\ \mu\text{m}$ region.
- C** : 1, 10, 52 - Linear, neutral visible slope often a slight rough bump around $0.6\ \mu\text{m}$; low but positive slope after 1.3 ; may exhibit slight feature longword of $1\ \mu\text{m}$.
- Cb** : 191, 210, 785 - Linear with a small positive slope that starts around $1.1\ \mu\text{m}$.
- Cg** : 175 - Small positive slope that begins around $1.3\ \mu\text{m}$; pronounced UV dropoff.
- Cgh** : 106, 706, 776 - Small positive slope that begins around $1\ \mu\text{m}$; pronounced UV dropoff similar to Cg; includes a broad, shallow absorption band centered near $0.7\ \mu\text{m}$ similar to Ch.
- Ch** : 19, 48, 49 - Small positive slope that begins around $1.1\ \mu\text{m}$; slightly pronounced UV dropoff; includes a broad, shallow absorption band centered near $0.7\ \mu\text{m}$.
- D** : 1143, 1542, 3248 - Linear with very steep slope; some show slight curvature or gentle kink around $1.5\ \mu\text{m}$.
- K** : 42, 579, 742 - Wide absorption band centered just longword of $1\ \mu\text{m}$; the fist maximum and the minimum are sharply pointed; the walls of the absorption are linear with very little curvature.
- L** : 236, 402, 606 - Steep slope in visible region leveling out abruptly around $0.7\ \mu\text{m}$; there is often a gentle concave down curvature in the infrared with a maximum around $1.5\ \mu\text{m}$; there may or may not be a $2\ \mu\text{m}$ absorption feature.

- O** : 3628 - Very rounded and deep, "bowl" shape absorption feature at 1 μm as well as a significant absorption feature at 2 μm .
- Q** : 1862, 3753, 5660 - Distinct 1 μm absorption feature with evidence of another feature near 1.3 μm ; a 2 μm feature exists with varying depths between objects.
- R** : 349 - Deep 1 and 2 μm features; the 1 μm feature is much narrower than a Q type, but slightly broader than a V type.
- S** : 5, 14, 20 - Moderate 1 and 2 μm features; the 2 μm feature may vary in depth between objects.
- Sa** : 984, 5261 - Has a deep and extremely broad absorption band at 1 μm ; has similar features to A types but is less red.
- Sq** : 3, 11, 43 - Has a wide 1 μm absorption band with evidence of a feature near 1.3 μm like the Q type, except the 1 μm feature is more shallow for the Sq.
- Sr** : 237, 808, 1228 - Has a fairly narrow 1 μm feature similar to but more shallow than an R type as well as a 2 μm feature.
- Sv** : 2965, 4451 - Has a very narrow 1 μm absorption band similar to but more shallow than a V type as well as a 2 μm feature.
- T** : 96, 308, 773 - Linear with moderate to high slope and often gently concaving down.
- V** : 4, 1929, 2851 - Very strong and very narrow 1 μm absorption and as well as a strong 2 μm absorption feature.
- X** : 22, 87, 153 - Linear with medium to high slope.
- Xc** : 21, 97, 739 - Low to medium slope and slightly curved and concave downward.
- Xe** : 64, 77, 3103 - Low to medium slope similar to either Xc or Xk type, but with an absorption band feature shortward of 0.55 μm .
- Xk** : 56, 110, 337 - Slightly curved and concave downward similar to Xc type but with a faint feature between 0.8 to 1 μm .
- Ld** : 279, 3734 - Diverged to L and D classes.
- Sk** : 3, 6585 - Diverged to the S and Sq classes.
- Sl** : 17, 30 - Merged with the S class.

The classification of an asteroid spectrum in Bus-DeMeo taxonomy can be done via MIT-SMASS online tool ¹.

The G-mode is a multivariate statistical clustering method that allows us to classify a statistical sample consisting of N elements with M variables. The parameter G is the analog of the distance in a NxM space. This statistical distance between an object and a taxonomic class shows the similarities of the characteristics of this object to those of its class [Barucci *et al.*,

¹<http://smass.mit.edu/busdemeoclass.html>

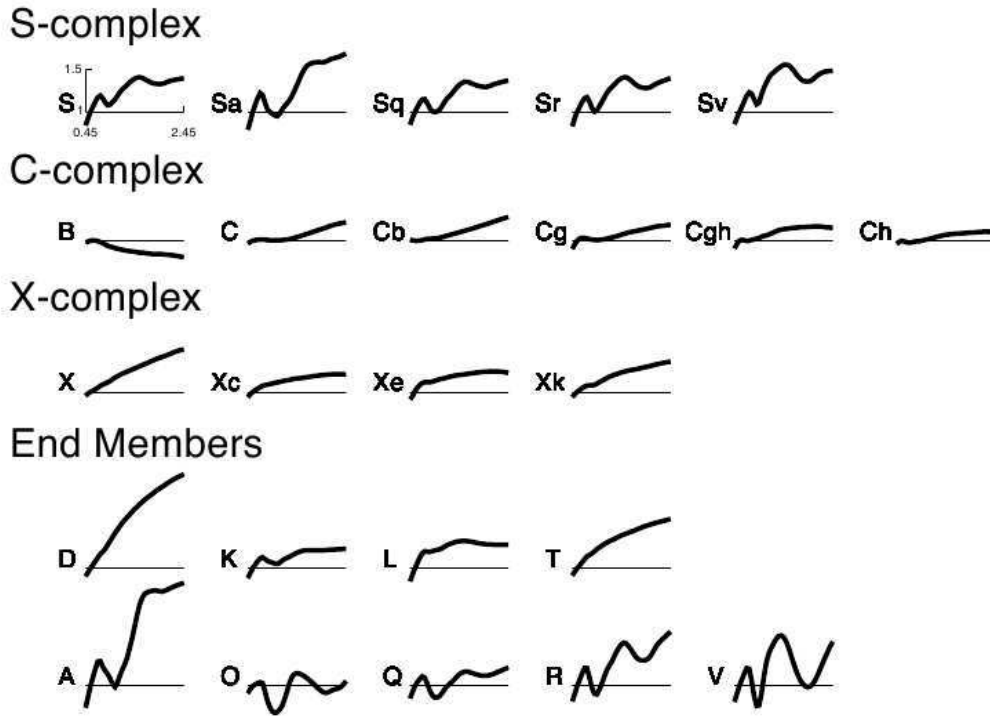


Figure 4.1: Bus-DeMeo taxonomy key figures. Source :<http://smass.mit.edu/busdemeoclass.html>

1987, Birlan *et al.*, 1996a]. One of the advantages of this method is that even if only a subset of variables is available for an object (only part of the spectrum), a preliminary classification can still be achieved.

4.1.2 Spectral comparison - Comparative planetology

Spectroscopy of different samples performed in the laboratory provides the basis upon which compositional information about unexplored planetary surfaces can be understood from remotely obtained reflectance spectra. Thus, confronting the spectral data derived from telescopic observations with laboratory measurements is an important step in study of asteroid physical properties [Britt *et al.*, 1992, Vernazza *et al.*, 2007, Popescu *et al.*, 2011].

Among the laboratory samples, meteorites can provide the most fruitful results for understanding asteroid composition. This is owed to the fact that, prior to their arrival meteorites are themselves small bodies of the solar system. Thus, spectral comparison represents a direct link for understanding of asteroid-meteorite relationships.

The traditional classification is based upon their appearance [de Pater & Lissauer, 2010]:

- metal meteorites are referred as *iron meteorites*. They are made primary of iron and nickel and smaller amounts of siderophile elements (elements which easily combine with molten iron);

- meteorites that contain comparable amounts of macroscopic metallic and rocky components are called *stony irons*.
- meteorites that do not contain large concentrations of metal are known as *stones*.

A second classification of meteorites takes into account their mineralogical changes: *achondrites* are igneous bodies, the product of melting, changes in composition and recrystallization, while *chondrites* are the primitive meteorites composed of material that formed the solar nebula and surviving interstellar grains, little modified in some cases by aqueous and/or thermal processes.

Chondrites keep the records of the origin and the early evolution of the Sun and planets. The name comes from Greek - "*chondros*", meaning grain or seed, a reference to the appearance produced by numerous small, rounded inclusions called chondrules. These chondrules are small droplets of olivine and pyroxene condensed and crystallized from the hot primordial solar nebula in form of small spheres. They accreted with other material that condensed from the solar nebula forming a matrix [McSween, 1999]. The chondritic meteorites are split into: *ordinary chondrites* so named because they are the most abundant type; the *carbonaceous chondrites* actually misnamed when they were believed to have much higher carbon contents than other chondrites; the *enstatite chondrites* named for their high abundances of enstatite, a magnesium silicate mineral. Rumuruti and Kakangari chondrite meteorites do not fit in any of these classes, being considered separate types [de Pater & Lissauer, 2010].

The most common primitive meteorites - ordinary chondrites are divided based on their Fe/Si ratio: *H* - high Fe content, *L* low Fe, and *LL* low Fe and low metal. The same criterion applies for enstatite chondrites *EH*, *EL*. The carbonaceous chondrites are split into eight classes which slightly differ in composition: *CI*, *CM*, *CO*, *CV*, *CR*, *CH*, *CB*, and *CK* [de Pater & Lissauer, 2010].

In Fig. 4.2a is given the microscopic view of a thin section of the Allende meteorite (CV3). It shows numerous chondrules, white calcium-aluminum inclusions (CAI), and opaque metal grains, all held together by dark, fine-grained matrix material. All of this diversity is contained within several square centimeters of surface area in this meteorite. For comparison, the abundance of elements in the Sun's photosphere is plotted against their abundance in the carbonaceous chondrites [Ringwood, 1979]. Most elements lie very close to the curve of equal abundance (normalized to Si).

Chondritic meteorites are assigned a petrographic type ranging from 1 to 7. This describes the degree of alteration by different processes. Type 3 chondrites appear to be least altered and provide the best data on the conditions within the protoplanetary disc. Types 5 to 7 are shocked materials, signature of collisional processes of parent bodies.

In contrast to chondrite, achondrites came from differentiated parent bodies (bodies that have undergone density-dependent phase separation). The igneous origin of these meteorites implies a partial or total melting of primordial chondritic matter. Igneous processes are the

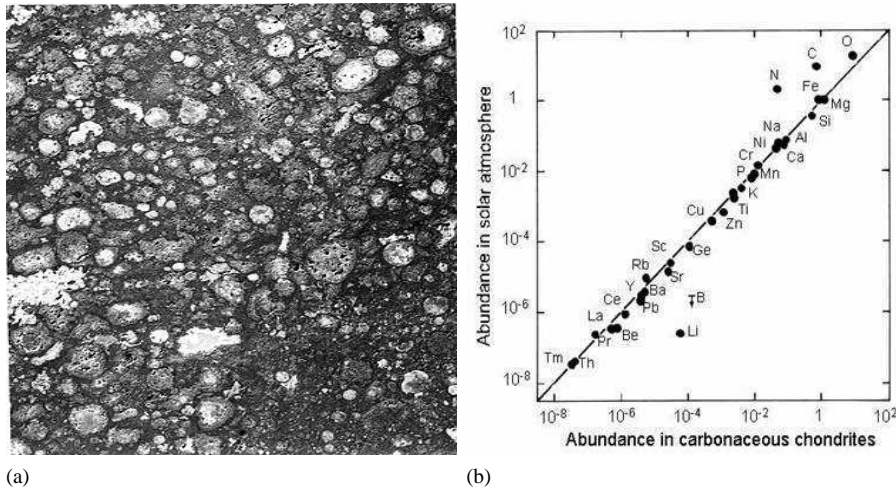


Figure 4.2: a) The photomicrograph of a thin section of the carbonaceous chondrite Allende, which was seen to fall in Chihuahua, Mexico on the night of February 8, 1969. Numerous round silicate chondrules together with irregular inclusions can be observed. b) Comparison of solar-system abundances (relative to silicon) determined by solar spectroscopy and by analysis of carbonaceous chondrites [Ringwood, 1979].

primary means by which planetary bodies evolve. The bulk compositions of achondrites are enriched in lithophile and chalcophile elements. The abundances of these elements are also enhanced in the Earth's crust. Achondrites are significantly depleted in iron and siderophile elements. The subtypes of achondritic meteorites include: Howardite - Eucrite - Diogenite (HED), Aubrites, Shergottite - Nakhilite - Chassignite (SNC), Ureilites, Acapulcoites and Lodranites. A small percentage of known achondrites are from two larger bodies - the Moon and Mars [de Pater & Lissauer, 2010].

Several spectral libraries are available for accomplishing spectral comparison, such as Relab², USGS Spectroscopy Laboratory³, the Johns Hopkins University (JHU) Spectral Library, the Jet Propulsion Laboratory (JPL) Spectral Library⁴, etc. I used the Relab spectral library, which is one of the largest libraries and contains more than 15,000 spectra for different types of materials from meteorites to terrestrial rocks, man-made mixtures, and both terrestrial and lunar soils.

4.1.3 Space weathering effects

It is now widely accepted that the space environment alters the optical properties of airless body surfaces (Fig. 4.3). Space weathering is the term that describes the observed phenomena caused by these processes operating at or near the surface of an atmosphere-less solar system body, that modify the remotely sensed properties of this body surface away from those of the unmodified, intrinsic, subsurface bulk of the body [Chapman, 1996, 2004].

²<http://www.planetary.brown.edu/relab/>

³<http://speclab.cr.usgs.gov/>

⁴<http://speclib.jpl.nasa.gov/>

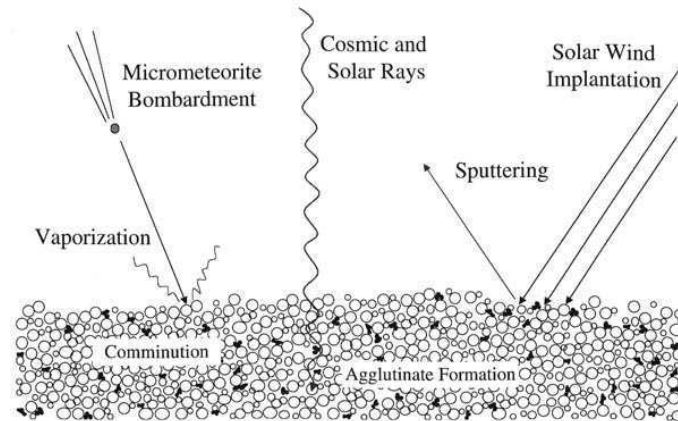


Figure 4.3: Different ways in which space weathering affects the visible and near-infrared spectra of soil. Space weathering processes alters the properties of the soil that covers the surface of all bodies which are not protected by an atmosphere (Source <http://en.wikipedia.org/>).

The objects that are most affected by the space weathering are silicate-rich objects for which a progressive darkening and reddening of the solar reflectance spectra appear in the 0.2 - 2.7 μm spectral region [Hapke, 2001]. Lunar-type space weathering is well-understood, while two well-studied asteroids (433 Eros and 243 Ida) exhibit different space weathering types. The mechanism of space weathering for asteroids is still currently far from being completely understood.

The latest approaches to the study of space weathering are based on laboratory experiments. Simulations of micrometeorites and cosmic ray impacts have been achieved using nanopulse lasers on olivine and pyroxene samples. These have shown that laser ablation lowers the albedo, dampens the absorption bands, and reddens the spectrum. These effects could explain the transition from "fresh" ordinary chondrite material to the observed asteroid spectra [Yamada *et al.*, 1999, Sasaki *et al.*, 2001]. The spectral effects generated by the solar wind irradiation to silicate materials were also investigated by Brunetto *et al.* [2006]. On the basis of ion irradiation experiments, they found "a weathering function" that could be used to fit the ratio of the spectra of irradiated to unirradiated samples, which was implemented in M4AST.

4.1.4 Band parameters

The "traditional" method used for mineralogical analysis is based on different parameters that can be computed from the reflectance spectra of the object. These parameters give information about the minerals that are present on the surface of the asteroid, their modal abundances, and the size of the grains.

Cloutis *et al.* [1986b] outlined an analytical approach that permits the interpretation of visible and near-infrared spectral reflectance to determine the mineralogic and petrologic parameters of olivine-orthopyroxene mixtures, including end-member abundances, chemistries, and

particle size. These parameters are the wavelength position of the reflectance minima around 1 μm and 2 μm , the band centers, and the band area ratio (BAR) which is the ratio of the areas of the second absorption band relative to the first absorption band.

Gaffey [2010] noted that mineralogically diagnostic spectral parameters (band centers, BARs) are "essentially immune to the effects of space weathering observed and modeled to date".

4.2 Algorithms

This section describes the algorithms used to analyze the different types of spectra. The description of these algorithms was part of the paper **Popescu et al.** [2012b].

4.2.1 Taxonomic classification

Different approaches for the taxonomies can be used.

To classify a spectrum in the Bus-DeMeo taxonomy, we determine how closely the asteroid spectrum is fitted by the standard spectrum of each class using a curve matching approach. This approach involves first fitting the spectrum with a polynomial curve and then comparing this curve to the standard spectrum at the wavelengths given in the taxonomy. We select the taxonomic classes producing the smallest standard deviation in the error (see Eq. 4.5).

For G-mode taxonomy, we used the algorithm defined in Fulchignoni *et al.* [2000]. This comprises the computation of the g parameter, which gives the statistical distance of a new sample, characterized by $\{x_i\}$ from the taxonomic class s

$$g_s = \sqrt{2 \cdot R_s \cdot \sum_i^M \left(\frac{x_i - \bar{x}_{is}}{\sigma_{is}} \right)^2} - \sqrt{2 \cdot R_s \cdot M - 1}, \quad (4.1)$$

where M is the number of points along the selected section of the spectrum, and $i = \overline{1 \dots M}$. The G-mode method defines for each taxonomic class s the mean values $\{\bar{x}_{is}\}$, the standard deviations $\{\sigma_{is}\}$, and a statistical indicator R_s . We select the classes that have the lowest g_s , the ideal case being $g_s = -\sqrt{2 \cdot R_s \cdot M - 1}$.

The taxonomic classes are defined depending on the taxonomy in different wavelength intervals (0.45 - 2.45 μm for Bus- DeMeo taxonomy, 0.337 -2.359 μm for G13 [Birlan *et al.*, 1996a] taxonomy, and 0.337 - 1.041 and for G9 taxonomy) and some of them also using the albedo. The curve matching or g factor computation can be made across a smaller wavelength interval (depending on the available wavelength range of the asteroid spectrum) but with a lower confidence, thus a reliability criterion is required [**Popescu et al.**, 2011]

$$Reliability = \frac{card([\lambda_m, \lambda_M] \cap \{\lambda_1^T, \lambda_2^T, \dots, \lambda_N^T\})}{N}, \quad (4.2)$$

where $[\lambda_m, \lambda_M]$ is the spectral interval between the minimum wavelength and the maximum wavelength in the asteroid spectrum, $\lambda_1^T, \lambda_2^T, \dots, \lambda_N^T$ are the N wavelengths for which the stan-

standard spectra of the taxonomy are given, and $\text{card}()$ represents the number of elements of a discrete set.

4.2.2 Curve matching

The methods for taxonomic classification and comparison with meteorite spectra are based on curve matching. These procedures involve minimizing a quantity (usually called Φ) in order to determine the best estimates for a given asteroid spectrum.

A quantity commonly used to test whether any given points are well-described by some hypothesized function is chi-square (χ^2), the determination being called the chi-square test for goodness of the fit [Bevington & Robinson, 1992].

The classical definition for the χ^2 is :

$$\chi^2 = \sum_i^N \frac{(x_i - \mu_i)^2}{\sigma_i^2}, \quad (4.3)$$

where there are N variables x_i normally distributed with the mean μ_i and variance σ_i^2 . If σ_i^2 are correctly estimated, the data are well-described by the values μ_i when $\Phi = \chi^2 \rightarrow 0$.

We denote by $\{e_i\}$ the error between the data (asteroid spectrum) and the fitting curve:

$$e_i = (x_i - \mu_i). \quad (4.4)$$

Our first approach to curve matching, derived from chi-square fitting, is based on the formula

$$\Phi_{std} = \frac{1}{N} \cdot \sqrt{\sum_i^N (e_i - \bar{e})^2}, \quad (4.5)$$

where we have denoted with \bar{e} the mean value of the set $\{e_i\}$ (Eq. 4.4).

The quantity to minimize in this case is the standard deviation of the errors. To apply this procedure, we smooth our asteroid spectrum by a polynomial curve (using the *polyfit* function from the Octave3.2 computation environment). This step is required to eliminate the outliers produced by the incomplete removal of telluric absorption lines.

We used this type of curve matching to find the taxonomic class of the asteroid in the Bus-DeMeo taxonomy and to compare with laboratory spectra. In the latter case, we determine how well the asteroid spectrum is fitted by different laboratory spectra, and select the closest 50 fits, in ascending order of Φ .

A second approach to curve matching can be made using χ^2 with the definition [Nedelcu *et al.*, 2007]:

$$\chi^2 = \frac{1}{N} \cdot \sum_i^N \frac{(x_i - \mu_i)^2}{x_i}, \quad (4.6)$$

where x_i are the values of a polynomial fit to the asteroid spectrum and μ_i are the reflectance values for the meteorite spectrum. The meaning of this formula is that of a relative error at each

wavelength (N being the number of wavelengths on which the comparison is made).

The third approach to curve fitting is based on the correlation coefficient

$$\rho_{X,M} = \frac{\text{cov}(X,M)}{\sigma_X \cdot \sigma_M}, \quad (4.7)$$

where, $X = \{x_i\}$ is the spectrum of the asteroid and $M = \{\mu_i\}$ is the laboratory spectrum. The correlation coefficient detects linear dependences between two variables. If the variables are independent (i.e. the asteroid and laboratory spectra), then the correlation coefficient is zero. A unitary value for the correlation coefficient indicates that the variables are in a perfect linear relationship, though in this case we search for laboratory spectra that match the desired asteroid spectrum with the highest $\rho_{X,M}$.

Finally, we concluded that a good fitting can be achieved by combining the standard deviation method and correlation coefficient method. In connection to the Eq. 4.5 and Eq. 4.7 a combined coefficient can be defined - Eq. 4.8.

$$\Phi_{comb} = \frac{\rho_{X,M}}{\Phi_{std}}, \quad (4.8)$$

where $\rho_{X,M}$ was defined in Eq. 4.7 and Φ_{std} was defined in Eq. 4.5. In this case, the laboratory spectra that match the asteroid spectrum are those with the highest value of Φ_{comb} .

4.2.3 Computing the space weathering effects

Our approach to computing space weathering effects applies the model proposed by Brunetto *et al.* [2006]. On the basis of laboratory experiments, they concluded that a weathered spectrum can be obtained by multiplying the spectrum of the unaltered sample by an exponential function (see Eq. 4.9) that depends on the precise parameter C_s .

By fitting the asteroid spectral curve with an exponential function using a least-square error algorithm, we can compute the C_s parameter

$$W(\lambda) = K \times \exp\left(\frac{C_s}{\lambda}\right) \quad (4.9)$$

Brunetto & Strazzulla [2005] demonstrated that ion-induced spectral reddening is related to the formation of displacements, with the C_s parameter being correlated with the number of displacements per cm^2 (named damage parameter - d). Brunetto *et al.* [2006] obtained an empirical relation between C_s and the number of displacements per cm^2

$$C_s = \alpha \times \ln(\beta \times d + 1), \quad (4.10)$$

where $\alpha = -0.33 \mu\text{m}$ and $\beta = 1.1 \times 10^{19} \text{ cm}^2$. Eq. 4.10 can be used to compute the damage parameter d .

This model for the space weathering effects describes the effects of solar-wind ion irradiation

tion. While this is not the only active weathering process, it seems to be the most important at 1 AU [Vernazza *et al.*, 2009, Brunetto *et al.*, 2006].

The removal of space weathering effects is made by dividing the asteroid spectrum by $W(\lambda)$ at each wavelength.

4.2.4 Application of the Cloutis model

Cloutis *et al.* [1986b] proposed a method for the mineralogical analysis of spectra showing absorption bands. We implemented an application to compute the spectral parameters defined by this method. The computation of all the parameters described in Section 4.2 is done for spectra that contains the V + NIR wavelength regions. If only the NIR region is given, then only the band minima can be computed.

The following steps are taken: we first compute the minima and maxima of the spectrum. This is done by starting with the assumption that there is a maximum around $0.7 \mu\text{m}$ followed by a minimum around $1 \mu\text{m}$, then a maximum between $1.3 - 1.7 \mu\text{m}$ and a minimum around $2 \mu\text{m}$. The spectrum is fitted around these regions by a polynomial function. The order of the polynomial is selected to be between three and eight, in order to obtain the smallest least square residuals. The minima and the maxima are the points where the first derivative of the fitted polynomial functions is zero.

In the second step, using the wavelengths and the reflectance at the two maxima and at the end of the spectrum (around $2.5 \mu\text{m}$), we compute two linear continua, tangential to the spectral curve. The continuum part is removed by dividing the spectrum by the two tangential lines (in the corresponding regions). The band centers are computed following a method similar to that applied to the band minima, but after the removal of the continuum.

The last step consists in computing the two absorption-band areas. The first absorption band is located around $1 \mu\text{m}$ and between the first and second maxima. The second absorption band is located around $2 \mu\text{m}$, between the second maximum and the end of the spectrum. The area is computed using a simple integration method. This method consists in computing the area between two consecutive points in the spectrum defined by a trapezoid and summing all these small areas corresponding to the absorption band.

$$\frac{OPX}{OPX + OL} = 0.4187 \times \left(\frac{BII}{BI} + 0.125 \right). \quad (4.11)$$

The ratio of the areas of the second to the first absorption band ($BAR = \frac{BII}{BI}$) gives the relative abundance orthopyroxene vs olivine presented in Eq. 4.11 [Fornasier *et al.*, 2003].

M4AST - Modeling of Asteroids Spectra

The increasing number of asteroid spectral measurements has lead to well-developed methods for analyzing asteroid spectra. There is however no centralized database for all the published data and a set of standard routines is also required.

This chapter describes a public software tool (called M4AST) that combines both data archives and analyses of asteroid spectra. M4AST (Modeling for asteroids) consists of an asteroid spectral database and a set of applications for analyzing asteroid spectra. These applications cover aspects related to taxonomy, curve matching with laboratory spectra, space weathering models, and mineralogical diagnosis. M4AST tool is fully available via a web interface. The database contains around 2,700 spectra of asteroids that can be either processed in M4AST and/or downloaded. M4AST applications can also be used to characterize new asteroid spectra.

The robustness of routines is proven by the solutions found for spectra of two NEAs: (99942) Apophis, and (175706) 1996 FG3. The results confirm those already published in the literature. M4AST was presented to the scientific community through a dedicated article published recently [Popescu et al., 2012b]. The presentation from this chapter closely follows the cited article.

Asteroid spectra have been obtained since the late 1960s. McCord *et al.* [1970] published the first spectral measurements in the 0.3-1.1 μm wavelength region for the asteroid (4) Vesta, and found that its spectrum is similar to those of basaltic achondritic meteorites. The most important surveys in the 1980s for measuring the spectral characteristics of asteroids are the Eight-Color Asteroid Survey¹ (ECAS, Zellner *et al.* [1985]), and the 52-color survey² [Bell *et al.*, 1988]. All these results showed the diversity of asteroid surface composition.

In the last two decades, the development of CCD spectrograph and the access to 3 - 8 m telescope class have made possible to obtain spectra of significantly fainter asteroids with a much higher spectral resolution than achievable by broad-band photometry. Several spectroscopic surveys have been performed, including SMASS [Xu *et al.*, 1995], SMASS2 [Bus & Binzel, 2002b], and S³OS² [Lazzaro *et al.*, 2004]. Other spectroscopic surveys have been dedicated only to NEAs such as SINEO [Lazzarin *et al.*, 2005] or the survey performed by de León *et al.* [2010]. The total number of asteroid spectra resulting from these surveys is in order of thousands and has led to a mature understanding of their population.

Currently, the spectral data of asteroids continues to grow. The most important spectral

¹ECAS is a photometric survey

²52-color is a spectrophotometric survey

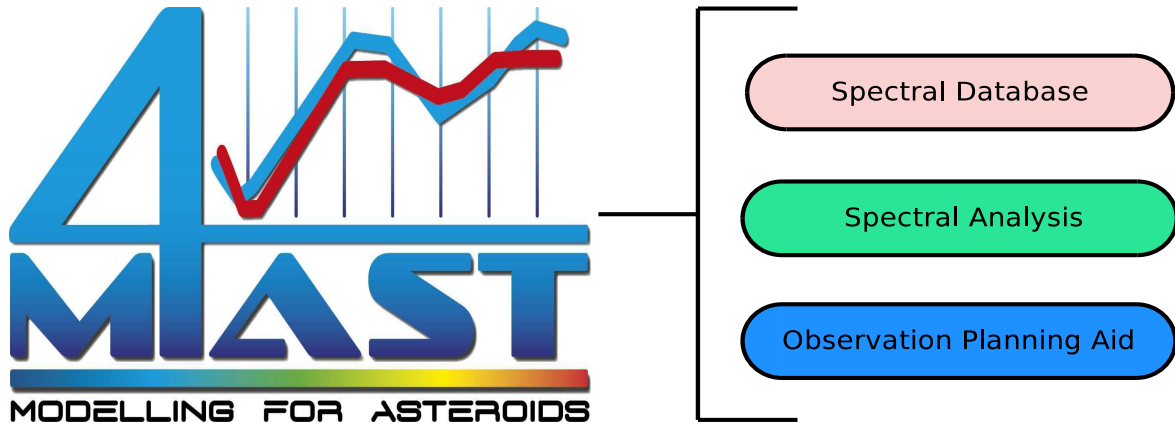


Figure 5.1: M4AST logo and the aims of this project.

surveys for asteroid have made their data available online. However, there is no centralized database containing all the asteroid spectra³. Moreover, the exploitation of these data in terms of construction of mineralogical models, comparison to laboratory spectra, and taxonomy is treated individually by each team working in this field. While the spectral databases for asteroids have become significant in size and the methods for modeling asteroid spectra are now well-defined and robust, there are no standard set of routines for handling these data.

I developed M4AST (Modeling for Asteroids), which is a tool dedicated to asteroid spectra [Popescu *et al.*, 2012b, 2011, Birlan & Popescu, 2011]. The logo of this project and the aims are given in Fig. 5.1. M4AST was conceived to be available via a web interface (<http://cardamine.imcce.fr/m4ast/>) and is free for access to the scientific community.

The flowchart of the M4AST project is presented in Fig. 5.2. This project consists of a database containing the results of the observational measurements and a set of applications for spectral analysis and interpretation. Additionally, we start up to build a tool dedicated to observations planing, already described in chapter 3. Bellow we discuss the spectral database and the modelling tools parts of M4AST.

5.1 Spectral database

The first component of the project is the spectral database. It contains the results of telescopic measurements for the reflectance spectra of different wavelength ranges (V - visible, NIR - near infrared, V+NIR - visible and near infrared) of the asteroids, and the observations logs.

5.1.1 Structure of M4AST database

The information in the database is organized into two type of files: *permanent* and *temporary* files. Additionally, there is a catalog to keep track of the permanent files recorded.

³Some of these data are archived within the Small Bodies Node of the Planetary Data System (<http://pds.nasa.gov/>)

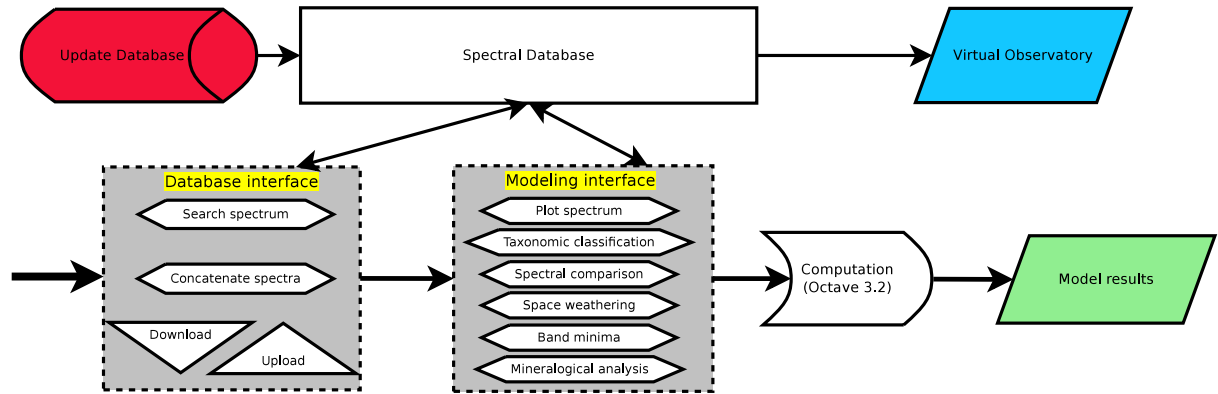


Figure 5.2: Block diagram and work flow of M4AST [Popescu *et al.*, 2012b].

Permanent files are uploaded through a dedicated interface protected by a password. Any new file submitted in this way is recorded in a catalog together with its observation log. The observation log is also kept in the header of each file containing the corresponding spectral data, including IAU designations of the asteroid, the date and hour (UT) of the observation, and the IAU code of the observatory. Additional information could be included such as the investigator name and e-mail address as well as the link to a reference, if the spectrum was published.

Each file containing the spectral data includes a header with the observation log and the measurements given in two columns: the first column contains the wavelength in μm , and the second column contains the corresponding reflectance values (normalized to unity at $0.55 \mu\text{m}$ if the visible part of the spectrum is contained, and otherwise at $1.25 \mu\text{m}$). If the dispersion in the measurements is available, then it is provided into a third column.

Temporary files are created by the users only for processing the data. They provide a way for the anonymous user to use the applications of M4AST for his own spectral data. Temporary files receive a random name and can be removed by the same user that created them (no administrative rights are required). The application library is fully available for modeling spectral data contained in temporary files. No permanent information is recorded.

5.1.2 The content

Historically, the database was designed for making available to the scientific community the spectra obtained after observations performed remotely from the Centre d’Observation à Distance en Astronomie à Meudon (CODAM) [Birlan *et al.*, 2004a, 2006]. The observations were obtained in the $0.8 - 2.5 \mu\text{m}$ spectral region using the SpeX/IRTF instrument, located on Mauna Kea, Hawaii. The project now includes around 2,700 permanent spectra (in the V and NIR wavelength regions) of both main belt and near-Earth asteroids.

Except the spectra obtained via CODAM, the main sources of the database are SMASSI [Xu *et al.*, 1995], SMASII [Bus & Binzel, 2002b], and S³OS² [Lazzaro *et al.*, 2004] and de León *et al.* [2010]. Together with our program of asteroid spectroscopic observations, some

The screenshot shows the M4AST database interface in a web browser. The address bar shows 'm4ast.imcce.fr/m4ast/userspec.php'. The interface is divided into four main sections:

- 1. Search spectra in database:** This section contains three input fields for search criteria: 'Criterion 1: Cuyo', 'Criterion 2: 2008', and 'Criterion 3: 568'. Below these is a 'Search Spectra' button.
- 2. Download file from database:** This section has a 'Select file for download:' text box and a 'Download' button.
- 3. Upload temporary spectrum in database:** This section includes a 'Choose a file to upload:' area with a 'Choose File' button and 'No file chosen' text. Below this are two more input fields: 'Wavelength is given in : um' (with a dropdown arrow) and 'Number of lines from the input file to be skipped :'. A 'Submit Spectrum' button is at the bottom of this section, followed by the text 'Please be patient while gathering and sorting information'.
- 4. Concatenate spectra:** This section has two input fields for 'Spectrum A:' and 'Spectrum B:', and a 'Concatenate' button.

At the bottom of the interface, a table displays the search results:

File name	Obj. Design.	Obj. No.	Obsv. Date	UAI code	Λ_{\min}	Λ_{\max}	Published
Cuyo_20080827_568_00	Cuyo	1917	2008-08-27:15:16	568	0.820	2.455	http://adsabs.harvard.edu/abs/2011A&A...535A...15P

Figure 5.3: The database interface of M4AST. Here is illustrated the search of a spectrum for (1917) Cuyo and the result of this search displayed at the bottom of the interface.

collaborations are intended in order to enlarge M4AST database.

The purpose of this database is not to duplicate other spectral libraries that already exist, but to offer an unique format for the data, a fast way of applying the existing models, and a rapid comparison of results.

5.1.3 M4AST database via the Virtual Observatory

The Virtual Observatory (VO) is an international astronomical community-based initiative. Its aims are to allow global electronic access to the available astronomical data archives of space and ground-based observatories and other sky survey databases and to enable data analysis techniques through a coordinating entity that will provide common standards.

The M4AST spectral database can be accessed via VO-Paris Data Centre⁴ using Simple Spectral Access Protocol [Doug Tody & the Data Access Layer Working Group., 2011]. The M4AST spectral data obtained via VO can be retrieved in both *VOTable* format or our native *ASCII* format. A "simple query search" based on asteroid designation correctly returns all the spectra from our database for the corresponding object.

New protocols, dedicated to planetology, (such as Table Access Protocol) will be implemented in the future.

5.2 The interface

M4AST includes two interfaces, one dedicated to database access (Fig. 5.3) and another for running the different applications dedicated to spectral analysis (Fig. 5.4). The access flow starts with the database interface and continues with the modeling tool interface. Fig. 5.2 gives an overview of the M4AST workflow.

5.2.1 Database interface

The database interface (Fig. 5.3), called **user input interface**, allows the users to access the spectra from the database or upload their own spectra for further processing. The following options are available:

Search spectra in database - the user can search spectra in the database based on a maximum of three keywords. These keywords include object designations, observing date, and the IAU observatory code.

Download file from database - the user can download any spectrum using as input the file-name provided by the previous option.

Upload temporary spectrum to database - the user can anonymously upload his own spectral data for further processing. The file with the spectrum should contain two or three columns, the first column containing the wavelengths (given in angstroms, nanometers, or microns), the second column containing the corresponding reflectance. Optionally, the third column may include the dispersion of observations. The file receive a temporary name over which the user has full control.

Concatenate spectra - spectra in different wavelength regions (V and NIR) can be merged. The procedure consists in the minimization of data into a common spectral region (usually 0.8 - 0.9 μm). The result is stored in a temporary file and can be further processed.

The results of all these operations are displayed at the bottom of each page (Fig. 5.3). These results can be either spectra found in the database or temporary files. The connection with the modeling tools is made using the name of the file containing the spectrum. This filename is provided as a link and a simple click allows the user to access the modeling tool interface.

⁴<http://voparis-srv.obspm.fr/portal/>

Spectrum File (from database):

Select action:

☒ Plot spectrum

Taxonomy: ☐ [Bus-DeMeo](#) ☐ [G13](#) ☐ [G9](#)

Search matching with spectra from [Relab](#) database: ☐ All spectra | ☐ Meteorites spectra

Chose method: ▾

☐ Space weathering effects. [See this article.](#)

☐ Band parameters (if present)

☐ Mineralogical analysis ([Cloutis model](#)) [To be applied only to V+NIR spectra with features]

Please be patient while gathering and sorting information, the run might take up to 3 minutes...
The results are displayed bellow (section Results) after processing.

Results

Figure 5.4: M4AST web application tool : modelling tool interface

5.2.2 Modeling tool interface

The second component of the M4AST project is the set of applications for modeling and analyzing the spectra from the database or any spectrum submitted by the user. The use of the **modeling tool interface** (Fig. 5.4) is based on the name of the file containing the spectral data.

The following applications are currently available in this interface:

Plot spectrum - plot the reflectance as a function of wavelength. Additional information related to the selected spectrum (the observing log) are also given.

Taxonomy - classify the spectrum according to different taxonomies. Taxonomic systems that can be selected are Bus-DeMeo [DeMeo *et al.*, 2009], G13 [Birlan *et al.*, 1996a], and G9 [Fulchignoni *et al.*, 2000]. The methods behind these classifications are outlined in chapter 4. The results of this application consist in the first three classes that match the asteroid spectrum, together with some matching quantitative values (coefficients). In addition, the asteroid spectrum is plotted together with standard spectra corresponding to the best matches.

Search matching with spectra from the Relab database - performs spectral comparison with spectra from Relab database. In general, only the meteorite spectra are of interest, thus an



Asteroid designations (Number, Name, Temporary designation): 9147, Kourakuen, 1977_DD1
 Observation was done on (UT) (format YYYY-MM-DD-hh): 2011 - 11 - 15 - 09:00
 Observation was made by : Mirel Birlan E-mail; mirel.birlan@imcce.fr
 At observatory with UAI code: 568
 Obsv. comments: Will be published in <http://www.scientificbulletin.upb.ro/>
 The spectrum was published in the article: In press
 The normalization of this spectrum was made for the wavelength: 1.250 microns.

Matching with spectra from Relab database

Index	Coefficient	Relab File	Sample ID	Sample name	GeneralType	Type	SubType
0	0.01884	cgp047	MR-MJG-094	Pavlovka	Meteorite	Achondrite	Howardite (AHOW)
1	0.02195	mgp047	MR-MJG-094	Pavlovka	Meteorite	Achondrite	Howardite (AHOW)
2	0.02731	cgp063	MR-MJG-099	Roda	Meteorite	Achondrite	Diogenite (ADIO)
3	0.03022	mgp051	MR-MJG-096	Le Teilleul	Meteorite	Achondrite	Howardite (AHOW)
4	0.03179	c1sn12	SN-CMP-012	Kapoeta P11410	Meteorite	Achondrite	Basaltic HED Howardite Regolith Breccia
5	0.03181	cgp051	MR-MJG-096	Le Teilleul	Meteorite	Achondrite	Howardite (AHOW)
6	0.03189	c1mp126	MP-TXH-126	"QUE97001.28 (Howardite) <125 um"	Meteorite	Achondrite	Basaltic HED Howardite

Figure 5.5: M4AST web tool application: screen-shoot from the table containing the list of the closest fifty best matches which are ordered upon the comparison coefficient (column two of the table).

option for selecting between all spectra and only meteorite spectra is included. However, the "all spectra" option includes spectral measurements for mixtures (olivine/pyroxene) prepared in the laboratory that can be considered when analyzing asteroid spectra. Four methods are available for the spectral matching. Their description is given in Chapter Methods of Analysis. This application provides the first fifty laboratory spectra that match the spectrum (ordered by the matching coefficient - defined in previous chapter). These results are given in a table, together with a link to visualize a comparative plot between laboratory spectrum and the asteroid one. This table includes all the information regarding the spectral measurements and the sample characteristics (Fig. 5.5).

Space weathering effects - uses the space weathering model defined by Brunetto *et al.* [2006].

The results consists in computing the parameters of the model and de-reddening the spectrum. The de-reddening (removal of space weathering effects) is done by dividing the spectrum by its continuum. The spectrum obtained can be further analyzed, being provided in a temporary file.

Band parameters and mineralogical analysis - computes the spectral parameters defined by Cloutis *et al.* [1986b]. If only the infrared part of the spectrum is given, the algorithm computes the band minima. If the spectrum contains both V and NIR regions, all the parameters described in chapter 4 are calculated. Along with the results, the plots necessary to interpret these parameters are also provided.

After each computation made in M4AST, the results are displayed at the bottom of the page. It must be noted that some of these applications provides meaningfully results only for certain types of spectra. Their applicability is indicated in the publications describing the models. The reference to the relevant publications is also available via the web interface.

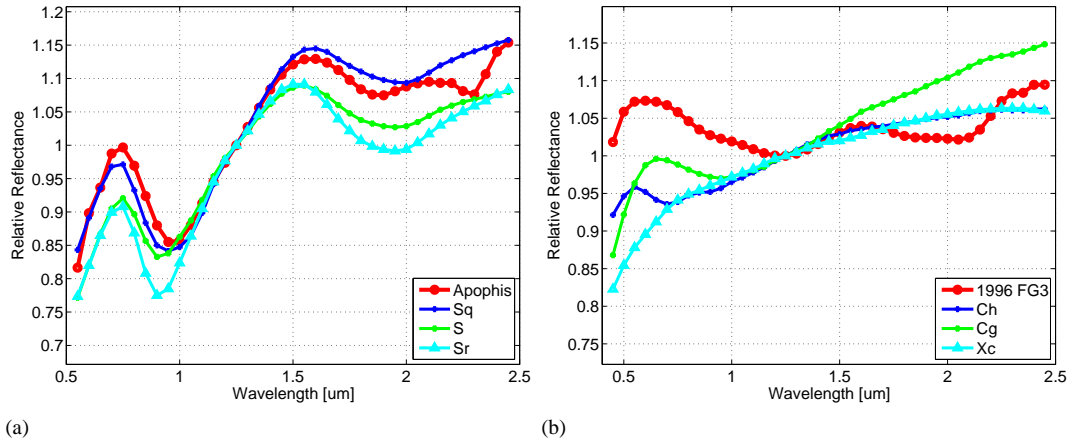


Figure 5.6: Classification in Bus-DeMeo taxonomical system for: a)) (99942) Apophis, and b) (175706) 1996 FG3. All the spectra are normalized to $1.25 \mu\text{m}$.

5.2.3 Updating the database

Permanent spectra can be added into the database via a dedicated interface - **update database** (Fig. 5.2) - that requires administrative rights. The information needed to add a new permanent file with spectral data are asteroid designations (an additional utility is provided to check the designations), information about the observation (date, investigator, and IAU code of the observatory), and information about the uploaded file containing the measurements. Each record submitted to the database can be removed only from this interface.

5.3 Testing of M4AST

The functionality of M4AST is exemplified here by the analysis of two spectra available in the database that were previously discussed by Binzel *et al.* [2009], and de León *et al.* [2011a]. Our selection here covers a wide variety of spectra, (99942) Apophis is an *Sq* type asteroid with moderate features, and (175706) 1996 FG3 is a primitive type with featureless spectra. My choice for these objects is not trivial. (99942) Apophis is a NEA which came very close to the Earth. The next approach will occur in 2029 and its Minimum Orbital Intersection Distance (MOID) is less than 40,000 km from the Earth surface. 1996 FG3 is the main target of the future mission Marco-Polo-R. Ground based science is highly required for this object if the mission will take place.

The discussion of the taxonomic type of each object is made with reference to both Fig. 5.6 for Bus-DeMeo taxonomy and Fig. 5.7 for G-mode taxonomies. Table 5.1 summarizes the comparison of asteroid spectra with spectra from the Relab database. The corresponding plots are given in Fig. 5.8.

Table 5.1: Summary of the results obtained by matching the asteroids spectra with spectra from the Relab database. For each asteroid, I show the best two matches, obtained by measuring the standard deviation (std. dev.) and the correlation coefficient (corr. coef.).

Spectrum	std. dev.	corr. coef.	Meteorite/Sample	Sample ID	Type	Texture
(99942)	0.01756	0.98013	Simulant	CM-CMP-001-B	Soil/Lunar	Particulate
	0.01970	0.98224	Hamlet	OC-TXH-002-C	OC-LL4	Particulate
(99942) de-reddened	0.01539	0.96245	Cherokee Springs	TB-TJM-090	OC-LL6	Particulate
	0.01609	0.97272	Cat Mountain	MB-DTB-035-A	OC-L5	Particulate
(175706)	0.01219	0.90546	Sete Lagoas	MH-JFB-021	OC-H4	Slab
	0.01504	0.85366	Murchison heated 1000 °C	MB-TXH-064-G	CC-CM2	Particulate

5.3.1 Results

The first spectrum considered to exemplify the M4AST routines is that of the potential hazardous asteroid **(99942) Apophis** [Binzel *et al.*, 2009]. On the basis of this spectrum this asteroid was found to be an Sq type, and has a composition that closely resemble those of LL ordinary chondrite meteorites.

M4AST classifies this spectrum in the Bus-DeMeo taxonomy as an Sq-type (Fig. 5.6a). The next two types, S and Sr, are relatively good matches, but have larger errors. Applying the G13 taxonomy, M4AST classifies this asteroid as being in class 2 (Fig. 5.7a). Two other classes (namely 6 and 7) are relatively close in terms of g factor (Fig 5.7a). Class 2 has the representative members (7) Iris and (11) Parthenope, which are S and Sq type asteroids according to DeMeo *et al.* (2009). The classes 2, 6, and 7 are equivalent to the S profile.

Being an Sq type, for this asteroid spectrum it can be applied the space weathering model proposed by Brunetto *et al.* [2006]. Thus, fitting the spectrum with an exponential continuum we found $C_s = -0.196 \mu\text{m}$, corresponding to a moderate spectral reddening. The result obtained by Binzel *et al.* [2009] is $C_s = -0.17 \pm 0.01 \mu\text{m}$. This difference could be caused by the different method that they used: their "best fit was performed as an integral part of the overall minimum RMS solution". The C_s value gives the number of displacements per cm^2 , $d = 0.74 \times 10^{19}$ displacements/ cm^2 . Next, will be analyzed both the original spectrum and the de-reddened spectrum.

Comparing the original spectrum of (99942) Apophis with all laboratory spectra from Relab, M4AST found matches with some ordinary chondrite meteorites (L and LL subtypes, and petrologic classes from 3 to 6) and some lunar soils (Figs. 5.8a and 5.8b). Referring to standard deviation and to correlation coefficient, the closest matches were those of particulate lunar soils and some spectra from Hamlet meteorite which is particulate with grain sizes smaller than $500 \mu\text{m}$. The meteorite Hamlet is an ordinary chondrite, subtype LL4.

In the case of the de-reddened spectrum, the majority of solutions correspond to ordinary chondrite meteorites, of subtype L and LL, with petrologic classes from 4 to 6. The best matches were those of the Cherokee Springs meteorite (an LL6 ordinary chondrite, Fig. 5.8c) and the Cat Mountain meteorite (an L5 ordinary chondrite, Fig. 5.8c). From spectral modeling

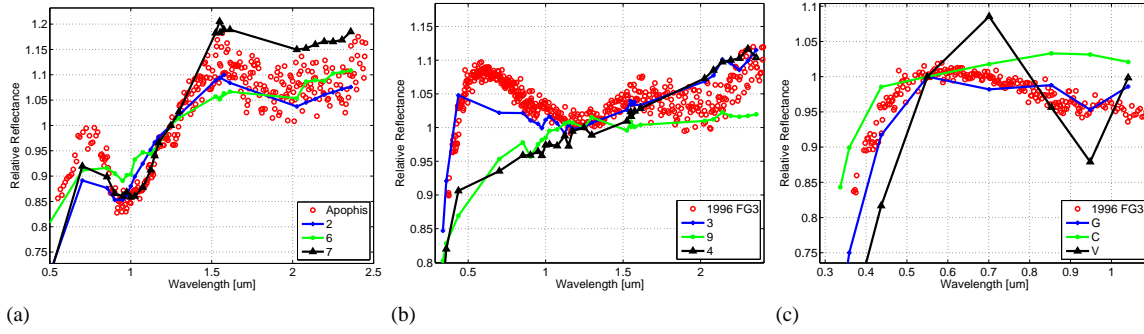


Figure 5.7: Classification in the G-mode taxonomical system for: a) (99942) Apophis using G13 taxonomy, b) (175706) 1996 FG3 using G13 taxonomy, and c) (175706) 1996 FG3 using G9 taxonomy. All the spectra are normalized either to $1.25 \mu\text{m}$ (left and central panel), or to $0.55 \mu\text{m}$ (c).

of mixtures of olivine, orthopyroxene, and clinopyroxene, Binzel *et al.* [2009] correlate the spectrum of (99942) Apophis to the spectra of LL meteorites. These results agrees with the spectral matching solutions found by M4AST.

No significant differences between the Cloutis model parameters computed for original and de-reddened spectrum are found. The application founds the first band center at $0.9721 \pm 0.0143 \mu\text{m}$ ($0.9755 \pm 0.0144 \mu\text{m}$ for the de-reddened spectrum), the second band center at $1.8200 \pm 0.0679 \mu\text{m}$ ($1.8404 \pm 0.0591 \mu\text{m}$ for the de-reddened spectrum), and the band area ratio 0.4059 ± 0.0047 (0.3886 ± 0.0015 for the de-reddened spectrum). These parameters correspond to an ordinary chondrite with an $OPX/(OPX + OL)$ ratio of 0.222 (0.215 for the de-reddened spectrum). This ratio agrees with the compatibility relation between NEA and LL ordinary chondrites found by Vernazza *et al.* [2008], which is similarly consistent with the spectral matching we found.

This value means that the ordinary chondrite consist of 78% olivine, which is consistent with an LL ordinary chondrite. And this result agrees to the spectral matching.

The dark primitive asteroid **(175706) 1996 FG3** is the primary target of the ESA Marco Polo-R mission. Some papers were dedicated to this object, namely de León *et al.* [2011b], Wolters *et al.* [2011], Rivkin *et al.* [2012], and Walsh *et al.* [2012]. There are few spectra published in both V and NIR. In the M4AST database, we included spectra from the MIT-UH-IRTF (MINUS) survey ⁵ and the spectrum of de León *et al.* [2011b].

On the basis of different spectra, the asteroid has been classified as belonging to primitive types (C, B, or X), but there is no consensus on its classification in the literature [de León *et al.*, 2011b, Walsh *et al.*, 2012]. In addition some spectral matchings have been noted with meteorites ranging from ordinary chondrite H-type to both CM2 and CV3 carbonaceous chondrite [de León *et al.*, 2011b, Rivkin *et al.*, 2012].

To exemplify the applications of M4AST, we used the spectrum obtained on March 30, 2009 by MIT-UH-IRTF (MINUS). The classification in the Bus-DeMeo taxonomy returned the Ch,

⁵<http://smass.mit.edu/minus.html>

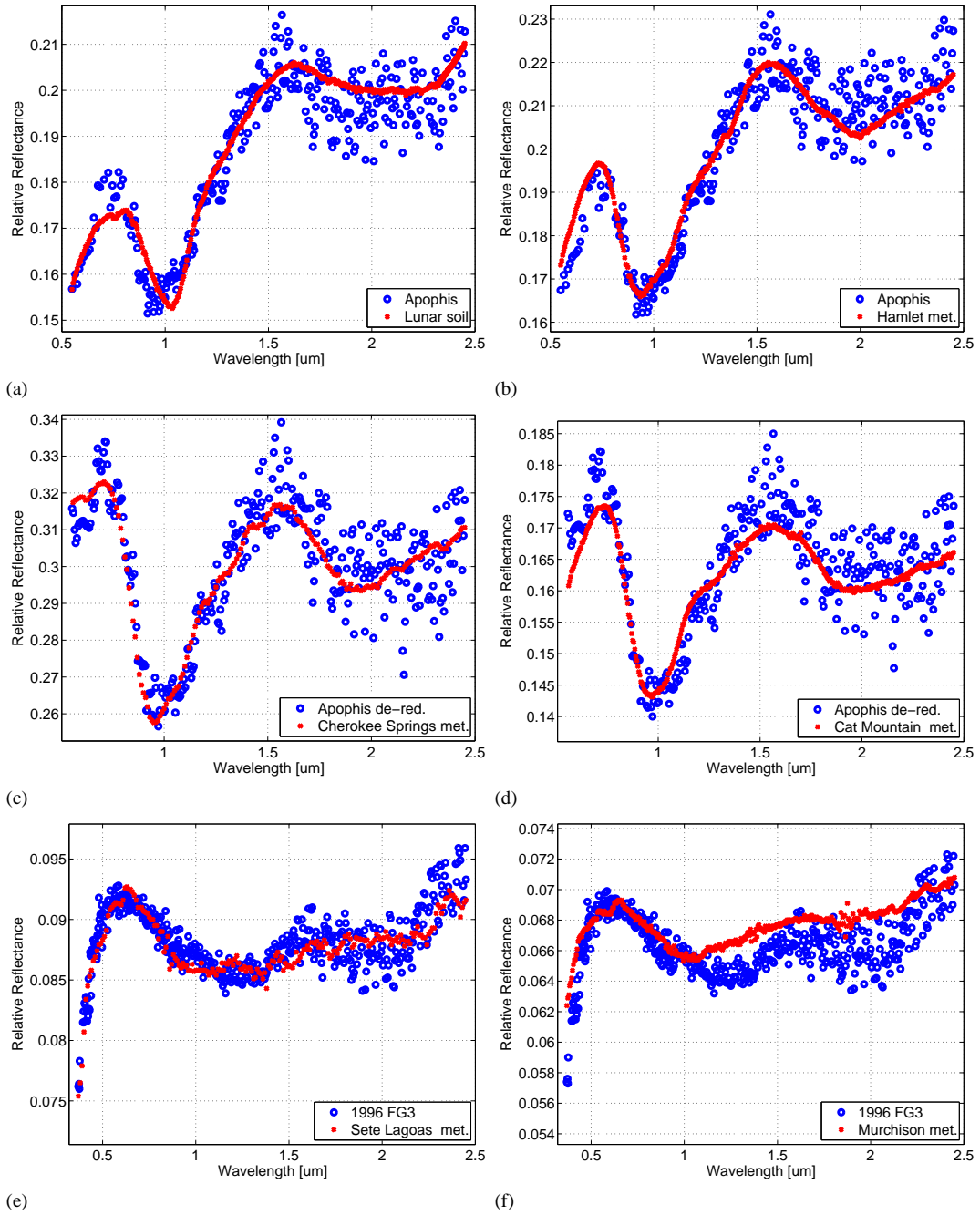


Figure 5.8: Asteroid spectra and the best two matches derived from a comparison with laboratory spectra:(a) spectrum of Apophis and the spectrum of a simulant Lunar soil, (b) spectrum of Apophis and the spectrum of a particulate sample from the Hamlet meteorite, (c) de-reddened spectrum of Apophis and the spectrum of a particulate sample from the Cherokee Springs meteorite, (d) de-reddened spectrum of Apophis and the spectrum of a particulate sample from the Cat Mountain meteorite, (e) spectrum of 1996 FG3 and the spectrum of a sample from the meteorite Sete Lagoas, and (f) spectrum of 1996 FG3 and the spectrum of a sample from the Murchison meteorite heated to 1000 °C.

Cg, and Xc taxonomic types (Fig. 5.6b). The scores obtained for the classes Ch, Cg, Xc, C, and Cgh are very similar. This object has neither the absorption band centered at $0.7 \mu\text{m}$ typical of Ch-type, nor the redder spectral slope of Xk-types [de León *et al.*, 2011b]. In addition, the slope in the NIR part of the spectrum, that is of Cg type does not corresponds to the spectrum of (175706) 1996 FG3.

Classifying this spectrum of (175706) 1996 FG3 using the G13 taxonomy, we obtain with high confidence ($g_s = -1.237$) the type corresponding to class 3. The other two types (classes 9 and 4) have greater g_s coefficients (Fig. 5.7b). Groups 3 and 4 are the equivalents for the C-type asteroids. As representative members of the class 3, there are (1) Ceres and (10) Hygiea, which are both primitive asteroids. The classification in the G9 taxonomy (Fig. 5.7c) confirms the classification as a primitive type, suggesting as the first options the classes G and C, while the third option (V) could be ignored because it has a larger g_s .

Considering these three classifications, the solution on which the applications of M4AST seems to converge is that the spectrum of (175706) 1996 FG3 is of a Cg taxonomic type.

Comparing the spectrum of (175706) 1996 FG3 to the laboratory spectra, it was obtained a good match to a sample of the meteorite Sete Lagoas (Fig. 5.8e). Other matches are the spectrum of a sample from meteorite Murchison heated to 1000°C (Fig. 5.8f), the spectrum of a sample from the Dhofar 225 meteorite, and the spectrum of a sample from Ozona. This is puzzling, since both the Sete Lagoas and Ozona meteorites are ordinary chondrites (H4 and H6, respectively), and both Murchinson and Dhofar 225 are carbonaceous chondrites. However, it can be noted that the majority of matching solutions are spectra of carbonaceous chondrite meteorites (CM type). If additionally, is taken into account the asteroid albedo⁶, then the spectrum of Dhofar 225 (sample ID: MA-LXM-078) and Murchison heated to 1000°C (sample ID: MB-TXH-064-G) seems to be the most probable analogs of this asteroid spectrum.

While the results of M4AST are in agreement with those already published, it can be concluded that the routines of M4AST work correctly and their implementation is robust.

5.3.2 Discussions regarding misinterpretations of spectra

Applying the correct methods for interpreting asteroid spectra can reveal a lot of information about the physical properties of these objects. However, each method has its own limitations which in general are well-described in their corresponding paper, and using the methods beyond their limits may of course lead to incorrect results.

The first misinterpretation that may occur is related to space weathering. Gaffey [2008] noted, "space weathering is commonly invoked to reconcile observational data to the incorrect expectation that ordinary chondrite assemblage are common in the asteroid belt". While space weathering for the lunar samples has been well-documented using the samples returned from the Apollo missions, it has been observed that different models are required to interpret the

⁶the geometric albedo was found as 0.039 ± 0.012 by Walsh *et al.* [2012]

space weathering processes that acted on different asteroid surfaces.

The model I applied for space weathering was based on laboratory experiments that consist in ion irradiation (Ar^+) of olivine and pyroxene powders. This model is suitable for asteroids that seem to consist of olivine and pyroxene, such as those from the S complex.

According to these experiments, the reddening in the infrared part of spectra due to solar-wind ion irradiation can be removed, by dividing the spectrum by an exponential function. However, there are several other effects that can modulate the spectra, such as either thermal influence [Rivkin *et al.*, 2005] or the debated phase-angle effect [Veverka *et al.*, 2000].

The second misinterpretation that may occur is related to the spectral matches with laboratory spectra [Gaffey, 2008]. Curve matching can provide clues to the nature of the asteroid surface composition. The efficiency of this method can be clearly observed in the case of asteroids that have strong spectral features, such as the vestoids⁷. Misinterpretations can occur when the asteroid surface is modified by space weathering effects, while the meteorite can be modified by terrestrial influences.

The four methods proposed take into account different characteristics of the spectra: spectral slope, band depths, and the various feature positions. In the context of taxonomic classification, albedo value, space-weathering effects, and similar solutions obtained from all four matching methods, the developers [Popescu *et al.*, 2012b] of M4AST believe that spectral matches with laboratory spectra provide valuable information on the asteroid surface nature.

By applying the methods of M4AST, it can be observed that a good solution for interpreting the asteroid spectrum is found when all the methods converge to the same mineralogical interpretation. For example, when the spectrum of (99942) Apophis was processed, despite the poor signal to noise ratio in the infrared part of its spectrum, we obtain the classification Sq in the Bus-DeMeo taxonomy and an analog of this class in the G13 taxonomy. We then found that the spectra of ordinary chondrite meteorites (L, LL subtypes) match this spectrum. These two results were confirmed and developed by applying the Cloutis model: the fraction of olivine-orthopyroxene is 22%, and the associated parameters are equivalent to those of an ordinary chondrite. This conclusion is in general valid for all the spectra analyzed via M4AST.

⁷Vesta-like asteroids

Part III

OBSERVATIONS AND RESULTS

Spectral properties of near-Earth asteroids

This chapter presents spectra of eight NEAs (1917, 8567, 16960, 164400, 188452, 2010 TD54, 5620, and 2001 SG286) obtained using the NASA telescope IRTF equipped with the spectro-imager SpeX. The analysis of these spectra includes taxonomic classification, comparison with laboratory spectra from Relab database, and for the S-type objects the correspondent mineralogical models. I also attempted to interpret our data using a space-weathering model.

The taxonomic classification of five objects was reviewed and a corresponding type was assigned to the other three asteroids that were not classified before. I found that (1917) Cuyo, (8567) 1996 HW1, (16960) 1998 QS52, (188452) 2004 HE62, and 2010 TD54 are in the S-complex. For these S-type asteroids a good matching was found with spectra of ordinary chondrites meteorites.

The asteroids (5620) Jasonwheeler and 2001 SG286 were classified as D-type objects. The spectrum of (5620) Jasonwheeler is similar to spectra of carbonaceous chondrite meteorites. The results found for the two objects confirm their primitive properties obtained in several other spectral intervals.

Four of the observed objects have delta - V lower than 7 km/sec, which make them suitable targets in terms of propulsion for a future spacecraft mission.

Near-Earth Asteroids (NEAs) are a continuously changing population of small bodies with orbits that come close to the Earth's orbit. Their chaoticity defines them as a critical population, while several important gravitational field (those of the Sun, Jupiter, and the inner planets) are superimposed influencing their orbital movement.

Because of the relatively short lifetime of these objects, it is necessary to understand the dynamical mechanisms of supplying those bodies which are lost (due to expulsion from the Solar System, falling into the Sun or on the telluric planets) and their reservoirs of objects from the Main Belt. According to Gladman *et al.* [2000] the median lifetime of the NEAs is 10 Myr.

On the other hand, NEAs are among the most accessible bodies in the Solar System in terms of the spacecraft propulsion requirements to reach them. In this sense, the knowledge of the ensemble of physical parameters for these objects, including their composition, is a critical point in defining any mission scientific objectives. Currently, several programs (like Marco Polo-R, Osiris-REx, Hayabusa2) are under development for space exploration of NEAs.

Another point is that the objects in near-Earth space are a valuable source of information as they represent a mixture of the different populations of small bodies: main-belt asteroids and cometary nuclei [DeMeo & Binzel, 2008], and a link with meteorites [Vernazza *et al.*, 2008,

Table 6.1: Some characteristics of the observed NEAs: orbit type, semi-major axis, eccentricity, inclination, absolute magnitude (H), and the delta-V.

Object	Orbit Type	a	e	i	ΔV [km/s]	H
Cuyo	Amor	2.15005205	0.50448184	23.943786	8.556	14.7
Jasonwheeler	Amor	2.15783969	0.42369152	7.861788	6.974	17.0
1996 HW1	Amor	2.04580925	0.44905867	8.439303	6.495	15.4
1998 QS52	Apollo	2.20249841	0.85791440	17.563883	11.11	14.2
2005 GN59	Apollo	1.65644063	0.46770919	6.627004	6.002	17.4
2004 HE62	Amor	2.55781560	0.56690184	24.685809	9.074	17.3
2001 SG286	Apollo	1.35819973	0.34708703	7.772096	5.604	20.9
2010 TD54	Apollo	1.97198039	0.64352131	4.809727	-	28.7

Popescu et al., 2011]. Their accessibility enables their scientific study, their practical study, and their detailed assessment for their future use as space resources.

In this chapter are describe spectroscopic results for eight NEAs in the 0.8-2.5 μm spectral region. Some of their dynamical characteristics are summarized in Table 6.1. The asteroids were observed during several runs between 2008 and 2010 as part of a project for studies of NEA physical properties, and potential targets of spacecraft missions. I modeled and interpreted the acquired spectra using the techniques described in chapter four with the goal of achieving basic interpretations regarding the composition and physical processes that took place at the surface of these asteroids.

6.1 Log of observations

In contrast to the Main-Belt asteroids, the asteroids classified as NEA do not often have a favorable geometry for ground-based observations. The small diameters of the majority of NEAs impose tight constraints on the suitable geometries of observations for determining the reflective properties of their surfaces. These conditions are usually met in the case of a close approach to the Earth, when the apparent magnitude decreases by several magnitudes. These suitable geometries occur on average, only five times per century.

The technical limitations like differential tracking, diameter of the principal mirror of the telescope and the sensitivity of the detectors should be also taken into account.

The spectral data described here were obtained in the 0.8 - 2.5 μm spectral region with the SpeX/IRTF instrument. The observations were carried out in two sessions: in August 2008 and in May 2009. The remotely observing procedure from CODAM was used. The spectrum of 2010 TD54 was received from professor R. Binzel (private communication). For all the observations the low resolution prism mode ($R \approx 100$) of the spectrograph was used. A 0.8×15 arcsec slit oriented north-south was used. The spectra of the asteroids and the solar analog stars were obtained using the nodding procedure.

Log of the observations is given in Table 6.2. In general, the asteroid spectra were obtained taking images with an integration time (I_{time}) of 120s, for several cycles, to increase the S/N

Table 6.2: Log of NEAs observations. Their designations, date of observation with the fraction of the day for the mid time of the observation, the apparent magnitude, the phase angle, the heliocentric distance, the airmass at the mean UT of each observation, the integration time for each spectrum (ITime), and the number of cycles are shown.

Asteroid	Date (UT)	V	Φ ($^{\circ}$)	r (UA)	Airmass	ITime(s)	Cycles
(1917) Cuyo	2008-08-27.637	14.6	66.0	1.105	1.038	120	6
(5620) Jasonwheeler	2009-05-04.569	16.5	20.9	1.345	1.344	120	6
(8567) 1996 HW1	2008-08-27.543	12.9	28.8	1.143	1.099	60	13
(16960) 1998 QS52	2008-08-27.588	16.9	30.0	1.784	1.105	120	13
(164400) 2005 GN59	2008-08-27.472	16.2	25.2	1.244	1.024	120	2
(188452) 2004 HE62	2008-08-27.404	16.7	60.8	1.109	1.513	120	12
2001 SG286	2009-05-19.594	16.7	102.0	1.006	1.962	120	2
2010 TD54	2010-10-12.303	15.5	17.3	1.000	1.252	120	8

Table 6.3: The solar analogs used for data reduction in the case of the NEAs spectra. The airmass at the moment of observations and relative distance to the asteroid are presented.

Asteroid	Solar analogue	Airmass	Distance[$^{\circ}$]
(1917) Cuyo	BD+41 309	1.141	29.1
(5620) Jasonwheeler	HD 154716	1.240	15.4
(8567) 1996 HW1	HD 217577	1.213	5.4
(16960) 1998 QS52	HD 27834	1.083	48.5
(164400) 2005 GN59	BD+28 3198	1.410	46.7
(188452) 2004 HE62	BD+28 3198	1.401	11.8
2001 SG286	HD 216516	1.742	3.4
2010 TD54	L115-271	1.092	8.71

ratio. For two objects of our sample (2005 GN59, and 2001 SG286), the atmospheric conditions and their faint magnitude imply a poor S/N ratio. In this case, in order to obtain reliable spectral measurements the images were selected by visual inspection, removing all those in which it could not distinguish the trace of the spectrum before the data reduction procedure.

Our strategy was to observe all asteroids as close to the zenith as possible (Table 6.2). Each observed asteroid was preceded by observations of a solar analog. The following stars were observed and used as solar analogs: BD+41 309, HD 154716, HD 217577, HD 27834, BD+28 3198, HD 216516, and L115-271 (Table 6.3). The differential airmass between the asteroid and the standard was usually restricted to less than 0.15. The photometric G2V standards were chosen. An exception was made for 2010 TD54, where the data reduction was performed using Landolt 115-271 star, commonly used for NIR spectral measurements.

6.2 S-type Near-Earth Asteroids

Spectroscopic observations in visible wavelengths show that 65% of NEAs have S- and Q-type spectral properties. When corrected for discovery biases, the near-Earth population of S- and Q-type asteroids is estimated to be 36 % of the total NEA population [Stuart & Binzel, 2004].

Six asteroids from our eight observed samples have spectra similar to the S-complex. These objects are: (1917) Cuyo, (8567) 1996 HW1, (16960) 1998 QS52, (164400) 2005 GN59,

(188452) 2004 HE62, and 2010 TD54. The summary of the results obtained by matching the asteroid spectra and the de-reddened asteroid spectra with spectra from the Relab database is given in Table 6.4.

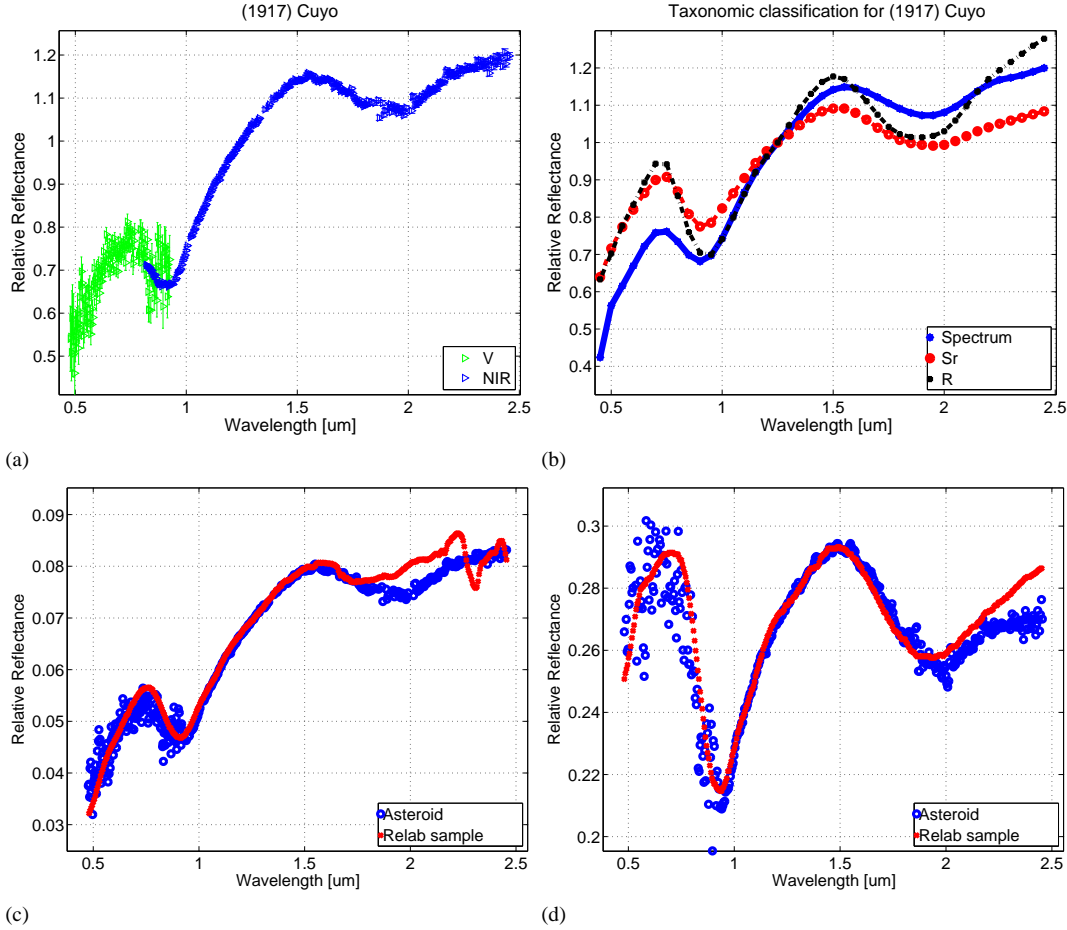


Figure 6.1: a) The visible [Binzel *et al.*, 2004b] and the NIR spectrum of (1917) Cuyo; b) a polynomial fit of the V+NIR spectrum of (1917) Cuyo compared with the theoretical spectra of R and Sr types; c) reflectance spectrum of (1917) Cuyo and the closest match resulting from meteorite comparison - H3-4 ordinary chondrite Dhajala; d) De-reddened spectrum of (1917) Cuyo and the closest match resulting from meteorite comparison, H6 ordinary chondrite Lancon.

6.2.1 (1917) Cuyo

With an absolute magnitude $H = 14.7$, this object has an estimated diameter of 5.2 km [Binzel *et al.*, 2002]. It is an Amor-type asteroid, with a rotation period of 2.6905 ± 0.0005 hrs [Wisniewski *et al.*, 1997].

Two spectra in the visible wavelengths are published for this object. For the first one, Binzel *et al.* [2004b] found that this asteroid is a S1-type in Bus taxonomy, with a high slope of ($0.7233 \mu\text{m}^{-1}$). The second one was classified by Michelsen *et al.* [2006] as an S-type asteroid in Tholen taxonomy. I joined the visible spectrum from the SMASS database [Binzel *et al.*,

2004b], with the data in NIR region (Fig. 6.1a). The analysis was performed on the composite V+NIR spectrum.

Using M4AST tool for taxonomic classification of a spectrum, the R and Sr types are obtained as possible classes for this object. The R-type is obtained with a slightly better matching coefficient than Sr-type, because of the trend in the 1-1.5 μm spectral region. With the tool from the MIT-SMASS website, this NEA was classified as Sr-type with a higher spectral slope of $0.5086 \mu\text{m}^{-1}$. By visual inspection of the two solutions, it can be seen that the features around 1 μm and 2 μm are more shallow than for R class (Fig. 6.1b), so it can be concluded that this object is an Sr type asteroid.

The comparison with the Relab database shows that the closest spectral fit is obtained for a tiny section from the Dhajala meteorite (Sample ID: LM-LAM-026, Fig. 6.1c). This corresponds to an ordinary chondrite meteorite rich in Fe (H3-4 Olivine-Bronzite). Das Gupta *et al.* [1978] estimated a total iron content of 27.1% of the total mass of Dhajala. This meteorite was also studied by analyzing the metallic grains in its OC structure [Kong & Ebihara, 1997]. While the formation of metallic iron is a consequence of the spatial alteration of an object, space weathering models are nevertheless justified.

Modeling the effects of space weathering on the basis of the exponential continuum, it can be found $C_s = -0.484 \mu\text{m}$, corresponding to strong spectral reddening. Owing to the size of this NEA, this value agrees with the general conclusion that larger objects are collisionally older, hence contain surfaces that are more space-weathered, or are not subject to other surface rejuvenating events as frequently as smaller NEAs. The number of displacements per cm^2 , which provides a measure of the solar-wind ion irradiation, is 3.25×10^{19} , which implies that the exposure has been longer than 1My [Brunetto *et al.*, 2006].

By removing the exponential continuum and fitting the unweathered spectrum with meteorite spectra from the Relab database, the closest match was found to be ordinary chondrites with high level content of Fe, but with a higher petrological type (H5, H6). The spectra of the following meteorites are very similar to the de-reddened spectrum of (1917) Cuyo: Lancon (Fig. 6.1d), Collescipoli, Ehole (Table 6.4).

6.2.2 (8567) 1996 HW1

This asteroid has an Amor type orbit and a $\Delta V = 6.495 \text{ km/s}$, though it is a suitable target in terms of propulsion for a space mission. The radar observations show a two-lobed object about 1.1 by 2.7 km in size [Taylor *et al.*, 2009]. The object is rotating with a synodic period of $8.7573 \pm 0.0009 \text{ hrs}$ [Higgins *et al.*, 2006].

Vernazza [2006] found this asteroid to be an S-type based on the visible spectrum (0.5 - 0.95 μm) acquired on August 29, 2005 at TNG. The NIR spectrum of (8567) 1996 HW1 was obtained in August 28, 2008 using an integration time of 60sec, due to the fact that the apparent magnitude was 12.9. I combined the visible spectrum from Vernazza [2006] with the NIR data

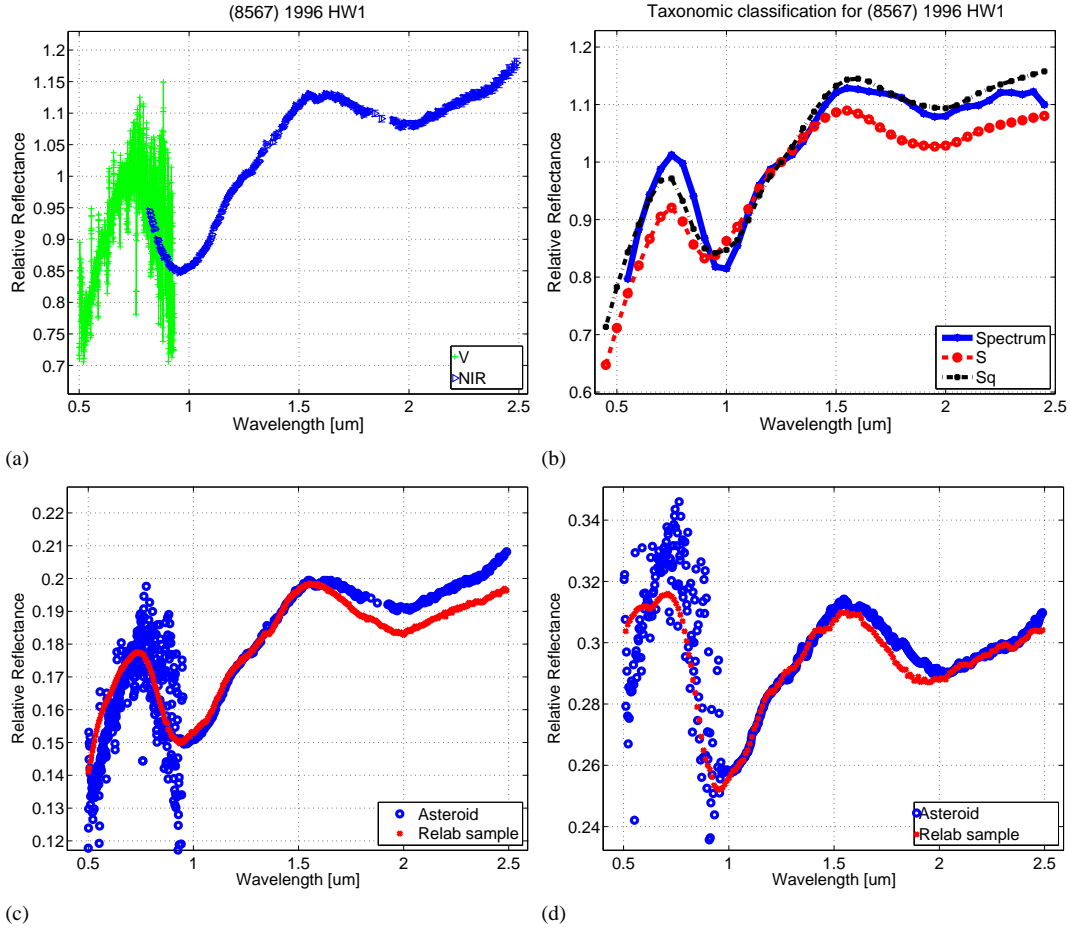


Figure 6.2: a) The visible [Vernazza, 2006] and the NIR spectra of (8567) 1996 HW1; b) a polynomial fit of the V+NIR spectrum of (8567) 1996 HW1 compared with the theoretical spectra of S and Sq types; c) reflectance spectrum of (8567) 1996 and the closest match resulting from the meteorite comparison - the LL4 ordinary chondrite Hamlet; d) de-reddened spectrum of (8567) 1996 HW1 and the closest match resulting from meteorite comparison - the LL6 ordinary chondrite Cherokee Springs.

(Fig. 6.2a) before analyzing the composite spectrum.

Using the taxonomic classification tool from the MIT-SMASS, this NEA is classified as an S-type with the spectral slope $0.2245 \mu\text{m}^{-1}$. Using the M4AST approach, it can be found that an Sq type provides a closer fit spectrum than an S (Fig. 6.2b). Sq type is at the transition between S and Q classes with two absorption bands around $1 \mu\text{m}$ and $2 \mu\text{m}$ that are more shallow than for Q-type [DeMeo *et al.*, 2009]. Comparing the features for the two considered spectral types with a polynomial fit of the spectrum, it can be observed that an Sq type matches more closely the obtained data than an S type. Since there are no measurement of the albedo for this object, assuming a value of 0.20 as typically found for the albedo of S-type asteroids [Fulchignoni *et al.*, 2000], the diameter can be estimated to be $\approx 2.5 \text{ km}$.

The spectrum from the Relab sample that provides the closest fit is a particulate ground sorted (0-125 μm) Hamlet meteorite (sample ID: OC-TXH-002-C), an ordinary chondrite with

Table 6.4: Summary of results obtained by matching the asteroid spectra and de-reddened asteroid spectra with spectra from the Relab database. The comparison was made using a χ^2 method and a selection of the obtained results was done based on spectral features (band, band-gap, concavity) positions, and albedo values. For (5620) Jasonwheeler, a de-reddening model was not applied

Spectrum	Matching results for asteroid spectra				
	Meteorite	Sample ID	Type	Texture	Size [μm]
(1917) Cuyo	Dhajala	LM-LAM-026	OC/H3-4	Thin Section	-
(8567) 1996 HW1	Hamlet	OC-TXH-002-C	OC/LL4	Particulates	0-125
(16960) 1998 QS52	Saratov	MB-CMP-028-H	OC/L4	Particulates	0-370
	Homestead	MR-MJG-048	OC/L5	-	-
	Hamlet 1	MR-MJG-069	OC/LL4	-	-
(188452) 2004 HE62	La Criolla	MH-FPF-050-B	OC/L6	Particulates	0-150
	Cherokee Springs	OC-TXH-001-A	OC/LL6	Chip	-
	Wold Cottage	MH-FPF-064	OC/L6	Particulates	-
2010 TD54	Saratov	MB-CMP-028-B	OC/L4	Particulates	10-45
	Mirzapur	TB-TJM-111	OC/L5	Particulates	0-150
	Rio Negro	TB-TJM-081	OC/L4	Particulates	0-150
	Matching results for de-reddened asteroid spectra				
	Meteorite	Sample ID	Type	Texture	Size [μm]
(1917) Cuyo	Lancon	MR-MJG-033	OC/H6	-	-
	Collescipoli	MR-MJG-030	OC/H5	-	-
	Ehole	TB-TJM-074	OC/H5	Particulates	0-150
(8567) 1996 HW1	Cherokee Springs	TB-TJM-090	OC/LL6	Particulates	0-150
	Hedjaz	OC-TXH-016-C	OC/L3-6	Particulates	0-125
	Ensisheim	TB-TJM-092	OC/LL6	Particulates	0-150
(16960) 1998 QS52	Hamlet 1	MR-MJG-069	OC/LL4	-	-
	Gruneberg	MR-MJG-040	OC/H4	-	-
(188452) 2004 HE62	Nanjemoy	MR-MJG-034	OC/H6	-	-
	Olmedilla de Alarcon	MR-MJG-075	OC/H5	-	-
	MAC88119.9	MB-TXH-044	OC/H5	Slab	0
2010 TD54	Gruneberg	MR-MJG-040	OC/H4	-	-
	Queen's Mercy	MR-MJG-035	OC/H6	-	-
	Ochansk	MR-MJG-027	OC/H4	-	-

a low level content of Fe and metal - LL4 (Table 6.4, Fig. 6.2c). The asteroid spectrum in the region 1.6 -2.5 μm is shallower than that of the meteorite spectrum, which could be explained by considering space-weathering effects.

Using the space weathering model of Brunetto *et al.* [2006], it can be found that $C_s = -0.258 \mu\text{m}$. Modelling this with a damage parameter due to the solar-wind ion irradiation the number of displacements per cm^2 can be found as $d = 1.08 \times 10^{19}$, showing that it has experienced an appreciable amount of space weathering.

By removing the exponential continuum and comparing again with Relab meteorite spectra, the closest matches are also ordinary chondrite (LL6, L3-6 types) spectra with a low metal, low Fe content. The meteorite spectra that provide the closest fit of the de-reddened spectrum of this asteroid are those of: Cherokee Spring (Fig. 6.2d), Hedjaz, and Ensisheim (Table 6.4). The Relab samples of these meteorites are particulates sorted in order of their sizes, which are smaller than 150 μm .

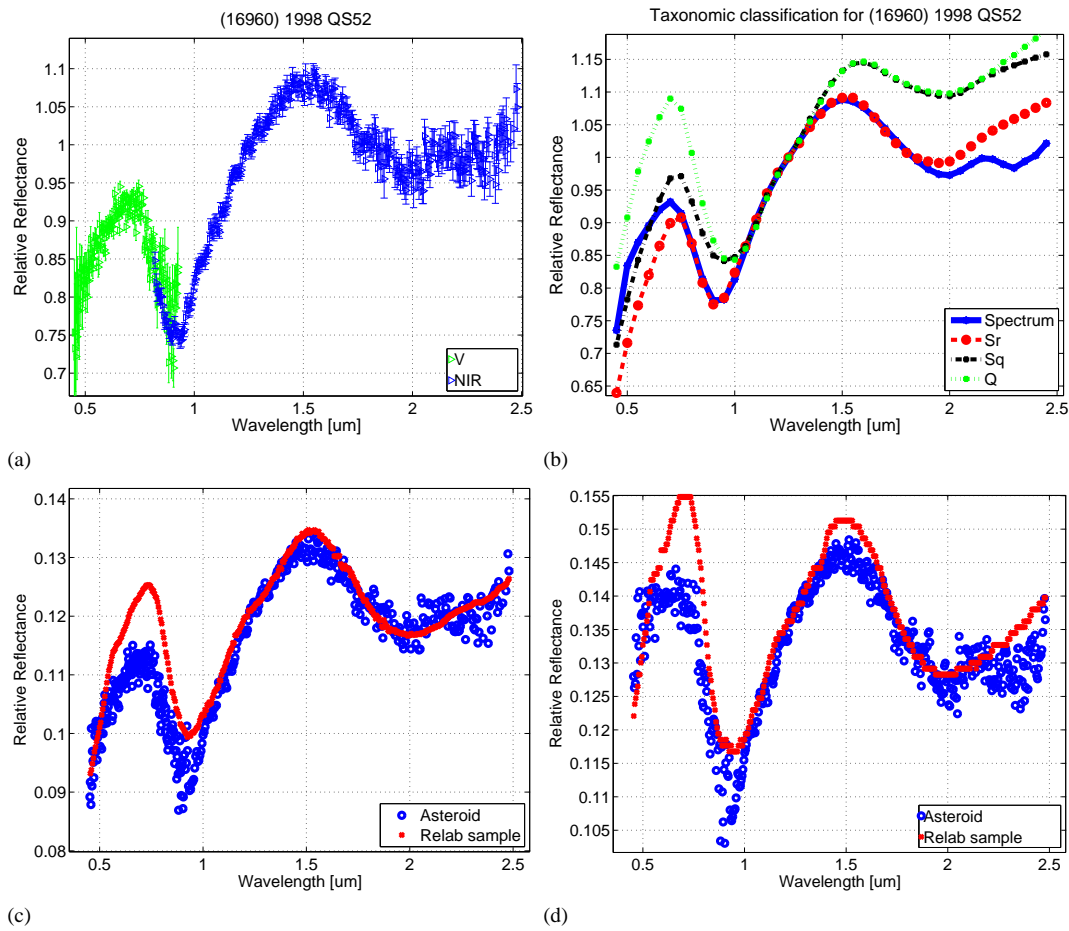


Figure 6.3: a) The visible [Binzel *et al.*, 2004b] and the NIR spectra of (16960) 1998 QS52; b) a polynomial fit of the V+NIR spectrum of (16960) 1998 QS52 compared with the theoretical spectra of Sr, Sq and Q types; c) the reflectance spectrum of (16960) 1998 QS52 and the closest fit resulting from spectral comparison - the L4 ordinary chondrite Saratov; d) the de-reddened spectrum of (16960) 1998 QS52 and the closest fit resulting from meteorite comparison - the LL4 ordinary chondrite Hamlet.

6.2.3 (16960) 1998 QS52

With an absolute magnitude $H = 14.20$, this asteroid has an estimated diameter of 4.3 km [Binzel *et al.*, 2002]. It is characterized by a synodic period of 2.900 ± 0.001 hrs [Warner, 2009]. It has an Apollo orbit type and $\Delta V = 6.5$ km/s, which makes it an accessible target for a spacecraft mission. (16960) 1998 QS52 is a PHA object type with 0.01408 AU MOID computed at epoch 55600.0 MJD (NeoDys¹).

On the basis of a visible spectrum acquired with the MDM 2.4 m telescope in 15 October 1998, Binzel *et al.* [2004b] classified this asteroid as Sq type. The spectrum of the visible region has a small negative slope of $-0.0205 \mu\text{m}^{-1}$. The following analysis was made on the combined V+NIR spectrum (Fig. 6.3a).

Both methods for taxonomic classification (M4AST and MIT-SMASS online tool) of clas-

¹<http://newton.dm.unipi.it/neodys/>

sification gave the same results: this object has the characteristics of an Sr type in Bus-DeMeo taxonomy, with a fairly $1\ \mu\text{m}$ feature (Fig. 6.3b). The slope of this composite spectrum is $0.1126\ \mu\text{m}^{-1}$.

Comparison with meteorite spectra from Relab database shows the match with ordinary chondrites samples with low content of Fe (L4, LL4, L5). The best fit is a powdered sample (dimensions: $10 - 45\ \mu\text{m}$) from Saratov meteorite, an ordinary chondrite L4 (Table 6.4, Fig. 6.3c).

Analyzing this composite spectrum with a space weathering model [Brunetto *et al.*, 2006], I computed the value of $C_s = -0.149$ which describes an unreddened spectrum corresponding to a fresh surface. It can be speculated that this young surface is due to a relatively recent close encounter with a planet [Binzel *et al.*, 2010].

To verify this hypothesis, 100 orbital clones of 1998 QS52 were generated using a random gaussian distribution centered at the nominal values in each of the six orbital elements. The 1σ values were obtained from the orbital elements uncertainties provided by the NeoDys service for this asteroid. The 100 clones were numerically integrated backward in time for 5,000 years using the computing routines proposed by Nedelcu [2010]. Each close encounter (MOID) with Venus, the Earth, and Mars was then carefully analyzed to find the closest one able to rejuvenate the surface of the object.

In addition to the 1989 close approach to Earth, an event already identified by NeoDys, the calculus confirms that five others close approaches to Venus had occurred in the past 3,000 years before the common origin signature of our cloud of clones was erased by close planetary encounters. The MOID values are larger than those predicted by Binzel *et al.* [2010]. The deterministic clones approach can reliably obtain NEAs positions only for a couple of thousands years backward in time [Nedelcu, 2010]. Systematic errors in osculating elements can affect the position of the object, and close encounters with telluric planets will modify in a non-linear way the uncertainty in the position. Thus, it can be estimated that for timescales of millions of years (the scale for SW determined by Brunetto *et al.* [2006]) the object might experience additional close encounters that cannot be reproduced by our numerical integration of orbit.

Comparing the de-reddened spectrum with the Relab database, it can be found a good fit to the spectrum with the one of Hamlet meteorite, a LL4 ordinary chondrite (Fig. 6.3d). This result was also found when comparing with the original spectrum. This agrees with the result that dividing the spectrum with the exponential continuum by the small value of C_s does not alter its characteristics.

6.2.4 (188452) 2004 HE62

Few physical parameters of (188452) 2004 HE62 are known. This asteroid has an Amor orbit and an absolute magnitude $H = 17.30$ (Table 6.1). No other spectral investigations have been published for this asteroid. The NIR spectrum observations (Fig. 6.4a) of this object were made

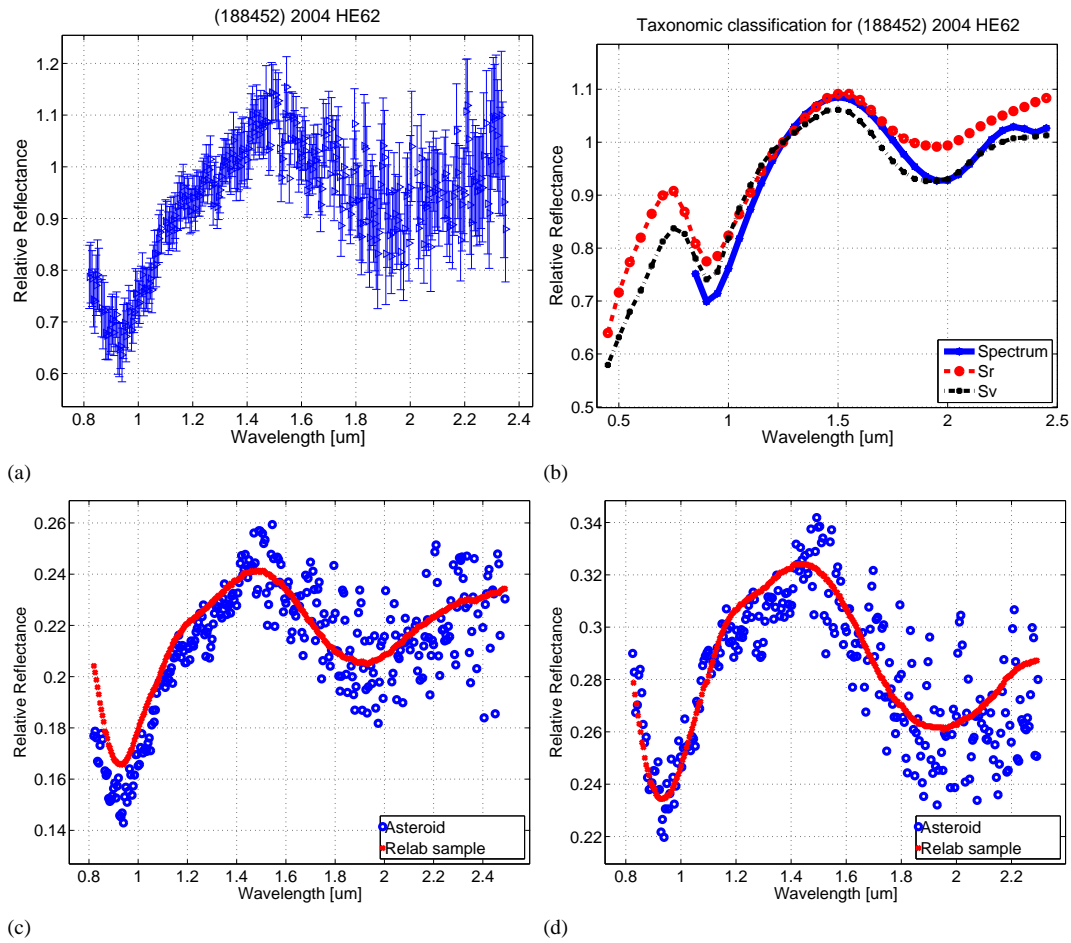


Figure 6.4: a) The NIR spectrum of (188452) 2004 HE62 normalized to $1.25 \mu\text{m}$; b) a polynomial fit for the spectrum of (188452) 2004 HE62 compared with the theoretical spectra of Sr and Sv types; c) the reflectance spectrum of (188452) 2004 HE62 and the closest fit resulting from meteorite spectra comparison - the L6 ordinary chondrite La Criolla; d) the de-reddened spectrum of (188452) 2004 HE62 and the closest matches resulting from meteorite comparison - the H6 ordinary chondrite Nanjemoy.

on August 27, 2008 when the object had an apparent magnitude of 16.7.

The spectrum of (188452) 2004 HE62 has two features around 1 and $2 \mu\text{m}$: these are two deep absorption bands that are larger than for Sv-type meteorites but not so deep to be classified as one of the end members R or V. However, the classification is between the Sr and Sv classes in the Bus-DeMeo taxonomy (Fig. 6.4b). A visible spectrum would help to clarify the object's classification. The spectral slope computed on the NIR part of the spectrum is $0.1167 \mu\text{m}^{-1}$. Assuming an average albedo of 0.2 - typical for S-type objects, the diameter can be estimated to be $\sim 1 \text{ km}$.

By comparing with data from the Relab database, this spectrum was found to be closely matched by the spectra of ordinary chondrite meteorites with low Fe, low metallic content, and high petrologic class (L6, L5, LL6) - Table 6.4. The best-fit solution was obtained with a spectrum of a particulate sample (0-150 μm) from the La Criolla meteorite (Sample ID:

MH-FPF-050-B) - Fig. 6.4c.

Modeling the spectra with the exponential continuum [Brunetto *et al.*, 2006], the parameter C_s is found to be of $-0.377 \mu\text{m}$, which characterizes a surface affected by space weathering effects. Removing this continuum and comparing with Relab meteorite spectra, the best fit are also the ordinary chondrites, the same petrologic class but with a high content of Fe (OC types H5, H6). The closest match in this case is a sample from a Nanjemoy meteorite, an H6 Olivine-Bronzite OC, which consists of 18% Fayalitic material (Fig. 6.4d).

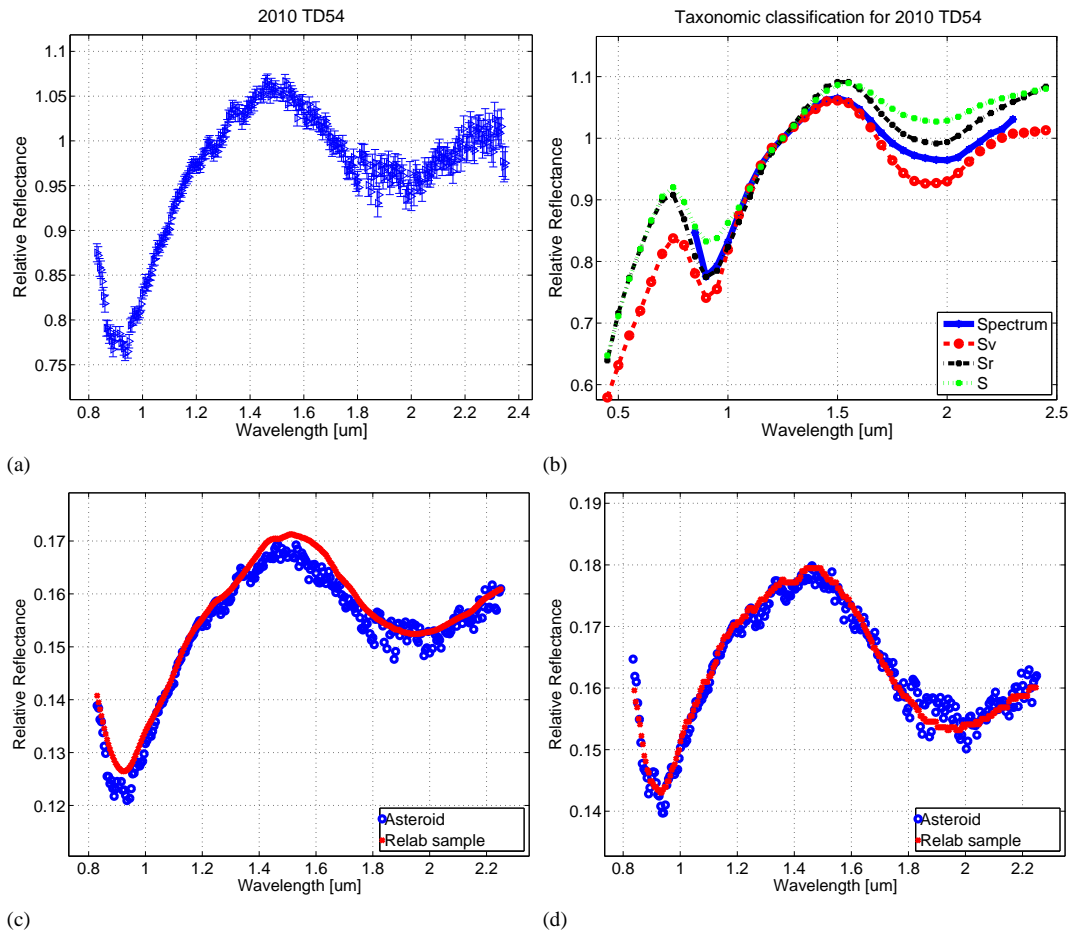


Figure 6.5: a) The NIR spectrum of 2010 TD54; b) a polynomial fit for the spectrum of 2010 TD54 compared with the theoretical spectra of Sv, Sr and S types; c) the reflectance spectrum of 2010 TD54 and the closest match resulting from meteorite comparison - the L4 ordinary chondrite Saratov; d) the de-reddened spectrum of 2010 TD54 and the closest match resulting from meteorite comparison - the H4 ordinary chondrite Gruneberg.

6.2.5 2010 TD54

The analysis of this object is interesting from the point of view of its size and the phenomena that occur on the surface of small bodies during a close encounter with Earth. With an absolute magnitude $H = 28.75$, 2010 TD54 was discovered by the Catalina Sky Survey in October 09, 2010. Having an Apollo orbit type, this object passed within 0.00035 AU of the Earth on 12.55

Oct 2010 [Hicks & Rhoades, 2010].

Preliminary measurements were done by Hicks & Rhoades [2010]. They found a rotational period of 42.0 sec, which implies that this small NEA is the most rapidly rotating natural body known in the Solar System. They also measured the object's average colors ($B-R = 1.284 \pm 0.045$ mag; $V-R = 0.461 \pm 0.030$ mag; $R-I = 0.344 \pm 0.022$ mag). These are compatible with an S-type spectral classification.

The NIR spectrum of 2010 TD54 is plotted in Fig. 6.5a. Using the MIT-SMASS online tool for Bus-DeMeo taxonomy, this asteroid is classified as belonging to a S complex, of subtypes Sr or Sq. An end class Q is also proposed but with a lower coefficient. By using the M4AST method, this spectrum can be classified to be between Sv and Sr classes (Fig. 6.5b). It has a fairly prominent feature around $1 \mu\text{m}$ and another around $2 \mu\text{m}$. When considering these two results and the depth of the two absorption bands, I found that the Sr type provides a more accurate description for this object. The slope for this NIR spectrum is $0.062 \mu\text{m}^{-1}$.

The matching with meteorite spectra (Fig. 6.5c) shows that the best fit is a spectrum for a sample from Saratov - an ordinary chondrite meteorite with a low content of Fe (L4). This sample contains particles with sizes between 10 and $45 \mu\text{m}$ (Sample ID: MB-CMP-028-B). The spectrum can also be closely fitted with spectra of powdered samples from the meteorites Mirzapur and Rio Negro, which are also L ordinary chondrites.

Modelling the space weathering effects, a $C_s = -0.223 \mu\text{m}$ can be computed, which describes a relatively fresh surface. This agrees with the small bodies having relatively young surfaces, and Earth encounters are one of the origins for rejuvenating surfaces on near-Earth asteroids [Binzel *et al.*, 2010]. Removing the exponential continuum and comparing again with spectra from the Relab database, it can be found a good fit to the spectrum with those of ordinary chondrite meteorites with high level of Fe, from petrologic class 4 (H4 - Olivine-Bronzite). Spectra of meteorites such as Gruneberg (Fig. 6.5d), Queen's Mercy, or Ochansk match the unweathered spectrum of this asteroid (Table 6.4).

6.2.6 (164400) 2005 GN59

This asteroid has an absolute magnitude $H = 17.40$, derived from astrometric observations. The synodic period of the asteroid was estimated to be 38.62 ± 0.01 hrs [Vander Haagen, 2011], but the monomodal solution of 19.31 ± 0.01 hrs cannot be totally excluded.

A preliminary spectrum of this object was presented by Birlan *et al.* [2009], while Taylor *et al.* [2009] presented thermal emission data corroborated with radar observations. From these radar observations, Taylor *et al.* [2009] discovered that this object has a two-lobed 0.35 by 1.1 km shape, with non-convex surface features.

Dynamically, (164400) 2005 GN59 is an Apollo asteroid. Its calculated $\Delta V = 6.002$ km/s make this asteroid a possible target in terms of propulsion for spacecraft mission.

The NIR spectrum of 164400 was obtained in August 28, 2008 for a total integration time

of 480 sec. While the spectrum is quite noisy, in order to obtain information about its taxonomic class, a five order polynomial function is used to reproduce the real data. The values for reflectance corresponding to wavelengths between 1.7 and 2 μm were excluded due to high noise caused by atmospheric turbulence (Fig. 6.6).

Both the MIT-SMASS on-line tool and the M4AST routine classifies this object as an L-type. However, the K taxonomic class is also a reasonable match to our data (Fig. 6.6).

An additional NIR spectrum of this object was obtained by the MIT-UH-IRTF Joint Campaign for NEO Spectral Reconnaissance². This spectrum has higher S/N than the one presented in Fig. 6.6. The classification of this additional spectrum is between Sq and Q types, while a K taxonomic class was proposed as a third solution. The L taxonomic class is also considered as a possible solution by the MIT-SMASS on-line tool.

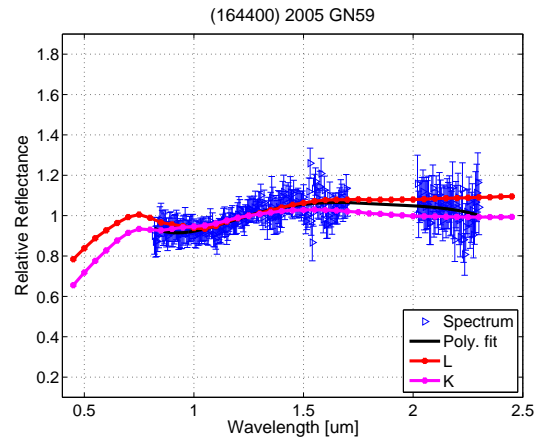


Figure 6.6: NIR spectrum of (164400) 2005 GN59 and its taxonomic classification.

The difference between the spectrum presented here and the one from MIT-UH-IRTF Joint Campaign, is caused by the SNR. For our spectrum [Popescu *et al.*, 2011], I did not take into account the feature between 1.7 and 2 μm . A visible spectrum would again help distinguish between the five possible solutions for the NIR part of the spectrum.

The spectrum of 2005 GN59 is noisy and I did not attempt to compare it with the Relab database and the de-reddening model.

6.3 Spectral properties of two primitive NEAs

Asteroids with low albedo are considered to contain the most primitive materials. They are found in the C, D, T and other dark taxonomic classes. The only images of such type of asteroid were those of (253) Mathilde, obtained by NEAR space-mission [Clark *et al.*, 1999]. This asteroid surface reflects only three percent of the Sun's light, making it twice as dark as a chunk of coal. Such a dark surface is believed to have carbon-rich material that has not been altered by planetary formation processes.

A strong correlation between the asteroid taxonomical classes and their heliocentric distance was showed based on the samples studied until now. The high albedo asteroids (like those of E and S type) can be found in the inner part of the main belt while, on the other hand C type are

²<http://smass.mit.edu/minus.html>

found mainly in the outer regions of the asteroid belt. D-type asteroids are found in the extreme outer parts of the asteroid belt and among the Trojan objects [de Pater & Lissauer, 2010]. Their distribution in space provides insight into the temperatures, pressures and chemistry of the solar nebula. de Pater & Lissauer [2010] noted that D type asteroids are probably even more primitive than the C-types and it may have formed at even lower temperatures.

Few things are known about the composition of D-type asteroids because few meteorites with similar spectral characteristics are available for study. One of the most interesting facts related to primitive asteroid is the fact that they are expected to contain organic materials³.

In this section we describe two D-types asteroids which have orbits close to the Earth orbit. They are a valuable resource from the scientific point of view, since they are reachable for sample and return space mission.

6.3.1 (5620) Jasonwheeler

This object has the geometric albedo $p_v = 0.094$ [Mueller *et al.*, 2011]. It is an Amor-type asteroid with a diameter of 1.77 km [Mueller *et al.*, 2011] and the synodic period of 5.307 ± 0.001 hrs [Durkee, 2010]. The light-curve amplitude of 1.2 magnitude [Durkee, 2010] is indicative of an object with an elongated shape, or a binary system. Having $\Delta V = 6.974$ km/s, this asteroid is a suitable target in terms of propulsion for a possible spacecraft mission.

No other spectroscopic studies of this object were found in the literature. The NIR spectrum obtained on May 5, 2009 when the object had the apparent magnitude 16.5, is plotted in Fig. 6.7a.

The MIT-SMASS online tool for taxonomy classified this object as belonging to D-class. With M4AST best-fit method, the spectrum is more similar to T-class (Fig 6.7b). In general, D-type asteroids have linear spectra with a very steep slope (greater than $0.38 \mu\text{m}^{-1}$) and display a slight curvature around $1.5 \mu\text{m}$. On the other hand, T-types also have linear spectra with a steep gradient - between 0.25 and $0.38 \mu\text{m}^{-1}$ - that nevertheless gradually curves concavely downward. [DeMeo *et al.*, 2009]. The spectrum of this asteroid has a steep slope in the $0.9 - 1.5 \mu\text{m}$ region and a slight curvature between $1.5 - 2.2 \mu\text{m}$, though the classification is at the boundary between D-type and T-type. The overall NIR slope is $0.2504 \mu\text{m}^{-1}$.

Taking into account the low geometrical albedo when comparing with spectra from the Relab database, I found close spectral matches for this spectrum with CM2 carbonaceous chondrite meteorites (Table 6.4, Fig. 6.7d, 6.7e, 6.7f). In general, the CM2 meteorites are characterized by 30% levels of chondrules with grain sizes of $\approx 300 \mu\text{m}$, the absence of Fe-Ni alloys, and the presence of CAI (Ca -Al inclusions) [Dobrica, 2010]. The closest description of the spectrum is provided by a sample of particulates ($0-75 \mu\text{m}$) from the meteorite Mighei/Meghei (Sample ID: MR-MJG-108). Other spectra of CM2 carbonaceous chondrite meteorites that fit the Jasonwheeler NIR spectrum are those of powdered samples with particle sizes smaller than

³<https://www.oca.eu/MarcoPolo-R/>

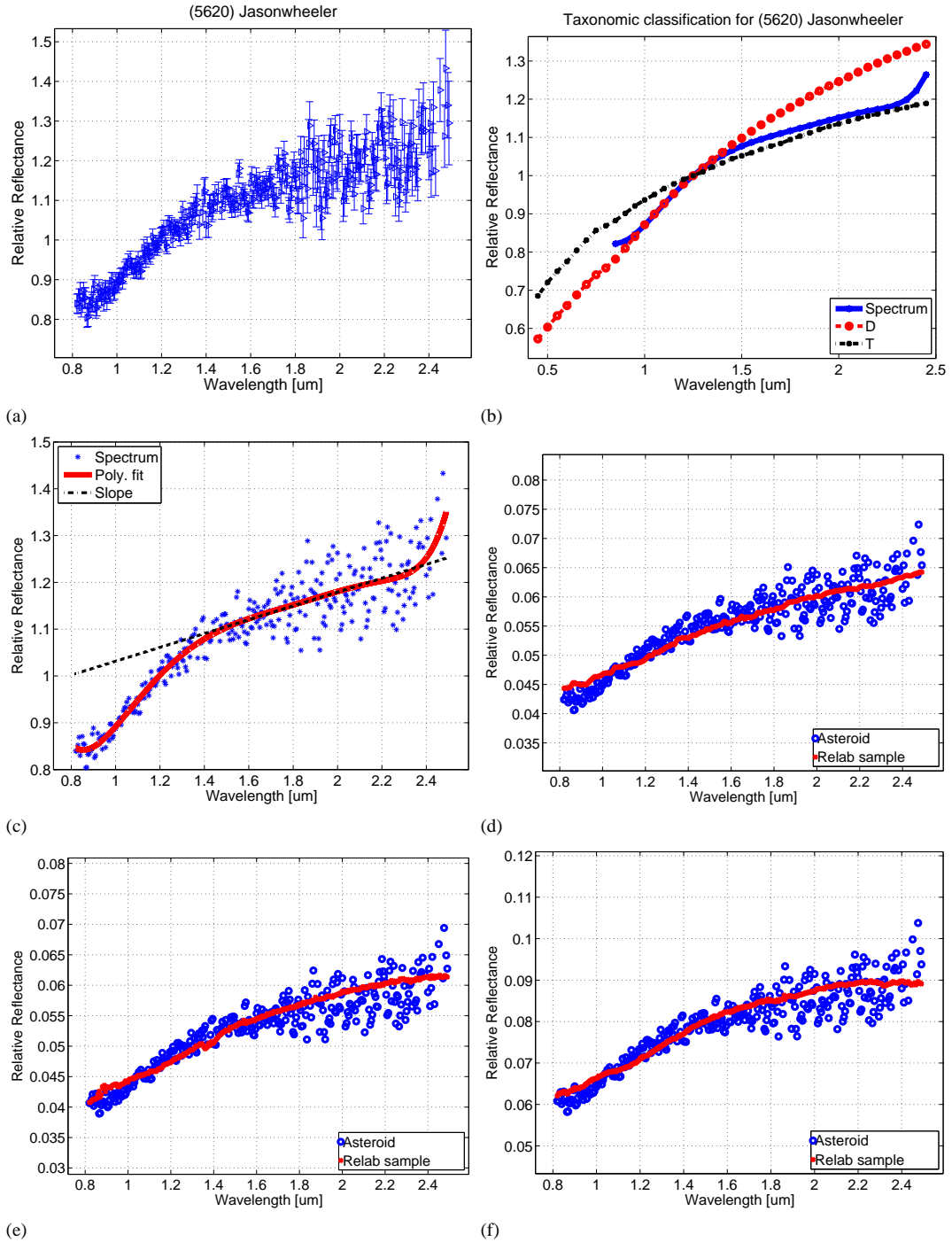


Figure 6.7: The NIR spectrum of (5620) Jasonwheeler; b) a polynomial fit for the spectrum of (5620) Jasonwheeler compared with the theoretical spectra of D and T types; c) estimation of thermal flux in the spectrum of (5620) Jasonwheeler - the dashed line indicates where a linearly extrapolated continuum would fall, the solid line shows the presence of thermal flux; d), e), f) the reflectance spectrum of (5620) Jasonwheeler and the closest three matches resulting from meteorite comparison: the CM2 carbonaceous chondrite Mighei/Meghei, the CM2 carbonaceous chondrite Cold Bokkeveld, and the CM2 carbonaceous chondrite ALH84029 [Popescu *et al.*, 2011].

125 μm . This fit suggests that the asteroid might be covered by a fine regolith layer.

By fitting the spectrum (Fig. 6.7c) with an eighth order polynomial function, it can be observed an excess of flux after 2.2 μm that cannot be explained by the general trend in the spectral region 1.4 - 2.2 μm and its taxonomical classification. Even if the level of noise is relatively important, it can be assumed that this feature is caused by asteroid thermal emission. Following Rivkin *et al.* [2005], I calculated the "thermal excess" parameter that describes this phenomenon:

$$\gamma = \frac{R_{2.5} + T_{2.5}}{R_{2.5}} - 1 = 0.092 \pm 0.0420 \quad (6.1)$$

where $R_{2.5}$ is the reflected flux at 2.5 μm and $T_{2.5}$ is the thermal flux at 2.5 μm . This value agrees with the geometrical albedo $p_v = 0.094$ for an asteroid at a 1.345 AU distance from the Sun and a phase angle of 20° [Rivkin *et al.*, 2005]. This value also agrees with the result obtained from mid-IR observations by Mueller *et al.* [2011].

Taking into account its dynamical parameters and that D and T types are considered to be of a primitive composition, it can be concluded that this object is very interesting from the point of view of "in-situ" exploration.

6.3.2 2001 SG286

This is an Apollo type asteroid with an absolute magnitude of 20.9. It is classified as PHA. Its $\Delta V = 5$ km/s makes it a suitable target for a spacecraft mission. Michel & Delbo [2010] estimated its median lifetime as an NEA to be about 22.19 Myr. The mechanism of injection into the NEA population is the secular v_6 resonance, but the 3:1 mean motion resonance with Jupiter could not be entirely excluded [Michel & Delbo, 2010].

On the basis of spectral data in the visible region, Binzel *et al.* [2004a] classified this asteroid as a D-type one. Using an average albedo of 0.09 for D-type asteroids, Binzel *et al.* [2004a] computed a diameter of about 350m for this object.

The object was observed on May 19, 2009 in the NIR for a total time of 480sec, in difficult conditions (considerable differential motion, only a few hours of visibility over three nights, limited atmospheric transparency). The NIR spectrum is reliable only for the spectral interval 0.8-1.7 μm .

The composite V+NIR spectrum was obtained by superposing data in the 0.82-0.9

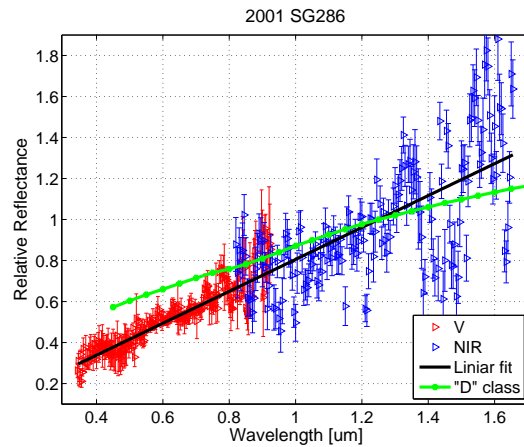


Figure 6.8: Visible [Binzel *et al.*, 2004a] and NIR spectrum of 2001 SG286. A linear fit and the D-type theoretical spectrum are plotted for comparison.

μm spectral interval (Fig. 6.8). The slope parameter for the composite spectrum is $0.7202 \mu\text{m}^{-1}$ (computed for a spectrum normalized to a reflectance value at $1.25 \mu\text{m}$) in agreement with the slope range for D-type taxonomic class.

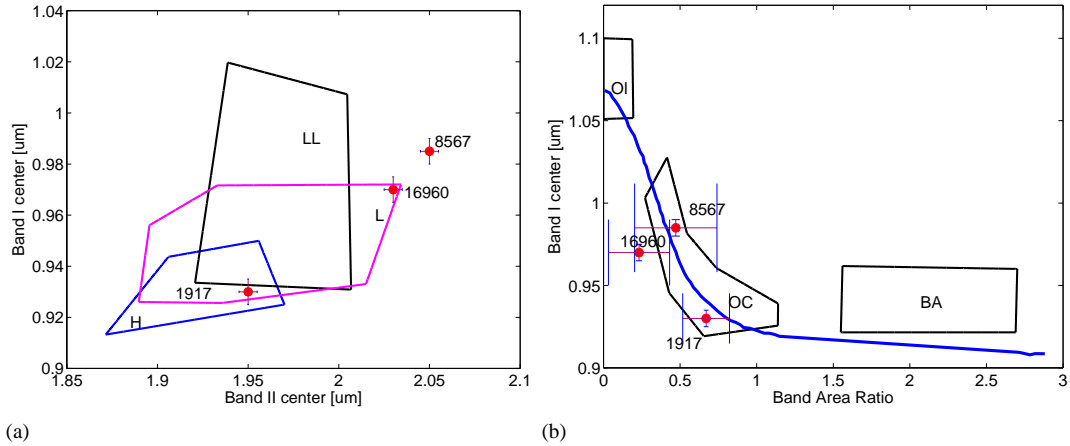


Figure 6.9: a) Wavelength position of the centers of the two absorption bands computed using Cloutis *et al.* [1986a]. The regions enclosed correspond to the band centers computed for the H, L, and LL chondrites, respectively [de León *et al.*, 2010]; b) BAR versus band I centers. The regions enclosed by continuous lines correspond to the values computed for basaltic achondrites, ordinary chondrites(OC), and olivine-rich meteorites(OL) [Gaffey *et al.*, 1993b].

6.4 Discussion

Luu & Jewitt [1990] suggested that the phase angle can affect the spectral slope. This was called "phase reddening" and consists of an increase in the spectral slope (reddening of the spectra) with the phase angle. Some studies have been performed based on laboratory measurements [Gradie & Veverka, 1986] and during the approach to (433) Eros by the NEAR spacecraft [Veverka *et al.*, 2000]. However, it should also be reminded the result mentioned in Binzel *et al.* [2004b] regarding a study conducted at MIT for which no correlation was found between the phase angle and the spectral slope for the ground-based asteroid reflectance spectra.

During the observing runs of these NEAs, all the asteroids were observed at phase angles as small as possible. Owing to this constraint, we [Popescu *et al.*, 2011] succeeded in observing only six objects at a phase angles between 17° and 30° (Table 6.2). The observations of (1917) Cuyo and (188452) 2004 HE62 were at a phase angle around 60° (Table 6.2).

Assuming similar surface mineralogies, the influence of phase angle on spectral slope is unclear from our measurements. For (1917) Cuyo, a high spectral slope was obtained, but for (188452) 2004 HE62 the computed spectral slope is comparable to the spectral slope of (8567) 1996 HW1 and (16960) 1998 QS52, which were measured at phase angles smaller than 30° (Table 6.5). Considering the trend of S-class objects, the reflectance value at $1.25 \mu\text{m}$ is higher than the reflectance value at $0.55 \mu\text{m}$, thus the comparison of slopes is correct. Therefore, no

Table 6.5: Slope and C_s parameter for the S-type objects studied in this article. The calculation was made by normalization of spectra to $0.55 \mu\text{m}$. Objects marked with (*) are normalized to $1.25 \mu\text{m}$ (only for NIR part).

Object	Slope(μm^{-1})	$C_s(\mu\text{m})$
(1917) Cuyo	0.5086	-0.484
(8567) 1996 HW1	0.2245	-0.258
(16960) 1998 QS52	0.1126	-0.149
(188452) 2004 HE62(*)	0.1167	-0.377
2010 TD54(*)	0.0620	-0.223

correction has been applied for this presumed effect of phase reddening.

Several NIR spectra for the asteroids (1917) Cuyo, (8567) 1996HW1, and (16960) 1998 QS52 were obtained by the MIT-UH-IRTF Joint Campaign for NEO Spectral Reconnaissance. However, a variation in spectral slope between the spectra of the same object was observed. Similar spectral variations in the NIR spectrum of a NEO was previously reported by de León *et al.* [2011b]. The asteroid (8567) 1996HW1 was observed five times, at phase angles between 20° and 55° . In this case, a variation in the spectral slope with phase angle was observed (i.e. the spectrum is redder for larger phase angles). While this object is not well-known in terms of spin axis and shape, it is difficult to draw any conclusions about the first order dependence of the slope on phase angle. A surface dichotomy and degrees of space weathering could compete with this effect.

The S-types objects have widely varying spectral slopes (Table 6.5), which is a general conclusion for the asteroids belonging to this complex [DeMeo *et al.*, 2009]. In the Bus-DeMeo taxonomy, the objects in the S-complex with a slope larger than $0.25 \mu\text{m}^{-1}$ receive the notation 'w' added to their type as an indication that they may be affected by space weathering effects. This is the case for (1917) Cuyo.

Although space weathering may occur on all asteroids, many types lack strong spectral-band contrasts that ensure that weathering effects are easily detectable [Clark *et al.*, 2002]. S-class asteroids are significantly reddened compared with their presumed meteorite analog, and this difference can be explained by space weathering phenomenon [Vernazza *et al.*, 2008]. This process may be the result of dust impacts and solar wind sputtering on the surface of atmosphereless bodies and cause a reddening of the spectral slope, a decrease in spectral absorption intensities, and a diminishing of albedo [Fornasier *et al.*, 2003].

An important concept in understanding space weathering processes is the development and accumulation of submicroscopic single-domain metallic Fe (4-30nm), produced in the space environment by a reduction of FeO in minerals. Referred to as nanophase reduced iron - " $npFe^0$ ", these are formed through the fractional processes that occur during ion-particle sputtering, vapor deposits from energetic micrometeorites impacts, or both. As more " $npFe^0$ " accumulates, the entire continuum becomes redder until it is almost linear through to the near-infrared region. With small amounts of " $npFe^0$ ", reddening of only the visible region of the spectra occur [Pieters *et al.*, 2000].

Table 6.6: Computed parameters from the Cloutis *et al.* [1986a] model applied to the V+NIR spectra of (1917) Cuyo, (8567) 1996 HW1, and (16960) 1998 QS52. The estimation error for band centers (BI, BII) is ± 0.005 .

Object	BI (μm)	BII (μm)	BAR	OPX (%)
(1917) Cuyo	0.93	1.95	0.670 ± 0.1526	33.28
(8567) 1996 HW1	0.99	2.06	0.485 ± 0.2687	25.50
(16960) 1998 QS52	0.97	2.03	0.232 ± 0.1996	14.94

A space weathering model has been applied for S-type objects. For two of the asteroids, (188452) 2004 HE62 and 2010 TD554, the models imply that the iron content ambiguity changes the best analog among meteorite samples. Thus, the best mineralogical analog will always be an OC meteorite, the same petrologic type, but the spectra for a sample containing Fe will be different. This could be explained in the following terms: highly curved continua occur for samples with small amounts of $npFe^0$, and the more linear continua occur for samples with large amounts of $npFe^0$ [Pieters *et al.*, 2000].

A quantitative comparison between the reflectance properties of (1917) Cuyo, (8567) 1996 HW1, and (16960) 1998 QS52 (since for these objects both visible and NIR data are available) and potential meteorite analogs could be made with the parameters computed from the model of Cloutis *et al.* [1986a]. The values of these parameters are given in Tabel 6.6. Plotting Band I center versus the BAR [Gaffey *et al.*, 1993b], it can be found that all three objects are located in the ordinary chondrite region (Fig. 6.9). (1917) Cuyo and (16960) 1998 QS52 are under the olivine-orthopyroxene mixing line, while (8567) 1996 HW1 is above the olivine-orthopyroxene mixing line.

Another comparison was made by plotting the Band I center versus the Band II center (Fig. 6.9). Considering the results of de León *et al.* [2010], I found that (1917) Cuyo is in the region of OC -H meteorites, while 16960 is in the region of OC -L meteorites. (8567) 1996 HW1 is outside the enclosed areas, between the regions for L and LL chondrites.

The statistical interpretation of the results agrees with the results obtained by comparison to Relab meteorite spectra. The measured parameters are direct indications of a spectrum's basic properties - revealing their distributions without making any assumptions about their underlying mineralogy [Vernazza *et al.*, 2008].

Spectral properties of Main Belt Asteroids

This chapter describes the spectral properties of six Main-Belt asteroids. The choice to study these objects was made based on the fact that they showed some peculiar physical properties. Thus, (9147) Kourakuen is a vestoid which dynamically could not belong to Vesta family, (854) Frostia is a binary asteroid, (1333) Cevenola and (3623) Chaplin are two asteroids with large amplitude lightcurves, and two asteroids for which it was reported to have pairs (10484) Hecht and (31569) 1999 FL18.

The observations presented here are part of the two long term programs which aim to study physical properties of vestoids and of asteroids pairs. The NIR spectra were acquired using the NASA telescope IRTF equipped with the spectro-imager SpeX. The spectra were analyzed applying the techniques described in chapter 4 and chapter 5.

I found that (9147) Kourakuen, (854) Frostia, (10484) Hecht and (31569) 1999 FL18 show the characteristics of V-type objects, while (1333) Cevenola, (3623) Chaplin belong to S-complex. The taxonomic classification, the comparison with the meteorite spectra from the Relab database and the mineralogical analysis converged to the same solutions for each of these objects, allowing to find important details for the chemical compositions.

Although more than 300,000 asteroids have well established orbital behavior, less than 3% of these have some of their compositional properties determined. To point out the scientific importance of these studies, it can be recalled that the majority of the asteroids have orbits in the region between 2.2 and 3.3 AU. This is the region that defines the transition between terrestrial and giant planets.

The majority of knowledge regarding compositional characterization is mainly due to three large surveys: the Eight-Color Asteroid Survey - ECAS [Zellner *et al.*, 1985], S³OS² [Lazzaro *et al.*, 2004], and the most fruitfully Small Main-Belt Spectroscopic Surveys (SMASSI, SMASSII, SMASS-IR) - Bus & Binzel [2002b].

The analysis of the spectra of six Main Belt asteroids which have some remarkable physical properties is made in the context of previously published physical and dynamical properties of these asteroids. Table 7.1 summarizes some parameters of the considered sample.

7.1 Log of observations

The spectral observations were carried out in two sessions: March 2007 and November 2011 using the 3.0 m NASA IRTF telescope located at Mauna Kea - Hawaii. The SpeX instrument

Table 7.1: Some characteristics of our observed MBAs: semi-major axis, eccentricity, inclination, absolute magnitude (H), and orbital period.

Object	a	e	i	Orbit. Period	H
	AU		°	Days	Mag.
(9147) Kourakuen	2.19161	0.106186	5.816	1185.06	13.4
(854) Frostia	2.36832	0.172996	6.091	1331.25	11.8
(1333) Cevenola	2.63344	0.133589	14.641	1560.93	11.5
(3623) Chaplin	2.85105	0.086814	3.071	1758.35	11.9
(10484) Hecht	2.32087	0.079053	5.729	1291.44	13.7
(31569) 1999 FL18	2.31427	0.123171	6.402	1285.94	14.0

Table 7.2: Log of asteroids observations. Asteroid designation, date of observation with the fraction of the day for the mid time of the observation, apparent magnitude, phase angle, heliocentric distance, the airmass at the mean UT of each observation, the integration time for each spectrum (ITime), and the number of cycles are presented.

Asteroid	Date	V	Φ	r	Airmass	ITime	Cycles
	UT	Mag.	°	UA		sec	
(9147) Kourakuen	2011-11-15.357	16.1	20.1	1.9596	1.116	120	16
(854) Frostia	2007-03-13.487	14.9	3.6	2.3484	1.070	120	10
(1333) Cevenola	2007-03-12.549	15.6	13.8	2.6696	1.035	120	24
(1333) Cevenola	2007-03-13.575	15.6	14.5	2.6710	1.031	120	10
(3623) Chaplin	2007-03-12.378	17.1	14.7	3.0366	1.085	120	18
(3623) Chaplin	2007-03-13.267	17.2	14.9	3.0371	1.018	120	20
(10484) Hecht	2011-11-16.420	17.0	16.3	2.1986	1.060	120	6
(31569) 1999 FL18	2011-11-16.330	17.1	19.9	2.0294	1.040	120	12

was used in low-resolution mode for these sessions. The observations were made in the 0.8-2.5 μm spectral interval. A 0.8 arcsec wide and 15 arcsec length slit, oriented North-South, allowed simultaneous measurements of the object and sky. The nodding procedure described in chapter 3 was applied. The observing conditions and parameters are given in Table 7.2.

The automatic guiding mode of the telescope was used for these observation. Since, for the main belt asteroids the relative speed ($\Delta\text{RA}/\Delta t$, $\Delta\text{DEC}/\Delta t$) is low, it does not impose difficulties for the differential tracking. In the moment of observations our objects had speed bellow 0.6''/min.

The apparent magnitude of the asteroids varies depending on the relative position with the Earth and the Sun. In the case of main belt asteroids this apparent magnitude variation could up to four magnitudes. The asteroids described here were observed when they were close to their brightest apparent magnitudes (at oppositions - Table 7.2).

Another constraint that should be taken into account when scheduling the observations is the airmass. In order to obtain good SNR for the spectra, I managed to observe all objects at an airmass smaller than 1.12 (zenith angle below 25 °) - Table 7.2.

The integration time for each image was 120 second. Depending on the weather conditions, and considering a basic SNR evaluation of the data, a different number of images for each object were taken.

Each observed asteroid was preceded by observations of solar analogs located in the vicinity.

Table 7.3: Solar analogs used for data reduction, their airmass at the moment of observations and their relative distance to the object.

Asteroid	Solar Analogue	Air mass	Distance [°]
(9147) Kourakuen	HD940	1.280	11.5
(854) Frostia	G104-335	1.070	11.3
(1333) Cevenola	HD127913	1.055	10.1
(1333) Cevenola	HD127913	1.031	10.2
(3623) Chaplin	HD73708	1.025	6.6
(3623) Chaplin	HD73708	1.018	6.6
(10484) Hecht	Land115-271	1.200	19.5
(31569) 1999 FL18	Land115-271	1.200	15.1

The following stars were observed and used as solar analogs: HD940, G104-335, HD127913, HD73708 and L115-256 (Table 7.3). Our choice was to observe the solar analogue as close as possible to the target (bellow 20°). The differential airmass between the asteroid and the standard was usually restricted to less than 0.16. The stars were chosen using the tool available on IRTF website¹. An exception was made for (10484) Hecht and (31569) 1999 FL18, where the data reduction were performed using L115-271, commonly used in NIR spectral measurements.

G104-335, HD127913, HD73708 are G2V type, while HD940 is a K0 star [Høg *et al.*, 2000, Cutri *et al.*, 2003, Landolt, 1992]. HD 940 was chosen as trade-off between the spectral type, airmass, and its relative distance to (9147) Kourakuen.

The data reduction followed the procedure described in chapter 3. For the computation of the final reflectance (ratio between the asteroid spectrum and the star spectrum) is considered the similar dynamic regimes of the detector [Vacca *et al.*, 2004, Rayner *et al.*, 2003].

7.2 (9147) Kourakuen - a V-type asteroid outside Vesta family

One of the most interesting asteroid family is the one of (4) Vesta. Located in the inner asteroid belt, the origins of this family is in a collision event that excavated a large crater in the surface of asteroid (4) Vesta [Asphaug, 1997]. The presence of such a crater in the south hemisphere of the asteroid has been confirmed by HST images [Thomas *et al.*, 1997] and recently by NASA's Dawn spacecraft. This crater, called Rheasilvia, has 505 Km in diameter and is one of the largest craters in the Solar System. The latest estimates indicate that the cratering event occurred at least 1.2 Gyr ago [Carruba *et al.*, 2005].

(4) Vesta is particularly interesting because it is the only large asteroid showing a basaltic crust [McCord *et al.*, 1970]. Basaltic asteroids are believed to derive from bodies whose interiors reached the melting temperature of silicate rocks and subsequently differentiated [Gaffey *et al.*, 2002]. Thus, (4) Vesta is a differentiated object with a basaltic crust and exposed mantle material [Gaffey, 1997] that survived during the Solar System history. It is considered

¹http://irtfweb.ifa.hawaii.edu/cgi-bin/spex/find_a0v.cgi

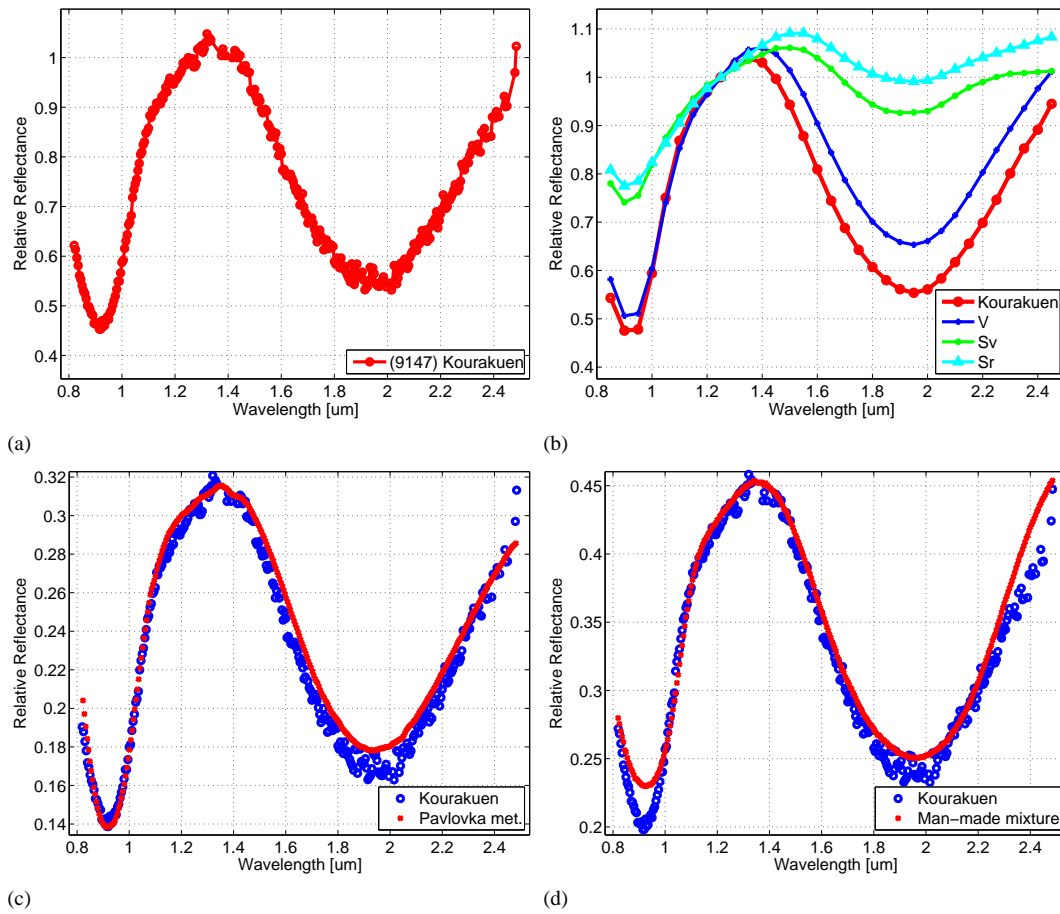


Figure 7.1: a) Spectrum of (9147) Kourakuen normalized to $1.25 \mu\text{m}$; b) a polynomial fit of the spectrum of (9147) Kourakuen compared with the theoretical spectra of V, Sv, and Sr types; c) the comparison between the spectrum of (9147) Kourakuen and the spectrum of a sample from Pavlovka, d) the comparison between the spectrum of (9147) Kourakuen and the spectrum of a mixture of Pyroxene-Hypersthene-Plagioclase-Bytownite-Ilmenite.

as *the smallest terrestrial planet* [Keil, 2002]. While (4) Vesta was the first known asteroid presenting a basaltic crust, in the last years an increasingly large number of small asteroids with a similar surface composition have been discovered [de Sanctis *et al.*, 2011a].

Vesta's density was derived from the estimation of its mass [Hilton, 2002] and shape [Thomas *et al.*, 1997]. The computed values of the bulk density span the range $3,000\text{--}4,300 \text{ kg/m}^3$. This interval is supported also by models of internal structure of large differentiated bodies. Ruzicka *et al.* [1997] calculated the density of silicate fraction in Vesta-like asteroids, assuming an average value of the bulk density of $3,540 \text{ kg/m}^3$. They conclude that Vesta could be modeled with an eucritic/diogenitic crust and an olivine mantle for a metallic core between zero and 25% of the total mass of the asteroid. In this case, the density of the crust could not be less than $3,000 \text{ kg/m}^3$.

Based on spectroscopic behavior and dynamical consideration from the main-belt through the resonances 3:1 and ν_6 resonances [Binzel & Xu, 1993], Vesta and the vestoids are supposed

to be at the origin of Howardite-Eucrite-Diogenite meteorites. The structure of HED meteorites is very close to mafic materials. Thus, the parent body of HED meteorites are supposed to have experienced volcanism and metamorphism in the process of formation during the early Solar System. The parent body of Vesta and vestoids underwent accretion, total melting, fractionation, and differentiation during the first few million of years of Solar System formation [Keil, 2002].

The V-type asteroids are objects with reflectance spectra similar to the asteroid (4) Vesta and to HED meteorites. These objects smaller in size than Vesta (commonly called 'vestoids') present spectral properties similar to this asteroid. Partly, the vestoids are identified as fragments of Vesta, a result of the catastrophic collision who excavated material from the crust and the mantle [Binzel & Xu, 1993] of (4) Vesta.

The V-type asteroids are mainly located in the population represented by the Vesta family, and is considered to be the reservoir of HED meteorites. However, basaltic asteroids, not yet considered members of Vesta family, are also located in the vicinity of the family [Florczak *et al.*, 2002, Duffard *et al.*, 2004]. Data on V-type asteroids such as (1459) Magnya are reported at different semi-major axis [Lazzaro *et al.*, 2000, Roig & Gil-Hutton, 2006, Duffard & Roig, 2009] and in the NEA population [Binzel *et al.*, 2002]. This picture of V-type asteroids supports the hypothesis of formation of several objects with basaltic crust in the Main-Belt.

At present, hundreds of asteroids are classified as potentially V-type bodies, based on the new photometric investigations. According to dynamical considerations some of these objects possibly belong to the Vesta-family, while others seem to have no clear connection. Ground-based observations allow to investigate the spectral properties and hence the mineralogical composition of such asteroids.

(9147) Kourakuen is a main belt asteroid with an estimated diameter of 5.1 Km. Having the semi-major axis $a = 2.19$ AU, eccentricity $e = 0.108$, and inclination $i = 6.892^\circ$, this object could not belong to Vesta family considering the dynamical criteria. However, its SDSS (Sloan Digital Sky Survey) colors [Roig & Gil-Hutton, 2006] suggests a surface composition similar to (4) Vesta (a V-type object). The cause could be a higher ejection velocity and a subsequent dynamical evolution.

The spectrum of (9147) Kourakuen (Fig. 7.1a) has the characteristics of a V-type asteroid [Popescu *et al.*, 2012b]. In Bus-DeMeo taxonomy, V-type asteroids are characterized by a very strong and very narrow $1\ \mu\text{m}$ absorption feature and a strong $2\ \mu\text{m}$ absorption feature [DeMeo *et al.*, 2009]. M4AST classify undoubtedly this spectrum as V-type. This agrees the classification made via MIT-SMASS online tool. A similar result was found by de Sanctis *et al.* [2011a] using a more noisy spectrum. The next two matches (the program always returns the first three matches), Sv and Sr types have a larger matching error (Fig. 7.1b).

The solution given by all four methods for comparison with laboratory spectra shows that the

spectrum of 9147 Kourakuen is almost identical with the spectrum of a sample from Pavlovka meteorite (Fig. 7.1c). This meteorite sample is of type achondrite howardite already studied so far [Olsen *et al.*, 1990, Labotka & Papike, 1980]. The bulk composition of the chondrules from this meteorite contains SiO₂ (50.1%), MgO(23.7%), FeO(15%), Al₂O₃(6.2%), CaO(3.8%) [Olsen *et al.*, 1990].

Other meteorite laboratory spectra similar to the spectrum of (9147) Kourakuen are those of the meteorites Roda (Achondrite Diogenite), Le Teilleul (Achondrite, Howardite) and Kapoeta (Basaltic HED Howardite). The first fifty solutions that matched our spectrum are HED (Howardite Eucrite Diogenite) meteorites. These are basaltic meteorites believed to result from large asteroids that melted to form a metallic core and basaltic magma after the formation.

Another solution of this application is a spectrum of a man-made mixture of Pyroxene Hypersthene Plagioclase Bytownite Ilmenite (Fig. 7.1d). This man-made mixture reproduces quite well the natural composition of volcanic rocks or melting rock of volcanic beds, and is consistent to the V-type mineralogical composition of asteroids. In all laboratory spectra proposed by M4AST to match this asteroid spectrum, the majority corresponds to HED achondrite meteorites.

While the standard deviation measures the overall matching between the two spectra, the correlation coefficient finds those spectra for which the spectral features positions and shapes are very close. In the case of spectrum of (9147) Kourakuen, a very high correlation coefficient (more than 0.99) characterize the first matching solutions (Table 7.4).

Since only the NIR part of the spectrum is available, we can only compute the band minima. The high signal to noise ratio of this spectrum ensures that there is a small error in computing the band minima. The first minimum is at $0.9217 \pm 0.0005 \mu\text{m}$ and the second minimum is at $1.9517 \pm 0.0062 \mu\text{m}$, which imply a band separation of $1.03 \mu\text{m}$. The band separation provides a way of estimating the iron content. Cloutis *et al.* [1990] noted that the band separation is a linear function of the BII minimum for orthopyroxenes and that both parameters increase with the iron content. If we refer to the relation obtained by de Sanctis *et al.* [2011b], the parameters that we found match their formula $y = 0.801 * x - 0.536$, where y is the band separation and x is the BII minimum. These parameters correspond to an iron content of around 40 wt%. However, the laboratory calibrations suggest that the correspondence is true for a number of low aluminum orthopyroxenes but invalid for mixtures of olivine, metal, and both ortho- and clino-pyroxenes [de Sanctis *et al.*, 2011b].

Concluding this section, based on an accurate near-infrared spectrum of the asteroid (9147) Kourakuen a description of its surface composition was made. The comparisons with meteorites spectra which revealed a spectral matching with HED type meteorites (in particular with the spectrum of Pavlovka meteorite) agrees and is complementary to the taxonomical classification and to the mineralogical solution found.

Table 7.4: Summary of results obtained by matching the main belt asteroids spectra with spectra from Relab database. The most relevant matches are presented. The comparison coefficients are given together with some details related to the laboratory samples.

Spectrum	std. dev.	corr. coef.	Meteorite/Sample	Sample ID	Type
9147	0.01884	0.99477	Pavlovka	MR-MJG-094	Achondrite(AHOW)
	0.02244	0.99207	Mixture	SC-EAC-039	Man-made
	0.02731	0.99048	Roda	MR-MJG-099	Achondrite(ADIO)
854	0.01894	0.98847	"ALHA76005,85"	MB-TXH-066-A	HED Eucrite
	0.01917	0.98842	"Y-793591,90"	MT-TXH-043-A	HED Eucrite
	0.02396	0.98332	"ALH-78132,61"	MB-TXH-072-A	HED Eucrite
1333	0.02065	0.97005	Saratov	MR-MJG-046	OC/L4
	0.02248	0.97188	Hamlet #1	MR-MJG-069	OC/LL4
	0.02413	0.95487	Paranaiba	MB-CMP-010-D	OC/L6
1333 De-reddened	0.01774	0.93893	Denver	TB-TJM-072	OC/L6
	0.02841	0.94397	Hamlet #1	MR-MJG-069	OC/LL4
3623	0.04344	0.83962	Gabbro 50S	RG-CMP-057	Rock/Igneous Plutonic
	0.04334	0.83360	14321,150P	LS-JBA-097	Rock/Polymict Breccia
3623 De-reddened	0.03296	0.79520	Fayetteville	MB-CMP-007-L	OC/H4
	0.04093	0.79900	Gabbro Ns	RG-CMP-017	Rock/Igneous Plutonic
1048	0.08761	0.93656	PYX:OLV:PLG:ILM	SC-EAC-045	Man - Made
	0.09487	0.93345	Mixture	SC-EAC-060	Man - Made
31569	0.04156	0.96088	Pasamonte	MR-MJG-090	HED Eucrite
	0.04112	0.95996	Mineral	SB-RGB-001	Pigeonite
	0.04433	0.95991	Macibini Clast 3	TB-RPB-027	HED Eucrite

7.3 A binary asteroid: (854) Frostia

The number of known multiple systems among asteroids has increased significantly in recent years. In the past, the binarity and multiplicity of asteroids was suggested by several authors [van Flandern *et al.*, 1979] based on occultations of stars (for example in the articles of Binzel [1978]², and Donnison [1979]³) or photometry [Tedesco, 1979, Binzel & van Flandern, 1979, Dunlap & Gehrels, 1969]. These observational facts were at the origin of theoretical problems related to spin evolution and stability [Wijesinghe & Tedesco, 1979, Zappala *et al.*, 1980, Leone *et al.*, 1984].

Analytical and numerical simulations of catastrophic collisions among small bodies, using several hypothesis, are published regularly by several teams [Dell'Oro & Cellino, 2007, Durda *et al.*, 2004, Holsapple & Michel, 2008]. This topic remains open despite an important acquisition of knowledge from laboratory experiments and numerical tests. The most important conclusion of these works is that elongated shapes, binarity or multiplicity could be explained for both large objects (≈ 100 km in size) and relatively small ones (kilometer-size asteroids). For instance, a *doublet system* is a binary system where both bodies are of nearly equal sizes. Their origin is not well understood, but several such systems have been reported (ex: (90) Antiope, (617) Patroclus, (69230) Hermes, 1998 WW31). Theoretical studies concerning the

²The article also presents historical facts of occultation of stars by asteroids.

³This satellite was not confirmed by direct imaging. [Storrs *et al.*, 1999]

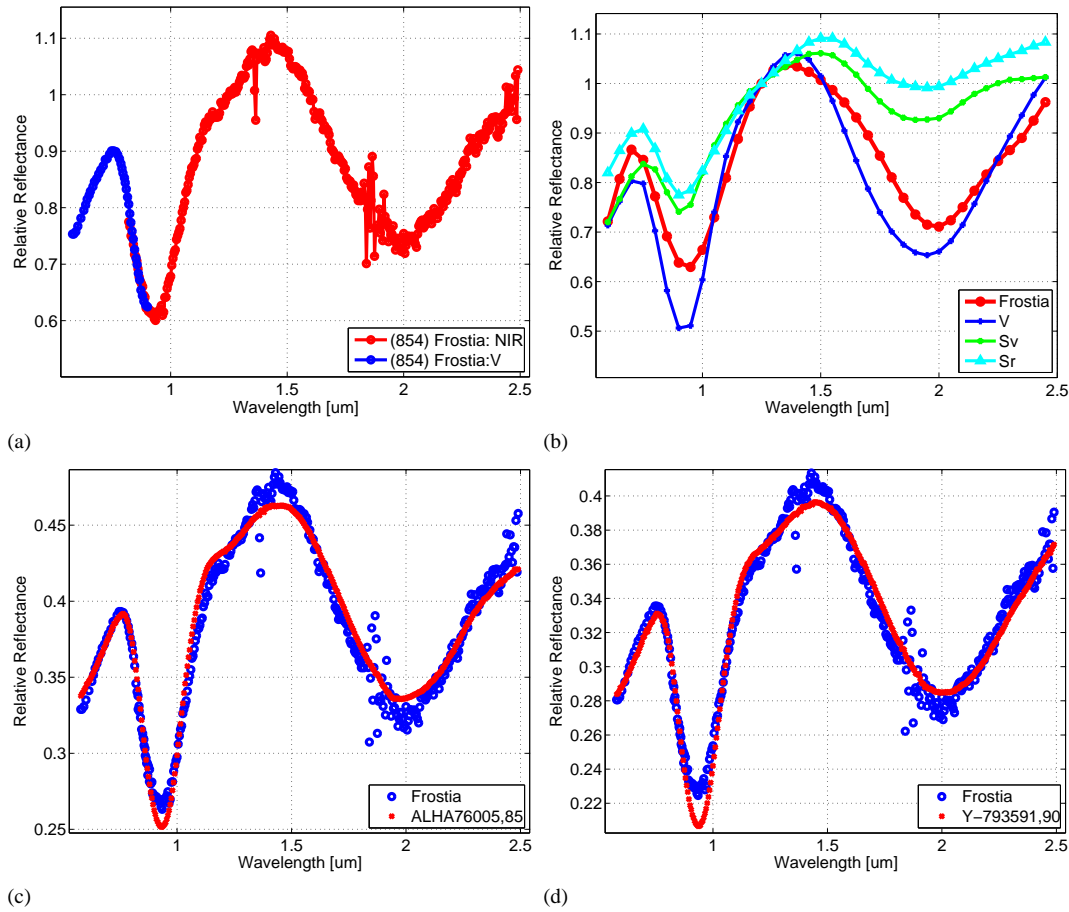


Figure 7.2: a) The visible and NIR spectrum of (854) Frostia; b) A polynomial fit for the spectrum of (854) Frostia compared with the theoretical spectra of V, Sv and Sr types; c) the comparison between the spectrum of (854) Frostia and the spectrum of a sample from "ALHA76005,85" meteorite; d) the comparison between the spectrum of (854) Frostia and the spectrum of a sample from Y – 793591,90 meteorite.

movement of components around their center of mass can be validated by observational results (obtained for instance using adaptive optics); results of their dynamics will be constrained by the physical model which takes into account shape, bulk density, and internal properties of the components. Furthermore, the interaction between a dynamical and a physical model allows the derivation of the most probable configuration of the system (in terms of separation of components, orbital parameters, shapes and densities).

(854) Frostia is a Main-Belt asteroid with an absolute magnitude $H = 11.8\text{mag}$. Its semi-major axis is $a = 2.36832\text{AU}$ (Table 7.1). This asteroid was observed intensely in photometry [Behrend *et al.*, 2006] by amateurs and professional astronomers⁴. (854) Frostia is a slow rotator with a synodic period of 37.728hrs. Its regular lightcurve with an amplitude of 0.33mag presents, for short periods of time, important attenuation, of about 0.7 – 0.8mag. The large magnitude is very well explained by mutual eclipse/occultation events for an object with two

⁴http://obswww.unige.ch/~behrend/page_cou.html

components of comparable size. Unfortunately, no physical ephemerides of Frostia are known to have a precise timing of possible mutual phenomena of this system. Nevertheless there is little chance for a geometry allowing mutual phenomena at the time of our observations.

Based on a physical model of a double system, Behrend *et al.* [2006] calculated a bulk density of 750 - 1,020 kg/m³. They explain such a low density value by a possible C-type asteroid with a high macro-porosity of about 45 %.

Sloan Digital Sky Survey (SDSS) colors (Ivezić *et al.* [2001])⁵ of this object were also reported. These data show large variations in color. It is important to note that the $v - i$ color is greater than the $v - z$ one⁶, which suggest the presence of absorption band around 1 μm .

Visible spectroscopy of Frostia was reported by Alvarez-Candal *et al.* [2006]. These results are in agreement with SDSS colors and the authors classified this asteroid in the V-taxonomic class.

NIR spectrum of (854) Frostia was obtained on March 13, 2007. The total integration time of 40 min allows an accurate spectrum with the S/N of 120. I joined the visible spectrum from Behrend *et al.* [2006] with our data in NIR region (Fig. 7.2a). The analysis was made on the composite V+NIR spectrum. This spectrum likely represents the asteroid globally, being a first characterization of the asteroid's mineralogy.

The spectrum of (854) Frostia reveals large and deep absorption bands around 1 and 2 μm . In Bus-DeMeo taxonomy the V+NIR spectrum is typical of V-type asteroids [DeMeo *et al.*, 2009], similar to the asteroid (4) Vesta. The next two matches returned by M4AST are Sv and Sr types but these types have larger matching error (Fig 7.2b).

(854) Frostia was not included in the family of (4) Vesta by Zappala *et al.* [1995]. The location of (854) Frostia inside the Main-Belt is very similar to that of Vesta family in semi-major axis and inclination and may justify its membership to the same clan. Frostia's eccentricity of 0.17 is slightly over the greater boundary (of 0.12) of Vesta family. This case is not particular while other V-type asteroids were already reported in the inner part of the Main Belt, relatively close to the Vesta family [Duffard *et al.*, 2004].

In the assumption of (854) Frostia as a fragment of Vesta's crust, a value of its density around 3,000 kg/m³ seems to be reasonable. The value calculated by Behrend *et al.* [2006] (around 1,000 kg/m³) is very difficult to explain even if an unrealistic porosities of 75% in a rubble-pile structure is assumed. In fact, large porosities for small fragments of large differentiated bodies are not realistic while the self-gravitation tendency is to decrease the volume of empty space inside the object. Behrend *et al.* [2006] inferred a C-type asteroid by analogy with the asteroid (90) Antiope. It is difficult to reconcile the C and V taxonomic classes while the objects experienced different temperatures in their history.

Descamps [2010] published recently a refined study of binary systems by accounting in-

⁵<http://sbn.psi.edu/ferret/>

⁶Sloan Digital Sky Survey was obtained using five broad band filters, namely u, g, r, i, z centered to 3,551, 4,686, 6,165, 7,481, and 8,931

homogeneous bodies with ellipsoidal shapes. This model allows the simultaneous fit of grain density and the bulk porosity. The author calculated a grain density of $(2,790 \pm 380) \text{ kg/m}^3$ in agreement to the one of Vesta-like asteroids, correlated to a bulk porosity of 63% ($\approx 55\%$ of macroscopic porosity + $\approx 8\%$ of microporosity).

For the laboratory spectra proposed by M4AST to match this asteroid spectrum, the majority corresponds to achondrite meteorites, subtype Basaltic HED -Eucrite. This fully agrees with the classification as a V-type asteroid. The first solution given by all four methods for comparison with laboratory spectra shows that the spectrum of (854) Frostia is almost identical with the spectrum of "ALHA76005,85" meteorite. Other relevant solutions of this application are the spectra of samples from Basaltic HED -Eucrite meteorites: "Y – 793591,90", "ALH – 78132,61" (Fig. 7.2c, 7.2d, Table 7.4). Another significant result of the spectral comparison was the fact that the first matches correspond to particulate samples with sizes less than $25 \mu\text{m}$. This suggests that (854) Frostia is covered by fine grains of regolith.

The meteorite number 5 discovered in 1976 in Allan Hills -Antartica ("ALHA76005,85") was study in many papers [Olsen *et al.*, 1978, Simon & Papike, 1983, Miyamoto *et al.*, 1979]. Olsen *et al.* [1978] noted about this meteorite that is a pale gray in color and consists of a finely divided microcrystalline pyroxene rich matrix that contains clastic fragments: white Plagioclase rich rocks, grey clasts of glass, monomineralic fragments of pyroxenes, silica, oxide minerals, sulfides and metal. On a plot of CaO against $\frac{Fe}{Fe+Mg}$, is placed in the middle of the eucrite field.

The mineralogy of (854) Frostia could be refined by taking into account the precise position of the band minima, band centers at 1 and $2 \mu\text{m}$ and the band area ratio (BAR). To estimate these parameters the mineralogical models can be applied [Cloutis *et al.*, 1986a, 1990] using M4AST routines on the composed V+NIR spectrum. The first minimum (BI minimum) is found at $0.9309 \pm 0.0015 \mu\text{m}$, while the BII minimum is located at $2.0049 \pm 0.0046 \mu\text{m}$, implying a band separation of $1.0740 \mu\text{m}$. These parameters fit in the empirical formula $y = 0.801 * x - 0.536$, where y is the band separation and x is the BII minimum. They correspond to an iron content of around 55 wt%, according to the calibrations shown by de Sanctis *et al.* [2011b]

After removing the continuum by considering a linear function for each band it can be found the band centers at $0.9355 \pm 0.0012 \mu\text{m}$ for the first band, respectively $1.9972 \pm 0.0038 \mu\text{m}$ for the second band. In the case of BII, the thermal correction can be computed using the formulas (2) and (4) from Burbine *et al.* [2009]. The value found $0.002 \mu\text{m}$ is closely to the value of the error-bar for BI center, thus its influence can be neglected. The positions of BI and BII centers are relatively similar to those obtained for the asteroid (1459) Magnya [Hardersen *et al.*, 2004]. If these values obtained for Frostia are placed in the context of the pyroxene studies of Adams [1974] and Cloutis & Gaffey [1991] it can be concluded a dominant presence of orthopyroxene on the asteroid surface. The position of the bands place the asteroid near the Eucrite region (see

Fig 10 from Gaffey [1997]).

The spectrum of (854) Frostia presents an inflexion near $1.2 \mu\text{m}$ which is an indication of the presence of feldspar in the basaltic achondrite materials. The mineralogical composition using the pyroxene calibration [Gaffey *et al.*, 2002] suggests the formula $Wo_8Fs_{43}En_{49}$ (with a 4% of uncertainty for wollastonite and ferrosilite). This composition is, within the error-bars, similar to that of (4) Vesta and (1459) Magnya, and similar to that of the asteroid (3269) De Sanctis [Duffard *et al.*, 2004].

The calculated BAR for (854) Frostia was 1.9052 ± 0.08 , in agreement with the basaltic achondrite minerals [Gaffey *et al.*, 1993b]. This ratio gives the relative abundance orthopyroxene vs olivine [Fornasier *et al.*, 2003]: 0.85 %. This fully agrees with the the mineralogical analysis performed above.

7.4 1333 and 3623 - two asteroids with large amplitude lightcurves

The lightcurve of an asteroid is the display of the variation of its magnitude over time. The lightcurve is related to the rotation of an asteroid around an instantaneous axis. In other words, the lightcurve could be interpreted as an observable of the angular momentum for a given object. This variation is primarily due to the shape [French & Binzel, 1989]. The lightcurve could be also due to the albedo variation [Harris & Lupishko, 1989] of the asteroids. The results of observations of lightcurves for asteroids are regularly synthesized in catalogs of lightcurves (for example Lagerkvist *et al.* [1987]).

Several asteroids exhibit large amplitude lightcurves, which remained unexplained until the last decade. Different explanations were proposed for these variations, starting with elongated shaped asteroids and including double and multiple systems of aggregates in a weak self-gravitational field [Cellino *et al.*, 1985].

This section is focused on the spectroscopic results obtained for two asteroids with large amplitude lightcurves. Near-Infrared (NIR) spectroscopic observations for (1333) Cevenola, and (3623) Chaplin are presented. A detailed analysis of their spectra, and the mineralogical models derived for each asteroid are discussed.

7.4.1 (1333) Cevenola

(1333) Cevenola has an absolute magnitude $H = 11.5 \text{ mag}$. The asteroid is placed in the Main Belt, having a semi-major axis $a = 2.63344 \text{ AU}$ and a eccentricity $e = 0.133589$ (Table 7.4). Photometry of this asteroid shows a large amplitude of $0.97 \pm 0.03 \text{ mag}$ and a synodical period of $4.88 \pm 0.02 \text{ hrs}$ [Warner, 2002].

(1333) Cevenola belongs to the Eunomia family [Zappala *et al.*, 1995, Mothé-Diniz *et al.*, 2005]. This family has more than 430 objects [Zappala *et al.*, 1995]. 44 members of Eu-

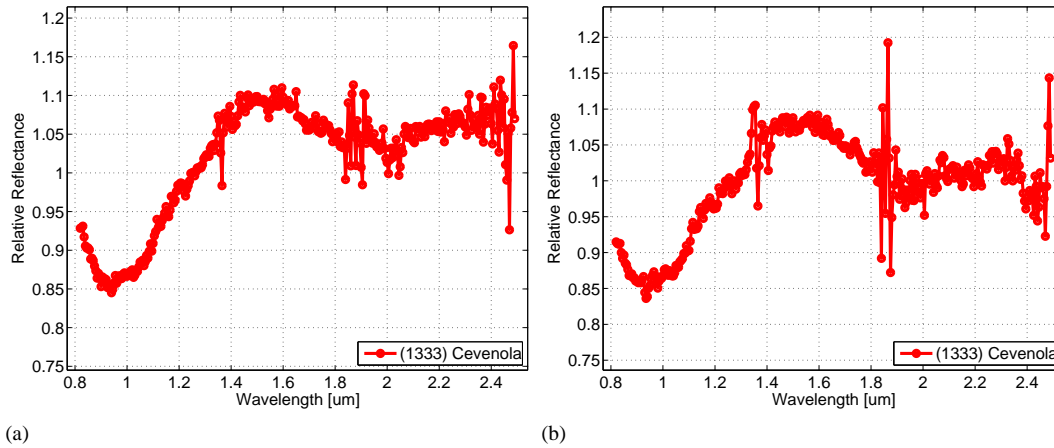


Figure 7.3: The NIR spectra with the error-bars for (1333) Cevenola; a) obtained in March 12, 2007; b) obtained in March 13, 2007. The spectra are normalized to $1.25 \mu\text{m}$.

nomia family (including Cevenola) were studied spectroscopically in the visible region by Lazzaro *et al.* [1999]. Based on the visible spectrum, 41 of them were classified as S-type objects, while three asteroids exhibit flat spectra and were considered as intruders. Considering these samples in the frame of the Bus-DeMeo taxonomy [DeMeo *et al.*, 2009], only three objects are re-observed in the near-infrared region.

The visible spectrum was reported by Lazzaro *et al.* [2004] in the framework of S^3OS^2 survey, and the analysis of spectral data places the asteroid into the S (S_q more precisely) complex. The Eunomia family is actually dominated by objects displaying S -type spectra.

Two NIR spectra were obtained for this asteroid (Fig. 7.3), on two consecutive nights, separated by 24 hours. The spectrum of March 12, 2007 is the result of the combination of individual spectra of 120 seconds each, for the total integration time of 1.4667hrs . The second spectrum was obtained in March 13, 2007 for the total integration time of 40min . Consequently, a S/N of 50 and 20 was estimated. The two NIR spectra are very similar. I made an average spectrum between the two spectra of (1333) Cevenola and I merged with the visible part from S^3OS^2 (Fig. 7.4a).

The SMASS-MIT online tool classifies this spectrum as an S_q type in Bus-DeMeo taxonomy. The S_q type has a wide 1-micron absorption band with evidence of a feature near $1.3 \mu\text{m}$ like the Q-type, except the 1-micron feature is more shallow for the S_q [DeMeo *et al.*, 2009]. Among the solutions proposed by M4AST for taxonomic classification of this spectrum are also the Q and K types. This is due to the fact that the spectrum is not as reddened as for S_q type in the infrared part (Fig. 7.4b). Using the G13 taxonomy [Birlan *et al.*, 1996a], it can be found that this spectrum belongs to S-complex, being in the class 2 of this taxonomy. The class 2 of G13 taxonomy includes asteroids like (7) Iris, (11) Parthenope, (26) Proserpina, (27) Euterpe.

The taxonomic type found for this asteroid spectrum, allows the application of space weath-

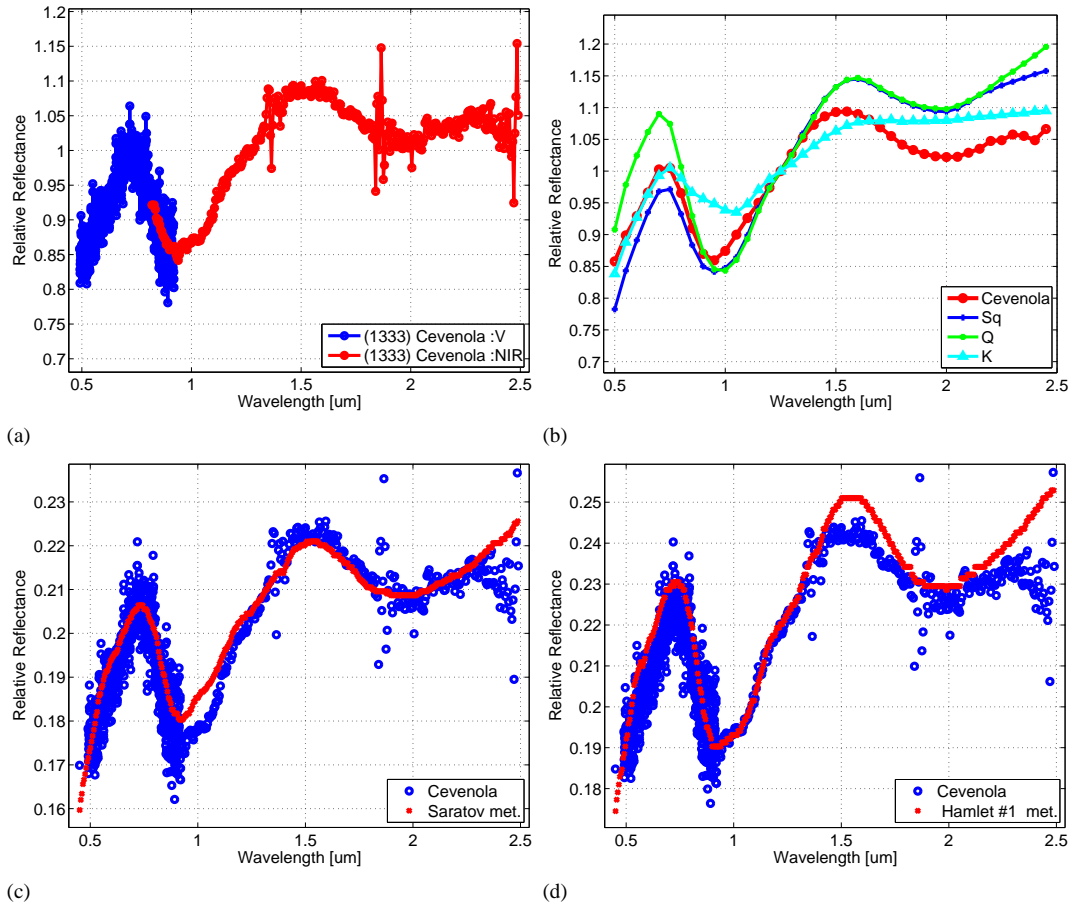


Figure 7.4: a) The visible and the averaged NIR spectrum of (1333) Cevenola; b) A polynomial fit for the V+NIR spectrum of (1333) Cevenola compared with the theoretical spectra of Sq, Q and K taxonomic types; c) the comparison between the spectrum of (1333) Cevenola and the spectrum of a sample from *Saratov* meteorite; d) the comparison between the spectrum of (1333) Cevenola and the spectrum of a sample from *Hamlet#1* meteorite.

ering model proposed by Brunetto *et al.* [2006]. Thus, fitting the spectrum with an exponential continuum I found $C_s = -0.133 \mu\text{m}$, corresponding to a relatively fresh surface. The C_s value gives the number of displacements per cm^2 , $d = 0.45 \times 10^{19}$ displacements/ cm^2 .

Comparing the original spectrum of (1333) Cevenola with all laboratory spectra from Relab, M4AST found matches with ordinary chondrite meteorites (L and LL subtypes, and petrologic classes 4 and 5). In terms of standard deviation and correlation coefficient, the best matches were those of samples from Saratov, Hamlet #1 (Fig. 7.4) and Paranaiba. These meteorites are ordinary chondrites with low iron content.

I compared also the de-reddened spectrum of (1333) Cevenola to laboratory spectra from Relab. In this case, the four methods used give relatively different solutions. The spectral solutions that can be selected are the spectrum of a sample from Denver meteorite and the spectrum of a sample from Hamlet #1 meteorite. Both meteorites are ordinary chondrites with low iron content.

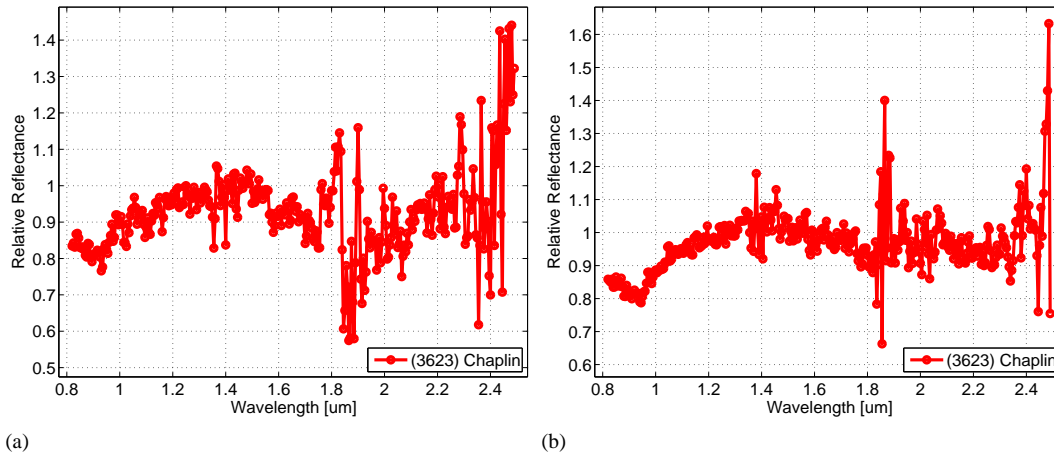


Figure 7.5: The NIR spectra of (3623) Chaplin; a) obtained in March 12, 2007; b) obtained in March 13, 2007. The spectra are normalized to $1.25 \mu\text{m}$.

Applying the Cloutis mineralogical model, the following parameters can be found: BI center is at $0.9803 \pm 0.0111 \mu\text{m}$, BII center is at $1.9630 \pm 0.0116 \mu\text{m}$, and the BAR is 0.3317 ± 0.0036 . These values imply an $\frac{OPX}{OPX+OL} \simeq 0.19$. The results of the model suggest a mineralogy similar with ordinary chondrites LL subtype. It agrees with the results found from the comparison with laboratory spectra.

This spectrum was analyzed by Birlan *et al.* [2011] using the modified Gaussian model (MGM) procedure [Sunshine & Pieters, 1993]. The procedure allows the quantitative characterization of absorption features, by simultaneous fitting of multiple Gaussian-like absorption bands [Pieters & McFadden, 1994]. This analysis strongly indicate that the presence of both olivine and pyroxene are necessary for reproducing the observational data of (1333) Cevenola. The mineralogical solution corresponds to fayalitic material with the molar percentage equal to 20 ± 5 [Sunshine *et al.*, 2007] and the width of these absorption bands span the same range as presented by Sunshine & Pieters [1998]. However, the strength ratio between the M1 and M2 olivine crystals is different from the calibration values proposed by Sunshine *et al.* [2007]. This imply that mineralogies with fayalitic-forsteritic components need to be completed with other components.

7.4.2 (3623) Chaplin

(3623) Chaplin belongs to the Koronis family [Zappala *et al.*, 1995, Mothé-Diniz *et al.*, 2005]. The asteroid has the synodic period of 8.361 ± 0.005 hrs, and a large amplitude in its composite lightcurve estimated to 0.97 ± 0.02 mag. [Birlan *et al.*, 1996b]. However, there is no estimation for its pole coordinates.

Two NIR spectra of the asteroid, presented in Fig 7.5a and Fig 7.5b were obtained at a time interval of about 23 hours. The spectrum of March 12, 2007 is the result of combined

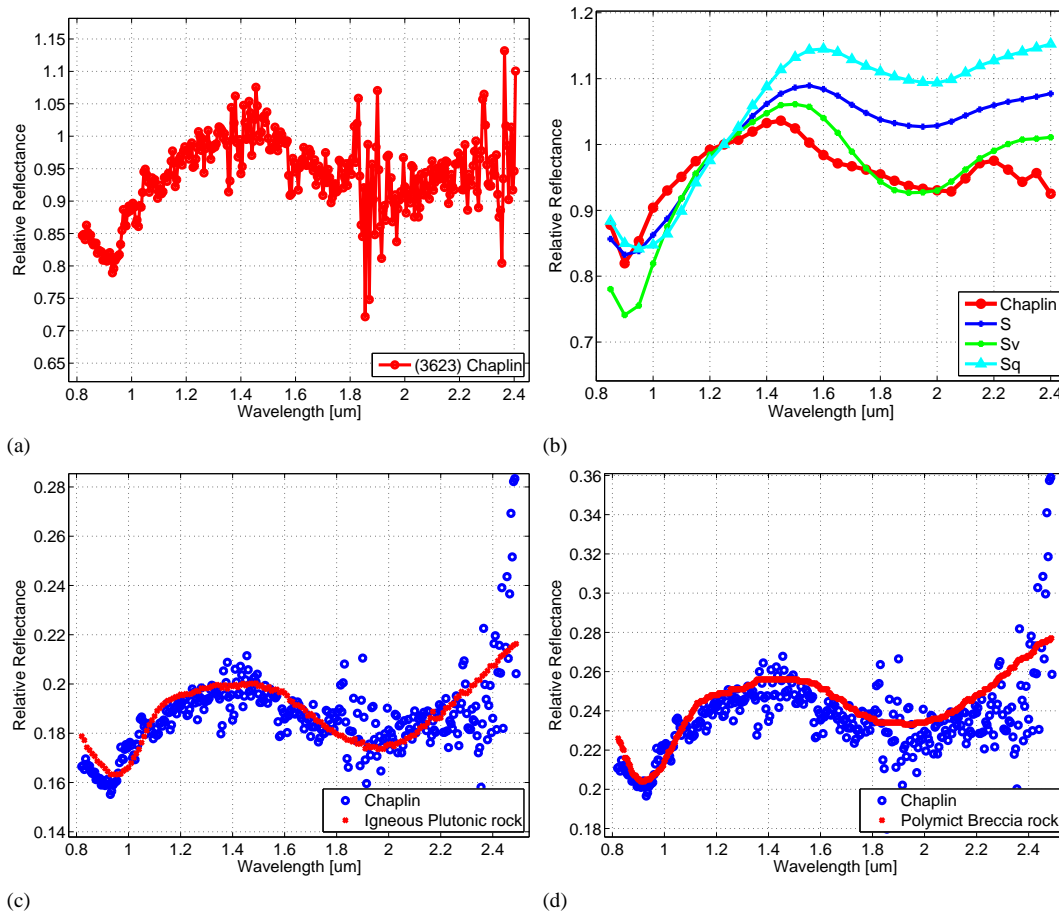


Figure 7.6: a) The NIR averaged spectrum of (3623) Chaplin; b) A polynomial fit for (3623) Chaplin compared with the theoretical spectra of S, Sv and Sq taxonomic types;; c) the comparison between the spectrum of (3623) Chaplin and the spectrum of a sample from igneous plutonic rock; d) the comparison between the spectrum of spectrum of (3623) Chaplin and the spectrum of a sample from low-calcium impact melt breccia rock.

individual spectra of 120 seconds each, for the total integration time of 72 min, while the the second spectrum (obtained in March 13, 2007) was obtained for the total integration time of 80 min. The S/N was estimated in the range of 15-20.

The NIR spectrum of (3623) Chaplin is typical to *S* complex asteroids, which is the taxonomic class of the Koronis family on which Koronis belongs. The classification made using M4AST gives relatively different solutions compared with the classification made via SMASS MIT online tool. M4AST gives the solutions: *Sv*, *L* and *S*, while the SMASS MIT online tool gives *S*, *Sq*, *Q* and *L*. By visual inspection between these solutions, I consider as possible types for this spectrum the solutions *S*, *Sv* and *Sq* Fig. 7.6b.

The comparison with laboratory spectra is presented in Table 7.4. The majority of matchings are among Igneous Plutonic rocks and Polymict Breccia rocks. The first matching corresponds to a spectrum of Igneous Plutonic rock, subtype - Gabro Shocked, with crumbed (particles size between 45 and 75 μm). The second match is a low-Calcium Impact Melt Breccia, a

rock brought by Apollo 14 mission. A meteorite spectrum that seems to match this asteroid spectrum is that of an Achondrite - Ureilite type, PCA82506,80.

Applying de-reddening model, it can be found that it is characterized by a low space-weathering effect ($C_s = -0.157 \mu\text{m}$). This small value of C_s can be explained by the fact that (3623) Chaplin resides in the outer part of the Main Belt, being less affected by the solar wind ion radiation. After removing the exponential continuum, the laboratory spectra that match this spectrum are those of a sample from Fayetteville meteorite - an ordinary chondrite meteorite and a Igneous Plutonic rock.

(1333) Cevenola and (3623) Chaplin were observed over two consecutive nights in order to detect spectral variations in their spectra. Their correspondent spectra has the same profile, which is interpreted as a homogeneity of the surfaces of each object.

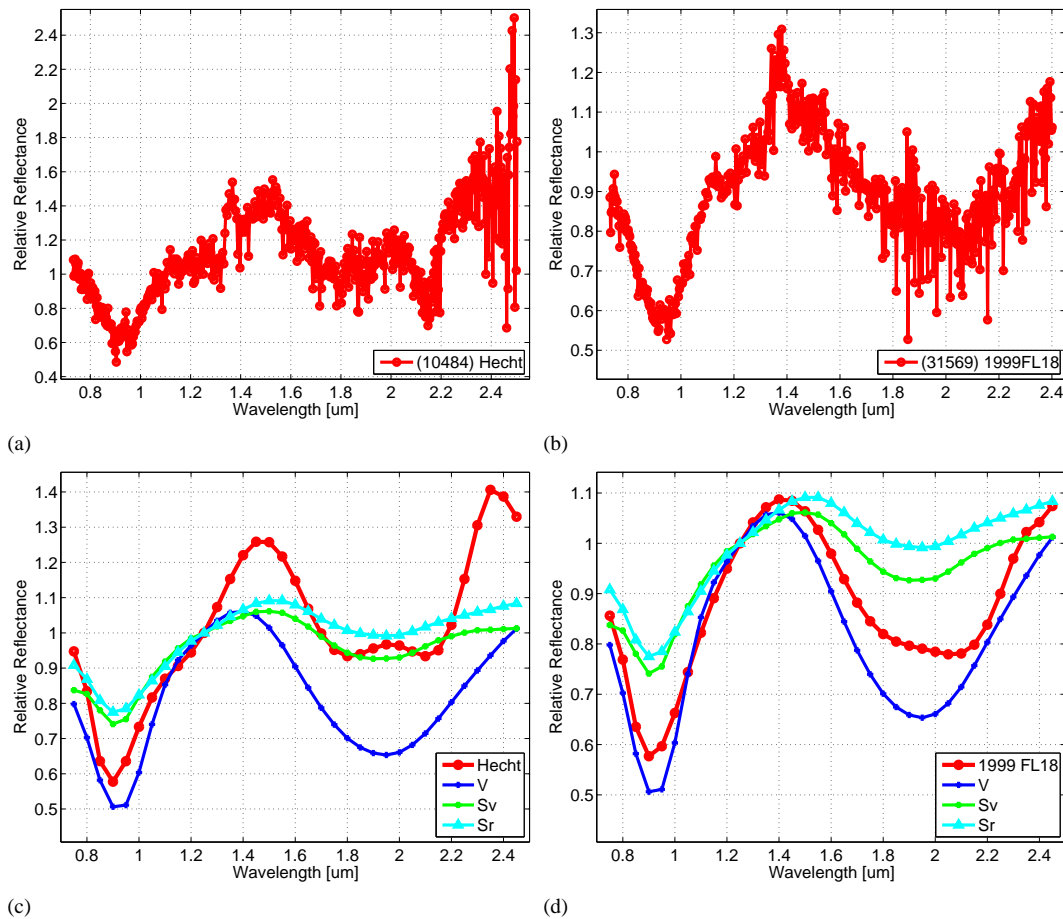


Figure 7.7: The NIR spectra of a) (10484) Hecht and b) (31569) 1999 FL18. Both spectra are normalized to $1.25 \mu\text{m}$. Taxonomic classification of c) (10484) Hecht and d) (31569) 1999 FL18.

7.5 Asteroid pairs: (10484) Hecht, (31569)1999 FL18

The identification of asteroid-pairs could be considered as the smallest cluster that could be derived using the asteroids dynamical parameters. Vokrouhlický & Nesvorný [2008] propose a set of pairs of asteroids of a common origin. This topic is further re-analyzed and quantified in terms of statistical significance by Pravec & Vokrouhlický [2009].

The formation of asteroid pairs could be explained using the following mechanisms: collision disruptions of km-sized and larger parent asteroids, Yarkovsky-O'Keefe-Radzievski-Paddack (YORP) effect which can induce spin-up and rotational fission of fast-rotating objects, and splitting of unstable asteroid binaries [Vokrouhlický & Nesvorný, 2008]. In the first case the asteroids would be parts of compact collisional families with many members that would be found by future asteroid surveys.

Physical characterization of asteroid pairs is still incipient and a challenging task since a large fraction of identified pairs have large magnitudes. Some recent results were proposed by [Duddy *et al.*, 2012]. In this framework we started an observing programs of these intriguing objects.

Here I briefly describe the NIR spectra (Fig. 7.7) of two objects from two different pairs identified by Pravec & Vokrouhlický [2009]: (10484) Hecht and (31569) 1999 FL18. The observations were performed using SpeX/IRTF in low resolution mode. While the S/N ratio is poor for (10484) Hecht only the spectral range 0.8-2.1 μm is considered as relevant. For the asteroid (31569) 1999 FL18 the spectrum is reliable over the spectral interval 0.8-2.4 μm .

(10484) Hecht has an apparent magnitude $H = 14.0$, while its twin (44645) 1999 RC118 has an apparent magnitude $H = 14.7$. The favorable positions to obtain the spectrum of (44645) 1999 RC118 are in July 2013 when the asteroid has an apparent magnitude 18.0 and in the beginning of January 2015 when the asteroid has an apparent magnitude 17.0.

(31569) 1999FL18 has also the apparent magnitude $H = 14.0$, while its twin (21321) 1997AN2 has an apparent magnitude $H = 14.3$. The favorable geometry to obtain the spectrum of (21321) 1997AN2 arise in October 2013 when the asteroid has an apparent magnitude 16.4.

(10484) Hecht data are close to the V, Sv, Sr (Fig. 7.7c) and R taxonomic classes into the Bus-DeMeo taxonomy. The result is mainly based on the deep 1 μm absorption band. The asteroid (31569) 1999 FL18 was classified as V or Sv taxonomic type (Fig. 7.7d).

The comparison to meteorite spectra confirms the affinity of both spectra to the one of HED meteorites. The best fit for (10484) Hecht are the man - made mixtures containing Pyroxene Hypersthene Olivine Forsterit Plagioclase Bytownite Ilmenite. However, due to the poor SNR of the data over 2.1 μm , the acapulcoide primitive achondrite meteorites could also be a relative good mineralogical solution. For (31569) 1999 FL18 the HED eucritic nature is proposed. Among the solutions it can be found the spectrum of a sample of Macibini Clast 3, a meteorite discovered in South Africa (Table 7.4).

The band minima for the (10484) Hecht are at $0.9244 \pm 0.0038 \mu\text{m}$, respectively $2.0461 \pm 0.1522 \mu\text{m}$, resulting in a band separation of $1.1217 \mu\text{m}$. These values indicate an iron content larger than 65 wt%, based on empirical relation obtained from the laboratory experiments. For a similar analysis of the spectrum of (31569) 1999 FL18 the following values can be found $0.9310 \pm 0.0011 \mu\text{m}$, respectively $2.0341 \pm 0.0094 \mu\text{m}$ for the band minima, and a band separation of $1.1031 \mu\text{m}$. These values are also equivalent with an iron content larger than 65 wt%.

(31569) 1999 FL18 belong to two different pairs which could be genetically related. The extrapolation of the results to these pairs shows four new objects possible V-type inside the asteroidal population.

The spectral observations and analysis of asteroid pairs is a new scientific program based on the dynamical findings by Vokrouhlický & Nesvorný [2008].

Part IV

CONCLUSIONS AND PERSPECTIVES

Conclusions and perspectives

During my Ph. D. studies, I applied the spectral techniques to determination of asteroids physical properties. The work consists of three main activities: telescope observations, developing of the methods and tools for asteroid spectral analysis, and interpretation of the asteroids spectra.

I observed for more than 40 hours on NASA SpeX/IRTF, in remote control from CODAM Center(Paris). The purpose of these observations was to obtain NIR asteroid spectra. The results where partially published [Birlan *et al.*, 2011, **Popescu et al.**, 2011, Birlan & **Popescu**, 2011, Birlan *et al.*, 2012, **Popescu et al.**, 2012b].

Additional to the main subject of the thesis, I observed around 20 nights for asteroids discovery (with particular interest for NEAs), recovery and follow up. These observations were made from Obsv. de Haute Provence (France), Pic du Midi (France), and ORM in La Palma (Canary). The results of these campaigns appeared in 12 Minor Planet Circulars and 21 Minor Planet Electronic Circulars.

For analysis of asteroids NIR spectra I applied the well known methods (taxonomic classifications, band analyses and comparative mineralogy) and I proposed new mathematical approaches for spectral comparison and taxonomical classification. I implemented all these methods into routines of a software package called M4AST (Modeling for Asteroids). The second component of M4AST is the spectral database which has around 2,700 asteroid spectra obtained from our observing program and different collaborations. The spectra from the database are in a standard format and are fully available for download. I developed M4AST using Octave computation environment, PHP programming language, and GNUPlot tools (with the free GNU license).

M4AST was conceived to be fully available via a web interface and can be used by the scientific community. Together with my colleagues, I presented in a paper [**Popescu et al.**, 2012b] the interfaces available to access this software tool and the algorithms behind each method used to perform the spectral analysis. The robustness of the routines has been demonstrated by using the software to model a variety of spectra.

Together with my colleagues, I obtained and analyzed NIR spectra for eight near-Earth asteroids [**Popescu et al.**, 2011]. Four of the observed objects have delta - V lower than 7

km/sec, which make them suitable targets in terms of propulsion for a future spacecraft mission. I modeled and interpreted the obtained spectra using a variety of techniques with the goal of interpreting the asteroidal surfaces in terms of their mineralogical composition. Each asteroid spectrum was analyzed to obtain its taxonomic class and the closest matching meteoritic analogs from the laboratory databases. The taxonomic classification of five of these objects was reviewed and I assigned a corresponding type to the other three asteroids that had not been previously classified. I found that (1917) Cuyo, (8567) 1996 HW1, (16960) 1998 QS52, (188452) 2004 HE62, and 2010 TD54 are in the S-complex. For these objects, a good matching with the spectra of ordinary chondrites meteorites has been obtained.

From this set of samples, the asteroid Jasonwheeler was found to have a NIR spectrum similar to that of carbonaceous chondrite meteorites. It was classified to be between D and T taxonomic classes. Since these classes are considered to have primitive compositions and the delta-V for this object is smaller than 7 km/sec, Jasonwheeler could be a very interesting candidate for a sample and return spacecraft mission.

In different collaborations [Birlan *et al.*, 2011, Birlan & Popescu, 2011, Popescu *et al.*, 2012a, Birlan *et al.*, 2012] I analyzed VNIR spectra for a variety of asteroids: vestoids, asteroid pairs, asteroids with large amplitude light-curve. Their spectral properties are in agreement with the V and S complex types. For the V-type a very good matching with HED meteorites was found. Mineralogical solutions were proposed for all these asteroids.

My future work includes two directions: developing M4AST tools and observational programs for asteroid spectra. Future developments of M4AST project consist in increasing the number of spectra in the database, additional methods for analyzing the spectra (such as mineralogical charts Birlan *et al.* [2011]), and a more friendly interface.

The first observational programs in which I am involved, as one of the co-investigators, aims to obtain using SpeX, NIR spectra of NEAs with MOID < 0.1 AU and orbits that are approaching Earth. The team is particularly interested to find V-types asteroids that may be at the origin of the meteor showers associated with the increased number of HED falls during June of each year. For this program we obtained 16 hours of observations on the IRTF/SpeX in the second half of 2012.

Another program on which I participate aims to gather physical characterization results for a large sample of potential target destinations for developing future space mission opportunities. Particular attention is given to asteroids presenting spectra similar to primitive mineralogical composition.

A

The GuideDog and the BigDog interfaces

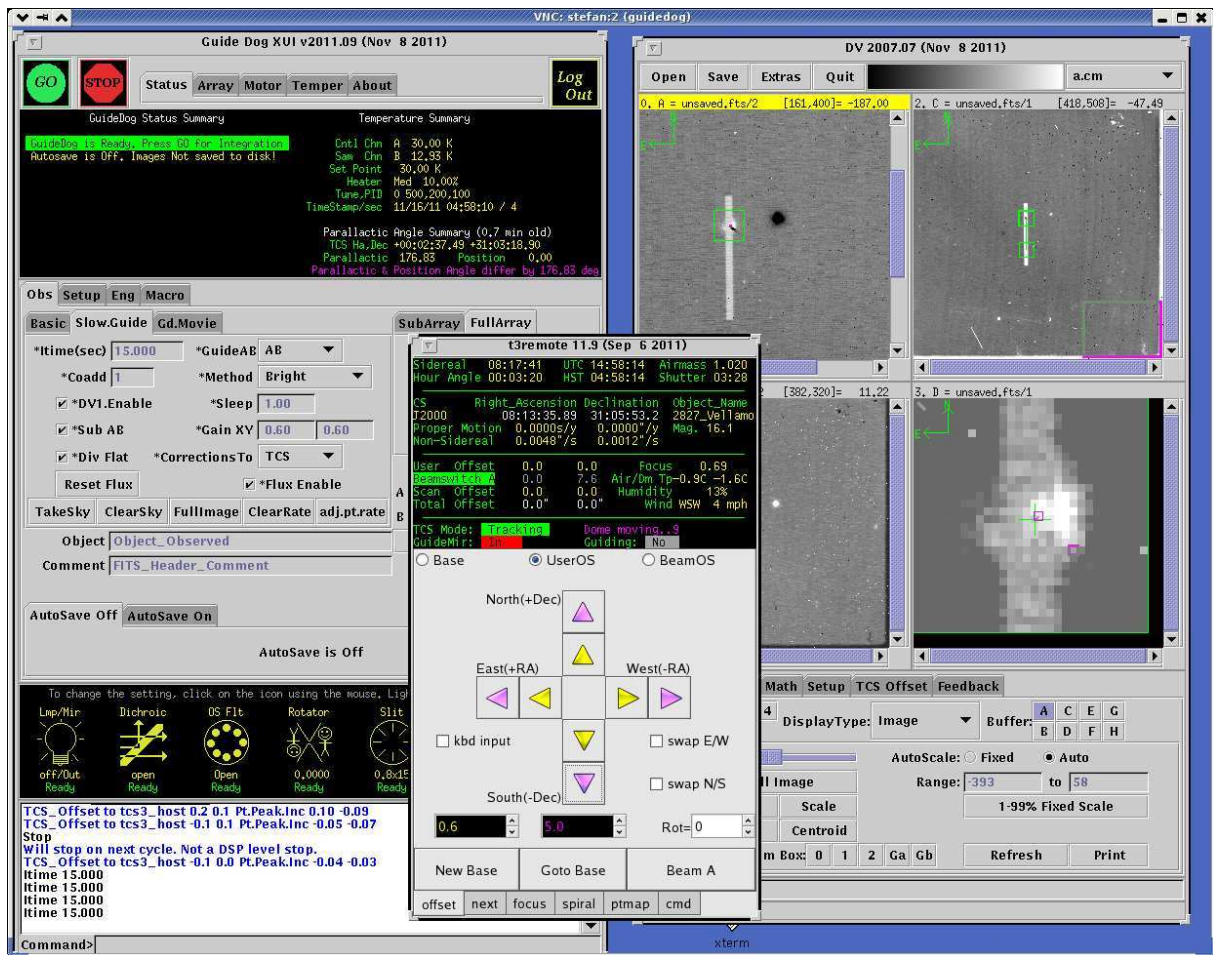


Figure A.1: The GuideDog interface is used to control the guider system of the telescope. Source: Rayner *et al.* [2004].

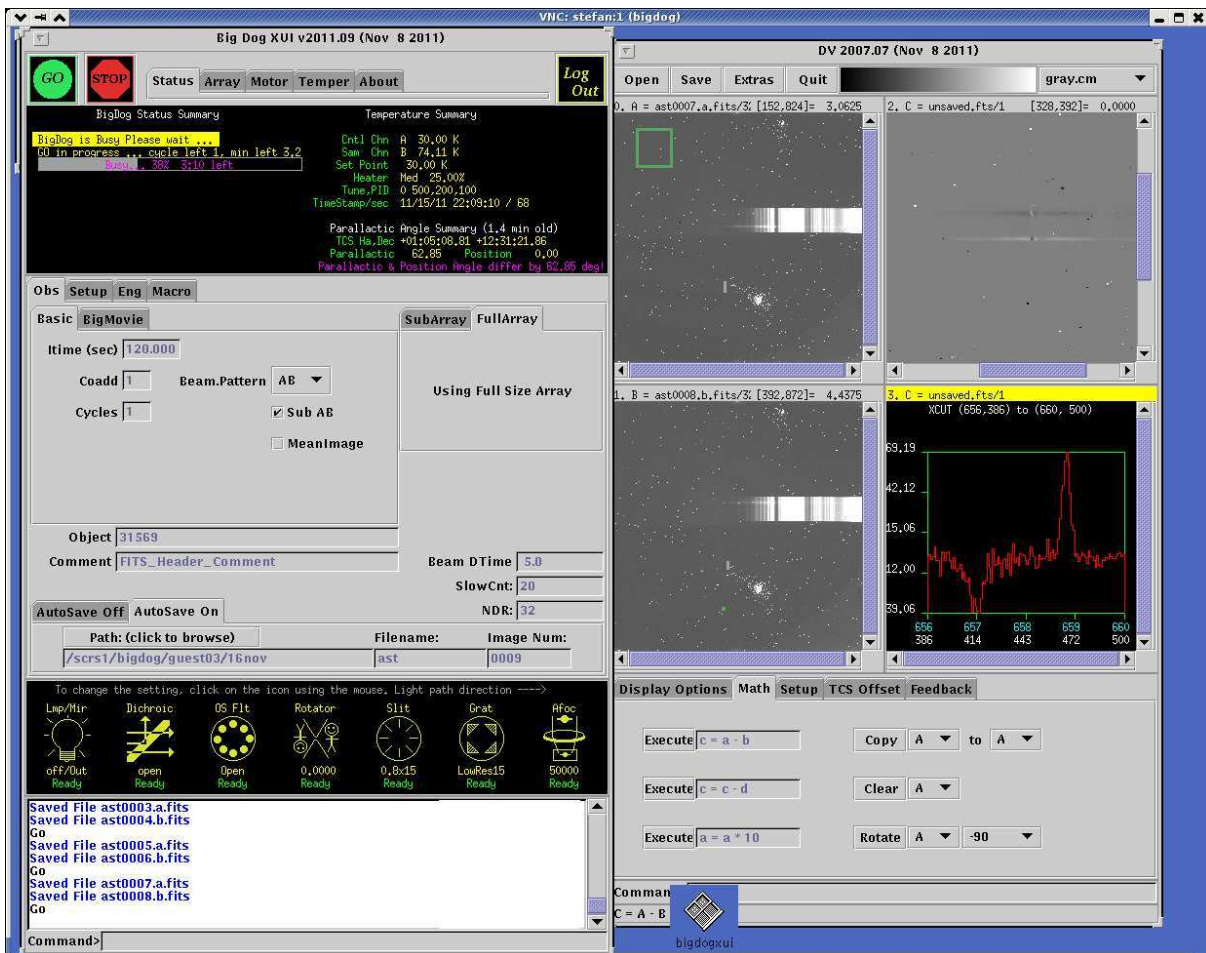


Figure A.2: The BigDog interface is used to control the spectrograph set-up and spectra acquisition. Source: Rayner *et al.* [2004].

B

List of publications

B.1 First Author

- **Popescu, M.**; Birlan, M.; Binzel, R.; Vernazza, P.; Barucci, A.; Nedelcu, D. A.; DeMeo, F.; Fulchignoni, M.
Spectral properties of eight near-Earth asteroids
Astronomy & Astrophysics, Volume 535, id.A15, 11/2011.
- **Popescu, M.**; Birlan, M.; Nedelcu, D. A.
Modeling of asteroid spectra - M4AST
Astronomy & Astrophysics, Volume 544, id.A130, 08/2012.
- **Popescu, M.**; Birlan, M.; Gherase, R. M.; Sonka, A. B.; Naiman, M.; Cristescu, C. P.
Applications of Visible and infrared spectroscopy in astronomy
UPB Scientific Bulletin, Series A, ISSN 1223-7027, Volume 3/2012.

B.2 Co-Author

- Birlan, M.; Nedelcu, D. A.; Descamps, P.; Berthier, J.; Marchis, F.; Merouane, S.; **Popescu, M.**
Spectral properties of (854) Frostia, (1333) Cevenola and (3623) Chaplin
Monthly Notices of the Royal Astronomical Society, Volume 415, Issue 1, pp. 587-595, 07/2011.
- Vaduvescu, O.; Birlan, M.; Tudorica, A.; Sonka, A.; Pozo, F. N.; Barr, A. D.; Asher, D. J.; Licandro, J.; Ortiz, J. L.; Unda-Sanzana, E.; **Popescu, M.**; Nedelcu, A.; et all.
EURONEAR-Recovery, follow-up and discovery of NEAs and MBAs using large field 1-2 m telescopes
Planetary and Space Science, Volume 59, Issue 13, p. 1632-1646, 10/2011.
- Vaduvescu, O.; **Popescu, M.**; Comsa, I; et. all.
Mining the ESO WFI and INT WFC archives for known Near Earth Asteroids. Mega-Precovery Software

Astronomische Nachrichten (Astronomical Notes), 2012, In press.

B.3 Conferences and Workshops

- Birlan, M.; Colas F.; **Popescu, M.**; Nedelcu, A.
Ground based observational campaigns of NEAs
Gaia-FUN-SSO 2012 workshop, 09/2012, Paris.
- Birlan, M.; **Popescu, M.**; Vernazza, P.; et. all.
Spectroscopy of Asteroid Pairs
Asteroids, Comets, Meteors 2012, Proceedings of the conference held May 16-20, 2012 in Niigata, Japan. LPI Contribution No. 1667, id.6098.
- Vaduvescu, O.; **Popescu, M.**; Tudorica, A.; et. all
Data Mining the Suprimecam Archive for Near Earth Asteroids
Asteroids, Comets, Meteors 2012, Proceedings of the conference held May 16-20, 2012 in Niigata, Japan. LPI Contribution No. 1667, id.6235.
- Birlan, M.; **Popescu, M.**; Colas F.; Nedelcu, A.
Focus on (175706)1996 FG3: modeling spectra using M4AST and new observational results from Pic du Midi
Marco Polo -R workshop, 01/2012, Paris.
- Birlan, M.; **Popescu, M.**
Modelling asteroid spectra: few examples
EPSC-DPS Joint Meeting 2011, held 2-7 October 2011 in Nantes, France.
- **Popescu, M.**; Birlan, M.
Modeling NEA spectra, a key to understand their physical properties
2011 IAA Planetary Defense Conference: From Threat to Action; 9-12 May 2011; Bucharest, Romanian.
- Birlan, M.; Binzel, R.; **Popescu, M.**; Vernazza, P.; Nedelcu, A.
Spectral Properties of Near-Earth Asteroids
2011 IAA Planetary Defense Conference: From Threat to Action; 9-12 May 2011; Bucharest, Romanian.
- Vaduvescu, O.; Birlan, M.; Tudorica, A.; **Popescu, M.**; et. all
The European Near Earth Asteroid Research (EURONEAR) - Status and Projects
2011 IAA Planetary Defense Conference: From Threat to Action; 9-12 May 2011; Bucharest, Romanian.
- Turcu, E.; **Popescu, M.**; Birlan, M.
NEAs astrometry for secure orbits in Observatoire de Haute Provence
2011 IAA Planetary Defense Conference: From Threat to Action; 9-12 May 2011; Bucharest, Romanian.

- **Popescu, M.;** Vaduvescu, O.; Birlan, M.

Mega-Precovery, a dedicated project for data mining worldwide image archives for poorly known asteroids

Journees Scientifiques 2010 de IMCCE, 11/2010, Paris.

- **Popescu, M.** and Vaduvescu, O.

Mega-Precovery, a dedicated project for data mining worldwide image archives for poorly known asteroids

Romanian Diaspora Conference, 09/2010, Bucharest.

Bibliography

- Adams, J. B. 1974. Visible and near-infrared diffuse reflectance spectra of pyroxenes as applied to remote sensing of solid objects in the solar system. *J. Geophys. Res.*, **79**(Nov.), 4829–4836.
- Alvarez-Candal, A., Duffard, R., Lazzaro, D., & Michtchenko, T. 2006. The inner region of the asteroid Main Belt: a spectroscopic and dynamic analysis. *A&A*, **459**(Dec.), 969–976.
- Asphaug, E. 1997. Impact origin of the Vesta family. *Meteoritics and planetary science*, **32**(Nov.), 965–980.
- Barucci, M. A., Capria, M. T., Coradini, A., & Fulchignoni, M. 1987. Classification of asteroids using G-mode analysis. *Icarus*, **72**(Nov.), 304–324.
- Behrend, R., Bernasconi, L., Roy, R., Klotz, A., Colas, F., Antonini, P., Aoun, R., Augustesen, K., Barbotin, E., Berger, N., Berrouachdi, H., Brochard, E., Cazenave, A., Cavadore, C., Coloma, J., Cotrez, V., Deconihout, S., Demeautis, C., Dorseuil, J., Dubos, G., Durkee, R., Frappa, E., Hormuth, F., Itkonen, T., Jacques, C., Kurtze, L., Laffont, A., Lavayssière, M., Lecacheux, J., Leroy, A., Manzini, F., Masi, G., Matter, D., Michelsen, R., Nomen, J., Oksanen, A., Pääkkönen, P., Peyrot, A., Pimentel, E., Pray, D., Rinner, C., Sanchez, S., Sonnenberg, K., Sposetti, S., Starkey, D., Stoss, R., Teng, J.-P., Vignand, M., & Waelchli, N. 2006. Four new binary minor planets: (854) Frostia, (1089) Tama, (1313) Berna, (4492) Debussy. *A&A*, **446**(Feb.), 1177–1184.
- Bell, J. F., Owensby, P. D., Hawke, B. R., & Gaffey, M. J. 1988. The 52-Color Asteroid Survey: Final Results and Interpretation. *Pages 57–+ of: Lunar and planetary institute conference abstracts*.
- Bevington, Philip R., & Robinson, D. Keith. 1992. *Data reduction and error analysis for the physical sciences*. McGraw-Hill, Inc.
- Binzel, R. P. 1978. Further Support for Minor Planet Multiplicity. *The minor planet bulletin*, volume 6, p.18-19, **6**(Dec.), 18–19.
- Binzel, R. P., & van Flandern, T. C. 1979. Minor planets - The discovery of minor satellites. *Science*, vol. 203, mar. 2, 1979, p. 903-905., **203**(Mar.), 903–905.
- Binzel, R. P., & Xu, S. 1993. Chips off of asteroid 4 Vesta - Evidence for the parent body of basaltic achondrite meteorites. *Science*, **260**(Apr.), 186–191.
- Binzel, R. P., Lupishko, D., di Martino, M., Whiteley, R. J., & Hahn, G. J. 2002. Physical Properties of Near-Earth Objects. *Asteroids iii*, 255–271.
- Binzel, R. P., Perozzi, E., Rivkin, A. S., Rossi, A., Harris, A. W., Bus, S. J., Valsecchi, G. B., & Slivan, S. M. 2004a. Dynamical and compositional assessment of near-Earth object mission targets. *Meteoritics and planetary science*, **39**(Mar.), 351–366.
- Binzel, R. P., Rivkin, A. S., Stuart, J. S., Harris, A. W., Bus, S. J., & Burbine, T. H. 2004b. Observed spectral properties of near-Earth objects: results for population distribution, source regions, and space weathering processes. *Icarus*, **170**(Aug.), 259–294.
- Binzel, R. P., Rivkin, A. S., Thomas, C. A., Vernazza, P., Burbine, T. H., DeMeo, F. E., Bus, S. J., Tokunaga, A. T., & Birlan, M. 2009. Spectral properties and composition of potentially hazardous Asteroid (99942) Apophis. *Icarus*, **200**(Apr.), 480–485.

- Binzel, R. P., Morbidelli, A., Merouane, S., DeMeo, F. E., Birlan, M., Vernazza, P., Thomas, C. A., Rivkin, A. S., Bus, S. J., & Tokunaga, A. T. 2010. Earth encounters as the origin of fresh surfaces on near-Earth asteroids. *Nature*, **463**(Jan.), 331–334.
- Birlan, M., & Nedelcu, A. 2010 (Mar.). The Physics of Asteroids and Their Junction with Dynamics. *Pages 229–250 of: Souchay, J., & Dvorak, R. (eds), Lecture notes in physics, berlin springer verlag. Lecture Notes in Physics, Berlin Springer Verlag, vol. 790.*
- Birlan, M., & **Popescu, M.** 2011 (Oct.). Modelling asteroid spectra: few examples. *Page 810 of: Epsc-dps joint meeting 2011.*
- Birlan, M., Barucci, M. A., & Fulchignoni, M. 1996a. G-mode analysis of the reflection spectra of 84 asteroids. *A&A*, **305**(Jan.), 984–+.
- Birlan, M., Barucci, M. A., Angeli, C. A., Doressoundiram, A., & de Sanctis, M. C. 1996b. Rotational properties of asteroids: CCD observations of nine small asteroids. *Planet. Space Sci.*, **44**(June), 555–558.
- Birlan, M., Barucci, M. A., Vernazza, P., Fulchignoni, M., Binzel, R. P., Bus, S. J., Belskaya, I., & Fornasier, S. 2004a. Near-IR spectroscopy of asteroids 21 Lutetia, 89 Julia, 140 Siwa, 2181 Fogelin and 5480 (1989YK8), potential targets for the Rosetta mission; remote observations campaign on IRTF. *New astronomy*, **9**(June), 343–351.
- Birlan, M., Barucci, A., & Thuillot, W. 2004b. Solar system observations by remote observing technique: useful experience for robotic telescope strategies. *Astronomische nachrichten*, **325**(Oct.), 571–573.
- Birlan, M., Vernazza, P., Fulchignoni, M., Barucci, M. A., Descamps, P., Binzel, R. P., & Bus, S. J. 2006. Near infra-red spectroscopy of the asteroid 21 Lutetia. I. New results of long-term campaign. *A&A*, **454**(Aug.), 677–681.
- Birlan, M., Binzel, R. P., Nedelcu, D., Vernazza, P., Barucci, A., Gasc, S., Fulchignoni, M., & Dotto, E. 2009 (Sept.). Physical Characterization of Asteroids Candidates of Marco Polo Mission. *Pages 34.08–+ of: Aas/division for planetary sciences meeting abstracts 41. AAS/- Division for Planetary Sciences Meeting Abstracts, vol. 41.*
- Birlan, M., Nedelcu, D. A., Descamps, P., Berthier, J., Marchis, F., Merouane, S., & **Popescu, M.** 2011. Spectral properties of (854) Frostia, (1333) Cevenola and (3623) Chaplin. *MNRAS*, **415**(July), 587–595.
- Birlan, M., **Popescu, M.**, Vernazza, P., Nedelcu, D. A., & Groussin, O. 2012. Spectroscopy of Asteroid Pairs. *Lpi contributions*, **1667**(May), 6098.
- Boattini, A., D’Abramo, G., Scholl, H., Hainaut, O. R., Boehnhardt, H., West, R., Carpino, M., Hahn, G., Michelsen, R., Forti, G., Pravec, P., Valsecchi, G. B., & Asher, D. J. 2004. Near Earth Asteroid search and follow-up beyond 22nd magnitude. A pilot program with ESO telescopes. *A&A*, **418**(May), 743–750.
- Britt, D. T., Tholen, D. J., Bell, J. F., & Pieters, C. M. 1992. Comparison of asteroid and meteorite spectra - Classification by principal component analysis. *Icarus*, **99**(Sept.), 153–166.
- Brunetto, R., & Strazzulla, G. 2005. Elastic collisions in ion irradiation experiments: A mechanism for space weathering of silicates. *Icarus*, **179**(Dec.), 265–273.

- Brunetto, R., Vernazza, P., Marchi, S., Birlan, M., Fulchignoni, M., Orofino, V., & Strazzulla, G. 2006. Modeling asteroid surfaces from observations and irradiation experiments: The case of 832 Karin. *Icarus*, **184**(Oct.), 327–337.
- Burbine, T. H., Buchanan, P. C., Dolkar, T., & Binzel, R. P. 2009. Pyroxene mineralogies of near-Earth vestoids. *Meteoritics and planetary science*, **44**(Oct.), 1331–1341.
- Bus, S. J., & Binzel, R. P. 2002a. Phase II of the Small Main-Belt Asteroid Spectroscopic Survey A Feature-Based Taxonomy. *Icarus*, **158**(July), 146–177.
- Bus, S. J., & Binzel, R. P. 2002b. Phase II of the Small Main-Belt Asteroid Spectroscopic Survey The Observations. *Icarus*, **158**(July), 106–145.
- Bus, S. J., Denault, A. J., Rayner, J. T., Binzel, R. P., & Birlan, M. 2002 (Nov.). Remote observing at the NASA Infrared Telescope Facility (IRTF). *Pages 94–99 of: Kibrick, R. I. (ed), Society of photo-optical instrumentation engineers (spie) conference series*. Society of Photo-Optical Instrumentation Engineers (SPIE) Conference Series, vol. 4845.
- Carruba, V., Michtchenko, T. A., Roig, F., Ferraz-Mello, S., & Nesvorný, D. 2005. On the V-type asteroids outside the Vesta family. I. Interplay of nonlinear secular resonances and the Yarkovsky effect: the cases of 956 Elisa and 809 Lundia. *A&A*, **441**(Oct.), 819–829.
- Cellino, A., Pannunzio, R., Zappala, V., Farinella, P., & Paolicchi, P. 1985. Do we observe light curves of binary asteroids? *A&A*, **144**(Mar.), 355–362.
- Chapman, C. R. 1996. S-Type Asteroids, Ordinary Chondrites, and Space Weathering: The Evidence from Galileo's Fly-bys of Gaspra and Ida. *Meteoritics and planetary science*, **31**(Oct.), 699–725.
- Chapman, C. R. 2004. Space Weathering of Asteroid Surfaces. *Annual review of earth and planetary sciences*, **32**(May), 539–567.
- Chapman, C. R., Johnson, T. V., & McCord, T. B. 1971. A Review of Spectrophotometric Studies of Asteroids. *Nasa special publication*, **267**, 51.
- Clark, B. E., Veverka, J., Helfenstein, P., Thomas, P. C., Bell, J. F., Harch, A., Robinson, M. S., Murchie, S. L., McFadden, L. A., & Chapman, C. R. 1999. NEAR Photometry of Asteroid 253 Mathilde. *Icarus*, **140**(July), 53–65.
- Clark, B. E., Hapke, B., Pieters, C., & Britt, D. 2002. Asteroid Space Weathering and Regolith Evolution. *Asteroids iii*, 585–599.
- Cloutis, E. A., & Gaffey, M. J. 1991. Pyroxene spectroscopy revisited - Spectral-compositional correlations and relationship to geothermometry. *J. Geophys. Res.*, **96**(Dec.), 22809.
- Cloutis, E. A., Gaffey, M. J., Jackowski, T. L., & Reed, K. L. 1986a. Calibrations of phase abundance, composition, and particle size distribution for olivine-orthopyroxene mixtures from reflectance spectra. *J. Geophys. Res.*, **91**, 641–653.
- Cloutis, E. A., Gaffey, M. J., Jackowski, T. L., & Reed, K. L. 1986b. Calibrations of phase abundance, composition, and particle size distribution for olivine-orthopyroxene mixtures from reflectance spectra. *J. Geophys. Res.*, **91**(Oct.), 11641.

- Cloutis, E. A., Gaffey, M. J., Smith, D. G. W., & Lambert, R. S. J. 1990. Metal Silicate Mixtures: Spectral Properties and Applications to Asteroid Taxonomy. *J. Geophys. Res.*, **95**(June), 8323–8338.
- Cristescu, C. P. 2004. *Introduction to optics and quantum physics*.
- Cutri, R. M., Skrutskie, M. F., van Dyk, S., Beichman, C. A., Carpenter, J. M., Chester, T., Cambresy, L., Evans, T., Fowler, J., Gizis, J., Howard, E., Huchra, J., Jarrett, T., Kopan, E. L., Kirkpatrick, J. D., Light, R. M., Marsh, K. A., McCallon, H., Schneider, S., Stiening, R., Sykes, M., Weinberg, M., Wheaton, W. A., Wheelock, S., & Zacarias, N. 2003. 2MASS All-Sky Catalog of Point Sources (Cutri+ 2003). *VizieR online data catalog*, **2246**(Mar.), 0.
- Das Gupta, S. P., Sen Gupta, P. R., Dube, A., Sen Gupta, N. R., & Das Gupta, D. R. 1978. The Dhajala Meteorite. *Mineralogical magazine*, **42**, 493–497.
- de León, J., Licandro, J., Serra-Ricart, M., Pinilla-Alonso, N., & Campins, H. 2010. Observations, compositional, and physical characterization of near-Earth and Mars-crosser asteroids from a spectroscopic survey. *A&A*, **517**(July), A23+.
- de León, J., Mothé-Diniz, T., Licandro, J., Pinilla-Alonso, N., & Campins, H. 2011a. New observations of asteroid (175706) 1996 FG3, primary target of the ESA Marco Polo-R mission. *A&A*, **530**(June), L12.
- de León, J., Mothé-Diniz, T., Licandro, J., Pinilla-Alonso, N., & Campins, H. 2011b. New observations of asteroid (175706) 1996 FG3, primary target of the ESA Marco Polo-R mission. *A&A*, **530**(June), L12+.
- de Pater, I., & Lissauer, J. J. 2010. *Planetary Sciences*.
- de Sanctis, M. C., Migliorini, A., Luzia Jasmin, F., Lazzaro, D., Filacchione, G., Marchi, S., Ammannito, E., & Capria, M. T. 2011a. Spectral and mineralogical characterization of inner main-belt V-type asteroids. *A&A*, **533**(Sept.), A77.
- de Sanctis, M. C., Migliorini, A., Luzia Jasmin, F., Lazzaro, D., Filacchione, G., Marchi, S., Ammannito, E., & Capria, M. T. 2011b. Spectral and mineralogical characterization of inner main-belt V-type asteroids. *A&A*, **533**(Sept.), A77.
- Dell’Oro, A., & Cellino, A. 2007. The random walk of Main Belt asteroids: orbital mobility by non-destructive collisions. *MNRAS*, **380**(Sept.), 399–416.
- DeMeo, F., & Binzel, R. P. 2008. Comets in the near-Earth object population. *Icarus*, **194**(Apr.), 436–449.
- DeMeo, F. E. 2010. *La variation compositionnelle des petits corps à travers le système solaire*. Ph.D. thesis, LESIA, Observatoire de Paris-Meudon.
- DeMeo, F. E., Binzel, R. P., Slivan, S. M., & Bus, S. J. 2009. An extension of the Bus asteroid taxonomy into the near-infrared. *Icarus*, **202**(July), 160–180.
- Descamps, P. 2010. Equilibrium figures of inhomogeneous synchronous binary asteroids. *Icarus*, **207**(June), 758–768.
- Dobrica, E. 2010. *Micrometeorites Concordia: des neiges antarctiques aux glaces cométaires*. Ph.D. thesis, University Paris Sud.

- Donnison, J. R. 1979. The satellite of Herculina. *MNRAS*, **186**(Mar.), 35P–37P.
- Doug Tody, Markus Dolensky, Jonathan McDowell Francois Bonnarel Tamas Budavari Ivan Busko Alberto Micol Pedro Osuna Jesus Salgado Petr Skoda Randy Thompson Frank Valdes, & the Data Access Layer Working Group. 2011. *Simple spectral access version 1.1*.
- Duddy, S. R., Lowry, S. C., Wolters, S. D., Christou, A., Weissman, P., Green, S. F., & Rozitis, B. 2012. Physical and dynamical characterisation of the unbound asteroid pair 7343-154634. *A&A*, **539**(Mar.), A36.
- Duffard, R., & Roig, F. 2009. Two new V-type asteroids in the outer Main Belt? *Planet. Space Sci.*, **57**(Feb.), 229–234.
- Duffard, R., Lazzaro, D., Licandro, J., de Sanctis, M. C., Capria, M. T., & Carvano, J. M. 2004. Mineralogical characterization of some basaltic asteroids in the neighborhood of (4) Vesta: first results. *Icarus*, **171**(Sept.), 120–132.
- Dunlap, J. L., & Gehrels, T. 1969. Minor Planets. III. Lightcurves of a Trojan Asteroid. *AJ*, **74**(Aug.), 796.
- Durda, D. D., Bottke, W. F., Enke, B. L., Merline, W. J., Asphaug, E., Richardson, D. C., & Leinhardt, Z. M. 2004. The formation of asteroid satellites in large impacts: results from numerical simulations. *Icarus*, **170**(July), 243–257.
- Durkee, I., R. 2010. Asteroids Observed from the Shed of Science Observatory: 2009 July–September. *Minor planet bulletin*, **37**(Jan.), 18–19.
- Florczak, M., Lazzaro, D., & Duffard, R. 2002. Discovering New V-Type Asteroids in the Vicinity of 4 Vesta. *Icarus*, **159**(Sept.), 178–182.
- Fornasier, S., Barucci, M. A., Binzel, R. P., Birlan, M., Fulchignoni, M., Barbieri, C., Bus, S. J., Harris, A. W., Rivkin, A. S., Lazzarin, M., Dotto, E., Michałowski, T., Doressoundiram, A., Bertini, I., & Peixinho, N. 2003. A portrait of 4979 Otawara, target of the Rosetta space mission. *A&A*, **398**(Jan.), 327–333.
- Francis, P. J., Hewett, P. C., Foltz, C. B., Chaffee, F. H., Weymann, R. J., & Morris, S. L. 1991. A high signal-to-noise ratio composite quasar spectrum. *ApJ*, **373**(June), 465–470.
- French, L. M., & Binzel, R. P. 1989. CCD photometry of asteroids. *Pages 54–65 of: Binzel, R. P., Gehrels, T., & Matthews, M. S. (eds), Asteroids ii; proceedings of the conference, tucson, az, mar. 8-11, 1988 (a90-27001 10-91). tucson, az, university of arizona press, 1989, p. 54-65. research supported by nsf and nasa.*
- Fulchignoni, M., Birlan, M., & Antonietta Barucci, M. 2000. The Extension of the G-Mode Asteroid Taxonomy. *Icarus*, **146**(July), 204–212.
- Gaffey, M. J. 1976. Spectral reflectance characteristics of the meteorite classes. *J. Geophys. Res.*, **81**(Feb.), 905–920.
- Gaffey, M. J. 1997. Surface Lithologic Heterogeneity of Asteroid 4 Vesta. *Icarus*, **127**(May), 130–157.
- Gaffey, M. J. 2008. Interpreting Asteroid Spectra - Avoiding the Three "Great Mistakes". *Lpi contributions*, **1405**, 8162.

- Gaffey, M. J. 2010. Space weathering and the interpretation of asteroid reflectance spectra. *Icarus*, **209**(Oct.), 564–574.
- Gaffey, M. J., Burbine, T. H., & Binzel, R. P. 1993a. Asteroid spectroscopy - Progress and perspectives. *Meteoritics*, **28**(June), 161–187.
- Gaffey, M. J., Burbine, T. H., Piatek, J. L., Reed, K. L., Chaky, D. A., Bell, J. F., & Brown, R. H. 1993b. Mineralogical variations within the S-type asteroid class. *Icarus*, **106**(Dec.), 573–+.
- Gaffey, M. J., Cloutis, E. A., Kelley, M. S., & Reed, K. L. 2002. Mineralogy of Asteroids. *Asteroids iii*, 183–204.
- Gladman, B., Michel, P., & Froeschlé, C. 2000. The Near-Earth Object Population. *Icarus*, **146**(July), 176–189.
- Gradie, J., & Veverka, J. 1986. The wavelength dependence of phase coefficients. *Icarus*, **66**(June), 455–467.
- Hapke, B. 2001. Space weathering from Mercury to the asteroid belt. *J. Geophys. Res.*, **106**(May), 10039–10074.
- Hardersen, P. S., Gaffey, M. J., & Abell, P. A. 2004. Mineralogy of Asteroid 1459 Magnya and implications for its origin. *Icarus*, **167**(Jan.), 170–177.
- Harris, A. W., & Lupishko, D. F. 1989. Photometric lightcurve observations and reduction techniques. *Pages 39–53 of: Binzel, R. P., Gehrels, T., & Matthews, M. S. (eds), Asteroids ii; proceedings of the conference, tucson, az, mar. 8-11, 1988 (a90-27001 10-91). tucson, az, university of arizona press, 1989, p. 39-53.*
- Hicks, M., & Rhoades, H. 2010. The near-Earth asteroid 2010 TD54: The fastest rotating natural body known in the solar system? *The astronomer's telegram*, **2984**(Oct.), 1–+.
- Higgins, D., Pravec, P., Kusnirak, P., Masi, G., Galad, A., Gajdos, S., Kornos, L., Vilagi, J., & Pray, D. 2006. Asteriod lightcurve analysis at Hunters Hill Observatory and collaborating stations - autumn/winter 2005. *Minor planet bulletin*, **33**(Mar.), 8–10.
- Hilton, J. L. 2002. Asteroid Masses and Densities. *Asteroids iii*, 103–112.
- Høg, E., Fabricius, C., Makarov, V. V., Urban, S., Corbin, T., Wycoff, G., Bastian, U., Schwendiek, P., & Wicenec, A. 2000. The Tycho-2 catalogue of the 2.5 million brightest stars. *A&A*, **355**(Mar.), L27–L30.
- Holsapple, K. A., & Michel, P. 2008. Tidal disruptions. II. A continuum theory for solid bodies with strength, with applications to the Solar System. *Icarus*, **193**(Jan.), 283–301.
- Ivezić, Ž., Tabachnik, S., Rafikov, R., Lupton, R. H., Quinn, T., Hammergren, M., Eyer, L., Chu, J., Armstrong, J. C., Fan, X., Finlator, K., Geballe, T. R., Gunn, J. E., Hennessy, G. S., Knapp, G. R., Leggett, S. K., Munn, J. A., Pier, J. R., Rockosi, C. M., Schneider, D. P., Strauss, M. A., Yanny, B., Brinkmann, J., Csabai, I., Hindsley, R. B., Kent, S., Lamb, D. Q., Margon, B., McKay, T. A., Smith, J. A., Waddel, P., York, D. G., & SDSS Collaboration. 2001. Solar System Objects Observed in the Sloan Digital Sky Survey Commissioning Data. *AJ*, **122**(Nov.), 2749–2784.

- Keil, K. 2002. Geological History of Asteroid 4 Vesta: The "Smallest Terrestrial Planet". *Asteroids iii*, 573–584.
- Kitchin, C. R. 1995. *Optical astronomical spectroscopy*.
- Kong, P., & Ebihara, M. 1997. The origin and nebular history of the metal phase of ordinary chondrites. *Geochim. Cosmochim. Acta*, **61**(June), 2317–2329.
- Labotka, T. C., & Papike, J. J. 1980. Howardites - Samples of the regolith of the eucrite parent-body: Petrology of Frankfort, Pavlovka, Yurtuk, Malvern, and ALHA 77302. *Pages 1103–1130 of: Bedini, S. A. (ed), Lunar and planetary science conference proceedings*. Lunar and Planetary Science Conference Proceedings, vol. 11.
- Lagerkvist, C.-I., Barucci, M. A., Capria, M. T., Fulchignoni, M., Guerriero, L., Perozzi, E., & Zappala, V. 1987. *Asteroid photometric catalogue*.
- Landolt, A. U. 1992. UBVRI photometric standard stars in the magnitude range 11.5–16.0 around the celestial equator. *AJ*, **104**(July), 340–371.
- Lazzarin, M., Marchi, S., Magrin, S., & Licandro, J. 2005. Spectroscopic investigation of near-Earth objects at Telescopio Nazionale Galileo. *MNRAS*, **359**(June), 1575–1582.
- Lazzaro, D., Mothé-Diniz, T., Carvano, J. M., Angeli, C. A., Betzler, A. S., Florczak, M., Cellino, A., Di Martino, M., Doressoundiram, A., Barucci, M. A., Dotto, E., & Bendjoya, P. 1999. The Eunomia Family: A Visible Spectroscopic Survey. *Icarus*, **142**(Dec.), 445–453.
- Lazzaro, D., Michtchenko, T., Carvano, J. M., Binzel, R. P., Bus, S. J., Burbine, T. H., Mothé-Diniz, T., Florczak, M., Angeli, C. A., & Harris, A. W. 2000. Discovery of a Basaltic Asteroid in the Outer Main Belt. *Science*, **288**(June), 2033–2035.
- Lazzaro, D., Angeli, C. A., Carvano, J. M., Mothé-Diniz, T., Duffard, R., & Florczak, M. 2004. S3OS2: the visible spectroscopic survey of 820 asteroids. *Icarus*, **172**(Nov.), 179–220.
- Leone, G., Paolicchi, P., Farinella, P., & Zappala, V. 1984. Equilibrium models of binary asteroids. *A&A*, **140**(Nov.), 265–272.
- Lord, S. D. 1992 (Dec.). *A new software tool for computing Earth's atmospheric transmission of near- and far-infrared radiation*. Tech. rept.
- Luu, J. X., & Jewitt, D. C. 1990. Charge-coupled device spectra of asteroids. I - Near-earth and 3:1 resonance asteroids. *AJ*, **99**(June), 1985–2011.
- Magrin, S. 2006. *Spectroscopic investigation of near Earth objects*. Ph.D. thesis, Padova University, astronomy departament.
- McCord, T. B., & Adams, J. B. 1977. Use of ground-based telescopes in determining the composition of the surfaces of solar system objects. *Nasa special publication*, **370**, 893–922.
- McCord, T. B., Adams, J. B., & Johnson, T. V. 1970. Asteroid Vesta: Spectral Reflectivity and Compositional Implications. *Science*, **168**(June), 1445–1447.
- McLean, I. S. 2008. *Electronic Imaging in Astronomy: Detectors and Instrumentation (Second Edition)*. Praxis Publishing.
- McSween, Harry Y. 1999. *Ometeorites and their Parent Planets*. Knoxville: University of Tennessee.

- Michel, P., & Delbo, M. 2010. Orbital and thermal evolutions of four potential targets for a sample return space mission to a primitive near-Earth asteroid. *Icarus*, **209**(Oct.), 520–534.
- Michelsen, R., Nathues, A., & Lagerkvist, C.-I. 2006. Spectroscopy of near-Earth asteroids. *A&A*, **451**(May), 331–337.
- Milani, A., & Gronchi, G. F. 2010. *Theory of Orbital Determination*. Cambridge University Press.
- Milani, A., & Knezevic, Z. 1990. Secular perturbation theory and computation of asteroid proper elements. *Celestial mechanics and dynamical astronomy*, **49**(Dec.), 347–411.
- Milani, A., Chesley, S. R., & Valsecchi, G. B. 2000. Asteroid close encounters with Earth: risk assessment. *Planet. Space Sci.*, **48**(Aug.), 945–954.
- Miyamoto, M., Takeda, H., & Yanai, K. 1979 (Mar.). Eucritic Polymict Breccias from Allan Hills and Yamato Mountains, Antarctica. *Pages 847–849 of: Lunar and planetary science x, p. 847-849. abstract.*, vol. 10.
- Morbidelli, A., Jedicke, R., Bottke, W. F., Michel, P., & Tedesco, E. F. 2002. From Magnitudes to Diameters: The Albedo Distribution of Near Earth Objects and the Earth Collision Hazard. *Icarus*, **158**(Aug.), 329–342.
- Mothé-Diniz, T., Roig, F., & Carvano, J. M. 2005. Reanalysis of asteroid families structure through visible spectroscopy. *Icarus*, **174**(Mar.), 54–80.
- Mueller, M., Delbo', M., Hora, J. L., Trilling, D. E., Bhattacharya, B., Bottke, W. F., Chesley, S., Emery, J. P., Fazio, G., Harris, A. W., Mainzer, A., Mommert, M., Penprase, B., Smith, H. A., Spahr, T. B., Stansberry, J. A., & Thomas, C. A. 2011. ExploreNEOs. III. Physical Characterization of 65 Potential Spacecraft Target Asteroids. *AJ*, **141**(Apr.), 109–+.
- Nedelcu, D. A. 2010. *Modelisation dynamique et spectroscopie des asteroides*. Ph.D. thesis, Observatoire de Paris.
- Nedelcu, D. A., Birlan, M., Vernazza, P., Descamps, P., Binzel, R. P., Colas, F., Kryszczynska, A., & Bus, S. J. 2007. Near infra-red spectroscopy of the asteroid 21 Lutetia. II. Rotationally resolved spectroscopy of the surface. *A&A*, **470**(Aug.), 1157–1164.
- Olsen, E. J., Noonan, A., Fredriksson, K., Jarosewich, E., & Moreland, G. 1978. Eleven new meteorites from Antarctica, 1976-1977. *Meteoritics*, vol. 13, june 30, 1978, p. 209-225., **13**(June), 209–225.
- Olsen, E. J., Fredriksson, K., Rajan, S., & Noonan, A. 1990. Chondrule-like objects and brown glasses in howardites. *Meteoritics*, **25**(Sept.), 187–194.
- Pieters, C. M., & McFadden, L. A. 1994. Meteorite and Asteroid Reflectance Spectroscopy: Clues to Early Solar System Processes. *Annual review of earth and planetary sciences*, **22**, 457–497.
- Pieters, C. M., Taylor, L. A., Noble, S. K., Keller, L. P., Hapke, B., Morris, R. V., Allen, C. C., McKay, D. S., & Wentworth, S. 2000. Space weathering on airless bodies: Resolving a mystery with lunar samples. *Meteoritics and planetary science*, **35**(Sept.), 1101–1107.

- Popescu, M.**, Birlan, M., Binzel, R., Vernazza, P., Barucci, A., Nedelcu, D. A., DeMeo, F., & Fulchignoni, M. 2011. Spectral properties of eight near-Earth asteroids. *A&A*, **535**(Nov.), A15.
- Popescu, M.**, Birlan, M., Gherase, R. M., Sonka, A. B., Naiman, M., & Cristescu, C. P. 2012a. Applications of Visible and infrared spectroscopy in astronomy. *UPB scientific bulletin, series a, issn 1223-7027*, **3**.
- Popescu, M.**, Birlan, M., & Nedelcu, D. A. 2012b. Modeling of asteroid spectra - M4AST. *A&A*, **544**(Aug.), A130.
- Pravec, P., & Vokrouhlický, D. 2009. Significance analysis of asteroid pairs. *Icarus*, **204**(Dec.), 580–588.
- Rayner, J. T., Toomey, D. W., Onaka, P. M., Denault, A. J., Stahlberger, W. E., Vacca, W. D., Cushing, M. C., & Wang, S. 2003. SpeX: A Medium-Resolution 0.8-5.5 Micron Spectrograph and Imager for the NASA Infrared Telescope Facility. *PASP*, **115**(Mar.), 362–382.
- Rayner, J. T., Onaka, P. M., Cushing, M. C., & Vacca, W. D. 2004 (Sept.). Four years of good SpeX. *Pages 1498–1509 of: Moorwood, A. F. M., & Iye, M. (eds), Ground-based instrumentation for astronomy. edited by alan f. m. moorwood and iye masanori. proceedings of the spie, volume 5492, pp. 1498-1509 (2004).* Presented at the Society of Photo-Optical Instrumentation Engineers (SPIE) Conference, vol. 5492.
- Ringwood, A. E. 1979. *Origin of the earth and moon*.
- Rivkin, A. S., Binzel, R. P., & Bus, S. J. 2005. Constraining near-Earth object albedos using near-infrared spectroscopy. *Icarus*, **175**(May), 175–180.
- Rivkin, A. S., Howell, E. S., DeMeo, F. E., Vervack, R. J., Binzel, R. P., Magri, C., Nolan, M. C., Fernandez, Y. R., Cheng, A. F., Barucci, M. A., & Michel, P. 2012 (Mar.). New Observations and Proposed Meteorite Analogs of the MarcoPolo-R Target Asteroid (175706) 1996 FG3. *Page 1537 of: Lunar and planetary institute science conference abstracts.* Lunar and Planetary Inst. Technical Report, vol. 43.
- Roig, F., & Gil-Hutton, R. 2006. Selecting candidate V-type asteroids from the analysis of the Sloan Digital Sky Survey colors. *Icarus*, **183**(Aug.), 411–419.
- Ruzicka, A., Snyder, G. A., & Taylor, L. A. 1997. Vesta as the HED Parent Body: Implications for the Size of a Core and for Large-Scale Differentiation. *Meteoritics and planetary science*, **32**(Nov.), 825–840.
- Sasaki, S., Nakamura, K., Hamabe, Y., Kurahashi, E., & Hiroi, T. 2001. Production of iron nanoparticles by laser irradiation in a simulation of lunar-like space weathering. *Nature*, **410**(Mar.), 555–557.
- Schmidt, M., & Green, R. F. 1983. Quasar evolution derived from the Palomar bright quasar survey and other complete quasar surveys. *ApJ*, **269**(June), 352–374.
- Simon, S. B., & Papike, J. J. 1983. Petrology of igneous lithic clasts from polymict eucrites ALHA76005 and ALHA77302. *Meteoritics (issn 0026-1114), vol. 18, march 31, 1983, p. 35-50.*, **18**(Mar.), 35–50.

- Storrs, A., Weiss, B., Zellner, B., Burleson, W., Sichertiu, R., Wells, E., Kowal, C., & Tholen, D. 1999. Imaging Observations of Asteroids with Hubble Space Telescope. *Icarus*, **137**(Feb.), 260–268.
- Stuart, J. S., & Binzel, R. P. 2004. Bias-corrected population, size distribution, and impact hazard for the near-Earth objects. *Icarus*, **170**(Aug.), 295–311.
- Sunshine, J. M., & Pieters, C. M. 1993. Estimating modal abundances from the spectra of natural and laboratory pyroxene mixtures using the modified Gaussian model. *J. Geophys. Res.*, **98**(May), 9075–9087.
- Sunshine, J. M., & Pieters, C. M. 1998. Determining the composition of olivine from reflectance spectroscopy. *J. Geophys. Res.*, **103**(June), 13675–13688.
- Sunshine, J. M., Bus, S. J., Corrigan, C. M., McCoy, T. J., & Burbine, T. H. 2007. Olivine-dominated asteroids and meteorites: Distinguishing nebular and igneous histories. *Meteoritics and planetary science*, **42**(Aug.), 155–170.
- Taylor, P. A., Howell, E. S., Magri, C., Vervack, R. J., Nolan, M. C., Fernandez, Y. R., Rivkin, A. S., & Mueller, M. 2009 (Sept.). Variability of Thermal Infrared Emission from Near-Earth Asteroids. *Pages 32.01–+ of: Aas/division for planetary sciences meeting abstracts. AAS/Division for Planetary Sciences Meeting Abstracts*, vol. 41.
- Tedesco, E. F. 1979. Binary asteroids - Evidence for their existence from lightcurves. *Science*, vol. 203, mar. 2, 1979, p. 905-907., **203**(Mar.), 905–907.
- Tennyson, J. 2005. *Astronomical spectroscopy : an introduction to the atomic and molecular physics of astronomical spectra*.
- Tholen, D. J. 1984 (Sept.). *Asteroid taxonomy from cluster analysis of Photometry*. Ph.D. thesis, Arizona Univ., Tucson.
- Thomas, P. C., Binzel, R. P., Gaffey, M. J., Zellner, B. H., Storrs, A. D., & Wells, E. 1997. Vesta: Spin Pole, Size, and Shape from HST Images. *Icarus*, **128**(July), 88–94.
- Tonry, J., & Davis, M. 1979. A survey of galaxy redshifts. I - Data reduction techniques. *AJ*, **84**(Oct.), 1511–1525.
- Trevese, D., Paris, D., Stirpe, G. M., Vagnetti, F., & Zitelli, V. 2007. Line and continuum variability of two intermediate-redshift, high-luminosity quasars. *A&A*, **470**(Aug.), 491–496.
- Vacca, W. D., Cushing, M. C., & Rayner, J. T. 2004. Nonlinearity Corrections and Statistical Uncertainties Associated with Near-Infrared Arrays. *PASP*, **116**(Apr.), 352–361.
- Vaduvescu, O., Popescu, M., Comsa, I., & et. all. 2012. Mining the ESO WFI and INT WFC archives for known Near Earth Asteroids. Mega-Precovery Software. *Astronomische nachrichten (astronomical notes)*, **In press**.
- van Flandern, T. C., Tedesco, E. F., & Binzel, R. P. 1979. *Satellites of asteroids*. Pages 443–465.
- Vander Haagen, G. A. 2011. Lightcurve for Near-Earth Asteroid (164400) 2005 GN59. *Minor planet bulletin*, **38**(Jan.), 10–11.
- Vernazza, P. 2006. *Etude des Proprietes Physiques des Asteroides*. Ph.D. thesis, Observatoire de Paris.

- Vernazza, P., Binzel, R. P., DeMeo, F. E., & Thomas, C. A. 2007 (Oct.). Mineralogical Characterization Of 150 S-type Asteroids And Comparison With OC Meteorites. *Page 476 of: Aas/division for planetary sciences meeting abstracts #39*. Bulletin of the American Astronomical Society, vol. 38.
- Vernazza, P., Binzel, R. P., Thomas, C. A., DeMeo, F. E., Bus, S. J., Rivkin, A. S., & Tokunaga, A. T. 2008. Compositional differences between meteorites and near-Earth asteroids. *Nature*, **454**(Aug.), 858–860.
- Vernazza, P., Binzel, R. P., Rossi, A., Fulchignoni, M., & Birlan, M. 2009. Solar wind as the origin of rapid reddening of asteroid surfaces. *Nature*, **458**(Apr.), 993–995.
- Veverka, J., Robinson, M., Thomas, P., Murchie, S., Bell, J. F., Izenberg, N., Chapman, C., Harch, A., Bell, M., Carcich, B., Cheng, A., Clark, B., Domingue, D., Dunham, D., Farquhar, R., Gaffey, M. J., Hawkins, E., Joseph, J., Kirk, R., Li, H., Lucey, P., Malin, M., Martin, P., McFadden, L., Merline, W. J., Miller, J. K., Owen, W. M., Peterson, C., Prockter, L., Warren, J., Wellnitz, D., Williams, B. G., & Yeomans, D. K. 2000. NEAR at Eros: Imaging and Spectral Results. *Science*, **289**(Sept.), 2088–2097.
- Vokrouhlický, D., & Nesvorný, D. 2008. Pairs of Asteroids Probably of a Common Origin. *AJ*, **136**(July), 280–290.
- Walsh, K. J., Delbo', M., Mueller, M., Binzel, R. P., & DeMeo, F. E. 2012. Physical Characterization and Origin of Binary Near-Earth Asteroid (175706) 1996 FG₃. *ApJ*, **748**(Apr.), 104.
- Warner, B. D. 2002. Asteroid Photometry at the Palmer Divide Observatory: Results for 1333 Cevenola and 2460 Mitlincoln. *The minor planet bulletin, volume 29, p.74-75*, **29**(Dec.), 74–75.
- Warner, B. D. 2009. Asteroid Lightcurve Analysis at the Palmer Divide Observatory: 2008 May - September. *Minor planet bulletin*, **36**(Jan.), 7–13.
- West, J. L., & Cameron, I. D. 2006. Using the Medical Image-Processing Package, ImageJ, for Astronomy. *JRASC*, **100**(Dec.), 242.
- Wijesinghe, M. P., & Tedesco, E. F. 1979. A test of plausibility of eclipsing binary asteroids. *Icarus*, **40**(Dec.), 383–393.
- Wisniewski, W. Z., Michalowski, T. M., Harris, A. W., & McMillan, R. S. 1997. Photometric Observations of 125 Asteroids. *Icarus*, **126**(Apr.), 395–449.
- Wolters, S. D., Rozitis, B., Duddy, S. R., Lowry, S. C., Green, S. F., Snodgrass, C., Hainaut, O. R., & Weissman, P. 2011. Physical characterization of low delta-V asteroid (175706) 1996 FG₃. *MNRAS*, **418**(Dec.), 1246–1257.
- Xu, S., Binzel, R. P., Burbine, T. H., & Bus, S. J. 1995. Small main-belt asteroid spectroscopic survey: Initial results. *Icarus*, **115**(May), 1–35.
- Yamada, M., Sasaki, S., Fujiwara, A., Hiroi, T., Hasegawa, S., Nagahara, H., Ohashi, H., Ohtake, H., & Yano, H. 1999 (Mar.). Simulation of Space Weathering by Nanosecond Pulse Laser Heating and Proton Implantation: Difference of Olivine and Pyroxene Samples. *Page 1566 of: Lunar and planetary institute science conference abstracts*. Lunar and Planetary Institute Science Conference Abstracts, vol. 30.

- Yin, Q., Jacobsen, S. B., Yamashita, K., Blichert-Toft, J., Télouk, P., & Albarède, F. 2002. A short timescale for terrestrial planet formation from Hf-W chronometry of meteorites. *Nature*, **418**(Aug.), 949–952.
- Zappala, V., Scaltriti, F., Farinella, P., & Paolicchi, P. 1980. Asteroidal binary systems - Detection and formation. *Moon and planets*, **22**(Apr.), 153–162.
- Zappala, V., Bendjoya, P., Cellino, A., Farinella, P., & Froeschle, C. 1995. Asteroid families: Search of a 12,487-asteroid sample using two different clustering techniques. *Icarus*, **116**(Aug.), 291–314.
- Zellner, B., Tholen, D. J., & Tedesco, E. F. 1985. The eight-color asteroid survey - Results for 589 minor planets. *Icarus*, **61**(Mar.), 355–416.

Spectral properties of eight near-Earth asteroids[★]

M. Popescu^{1,2,9}, M. Birlan¹, R. Binzel³, P. Vernazza^{4,8}, A. Barucci⁵, D. A. Nedelcu⁶, F. DeMeo³, and M. Fulchignoni⁷

¹ Institut de Mécanique Céleste et de Calcul des Éphémérides (IMCCE), Observatoire de Paris, 77 avenue Denfert-Rochereau, 75014 Paris Cedex, France
e-mail: mpopescu@imcce.fr

² Polytechnic University of Bucharest, Faculty of Applied Sciences, Department of Physics, Bucharest, Romania

³ Department of Earth, Atmospheric, and Planetary Sciences, Massachusetts Institute of Technology, 77 Massachusetts Avenue, Cambridge, MA 02139, USA

⁴ Laboratoire d'Astrophysique de Marseille, Université de Provence-CNRS, 38 rue Frédéric Joliot-Curie, 13388 Marseille Cedex 13, France

⁵ LESIA, Observatoire de Paris, 5 place Jules Janssen, 92195 Meudon Principal Cedex, France

⁶ Astronomical Institute of the Romanian Academy, 5 Cujitului de Argint, 040557 Bucharest, Romania

⁷ Université Paris Diderot – Paris 7, 4 rue Elsa Morante, 75013 Paris, France

⁸ European Southern Observatory, K. Schwarzschild-Str. 2, 85748 Garching, Germany

⁹ Bucharest Astroclub, B-dul LascarCatargiu 21, sect 1, Bucharest, Romania

Received 20 April 2011 / Accepted 21 July 2011

ABSTRACT

Context. Near-Earth objects are among the most accessible bodies in the solar system in terms of the spacecraft propulsion requirements to reach them. The choice of targets and the planning of space missions are based on high quality ground-based science.

Aims. The knowledge of the ensemble of physical parameters for these objects, including their composition, is a critical point in defining any mission scientific objectives. Determining the physical properties of near-Earth asteroids (NEAs) is also possible from the ground by analyzing spectroscopy at both visible and infrared wavelengths.

Methods. We present spectra of eight NEAs (1917, 8567, 16960, 164400, 188452, 2001 SG286, and 2010 TD54) obtained using the NASA telescope IRTF equipped with the spectro-imager SpeX. The observations were performed in the 0.8–2.5 μm spectral region using the low resolution mode of the spectrograph. We completed the taxonomic classification using the Bus-DeMeo taxonomy. We analyzed the spectra by comparing them to meteorite spectra from the Relab database using a χ^2 approach. For the S-type asteroids of our sample, the band centers and BAR were calculated. We also attempted to interpret our data using a space-weathering model.

Results. The taxonomic classification of five objects was reviewed and we assigned a corresponding type to the other three asteroids that were not classified before. We found that (1917) Cuyo, (8567) 1996 HW1, (16960) 1998 QS52, (188452) 2004 HE62, and 2010 TD54 are in the S-complex. We achieved a good matching of our S-type asteroids with the spectra of ordinary chondrites meteorites. The asteroid (5620) Jasonwheeler was found to have a NIR spectrum similar to carbonaceous chondrite meteorites. Thus, our results confirm its primitive properties obtained in several other spectral intervals.

Key words. minor planets, asteroids: general – methods: observational – techniques: spectroscopic

1. Introduction

Asteroids are leftovers from the formation of the solar system and studying their properties in detail will allow us to constrain more reliably the formation and evolution of our solar system.

There are more than 500 000 known asteroids, most of them belonging to the main belt. Owing to some mechanisms, which are still the subject of dynamical studies, some of these objects have migrated into the inner part of the solar system (Morbideilli et al. 2002). These are near-Earth asteroids (denoted NEAs), small bodies of the solar system with perihelion distances $q \leq 1.3$ AU and aphelion distances $Q \geq 0.983$ AU, whose orbits approach or intersect the Earth orbit. Depending on their orbital parameters, NEAs are divided into Apollos ($a \geq 1.0$ AU; $q \leq 1.016$ AU), Athens ($a < 1.0$ AU; $Q \geq 0.983$ AU), and Amors ($1.016 < q < 1.3$ AU).

Potentially hazardous asteroids (PHAs) are currently defined based on parameters that measure the asteroid's potential

to make threatening close approaches to the Earth. All asteroids with an Earth minimum orbit intersection distance (MOID) smaller than 0.05 AU and an absolute magnitude (H) of 22.0 or brighter are considered PHAs (Milani et al. 2000).

One of the most important aspects related to the NEAs is their accessibility to be investigated by spacecrafts. This enables their scientific study and the detailed assessment of their future use as space resources. Several programs for space exploration of these objects (Marco Polo-R, OSIRIS-REx, Hayabusa2) are now under study around the World. The choice of targets and the planning of space exploration are based on strong ground-based science. Thus, the knowledge of the ensemble of physical parameters of objects and their composition is a critical point in defining the mission scientific objectives.

A major scientific goal of studies of the NEA population is their global characterization in terms of spectral trends, relating the spectral data to the laboratory measurements. Given the dominance of S-type asteroids among the NEA population, and the abundance of ordinary chondrites (OC) among the meteorites, it has been generally and widely assumed that they are connected,

[★] Appendices A and B are available in electronic form at <http://www.aanda.org>

Table 1. Log of asteroids observations.

Asteroid	Date (UT)	V	Φ (°)	r (UA)	Airmass	ITime(s)	Cycles	Solar analogue	Airmass
(1917) Cuyo	2008/08/27.637	14.6	66.0	1.105	1.038	120	6	BD+41 309	1.141
(5620) Jasonwheeler	2009/05/04.569	16.5	20.9	1.345	1.344	120	6	HD 154716	1.240
(8567) 1996 HW1	2008/08/27.543	12.9	28.8	1.143	1.099	60	13	HD 217577	1.213
(16960) 1998 QS52	2008/08/27.588	16.9	30.0	1.784	1.105	120	13	HD 27834	1.083
(164400) 2005 GN59	2008/08/27.472	16.2	25.2	1.244	1.024	120	2	BD+28 3198	1.410
(188452) 2004 HE62	2008/08/27.404	16.7	60.8	1.109	1.513	120	12	BD+28 3198	1.401
2001 SG286	2009/05/19.594	16.7	102.0	1.006	1.962	120	2	HD 216516	1.742
2010 TD54	2010/10/12.303	15.5	17.3	1.000	1.252	120	8	L115-271	1.092

Notes. Asteroid designations, date of observation with the fraction of the day for the mid time of the observation, the apparent magnitude, the phase angle, the heliocentric distance, the airmass at the mean UT of each observation, the integration time for each spectrum (ITime), and the number of cycles are presented. The last two columns describe the solar analogs used for data reduction, as well as their airmass at the moment of observations.

and that NEAs are the most probably parent bodies of meteorites (Vernazza et al. 2008; de León et al. 2010). Vernazza et al. (2008) reported that about two-thirds of near-Earth asteroids in their sample of 38 objects have spectral properties quantitatively similar to the LL meteorites.

Statistical analysis of spectral data allows the construction of taxonomies and taxonomic classes. These analyzes represent a first step in studies of comparative planetology, which permit us to characterize the specific mineralogy of each class that they identify. The new taxonomy for asteroids obtained by DeMeo et al. (2009) underlines the importance of both visible and near-infrared spectral data to determining the asteroid statistics. This is quite understandable while the spectral data of regoliths on the asteroid's surface are of the 0.4–3.6 μm spectral region¹. With few exceptions, this spectral region is accessible from the ground, the atmosphere being transparent at these wavelengths. This new Bus-DeMeo taxonomy, based on the spectra of more than 310 objects, defines 24 classes.

Irradiation by cosmic and solar wind ions, as well as bombardment by interplanetary dust particles (micro-meteorites) produce relevant surface modifications to airless bodies of the solar system. These processes are known as space weathering (Hapke 2001). The most affected by this alteration are silicate-rich objects, for which a progressive darkening and reddening of the solar reflectance spectra appear in the 0.2–2.7 μm spectral region (Hapke 2001). Space weathering processes can explain the spectral differences between the ordinary chondrite meteorites and their presumed parent bodies – the S-type asteroids (Pieters et al. 2000). Vernazza et al. (2009) demonstrate the necessity to take the composition into account when evaluating weathering effectiveness. The laboratory experiments show that solar-wind ion implantation is the most rapid of several competing processes (Brunetto et al. 2006; Vernazza et al. 2009; Loeffler et al. 2009).

On the basis of laboratory experiments, Brunetto et al. (2006) describe the spectral effects of solar wind irradiation by an exponential continuum in terms of the ratio of weathered spectra to unweathered spectra. Since ion-induced spectral reddening is related to the formation of displacements, they correlated the model with a damage parameter of the surface given as the number of displacements per cm^2 .

In this paper, we present spectroscopic results for eight NEAs in the 0.8–2.5 μm spectral region. The asteroids were observed during several runs between 2008 and 2010 to study NEA physical properties, and are subsidiary to the potential targets of spacecraft missions. In Sect. 2, the details related to observation

methods and the steps followed for data reduction are given. We modeled and interpreted the acquired spectra using different techniques with the goal of achieving basic interpretations regarding of the composition and physical processes that took place at the surface of the asteroids (Sect. 3). The results of spectral analysis for each of the eight objects are described in Sect. 4. Some general characteristics of our sample are discussed in Sect. 5. Finally, the conclusions summarize the obtained results.

2. The observing method and data reduction

In contrast to the main-belt asteroids, the asteroids classified as NEA do not often have a favorable geometry for ground-based observations. The small diameters of the majority of NEAs impose tight constraints on the suitable geometries of observations for determining the reflective properties of their surfaces. These conditions are usually met in the case of a close approach to the Earth, when the apparent magnitude decreases by several magnitudes. These suitable geometries occur on average, only five times per century.

During the observing run, the asteroids and the solar analog were alternatively observed. Our strategy was to observe all asteroids as close to the zenith as possible (Table 1). Each observed asteroid was preceded by observations of solar analogs located in the vicinity. The following stars were observed and used as solar analogs: BD+41 309, HD 154716, HD 217577, HD 27834, BD+28 3198, HD 216516, and L115-271 (Table 1). Our choice was to observe the solar analogue as close as possible to the target. The differential airmass between the asteroid and the standard was usually restricted to less than 0.15. The photometric G2V standards were chosen. We made an exception for 2010 TD54, where the data reduction were performed using L115-271, commonly used in NIR spectral measurements.

The asteroids were observed in the 0.8–2.5 μm spectral region with the SpeX/IRTF instrument, located on Mauna Kea, Hawaii. These observations were performed remotely from the Centre d'Observation à Distance en Astronomie à Meudon (CODAM) (Birlan et al. 2004, 2006) using the low resolution prism mode ($R = 100$) of the spectrograph. We used a 0.8×15 arcsec slit oriented north-south. The spectra for the asteroid and the solar analog stars were obtained alternatively at two separate locations along the slit denoted A and B following the *nodding* procedure (Nedelcu 2010).

The data reduction process consists of two main steps (Birlan et al. 2007; Nedelcu 2010): first, obtaining the raw spectra for the object and the solar analog and second, computation of a

¹ We refer here only to the reflectance spectra.

Table 2. Some characteristics of our NEAs: orbit type, semi-major axis, eccentricity, inclination, absolute magnitude (H), the Delta- V , and taxonomic classification.

Object	Orbit type	a	e	i	ΔV [km s ⁻¹]	H	Taxonomic type	
							Previous	This work
(1917) Cuyo	Amor	2.15005205	0.50448184	23.943786	8.556	14.7	Sl:S	Srw
(5620) Jasonwheeler	Amor	2.15783969	0.42369152	7.861788	6.974	17.0	–	D;T
(8567) 1996 HW1	Amor	2.04580925	0.44905867	8.439303	6.495	15.4	S	Sq
(16960) 1998 QS52	Apollo	2.20249841	0.85791440	17.563883	11.11	14.2	Sq;Q	Sr
(164400) 2005 GN59	Apollo	1.65644063	0.46770919	6.627004	6.002	17.4	–	L
(188452) 2004 HE62	Amor	2.55781560	0.56690184	24.685809	9.074	17.3	–	Sr;Sv
2001 SG286	Apollo	1.35819973	0.34708703	7.772096	5.604	20.9	D	D
2010 TD54	Apollo	1.97198039	0.64352131	4.809727	–	28.7	S	Sr;Sv

normalized reflectance spectrum by dividing the asteroid spectrum by the solar analog spectrum and performing a correction for telluric lines.

For the first step, the Image Reduction and Analysis Facility (Tody 1986) was used. Preprocessing of the CCD images included bias and flat field correction. An averaged bias frame taken at the telescope at the beginning of each observing night was used to perform bias subtraction. Flat fields images were obtained for each object using calibration lamps, at the beginning or end of the night. For the wavelength calibration, the Ar lamp spectrum was used. In the second step, specific IDL routines were used to help diminish the influence of telluric bands in our spectra (Rivkin et al. 2004). No other correction for the differential refraction was performed. For the computation of the final reflectance (ratio of the asteroid spectrum to the star spectrum), we took into account the similar dynamic regimes of the detector (Vacca et al. 2004; Rayner et al. 2003).

Log of asteroids observations is given in Table 1. In general, the asteroid spectra were obtained taking images with an integration time (Itime) of 120s in the nodding procedure, for several cycles, to increase the S/N ratio. For two objects of our sample (2005 GN59, and 2001 SG286), the atmospheric conditions and their low brightness imply a poor S/N ratio. In this case, to obtain reliable spectral measurements, the images were selected by visual inspection, removing all those in which we could not distinguish the trace of the spectrum before the data reduction procedure.

3. Methods used to analyze data

We consider our analysis of spectra in the context of previously published physical and dynamical properties of these objects. Table 2 summarizes some parameters of our sample.

We complete our spectral data with the visible counterpart, when available. This is the case for four of our asteroids: (1917) Cuyo, (8567) 1996 HW1, (16960) 1998 QS52, and 2001 SG286. For each of them, the visible spectrum was merged with our NIR data using a procedure of minimization of data in the common spectral region 0.82–0.9 μm .

We computed the slope for each spectrum using a first-order polynomial fit. For the case of composite spectra ($V + \text{NIR}$), the slope was computed for the spectra normalized to 0.55 μm to compare with the conclusions of the DeMeo et al. (2009) taxonomy. Otherwise, when only NIR was available, the slope was computed for the spectra normalized to 1.25 μm .

Taxonomic types, although not usable to determine the mineralogic compositions of the objects, help constrain mineral species that may be present on the surface of the asteroid. Currently, the most commonly taxonomies are: Tholen

taxonomy (Tholen 1984), Barucci taxonomy (Barucci et al. 1987; Birlan et al. 1996), based on Eight-Color Asteroid Survey data (Zellner et al. 1985), SMASII spectral taxonomy (Bus & Binzel 2002), and Bus-DeMeo taxonomy (DeMeo et al. 2009). We used the last one, which is an extension of the Bus & Binzel (2002) taxonomy to the near-infrared, considering the data spanning the wavelength range between 0.45 μm to 2.45 μm . The Bus-DeMeo taxonomy is based on Principal Component Analysis and comprised 24 classes. This taxonomy allows us to analyze spectra using only NIR data, although we are in this case unable to obtain a unique classification. We used two independent methods to establish the taxonomical class of each asteroid in our sample. In a first approach, spectral data of our asteroids were compared with Bus-DeMeo taxonomic classes via the MIT-SMASS on-line tool². The second approach to taxonomic classification was a procedure developed during this study using a χ^2 minimization method accounting for the mean and standard-deviation values of the Bus-DeMeo taxonomic classes. For this method, we define a reliability criterion:

$$\text{Reliability} = \frac{\text{card}([\lambda_m, \lambda_M] \cap \{\lambda_1^T, \lambda_2^T, \dots, \lambda_{41}^T\})}{41} \quad (1)$$

where $[\lambda_m, \lambda_M]$ is the spectral interval between the minimum and maximum wavelengths of the spectrum, $\lambda_1^T, \lambda_2^T, \dots, \lambda_{41}^T$ are the 41 wavelengths from Bus-DeMeo taxonomy, spanning the interval between 0.45 μm and 2.45 μm , and $\text{card}()$ represents the number of elements of a discrete set. To apply this procedure, we smoothed our data by curve fitting with polynomial functions. This was done using *polyfit* from the Octave3.2 computation environment. The degree of the polynomial was selected to be between 15 to 21 such that the fit produces the smallest least squares fitting residuals. The obtained fitting curves are given in Fig. 3. Overall, we observed that both procedures gave similar results.

We also compared our observational data with laboratory spectra. Spectroscopy of different samples made in the laboratory provides the basis upon which compositional information about unexplored or unsampled planetary surfaces is derived from remotely obtained reflectance spectra. The Relab³ spectral database contains more than 15 000 spectra for different types of materials from meteorites to terrestrial rocks, man-made mixtures, and terrestrial and lunar soils. The comparison was made in the first step using a χ^2 minimization method between asteroid spectrum and all the spectra from the Relab database, which were first normalized to 1.25 μm . In this way, the best fifty spectral curves of different Relab samples were selected for further analysis. From these results, only the meteorite spectra were

² <http://smass.mit.edu/busdemeoclass.html>

³ <http://www.planetary.brown.edu/relab/>

kept. After that, we considered only those meteorite spectra for which the mean reflectance value remains roughly in an interval of $\pm 50\%$ centered on the albedo value (or mean albedo value corresponding to taxonomic class for that asteroid). A third selection was made by taking into account the spectral-feature position (band maxima, band minima) and slope. This was done by comparing each asteroid spectrum with a meteorite spectrum, and selecting the meteorite spectra for which the spectral features do not differ by roughly more than 10% and the difference in slope is not notably larger than 10%. Our initial intention had been to publish the first three most closely fitting solutions satisfying this criteria, for each asteroid spectrum. However, for some asteroid spectra we found only one or two solutions corresponding to the above mentioned criteria.

In our sample, the asteroids belonging to the S-complex were also investigated by considering space weathering effects. Our approach involved applying the model proposed by Brunetto et al. (2006) and calculating the C_s parameter for each of these objects using the formula:

$$W(\lambda) = K \times \exp\left(\frac{C_s}{\lambda}\right). \quad (2)$$

Brunetto et al. (2006) demonstrated that for laboratory experiments this provides a good approximation of the effects of irradiated materials, regardless of whether they are powder or bulk samples, meteorite or terrestrial samples, or samples of either olivine or orthopyroxene. They concluded that a weathered spectrum can be obtained by multiplying the spectrum of the unaltered sample by the exponential function (Eq. (2)) depending on the precise value of the parameter C_s .

$$C_s = \alpha \times \ln(\beta \times d + 1) \quad (3)$$

where $\alpha = -0.33 \mu\text{m}$ and $\beta = 1.1 \times 10^{19} \text{ cm}^2$.

Brunetto & Strazzulla (2005) demonstrated that ion-induced spectral reddening is related to the formation of displacements, though this C_s parameter is also correlated with the number of displacements per cm^2 (damage parameter, noted here by the letter d). By fitting experimental data, Brunetto et al. (2006) obtained the relation between C_s and the number of displacements per cm^2 (Eq. (3)). We computed this damage parameter by considering the values from Brunetto et al. (2006).

This model for the space weathering effects, which we applied to our data, describes the effects of solar-wind ion irradiation. This is not the only active weathering process, but it seems to be the most efficient at 1 AU (Vernazza et al. 2009; Brunetto et al. 2006).

We managed to remove the effects of space weathering by dividing the spectrum with the computed exponential continuum $W(\lambda)$. The de-reddened spectra obtained for the S-type asteroids were compared again with the laboratory measurements from the Relab database.

The computations for the modeling methods described above were done using M4AST⁴ (Popescu & Birlan 2011), which is software developed at IMCCE Paris to analyze asteroid spectra. This tool implements the algorithms for the aforementioned models.

$$\frac{\text{OPX}}{\text{OPX} + \text{OL}} = 0.4187 \times \left(\frac{\text{BII}}{\text{BI}} + 0.125 \right). \quad (4)$$

Since for (1917) Cuyo, (8567) 1996 HW1, and 16960 (1998 QS52) we had V+NIR spectra, we were able to apply the model

proposed by Cloutis et al. (1986). Thus, we computed the two-band centers (at $1 \mu\text{m}$ and $2 \mu\text{m}$), the ratio of the areas of the second to the first absorption band (BAR) and we analyzed the percentage of orthopyroxene using Eq. (4). The computations were done using the standard procedures described by Cloutis et al. (1986). These results are presented in Table 5.

4. Results

This section describes the results obtained for the observed asteroids: (1917) Cuyo, (5620) Jasonwheeler, (8567) 1996 HW1, (16960) 1998 QS52, (188452) 2004 HE62, 2010 TD54, (164400) 2005 GN59, and 2001 SG286. All spectra were normalized to $1.25 \mu\text{m}$. The spectra for the first six objects are plotted in Fig. 1 with error bars and joined with the visible part available from the literature (Binzel et al. 2004b; Vernazza 2006). The data obtained for the last two objects, (164400) 2005 GN59 and 2001 SG286, are plotted in Fig. 4 together with some curves that model these spectra.

The discussion about the taxonomic type of each object is made with reference to Fig. 3. The results for the taxonomic classification of spectra are synthesized in Table 2 to allow a comparison with the physical properties and previously taxonomic classification.

Table 3 summarizes the comparison of asteroid spectra with those of meteorites from the Relab database considering both the original and de-reddened spectra (the case of S-type asteroids). The corresponding figures are presented in Appendices A and B. Some additional data related to meteorites with similar spectra to our objects are given in Table 3.

4.1. (1917) Cuyo

With an absolute magnitude $H = 14.7$, this object has an estimated diameter of 5.2 km (Binzel et al. 2002). It is an Amor-type asteroid, with a synodic period of $2.6905 \pm 0.0005 \text{ h}$ (Wisniewski et al. 1997).

Two spectra in the visible are published for this object. For the first one, Binzel et al. (2004b) found that this asteroid is a SI-type in Bus taxonomy, with a high slope of $(0.7233 \mu\text{m}^{-1})$. The second one was classified by Michelsen et al. (2006) as an S-type asteroid in Tholen taxonomy. We joined the visible spectrum from the SMASS database corresponding to Binzel et al. (2004b), with our data in NIR region (Fig. 1). The analysis was made on the composite V + NIR spectrum.

With the tool from the MIT-SMASS website, this NEA was classified as Sr-type with a higher spectral slope of $0.5086 \mu\text{m}^{-1}$. Using our χ^2 method, R- and Sr-types are obtained as possible classes for this object. The R-type is obtained with a slightly better coefficient of reliability than Sr-type, because of the trend in the $1\text{--}1.5 \mu\text{m}$ spectral region. By visual inspection of the two solutions, we can see that the features around $1 \mu\text{m}$ and $2 \mu\text{m}$ are more shallow than for R class (Fig. 3), so we can conclude that this object is an Sr type asteroid.

The comparison with the Relab database shows that the closest spectral fit is obtained for a tiny section from the Dhajala meteorite (Sample ID: LM-LAM-026, Fig. A.1). This corresponds to an ordinary chondrite meteorite rich in Fe (H3-4 olivine-bronzite). Das Gupta et al. (1978) estimated a total iron content of 27.1% of the total mass of Dhajala. This meteorite was also studied by analyzing the metallic grains in its OC structure (Kong & Ebihara 1997). While the formation of metallic iron is a consequence of the spatial alteration of an object, space weathering models are nevertheless justified.

⁴ <http://cardamine.imcce.fr/m4ast/>

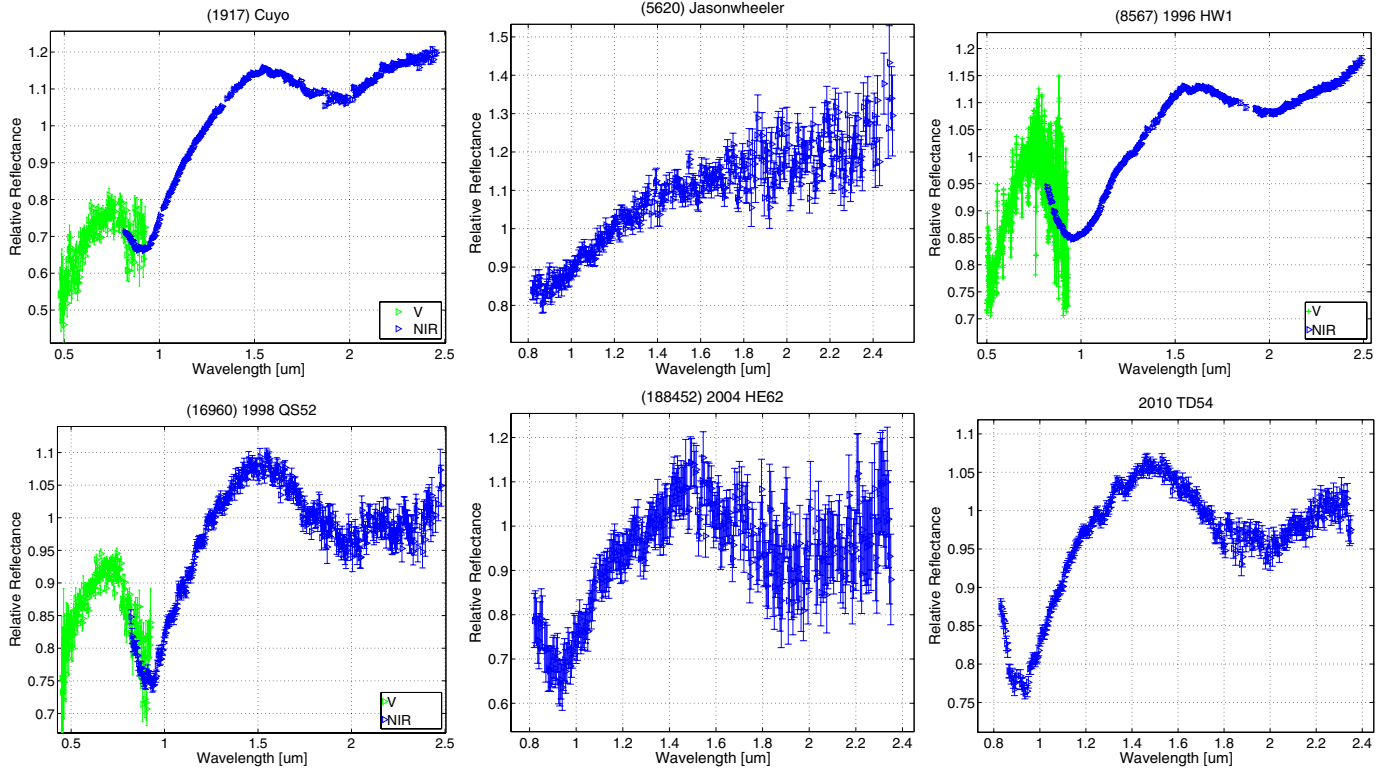


Fig. 1. Spectra of (1917) Cuyo, (5620) Jasonwheeler, (8567) 1996 HW1, (16960) 1998 QS52, (188452) 2004 HE62, and 2010 TD54, with error bars. All spectra are normalized to $1.25 \mu\text{m}$. For (1917) Cuyo, (8567) 1996 HW1, and (16960) 1998 QS52, we added the visible part (plotted with green) from the literature (Binzel et al. 2004b; Vernazza 2006).

Modeling the effects of space weathering on the basis of the exponential continuum, we find that $C_s = -0.484 \mu\text{m}$, corresponding to strong spectral reddening. Owing to the size of this NEA, this value agrees with the general conclusion that larger objects are collisionally older, hence contain surfaces that are more space-weathered, or are not subject to other surface rejuvenating events as frequently as smaller NEAs. The number of displacements per cm^2 , which provides a measure of the solar-wind ion irradiation, is 3.25×10^{19} , which implies that the exposure has been longer than 1 My (Brunetto et al. 2006).

By removing the exponential continuum and fitting the unweathered spectrum with meteorite spectra from the Relab database, the closest match was found for ordinary chondrites with high level content of Fe but with a higher petrological type (H5, H6). The spectra of the following meteorites are very similar to the de-reddened spectrum of (1917) Cuyo: Lancon, Collescipoli, Ehole (Table 3, Fig. B.1).

4.2. (5620) Jasonwheeler

This object has the geometric albedo $p_v = 0.094$ (Mueller et al. 2011). It is an Amor-type asteroid with a diameter of 1.77 km (Mueller et al. 2011) and the synodic period of 5.307 ± 0.001 h (Durkee 2010). The light-curve amplitude of 1.2 magnitude (Durkee 2010) is indicative of an object with an elongated shape, or a binary system. Having $\Delta V = 6.974 \text{ km s}^{-1}$, this asteroid is a suitable target in terms of propulsion for a possible spacecraft mission.

No other spectroscopic studies of this object were found in the literature. The NIR spectrum obtained on May 5, 2009 when the object had the apparent magnitude 16.5, is plotted in Fig. 1.

The MIT-SMASS online tool for taxonomy classified this object as belonging to D-class. With our best-fit method, the spectrum is more similar to T-class (Fig. 3). In general, D-type asteroids have linear spectra with a very steep slope (greater than $0.38 \mu\text{m}^{-1}$) and display a slight curvature around $1.5 \mu\text{m}$. On the other hand, T-types also have linear spectra with a steep gradient – between 0.25 and $0.38 \mu\text{m}^{-1}$ – that nevertheless gradually curves concavely downward (DeMeo et al. 2009). The spectrum of this asteroid has a steep slope in the 0.9 – $1.5 \mu\text{m}$ region and a slight curvature between 1.5 – $2.2 \mu\text{m}$ (Fig. 3), though the classification is at the boundary between D-type and T-type. The overall NIR slope is $0.2504 \mu\text{m}^{-1}$.

Taking into account the low geometrical albedo when comparing with spectra from the Relab database, we found close spectral matches for this spectrum with CM2 carbonaceous chondrite meteorites (Table 3, Fig. A.2). In general, the CM2 meteorites are characterized by 30% levels of chondrules with grain sizes of $\approx 300 \mu\text{m}$, the absence of Fe-Ni alloys, and the presence of CAI (Ca-Al inclusions) (Dobriza 2010). The closest description of the spectrum is provided by a sample of particulates (0 – $75 \mu\text{m}$) from the meteorite Mighei/Meghei (Sample ID: MR-MJG-108). Other spectra of CM2 carbonaceous chondrite meteorites that fit the Jasonwheeler NIR spectrum are those of powdered samples with particle sizes smaller than $125 \mu\text{m}$. This fit suggests that the asteroid might be covered by a fine regolith layer.

By fitting the spectrum (Fig. 2) with an eighth order polynomial function, we can observe an excess of flux after $2.2 \mu\text{m}$ that cannot be explained by the general trend in the spectral region 1.4 – $2.2 \mu\text{m}$ and its taxonomical classification. Even if the level of noise is relatively important, it can be assumed that this

Table 3. Summary of results obtained by matching the asteroid spectra and de-reddened asteroid spectra with spectra from the Relab database.

Matching results for asteroid spectra					
Spectrum	Meteorite	Sample ID	Type	Texture	Size [μm]
(1917) Cuyo	Dhajala	LM-LAM-026	OC/H3-4	Thin Section	–
(5620) Jasonwheeler	Meghei (Mighei)	MR-MJG-108	CC/CM2	Particulates	0–75
	Cold Bokkeveld	MB-TXH-061	CC/CM2	Particulates	0–125
	ALH84029	MB-TXH-052	CC/CM2	Particulates	0–100
(8567) 1996 HW1	Hamlet	OC-TXH-002-C	OC/LL4	Particulates	0–125
(16960) 1998 QS52	Saratov	MB-CMP-028-H	OC/L4	Particulates	0–370
	Homestead	MR-MJG-048	OC/L5	–	–
	Hamlet 1	MR-MJG-069	OC/LL4	–	–
(188452) 2004 HE62	La Criolla	MH-FPF-050-B	OC/L6	Particulates	0–150
	Cherokee Springs	OC-TXH-001-A	OC/LL6	Chip	–
	Wold Cottage	MH-FPF-064	OC/L6	Particulates	–
2010 TD54	Saratov	MB-CMP-028-B	OC/L4	Particulates	10–45
	Mirzapur	TB-TJM-111	OC/L5	Particulates	0–150
	Rio Negro	TB-TJM-081	OC/L4	Particulates	0–150
Matching results for de-reddened asteroid spectra					
(1917) Cuyo	Lancon	MR-MJG-033	OC/H6	–	–
	Collescipoli	MR-MJG-030	OC/H5	–	–
	Ehole	TB-TJM-074	OC/H5	Particulates	0–150
(8567) 1996 HW1	Cherokee Springs	TB-TJM-090	OC/LL6	Particulates	0–150
	Hedjaz	OC-TXH-016-C	OC/L3-6	Particulates	0–125
	Ensisheim	TB-TJM-092	OC/LL6	Particulates	0–150
(16960) 1998 QS52	Hamlet 1	MR-MJG-069	OC/LL4	–	–
	Gruneberg	MR-MJG-040	OC/H4	–	–
(188452) 2004 HE62	Nanjemoy	MR-MJG-034	OC/H6	–	–
	Olmedilla de Alarcon	MR-MJG-075	OC/H5	–	–
	MAC88119.9	MB-TXH-044	OC/H5	Slab	0
2010 TD54	Gruneberg	MR-MJG-040	OC/H4	–	–
	Queen's Mercy	MR-MJG-035	OC/H6	–	–
	Ochansk	MR-MJG-027	OC/H4	–	–

Notes. The comparison was made using a χ^2 method and a selection of the obtained results was done based on spectral features (band, band-gap, concavity) positions, and albedo values. For (5620) Jasonwheeler, a de-reddening model was not applied. The figures for this comparison can be found in Appendices A and B.

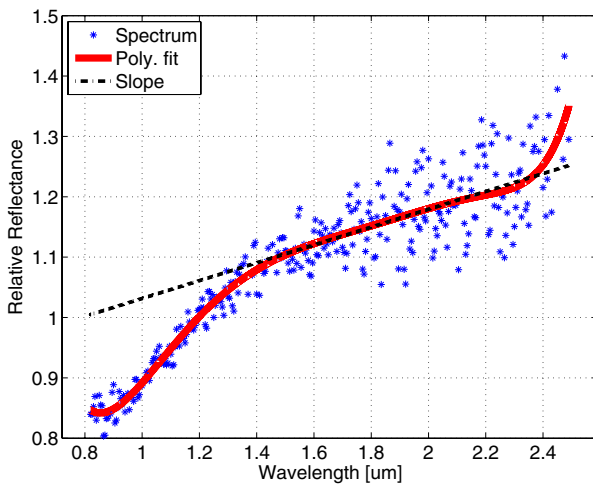


Fig. 2. Spectrum of (5620) Jasonwheeler. The dashed line indicates where a linearly extrapolated continuum would fall, the solid line shows the presence of thermal flux.

feature is caused by asteroid thermal emission. Following Rivkin et al. (2005), we calculated the “thermal excess” parameter that describes this phenomenon:

$$\gamma = \frac{R_{2.5} + T_{2.5}}{R_{2.5}} - 1 = 0.092 \pm 0.0420 \quad (5)$$

where $R_{2.5}$ is the reflected flux at $2.5 \mu\text{m}$ and $T_{2.5}$ is the thermal flux at $2.5 \mu\text{m}$. This value agrees with the geometrical albedo $p_v = 0.094$ for an asteroid at a 1.345 AU distance from the Sun and a phase angle of 20° (Rivkin et al. 2005). This value also agrees with the result obtained from mid-IR observations by Mueller et al. (2011).

Taking into account its dynamical parameters and that D and T types are considered to be of a primitive composition, we can conclude that this object is very interesting from the point of view of “in situ” exploration.

4.3. (8567) 1996 HW1

This asteroid has an Amor type orbit and a $\Delta V = 6.495 \text{ km s}^{-1}$, though it is a suitable target in terms of propulsion for a space mission. The radar observations show a two-lobed object about 1.1 by 2.7 km in size (Taylor et al. 2009). The object is rotating with a synodic period of $8.7573 \pm 0.0009 \text{ h}$ (Higgins et al. 2006).

Vernazza (2006) found this asteroid to be an S-type based on the visible spectrum ($0.5\text{--}0.95 \mu\text{m}$) acquired on August 29, 2005 at TNG. Our NIR spectrum of (8567) 1996 HW1 was obtained in August 28, 2008 using an integration time of 60 s, since the apparent magnitude was 12.9. We combined the visible spectrum from Vernazza (2006) with our NIR data (Fig. 1) before analyzing the composite spectrum.

Using the classification tool from the MIT-SMASS website, this NEA was classified as an S-type with the spectral slope

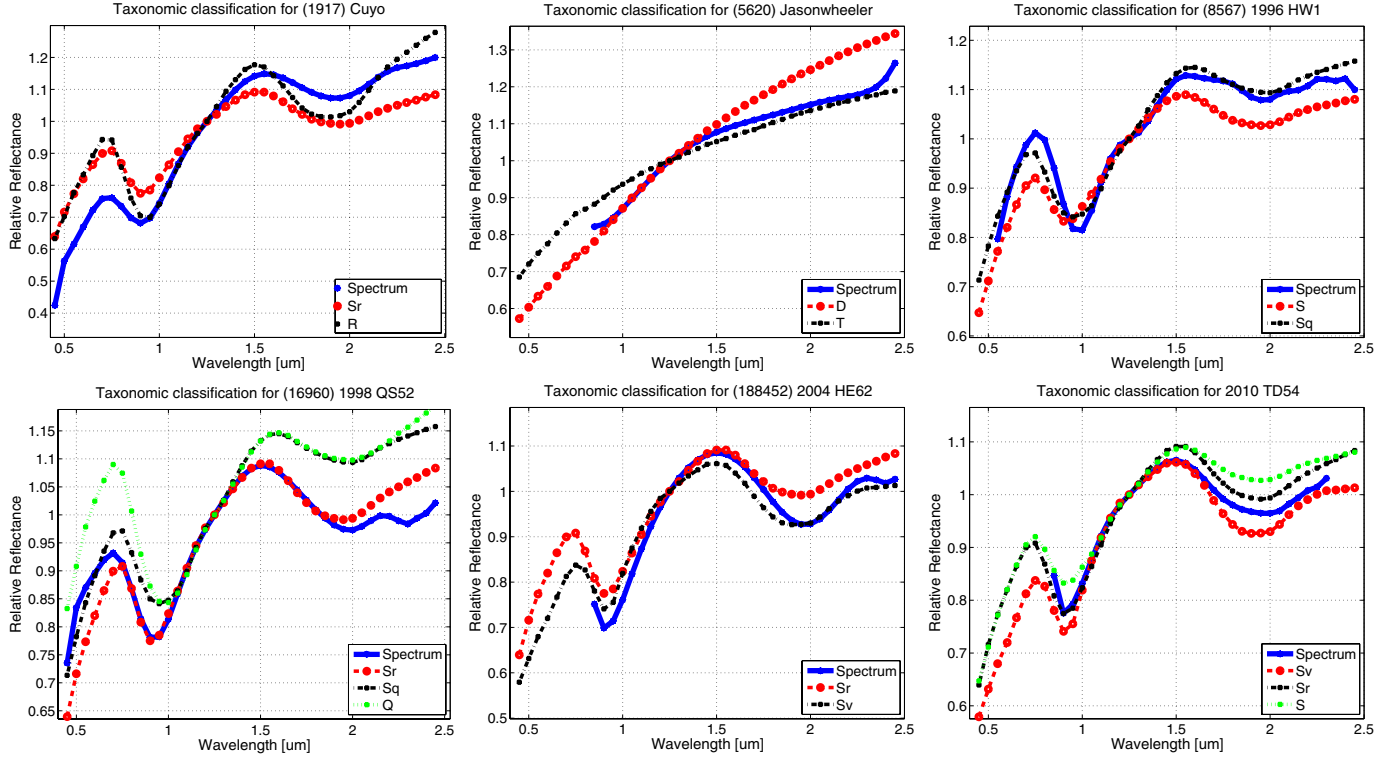


Fig. 3. Classification in Bus-DeMeo taxonomical system for (1917) Cuyo, (5620) Jasonwheeler, (8567) 1996 HW1, (16960) 1998 QS52, (188452) 2004 HE62, and 2010 TD54. The polynomial fit of the spectra are plotted against the curves for the resulting classes. The reflectances are normalized at $1.25 \mu\text{m}$.

$0.2245 \mu\text{m}^{-1}$. Using the χ^2 approach, it can be found that an Sq type provides a closer fit spectrum than an S (Fig. 3), being at the transition between S and Q classes with two absorption bands around $1 \mu\text{m}$ and $2 \mu\text{m}$ that are more shallow than for Q-type (DeMeo et al. 2009). Comparing the features for the two considered spectral types with a polynomial fit of the spectrum, it can be observed that an Sq type matches more closely our data than an S type. Since there has been no measurement of the albedo for this object, assumes a value of 0.20 as typically found for the albedo of S-type asteroids (Fulchignoni et al. 2000), hence the diameter can be estimated to be 2.5 km .

The spectrum from the Relab sample that provides the closest fit is a particulate ground sorted (0–125 μm) Hamlet meteorite (sample ID: OC-TXH-002-C), an ordinary chondrite with a low level content of Fe and metal – LL4 (Table 3, Fig. A.3). The asteroid spectrum in the region $1.6\text{--}2.5 \mu\text{m}$ is shallower than that of the meteorite spectrum, which could be explained by considering space-weathering effects.

Using the space weathering model of Brunetto et al. (2006), we calculated $C_s = -0.258 \mu\text{m}$, which corresponds to the reddening of the spectra. Modelling this with a damage parameter due to the solar-wind ion irradiation we found $d = 1.08 \times 10^{19}$ displacements per cm^2 , thus it has experienced an appreciable amount of space weathering.

By removing the exponential continuum and comparing again with Relab meteorite spectra, we also found the closest match with an ordinary chondrite (LL6, L3-6 types) spectrum with a low metal, low Fe content. The meteorite spectra that provide the closest descriptions of the de-reddened spectrum of this asteroid are those of: Cherokee Spring, Hedjaz, and Ensisheim (Table 3, Fig. B.2). The Relab samples of these meteorites are particulates sorted in order of their sizes, which are smaller than $150 \mu\text{m}$.

4.4. (16960) 1998 QS52

With an absolute magnitude $H = 14.20$, this asteroid has an estimated diameter of 4.3 km (Binzel et al. 2002). It is characterized by a synodic period of $2.900 \pm 0.001 \text{ h}$ (Warner 2009). It has an Apollo orbit type and $\Delta V = 6.5 \text{ km s}^{-1}$, which makes it an accessible target for a spacecraft mission. (16960) 1998 QS52 is a PHA object type with 0.01408 AU MOID computed at epoch 55600.0 MJD (Neody5⁵).

On the basis of a visible spectrum acquired with the MDM 2.4 m telescope in 15 October 1998, Binzel et al. (2004b) classified this asteroid as an Sq type. The spectrum of the visible region has a small negative slope of $-0.0205 \mu\text{m}^{-1}$. We joined the SMASS visible spectrum with our NIR spectrum (Fig. 1). The following analysis was made on the combined V + NIR spectrum.

Both methods of classification gave the same results: this object has the characteristics of an Sr type in Bus-DeMeo taxonomy, with a fairly $1 \mu\text{m}$ feature (Fig. 3). The slope of this composite spectrum is $0.1126 \mu\text{m}^{-1}$.

Comparison with meteorite spectra from Relab database shows the match with ordinary chondrites samples with low content of Fe (L4, LL4, L5). The best fit is a powdered sample (dimensions: $10\text{--}45 \mu\text{m}$) from Saratov meteorite, an ordinary chondrite L4 (Table 3, Fig. A.4).

Analyzing this composite spectrum with a space weathering model (Brunetto et al. 2006), we computed the value of $C_s = -0.149$ which describes an unreddened spectrum corresponding to a fresh surface. It can be speculated that this young surface is due to a relatively recent close encounter with a planet (Binzel et al. 2010).

⁵ <http://newton.dm.unipi.it/neody5/>

To verify this hypothesis, we generated 100 orbital clones of 1998 QS52 using a random Gaussian distribution centered at the nominal values in each of the six orbital elements. The 1σ values were obtained from the orbital elements uncertainties provided by the Neodydys service for this asteroid. The 100 clones were numerically integrated backward in time for 5000 years using the computing routines proposed by Nedelcu (2010). Each close encounter (MOID) with Venus, the Earth, and Mars was then carefully analyzed to find the closest one able to rejuvenate the surface of the object.

In addition to the 1989 close approach with Earth, an event already identified by Neodydys, we were able to confirm that another five close approaches with Venus had occurred in the past 3000 years before the common origin signature of our cloud of clones was erased by close planetary encounters. The MOID values are larger than those predicted by Binzel et al. (2010), whose findings, however, we cannot exclude. Our deterministic clones approach can reliably obtain NEAs positions only for a couple of thousands years backward in time (Nedelcu 2010). Systematic errors in osculating elements can affect the position of the object, and close approaches with telluric planets will modify in a non-linear way the uncertainty in the position. Thus, we estimate that for timescales of millions of years (the scale for SW determined by Brunetto et al. 2006) the object might experience additional close encounters that cannot be reproduced by our numerical integration of orbit.

Comparing the de-reddened spectrum with the Relab database, we found a good fit to the spectrum with a Hamlet meteorite, a LL4 ordinary chondrite (Fig. A.4). This result was also found when comparing with the original spectrum. This agrees with our finding that dividing the spectrum with the exponential continuum by the small value of C_s does not alter its characteristics.

4.5. (188452) 2004 HE62

Few physical parameters of (188452) 2004 HE62 are known. This asteroid has an Amor orbit and an absolute magnitude $H = 17.30$ (Table 2). No other spectral investigations have been published for this asteroid. Our NIR spectrum observations (Fig. 1) of this object were made on August 27, 2008 when the object had an apparent magnitude of 16.7.

The spectrum of (188452) 2004 HE62 has two features around 1 and 2 μm : these are two deep absorption bands that are larger than for Sv-type meteorites but not so deep to be classified as one of the end members R or V. However, the classification is between the Sr and Sv classes in the Bus-DeMeo taxonomy (Fig. 3). A visible spectrum would help us to clarify the object's classification, which in the end was obtained with both methods of classification. The spectral slope computed on the NIR part of the spectrum is $0.1167 \mu\text{m}^{-1}$. Assuming an average albedo of 0.2, which is typical of S-type objects, we can estimate the diameter to be ~ 1 km.

By comparing with data from the Relab database, this spectrum was found to be closely matched by the spectra of ordinary chondrite meteorites with low Fe, low metallic content, and high petrologic class (L6, L5, LL6) – see Table 3 and Fig. A.5 for details. The best-fit solution was obtained with a spectrum of a particulate sample (0–150 μm) from the La Criolla meteorite (Sample ID: MH-FPF-050-B).

Modeling the spectra with the exponential continuum (Brunetto et al. 2006), the parameter C_s is found to be of $-0.377 \mu\text{m}$, which characterizes a surface affected by space weathering effects. Removing this continuum and comparing

with Relab meteorite spectra, the best fit is also an ordinary chondrite (Fig. B.4), the same petrologic class but with a high content of Fe (OC types H5, H6). The closest match in this case is a sample from a Nanjemoy meteorite, a H6 olivine-bronzite OC, which consists of 18% Fayalitic material (Fig. B.4).

4.6. 2010 TD54

The analysis of this object is interesting from the point of view of its size and the phenomena that occur on the surface of small bodies during a close encounter with Earth. With an absolute magnitude $H = 28.75$, 2010 TD54 was discovered by the Catalina Sky Survey in October 09, 2010. Having an Apollo orbit type, this object passed within 0.00035 AU of the Earth on 12.55 Oct. 2010 (Hicks & Rhoades 2010).

Preliminary measurements were done by Hicks & Rhoades (2010). They found a rotational period of 42.0 s, which implies that this small NEA is the most rapidly rotating natural body known in the solar system. They also measured the object's average colors ($B - R = 1.284 \pm 0.045$ mag; $V - R = 0.461 \pm 0.030$ mag; $R - I = 0.344 \pm 0.022$ mag). These are compatible with an S-type spectral classification.

The NIR spectrum of 2010 TD54 is plotted in Fig. 1. Using the MIT-SMASS online tool for Bus-DeMeo taxonomy, this asteroid is classified as belonging to a S complex, of subtypes Sr or Sq. An end class Q is also proposed but with a lower coefficient. By using the χ^2 method, this spectrum can be classified to be between Sv and Sr classes (Fig. 3). It has a fairly prominent feature around 1 μm and another around 2 μm . When considering these two results and the depth of the two absorption bands, we found that the Sr type provides a more accurate description for this object. The slope for this NIR spectrum is $0.062 \mu\text{m}^{-1}$.

The matching with meteorite spectra (Fig. A.6) shows that the best fit is a spectrum for a sample from Saratov – an ordinary chondrite meteorite with a low content of Fe (L4). This sample contains particles with sizes between 10 and 45 μm (Sample ID: MB-CMP-028-B). The spectrum can also be closely fitted with spectra of powdered samples from the meteorites Mirzapur and Rio Negro, which are also L ordinary chondrites.

Modelling the space weathering effects, we computed $C_s = -0.223 \mu\text{m}$, which describes a relatively fresh surface. This agrees with the small bodies having relatively young surfaces, and Earth encounters being one of the origins for rejuvenating surfaces on near-Earth asteroids (Binzel et al. 2010). Removing the exponential continuum and comparing again with spectra from the Relab database, we found a good fit to the spectrum with those of ordinary chondrite meteorites with high level of Fe, from petrologic class 4 (H4 – olivine-bronzite). Spectra of meteorites such as Grunenberg, Queen's Mercy, or Ochansk match the unweathered spectrum of this asteroid (Table 3, Fig. A.6).

4.7. (164400) 2005 GN59

This asteroid has an absolute magnitude $H = 17.40$, derived from astrometric observations. The synodic period of the asteroid was estimated to be 38.62 ± 0.01 h (Vander Haagen 2011), but the monomodal solution of 19.31 ± 0.01 h cannot be totally excluded.

A preliminary spectrum of this object was presented by Birlan et al. (2009), while Taylor et al. (2009) presented thermal emission data corroborated with radar observations. From these radar observations, Taylor et al. (2009) uncovered that this

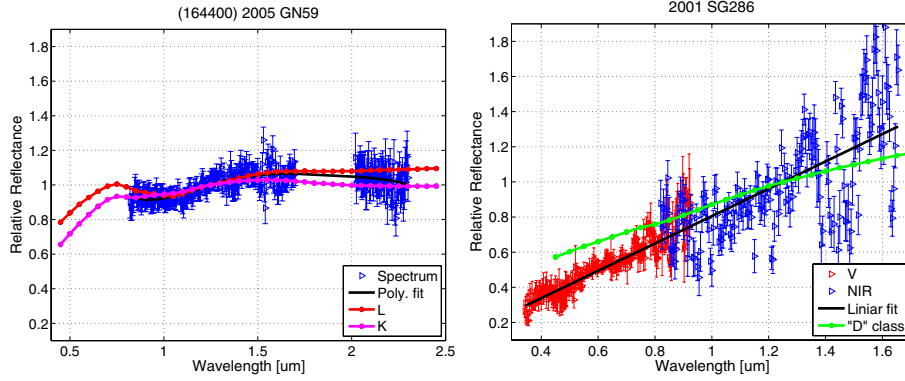


Fig. 4. NIR spectrum of (164400) 2005 GN59 and 2001 SG286. These spectra are normalized to $1.25 \mu\text{m}$.

object has a two-lobed 0.35 by 1.1 km shape, with non-convex surface features.

Dynamically, (164400) 2005 GN59 is an Apollo asteroid. Its calculated $\Delta V = 6.002 \text{ km s}^{-1}$ imply that it is a suitable target in terms of propulsion for spacecraft mission.

The NIR spectrum of 164400 was obtained in August 28, 2008 for a total integration time of 480 s. While the spectrum is quite noisy, to obtain information about its taxonomic class, we used a five order polynomial function to reproduce the real data. The values for reflectance corresponding to wavelengths between 1.7 and $2 \mu\text{m}$ were excluded because of the very high noise caused by atmospheric turbulence (Fig. 4).

Both the MIT-SMASS on-line tool and the χ^2 routine classify this object as an L-type. However, the K taxonomic class is also a reasonable match to our data (Fig. 4).

An additional NIR spectrum of this object was obtained by the MIT-UH-IRTF Joint Campaign for NEO Spectral Reconnaissance⁶. This spectrum has higher S/N than ours. We classified this spectrum with both methods and found it to be between Sq and Q types, while a K taxonomic class was proposed as a third solution. The L taxonomic class is also considered as a possible solution by the MIT-SMASS on-line tool. The difference between our spectrum and this one is caused by the low signal-to-noise ratio of our spectrum, which prevented us taking into consideration the feature between 1.7 and $2 \mu\text{m}$. A visible spectrum would again help us to distinguish between the five possible solutions for the NIR part of the spectrum.

The spectrum of 2005 GN59 is noisy and we did not attempt to compare it with the Relab database and the de-reddening model.

4.8. 2001 SG286

This is an Apollo type asteroid with an absolute magnitude of 20.9. It is classified as PHA. Its $\Delta V = 5 \text{ km s}^{-1}$ makes it a suitable target for a spacecraft mission. Michel & Delbo (2010) estimated its median lifetime as an NEA to be about 22.19 Myr. The mechanism of injection into the NEA population is the secular ν_6 resonance, but the 3:1 mean motion resonance with Jupiter could not be entirely excluded (Michel & Delbo 2010).

On the basis of spectral data in the visible region, Binzel et al. (2004a) classified this asteroid as a D-type one. Using an average albedo of 0.09 for D-type asteroids, Binzel et al. (2004a) computed a diameter of about 350 m for this object.

The object was observed on May 19, 2009 in the NIR for a total time of 480 s, in difficult conditions (considerable

Table 4. Slope and C_s parameter for the S-type objects studied in this article.

Object	Slope (μm^{-1})	C_s (μm)
(1917) Cuyo	0.5086	−0.484
(8567) 1996 HW1	0.2245	−0.258
(16960) 1998 QS52	0.1126	−0.149
(188452) 2004 HE62(*)	0.1167	−0.377
2010 TD54(*)	0.0620	−0.223

Notes. The calculation was made by normalization of spectra to $0.55 \mu\text{m}$. Objects marked with (*) are normalized to $1.25 \mu\text{m}$ (only for NIR part).

differential motion, only a few hours of visibility over three nights, limited atmospheric transparency). The NIR spectrum is reliable only for the spectral interval 0.8 – $1.7 \mu\text{m}$.

The composite V+NIR spectrum was obtained by superposing data in the 0.82 – $0.9 \mu\text{m}$ spectral interval (Fig. 4). The slope parameter for the composite spectrum is $0.7202 \mu\text{m}^{-1}$ (computed for a spectrum normalized to a reflectance value at $1.25 \mu\text{m}$) in agreement with the slope range for D-type taxonomic class.

5. Discussion

Luu & Jewitt (1990) suggested that the phase angle can affect the spectral slope. This was called “phase reddening” and consists of an increase in the spectral slope (reddening of the spectra) with the phase angle. Some studies have been performed based on laboratory measurements (Gradie & Veverka 1986) and during the approach to (433) Eros by the NEAR spacecraft (Veverka et al. 2000). However, for our method of observation we retain the result mentioned in Binzel et al. (2004b) regarding a study conducted at MIT for which no correlation was found between the phase angle and the spectral slope for the ground-based asteroid reflectance spectra.

During our observing runs, all the asteroids were observed at phase angles as small as possible. Owing to this constraint, we succeeded in observing only six objects at a phase angles between 17° and 30° (Table 1). We observed (1917) Cuyo and (188452) 2004 HE62 at a phase angle around 60° (Table 1).

Assuming similar surface mineralogies, the influence of phase angle on spectral slope is unclear from our measurements. For (1917) Cuyo, a high spectral slope was obtained, but for (188452) 2004 HE62 the computed spectral slope is comparable to the spectral slope of (8567) 1996 HW1 and (16960) 1998 QS52, which were measured at phase angles smaller than

⁶ <http://smass.mit.edu/minus.html>

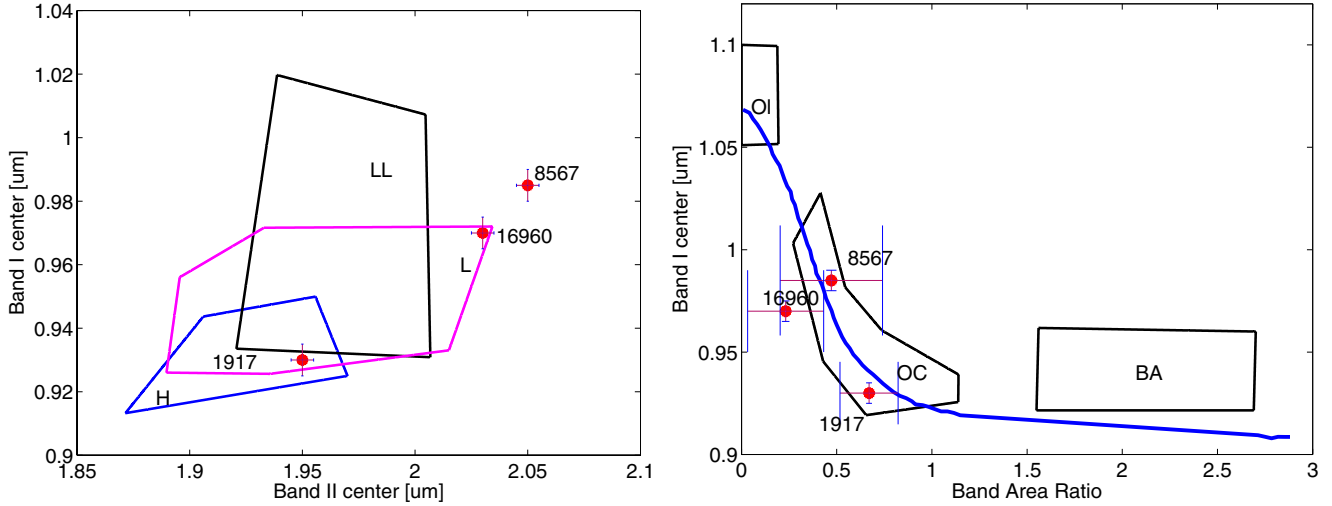


Fig. 5. (Left) Wavelength position of the centers of the two absorption bands computed using Cloutis et al. (1986). The regions enclosed correspond to the band centers computed for the H, L, and LL chondrites, respectively (de León et al. 2010). (Right) Band area ratio (BAR) versus band I centers. The regions enclosed by continuous lines correspond to the values computed for basaltic achondrites, ordinary chondrites (OC), and olivine-rich meteorites (Ol) (Gaffey et al. 1993).

30° (Table 4). Considering the trend of S-class objects, the reflectance value at 1.25 μm is higher than the reflectance value at 0.55 μm, thus our comparison of slopes is correct. Therefore, no correction has been applied for this presumed effect of phase reddening.

Several NIR spectra for the asteroids (1917) Cuyo, (8567) 1996HW1, and (16960) 1998 QS52 were obtained by the MIT-UH-IRTF Joint Campaign for NEO Spectral Reconnaissance. These spectra are similar to those presented in this paper in terms of spectral features. However, a variation in spectral slope between the spectra of the same object was observed. Similar spectral variations in the NIR spectrum of a NEO was previously reported by de León et al. (2011). For our sample, the asteroid (8567) 1996HW1 was observed five times, at phase angles between 20° and 55°. In this case, a variation in the spectral slope with phase angle was observed (i.e. the spectrum is redder for larger phase angles). While this object is not well-known in terms of spin axis and shape, it is difficult to draw any conclusions about the first order dependence of the slope on phase angle, while a surface dichotomy and degrees of space weathering could compete with this effect.

The S-types objects in our sample have widely varying spectral slopes (Table 4), which is a general conclusion for the asteroids belonging to this complex (DeMeo et al. 2009). In the Bus-DeMeo taxonomy, the objects in the S-complex with a slope larger than 0.25 μm⁻¹ receive the notation “w” added to their type as an indication that they may be affected by space weathering effects. This is the case for (1917) Cuyo.

Although space weathering may occur on all asteroids, many types lack strong spectral-band contrasts that ensure that weathering effects are easily detectable (Clark et al. 2002). S-class asteroids are significantly reddened compared with their presumed meteorite analog, and this difference can be explained by space weathering phenomenon (Vernazza et al. 2008). This process may be the result of dust impacts and solar wind sputtering on the surface of atmosphereless bodies and cause a reddening of the spectral slope, a decrease in spectral absorption intensities, and a diminishing of albedo (Fornasier et al. 2003).

An important concept in understanding space weathering processes is the development and accumulation of

Table 5. Computed parameters from the Cloutis et al. (1986) model applied to the V+NIR spectra of (1917) Cuyo, (8567) 1996 HW1, and (16960) 1998 QS52.

Object	BI (μm)	BII (μm)	BAR	OPX (%)
(1917) Cuyo	0.93	1.95	0.670 ± 0.1526	33.28
(8567) 1996 HW1	0.99	2.06	0.485 ± 0.2687	25.50
(16960) 1998 QS52	0.97	2.03	0.232 ± 0.1996	14.94

Notes. The estimation error for band centers (BI, BII) is ±0.005.

submicroscopic single-domain metallic Fe (4–30 nm), produced in the space environment by a reduction of FeO in minerals. Referred to as nanophase reduced iron – “npFe⁰”, these are formed through the fractional processes that occur during ion-particle sputtering, vapor deposits from energetic micrometeorites impacts, or both. As more “npFe⁰” accumulates, the entire continuum becomes redder until it is almost linear through to the near-infrared region. With small amounts of “npFe⁰”, reddening of only the visible region of the spectra occur (Pieters et al. 2000).

A space weathering model has been applied to five spectra in our samples (of S-type objects). For two asteroids, (188452) 2004 HE62 and 2010 TD554, the models imply that the iron content ambiguity changes the best analog among meteorite samples. Thus, the best mineralogical analog will always be an OC meteorite, the same petrologic type, but the spectra for a sample containing Fe will be different. This could be explained in the following terms: highly curved continua occur for samples with small amounts of npFe⁰, and the more linear continua occur for samples with large amounts of npFe⁰ (Pieters et al. 2000).

A quantitative comparison between the reflectance properties of (1917) Cuyo, (8567) 1996 HW1, and (16960) 1998 QS52 (since for these objects we have both visible and NIR data) and potential meteorite analogs could be made with the parameters computed from the model of Cloutis et al. (1986). The values of these parameters are given in Tabel 5. Plotting Band I center versus the BAR (Gaffey et al. 1993), we found

that all three objects are located in the ordinary chondrite region (Fig. 5). (1917) Cuyo and (16960) 1998 QS52 are under the olivine-orthopyroxene mixing line, while (8567) 1996 HW1 is above the olivine-orthopyroxene mixing line.

Another comparison was made by plotting the Band I center versus the Band II center (Fig. 5). Considering the results of de León et al. (2010), we found that (1917) Cuyo is in the region of OC-H meteorites, while 16960 is in the region of OC-L meteorites. (8567) 1996 HW1 is outside the enclosed areas, between the regions for L and LL chondrites.

This statistical interpretation of the results agrees with our results obtained by comparison to Relab meteorite spectra. These measured parameters are direct indications of a spectrum's basic properties – revealing their distributions without making any assumptions about their underlying mineralogy (Vernazza et al. 2008).

6. Conclusions

We obtained NIR spectra for eight near-Earth asteroids using IRTF/SpEx. The observations were performed remotely between the IRTF and Observatoire de Paris-Meudon. This technique proved to be robust while providing full control of the spectrograph and access to several telescope operations (focus, tracking, etc.).

Four of the observed objects have ΔV lower than 7 km s^{-1} , which make them suitable targets in terms of propulsion for a future spacecraft mission.

We have modelled and interpreted the obtained spectra using a variety of techniques with the goal of interpreting the asteroidal surfaces in terms of their mineralogical composition. Each asteroid spectrum was analyzed to obtain its taxonomic class and the closest matching meteoritic analogs in the laboratory. We have considered and discussed the effects of space weathering based on the model of Brunetto et al. (2006).

The taxonomic classification of five objects was reviewed and we assigned a corresponding type to the other three asteroids that had not been previously classified. We found that (1917) Cuyo, (8567) 1996 HW1, (16960) 1998 QS52, (188452) 2004 HE62, and 2010 TD54 are in the S-complex. For these objects, a good matching with the spectra of ordinary chondrites meteorites has been obtained.

The asteroid Jasonwheeler was found to have a NIR spectrum similar to that of carbonaceous chondrite meteorites. It was classified to be between D and T taxonomic class. Since these classes are considered to have primitive compositions and the ΔV for this object is smaller than 7 km s^{-1} , Jasonwheeler could be a very interesting candidate for a sample and return spacecraft mission.

Acknowledgements. The article is based on observations acquired with InfraRed Telescope Facilities as well as the CODAM remote facilities. We thank all the telescope operators for their contribution. This research utilizes spectra acquired with the NASA RELAB facility at Brown University.

The work of Marcel Popescu was supported by the ESA traineeships program Ref: RES-HM/1636.

The work of Dan Alin Nedelcu was partially supported by the Romanian National Authority for Scientific Research (ANCS) under the project POSCCE-A2-O2.1.2-2009-2/651.

References

- Barucci, M. A., Capria, M. T., Coradini, A., & Fulchignoni, M. 1987, *Icarus*, 72, 304
- Binzel, R. P., Lupishko, D., di Martino, M., Whiteley, R. J., & Hahn, G. J. 2002, *Asteroids III*, 255
- Binzel, R. P., Perozzi, E., Rivkin, A. S., et al. 2004a, *Meteoritics and Planetary Science*, 39, 351
- Binzel, R. P., Rivkin, A. S., Stuart, J. S., et al. 2004b, *Icarus*, 170, 259
- Binzel, R. P., Morbidelli, A., Merouane, S., et al. 2010, *Nature*, 463, 331
- Birlan, M., Barucci, M. A., & Fulchignoni, M. 1996, *A&A*, 305, 984
- Birlan, M., Barucci, M. A., Vernazza, P., et al. 2004, *New Astron.*, 9, 343
- Birlan, M., Vernazza, P., Fulchignoni, M., et al. 2006, *A&A*, 454, 677
- Birlan, M., Vernazza, P., & Nedelcu, D. A. 2007, *A&A*, 475, 747
- Birlan, M., Binzel, R. P., Nedelcu, D., et al. 2009, in *AAS/Division for Planetary Sciences Meeting Abstracts*, 41, 34.08
- Brunetto, R., & Strazzulla, G. 2005, *Icarus*, 179, 265
- Brunetto, R., Vernazza, P., Marchi, S., et al. 2006, *Icarus*, 184, 327
- Bus, S. J., & Binzel, R. P. 2002, *Icarus*, 158, 146
- Clark, B. E., Hapke, B., Pieters, C., & Britt, D. 2002, in *Asteroids III*, ed. W. F. Bottke Jr., A. Cellino, P. Paolicchi, & P. Binzel (University of Arizona Press: Tucson), 585
- Cloutis, E. A., Gaffey, M. J., Jackowski, T. L., & Reed, K. L. 1986, *J. Geophys. Res.*, 91, 641
- Das Gupta, S. P., Sen Gupta, P. R., Dube, A., Sen Gupta, N. R., & Das Gupta, D. R. 1978, *Mineralogical Magazine*, 42, 493
- de León, J., Licandro, J., Serra-Ricart, M., Pinilla-Alonso, N., & Campins, H. 2010, *A&A*, 517, A23
- de León, J., Mothé-Diniz, T., Licandro, J., Pinilla-Alonso, N., & Campins, H. 2011, *A&A*, 530, L12
- DeMeo, F. E., Binzel, R. P., Slivan, S. M., & Bus, S. J. 2009, *Icarus*, 202, 160
- Dobrica, E. 2010, Ph.D. Thesis, University Paris Sud
- Durkee, I. R. 2010, *Minor Planet Bulletin*, 37, 18
- Fornasier, S., Barucci, M. A., Binzel, R. P., et al. 2003, *A&A*, 398, 327
- Fulchignoni, M., Birlan, M., & Antonietta Barucci, M. 2000, *Icarus*, 146, 204
- Gaffey, M. J., Burbine, T. H., Piatek, J. L., et al. 1993, *Icarus*, 106, 573
- Gradie, J., & Veverka, J. 1986, *Icarus*, 66, 455
- Hapke, B. 2001, *J. Geophys. Res.*, 106, 10039
- Hicks, M., & Rhoades, H. 2010, *The Astronomer's Telegram*, 2984, 1
- Higgins, D., Pravec, P., Kusnirak, P., et al. 2006, *Minor Planet Bulletin*, 33, 8
- Kong, P., & Ebihara, M. 1997, *Geochim. Cosmochim. Acta*, 61, 2317
- Loeffler, M. J., Dukes, C. A., & Baragiola, R. A. 2009, *J. Geophys. Res. (Planets)*, 114, E03003
- Luu, J. X., & Jewitt, D. C. 1990, *AJ*, 99, 1985
- Michel, P., & Delbo, M. 2010, *Icarus*, 209, 520
- Michelsen, R., Nathues, A., & Lagerkvist, C. 2006, *A&A*, 451, 331
- Milani, A., Chesley, S. R., & Valsecchi, G. B. 2000, *Planet. Space Sci.*, 48, 945
- Morbidelli, A., Jedicke, R., Bottke, W. F., Michel, P., & Tedesco, E. F. 2002, *Icarus*, 158, 329
- Mueller, M., Delbo, M., Hora, J. L., et al. 2011, *AJ*, 141, 109
- Nedelcu, D. A. 2010, Ph.D. Thesis, Observatoire de Paris
- Pieters, C. M., Taylor, L. A., Noble, S. K., et al. 2000, *Meteor. Planet. Sci.*, 35, 1101
- Popescu, M., & Birlan, M. 2011, unpublished
- Rayner, J. T., Toomey, D. W., Onaka, P. M., et al. 2003, *PASP*, 115, 362
- Rivkin, A. S., Binzel, R. P., Sunshine, J., et al. 2004, *Icarus*, 172, 408
- Rivkin, A. S., Binzel, R. P., & Bus, S. J. 2005, *Icarus*, 175, 175
- Taylor, P. A., Howell, E. S., Magri, C., et al. 2009, in *AAS/Division for Planetary Sciences Meeting Abstracts*, 41, 32.01
- Tholen, D. J. 1984, Ph.D. Thesis, Arizona Univ., Tucson
- Tody, D. 1986, in *SPIE Conf. Ser.* 627, ed. D. L. Crawford, 733
- Vacca, W. D., Cushing, M. C., & Rayner, J. T. 2004, *PASP*, 116, 352
- Vander Haagen, G. A. 2011, *Minor Planet Bulletin*, 38, 10
- Vernazza, P. 2006, Ph.D. Thesis, Observatoire de Paris
- Vernazza, P., Binzel, R. P., Thomas, C. A., et al. 2008, *Nature*, 454, 858
- Vernazza, P., Binzel, R. P., Rossi, A., Fulchignoni, M., & Birlan, M. 2009, *Nature*, 458, 993
- Veverka, J., Robinson, M., Thomas, P., et al. 2000, *Science*, 289, 2088
- Warner, B. D. 2009, *Minor Planet Bulletin*, 36, 7
- Wisniewski, W. Z., Michalowski, T. M., Harris, A. W., & McMillan, R. S. 1997, *Icarus*, 126, 395
- Zellner, B., Tholen, D. J., & Tedesco, E. F. 1985, *Icarus*, 61, 355

Modeling of asteroid spectra – M4AST[★]

M. Popescu^{1,2,3}, M. Birlan¹, and D. A. Nedelcu⁴

¹ Institut de Mécanique Céleste et de Calcul des Éphémérides (IMCCE) CNRS-UMR8028, Observatoire de Paris,
77 avenue Denfert-Rochereau, 75014 Paris Cedex, France
e-mail: mpopescu@imcce.fr

² Polytechnic University of Bucharest, Faculty of Applied Sciences, Department of Physics, 040557 Bucharest, Romania

³ Astroclub Bucharest, Lascăr Catargiu Boulevard, Nr. 21, 040557 Bucharest, Romania

⁴ Astronomical Institute of the Romanian Academy, 5 Cuțitul de Argint, 040557 Bucharest, Romania

Received 11 May 2012 / Accepted 3 July 2012

ABSTRACT

Context. The interpretation of asteroid spectra provides the basis for determining the chemical composition and physical process that modified the surface of the asteroids. The increasing number of asteroid spectral measurements has lead to well-developed methods for analyzing asteroid spectra. There is however no centralized database for all the published data and a set of standard routines is also required.

Aims. We present a public software tool that combines both data archives and analyses of asteroid spectra.

Methods. Our project M4AST (Modeling for asteroids) consists of an asteroid spectral database and a set of applications for analyzing asteroid spectra. These applications cover aspects related to taxonomy, curve matching with laboratory spectra, space weathering models, and mineralogical diagnosis.

Results. M4AST project is fully available via a web interface. The database contains around 2700 spectra that can be either processed in M4AST and/or downloaded. The paper presents the algorithms we developed for spectral analyses based on existing methods. The robustness of routines is proven by the solutions found for spectra of three different asteroids: (9147) Kourakuen, (99 942) Apophis, and (175 706) 1996 FG3. The available results confirm those in the literature. M4AST applications can also be used to characterize any new asteroid spectra.

Conclusions. M4AST is a robust and reliable tool dedicated to asteroid spectra.

Key words. minor planets, asteroids: general – methods: data analysis – techniques: spectroscopic

1. Introduction

Spectroscopic studies of celestial bodies connect astronomy with fundamental physics on both atomic and molecular levels. The interpretation of the visible and near-infrared reflectance spectra of asteroids provides a powerful remote method for characterizing their surface composition. The mineralogical and the chemical properties of these objects provide direct information about the conditions and processes that were present during the very early stages of the evolution of the solar system. Another important aspect related to asteroids is their relative accessibility to spacecraft investigations. This enables their scientific study and the detailed assessment of their future use as space resources. The choice of targets and the planning of space missions are based on the ensemble of physical and dynamical parameters of these objects, which are properties inferred from ground-based observations.

Asteroid spectra have been obtained since the late 1960s. McCord et al. (1970) published the first spectral measurements in the 0.3–1.1 μm wavelength region for the asteroid (4) Vesta, and found that its spectrum is similar to those of basaltic achondritic meteorites. The most important surveys in the 1980s for measuring the spectral characteristics of asteroids were the Eight-Color Asteroid Survey (ECAS, Zellner et al. 1985), and the 52-color survey (Bell et al. 1988). All these results showed the diversity of asteroid surface composition.

In the past two decades, the development of CCD spectrographs have made it possible to obtain spectra of significantly fainter asteroids with a much higher spectral resolution than achievable with filter photometry. Several spectroscopic surveys have been performed, including SMASS (Xu et al. 1995), SMASS2 (Bus & Binzel 2002b), and S³OS² (Lazzaro et al. 2004). Other spectroscopic surveys have been dedicated only to near-Earth asteroids such as SINEO (Lazzarin et al. 2005) or the survey performed by de León et al. (2010). The total number of asteroid spectra resulting from these surveys is on the order of thousands and has led to a mature understanding of their population.

Currently, the spectral data of asteroids continues to grow. The most important spectral surveys for asteroid have made their data available online. There is no centralized database containing all the asteroid spectra¹. Moreover, the exploitation of these data in terms of the construction of mineralogical models, comparison to laboratory spectra, and taxonomy is treated individually by each team working in this field. While the spectral databases for asteroids have become significant in size and the methods for modeling asteroid spectra are now well-defined and robust, there are no standard set of routines for handling these data.

We developed M4AST (Modeling for Asteroids), which is a tool dedicated to asteroid spectra (Popescu et al. 2011; Birlan & Popescu 2011). It consists of a database containing the results

[★] M4AST is available via the web interface:
<http://cardamine.imcce.fr/m4ast/>

¹ Some of these data are archived within the Small Bodies Node of the Planetary Data System (<http://pds.nasa.gov/>).

of the observational measurements and a set of applications for spectral analysis and interpretation. M4AST covers several aspects related to the statistics of asteroids – taxonomy, curve matching with laboratory spectra, modeling of space weathering effects, and mineralogical diagnosis. M4AST was conceived to be available via a web interface and is free for access to the scientific community.

This paper presents M4AST as follows: in Sect. 2, we briefly review the general methods used to analyze asteroid spectra. In Sect. 3, we describe the structure of the database, and in Sect. 4 we give details about the M4AST interfaces and their use. Section 5 presents the algorithms behind the different models implemented in M4AST. Section 6 shows some examples of spectral analysis and discusses the applicability of the models. We end up with the conclusions and further perspectives.

2. Methods for asteroid spectra analysis

“Asteroids” actually means “star-like” and viewed through a telescope, as these planetesimals are merely a point source of light. A panoply of new observational techniques (e.g. spectroscopy, photometry, polarimetry, adaptive optics, radar, etc.) has transformed these star-like objects into individual little worlds.

One of the techniques used to characterize the surface of asteroids is reflectance spectroscopy in the visible and near-infrared wavelength regions. Diagnostic features in spectra related to electronic and vibrational transitions within minerals or molecules are detectable in the 0.35–2.50 μm spectral range. The overlapping of the absorption bands from different mineral species provides a distinctive signature of the asteroid surface. Olivine, pyroxene (clino- and ortho-pyroxene), iron-nickel (Fe-Ni) metal, spinel, and feldspar are some of the most important minerals that can be identified by carefully analyzing the reflection spectra of the asteroid (McSweeney 1999).

The analysis of reflectance spectra can be done using several methods, such as taxonomic classification, comparison with laboratory spectra, band parameter determination, and modeling of the space weathering effects. We briefly discuss below the methods implemented via M4AST.

2.1. Taxonomy

Taxonomy is the classification of asteroids into categories (classes, taxons) using some parameters and *a priori* rules. The main goal is to identify groups of asteroids that have similar surface compositions. The classification into taxons is the first step for further studies of comparative planetology. In the case of asteroids, a precise taxonomic system gives an approach to a specific mineralogy for each of the defined classes.

Taxonomic systems of asteroids were initially based on asteroid broadband colors (Chapman et al. 1971), which allowed us to distinguish between two separate types of objects, denoted “S” (stony) and “C” (carbonaceous). Based on the increasing amount of information from different types of observations, new taxonomic classes were defined. Historically, the most widely used taxonomies are the following: Tholen (1984) and Barucci et al. (1987), which used data from the Eight-Color Asteroid Survey (Zellner et al. 1985); Bus & Binzel (2002a), which used data from the SMASS2 survey; and DeMeo et al. (2009), which is an extension of a previous taxonomy scheme into the near-infrared.

Statistical methods are used for defining taxonomic systems of asteroids. We point out two of them, namely principal component analysis (PCA) and the G-mode clustering method.

Principal component analysis (PCA) is a method for reducing the dimensionality of a data set of M variables, involving linear coordinate transformations to minimize the variance. The first transformation rotates the data to maximize the variance along the first axis, known as the principal component 1 (PC1), then along the second axis – the second principal component, and so on. Overall, the new coordinates are ordered decreasingly in terms of the dispersion in the principal components.

The G-mode is a multivariate statistical clustering method that allows us to classify a statistical sample consisting of N elements with M variables. The parameter G is the analog of the distance in a $N \times M$ space. This statistical distance between an object and a taxonomic class shows the similarities of the characteristics of this object to those of its class (Birlan et al. 1996). One of the advantages of this method is that even if only a subset of variables are available for an object (only part of the spectrum), a preliminary classification can still be achieved.

2.2. Spectral comparison

Spectroscopy of different samples performed in the laboratory provides the basis upon which compositional information about unexplored planetary surfaces can be understood from remotely obtained reflectance spectra. Thus, confronting the spectral data derived from telescopic observations with laboratory measurements is an important step in study of asteroid physical properties (Britt et al. 1992; Vernazza et al. 2007; Popescu et al. 2011).

Several spectral libraries are available for accomplishing this task, such as Relab², USGS Spectroscopy Laboratory³, the Johns Hopkins University (JHU) Spectral Library, the Jet Propulsion Laboratory (JPL) Spectral Library⁴, etc. We use the Relab spectral library in M4AST, which is one of the largest libraries and contains more than 15 000 spectra for different types of materials from meteorites to terrestrial rocks, man-made mixtures, and both terrestrial and lunar soils.

2.3. Space weathering effects

It is now widely accepted that the space environment alters the optical properties of airless body surfaces. Space weathering is the term that describes the observed phenomena caused by these processes operating at or near the surface of an atmosphere-less solar system body, that modify the remotely sensed properties of this body surface away from those of the unmodified, intrinsic, subsurface bulk of the body (Chapman 1996, 2004).

The objects that are most affected by the space weathering are silicate-rich objects for which a progressive darkening and reddening of the solar reflectance spectra appear in the 0.2–2.7 μm spectral region (Hapke 2001). Lunar-type space weathering is well-understood, but two well-studied asteroids (433 Eros and 243 Ida) exhibit different space weathering types. The mechanism of space weathering for asteroids is still currently far from being completely understood.

The latest approaches to the study of space weathering are based on laboratory experiments. Simulations of micrometeorites and cosmic ray impacts have been achieved using nanosecond lasers on olivine and pyroxene samples. These have

² <http://www.planetary.brown.edu/relab/>

³ <http://speclab.cr.usgs.gov/>

⁴ <http://speclib.jpl.nasa.gov/>

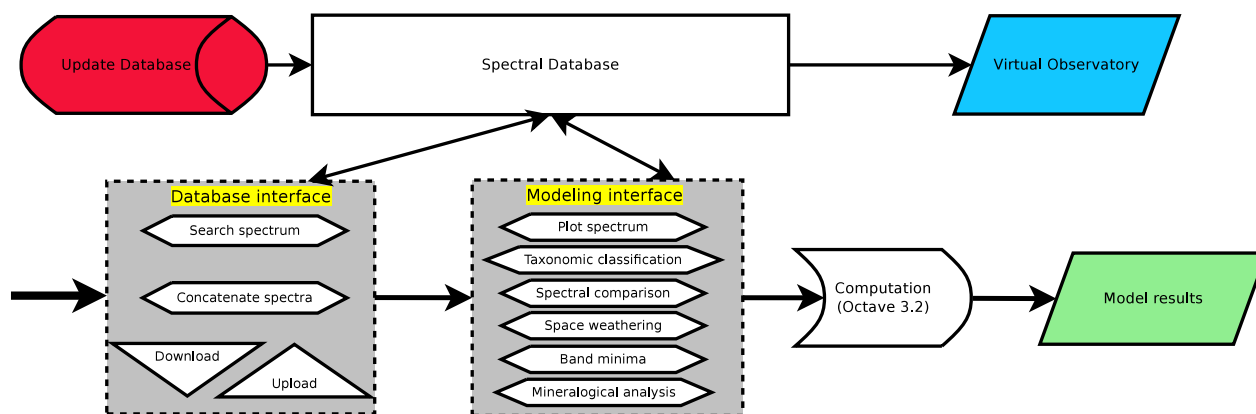


Fig. 1. Block diagram and work flow of M4AST.

shown that laser ablation lowers the albedo, dampens the absorption bands, and reddens the spectrum. These effects could explain the transition from “fresh” ordinary chondrite material to the observed asteroid spectra (Yamada et al. 1999; Sasaki et al. 2001). The spectral effects generated by the solar wind irradiation to silicate materials were investigated by Brunetto et al. (2006). On the basis of ion irradiation experiments, they found “a weathering function” that could be used to fit the ratio of the spectra of irradiated to unirradiated samples, which was implemented in M4AST.

2.4. Band parameters

The “traditional” method used for mineralogical analysis is based on different parameters that can be computed from the reflectance spectra of the object. These parameters give information about the minerals that are present on the surface of the asteroid, their modal abundances, and the size of the grains.

Cloutis et al. (1986) outlined an analytical approach that permits the interpretation of visible and near-infrared spectral reflectance to determine the mineralogic and petrologic parameters of olivine-orthopyroxene mixtures, including end-member abundances, chemistries, and particle size. These parameters are the wavelength position of the reflectance minima around $1\ \mu\text{m}$ and $2\ \mu\text{m}$, the band centers, and the band area ratio (BAR) which is the ratio of the areas of the second absorption band relative to the first absorption band.

Gaffey (2010) noted that mineralogically diagnostic spectral parameters (band centers, BARs) are “essentially immune to the effects of space weathering observed and modeled to date”.

3. Spectral database

The schematic of the M4AST project is given in Fig. 1. The first component is the spectral database. It contains the results of telescopic measurements for the reflectance spectra of different wavelength ranges (V – visible, NIR – near infrared, V+NIR – visible and near infrared) of the asteroids and the observations logs.

3.1. Structure of M4AST database

The information in the database is organized into two type of files: *permanent* and *temporary* files. Additionally, there is a catalog to keep track of the permanent files recorded.

Permanent files are uploaded through a dedicated interface protected by a password. Any new file submitted in this way is recorded in a catalog together with its observation log. The observation log is also kept in the header of the file containing the corresponding spectral data, including IAU designations of the asteroid, the date and hour (UT) of the observation, and the IAU code of the observatory. Additional information could be included such as the investigator name and e-mail address as well as the link to a reference if the spectrum was published.

Each file containing the spectral data includes a header with the observation log and the measurements given in two columns: the first column contains the wavelength in μm , and the second column contains the corresponding reflectance values (normalized to unity at $0.55\ \mu\text{m}$ if the visible part of the spectrum is contained, and otherwise at $1.25\ \mu\text{m}$). If the dispersions in the measurements are available, they are provided in the third column.

Temporary files are created by the users only for processing the data. They provide a way for the anonymously user to use the applications of M4AST for his own spectral data. Temporary files receive a random name and can be removed by the same user that created them (no administrative rights are required). The application library is fully available for modeling spectral data contained in temporary files. No permanent information is recorded.

3.2. The content

Historically, the database was designed for making available to the scientific community the spectra obtained after observations performed remotely from the Centre d’Observation à Distance en Astronomie à Meudon (CODAM) (Birlan et al. 2004, 2006). The observations were obtained in the $0.8\text{--}2.5\ \mu\text{m}$ spectral region using the SpeX/IRTF instrument, located on Mauna Kea, Hawaii. The project now includes around 2,700 permanent spectra (in the V and NIR wavelength regions) of both main belt and near-Earth asteroids.

Along with the spectra obtained via CODAM, the main sources of the project are SMASSI (Xu et al. 1995), SMAII (Bus & Binzel 2002b), and S³OS² (Lazzaro et al. 2004) and de León et al. (2010). Together with our program of asteroid spectroscopic observations, some collaborations are intended in order to enlarge M4AST database.

The purpose of this database is not to duplicate other spectral libraries that already exist, but to offer a unique format for the data, a fast way of applying the existing models, and a rapid comparison of the results.

3.3. M4AST database via the Virtual Observatory

The Virtual Observatory (VO) is an international astronomical community-based initiative. Its aims are to allow global electronic access to the available astronomical data archives of space and ground-based observatories and other sky survey databases and to enable data analysis techniques through a coordinating entity that will provide common standards.

The M4AST spectral database can be accessed via VO-Paris Data Centre⁵ using Simple Spectral Access Protocol (Tody 2011). The M4AST spectral data obtained via VO can be retrieved in both *VOTable* format or our native *ASCII* format. A “simple query search” based on asteroid designation correctly returns all the spectra from our database for the corresponding object.

New protocols, dedicated to planetology, (such as table access protocol) will be implemented in the future.

4. The interface

M4AST includes two interfaces, one dedicated to database access and another for running the different applications dedicated to spectral analysis⁶. The access flow starts with the database interface and continues with the modeling tool interface. Figure 1 gives an overview of the M4AST work-flow.

4.1. Database interface

The database interface (Fig. 1), called user input interface, allows the users to access the spectra from the database or upload their own spectra for further processing. The following options are available:

Search spectra in database – the user can search spectra in the database based on a maximum of three keywords. These keywords include object designations, observing date, and the IAU observatory code.

Download file from database – the user can download any spectrum using as input the filename provided by the previous option.

Upload temporary spectrum to database – the anonymously user can upload his own spectral data for further processing. The file with the spectrum should contain two or three columns, the first column containing the wavelengths (given in angstroms, nanometers, or microns), the second column containing the corresponding reflectance. Optionally, the third column may include the dispersion of measurements. The file is given a temporary name over which the user has full control.

Concatenate spectra – spectra in different wavelength regions (V and NIR) can be merged. The procedure consists in the minimization of data into a common spectral region (usually 0.8–0.9 μm). The result is stored in a temporary file and can be further processed.

The results of all these options are displayed at the bottom of each page. These results can be either spectra found in the database or temporary files. The connection with the modeling tools is made using the name of the file containing the spectrum. This filename is provided as a link and a simple click allows us to access the modeling tool interface.

⁵ <http://voparis-srv.obspm.fr/portal/>

⁶ <http://cardamine.imcce.fr/m4ast/>

4.2. Modeling tool interface

The second component of the M4AST project is the set of applications for modeling and analyzing the spectra from the database or any spectrum submitted by the user. The usage of this tool (Fig. 1), called the modeling interface, is based on the name of the file containing the spectral data.

The following applications are currently available in this interface:

Plot spectrum – plot the reflectance as a function of wavelength. Additional information related to the selected spectrum (the observing log) are also given.

Taxonomy – classify the spectrum according to different taxonomies. Taxonomic systems that can be selected are Bus-DeMeo (DeMeo et al. 2009), G13 (Birlan et al. 1996), and G9 (Fulchignoni et al. 2000). The methods behind these classifications are outlined in Sect. 5. The results of this application consist in the first three classes that match the asteroid spectrum, together with some matching quantitative values (coefficients). In addition, the asteroid spectrum is plotted together with standard spectra corresponding to the best matches.

Search matching with spectra from the Relab database – performs spectral comparison with spectra from Relab database. In general, only the meteorite spectra are of interest, thus an option for selecting between all spectra and only meteorite spectra is included. However, the “all spectra” option includes spectral measurements for mixtures (olivine/pyroxene) prepared in the laboratory that can be considered when analyzing asteroid spectra. Four methods are available for the spectral matching. Their description is given in Sect. 5. This application provides the first 50 laboratory spectra that matched the spectrum (in order of the matching coefficient). These results are given in a table, along with a link to visualize a comparative plot of laboratory spectra and asteroid spectra. The table includes all the information regarding the spectral measurements and the sample characteristics.

Space weathering effects – uses the space weathering model defined by Brunetto et al. (2006). The results consists in computing the parameters of the model and de-reddening the spectrum. The de-reddening (removal of space weathering effects) is done by dividing the spectrum by its continuum. The spectrum obtained can be further analyzed, being provided in a temporary file.

Band parameters and mineralogical analysis – computes the spectral parameters defined by Cloutis et al. (1986). If only the infrared part of the spectrum is given, the algorithm computes the band minima. If the spectrum contains both V and NIR regions, all the parameters described in Sect. 2.4 are calculated. Along with the results, the plots required to interpret these parameters are also provided.

After each computation made in M4AST, the results are displayed at the bottom of the page. It must be noted that some of these applications provides meaningfully results only for certain types of spectra. Their applicability is indicated in the publications describing the models. The reference to the relevant publications is also available via the web interface.

4.3. Updating the database

Permanent spectra can be added into the database via a dedicated interface – update database (Fig. 1) – that requires administrative

rights. The information needed to add a new permanent file with spectral data are asteroid designations (an additional utility is provided to check the designations), information about the observation (date, investigator, and IAU code of the observatory), and information about the uploaded file containing the measurements. Each record submitted to the database can be removed only from this interface.

5. Algorithms – the mathematical approach

This section describes the algorithms used to analyze the different types of spectra.

5.1. Taxonomic classification

We used different approaches for the three taxonomies types proposed in M4AST.

To classify a spectrum in the Bus-DeMeo taxonomy, we determine how closely this asteroid spectrum is fitted by the standard spectrum of each class using a curve matching approach. This approach involves first fitting the spectrum with a polynomial curve and then comparing this curve to the standard spectrum at the wavelengths given in the taxonomy. We select the taxonomic classes producing the smallest standard deviation in the error (see Eq. (5)).

For G-mode taxonomy, we used the algorithm defined in Fulchignoni et al. (2000). This comprises the computation of the g parameter, which gives the statistical distance of a new sample, characterized by $\{x_i\}$ from the taxonomic class s

$$g_s = \sqrt{2 R_s \sum_i^M \left(\frac{x_i - \bar{x}_{is}}{\sigma_{is}} \right)^2} - \sqrt{2 R_s M - 1}, \quad (1)$$

where M is the number of points and $i = \overline{1 \dots M}$. The G-mode method defines for each taxonomic class s the mean values $\{\bar{x}_{is}\}$, the standard deviations $\{\sigma_{is}\}$, and a statistical indicator R_s . We select the classes that have the lowest g_s , the ideal case being $g_s = -\sqrt{2 R_s M - 1}$.

The taxonomic classes are defined depending on the taxonomy in different wavelength intervals (0.45–2.45 μm for Bus-DeMeo taxonomy, 0.337–2.359 μm for G13 taxonomy, and 0.337–1.041 μm for G9 taxonomy) and some of them also using the albedo. The curve matching or g factor computation can be made across a smaller wavelength interval (depending on the available wavelength range of the asteroid spectrum) but with a lower confidence, thus a reliability criterion is required (Popescu et al. 2011)

$$\text{Reliability} = \frac{\text{card}([\lambda_m, \lambda_M] \cap \{ \lambda_1^T, \lambda_2^T, \dots, \lambda_N^T \})}{N}, \quad (2)$$

where $[\lambda_m, \lambda_M]$ is the spectral interval between the minimum wavelength and the maximum wavelength in the asteroid spectrum, $\lambda_1^T, \lambda_2^T, \dots, \lambda_N^T$ are the N wavelengths for which the standard spectra of the taxonomy are given, and $\text{card}()$ represents the number of elements of a discrete set.

5.2. Curve matching

The methods for taxonomic classification and comparison with meteorite spectra are based on curve matching. These procedures involve minimizing a quantity (usually called Φ) in order to determine the best estimates for a given asteroid spectrum.

A quantity commonly used to test whether any given points are well-described by some hypothesized function is chi-square (χ^2), the determination being called the chi-square test for goodness of the fit (Bevington & Robinson 1992).

The classical definition for the χ^2 is:

$$\chi^2 = \sum_i^N \frac{(x_i - \mu_i)^2}{\sigma_i^2}, \quad (3)$$

where there are N variables x_i normally distributed with the mean μ_i and variance σ_i^2 . If σ_i^2 are correctly estimated, the data are well-described by the values μ_i when $\Phi = \chi^2 \rightarrow 0$.

We denote by $\{e_i\}$ the error between the data (asteroid spectrum) and the curve that was fitted

$$e_i = (x_i - \mu_i). \quad (4)$$

Our first approach to curve matching, derived from chi-square fitting, is based on the formula

$$\Phi_{std} = \frac{1}{N} \sqrt{\sum_i^N (e_i - \bar{e})^2}, \quad (5)$$

where we have denoted with \bar{e} the mean value of the set $\{e_i\}$ (Eq. (4)).

The quantity to minimize in this case is the standard deviation of the errors. To apply this procedure, we smooth our asteroid spectrum by a polynomial curve (using the *polyfit* function from the Octave3.2 computation environment). This step is required to eliminate the outlier points produced by the incomplete removal of telluric absorption lines.

We used this type of curve matching to find the taxonomic class of the asteroid in the Bus-DeMeo taxonomy and to compare with laboratory spectra. In the latter case, we determine how well the asteroid spectrum is fitted by different laboratory spectra, and select the closest 50 fits, in ascending order of Φ .

A second approach to curve matching can be made using χ^2 with the definition (Nedelcu et al. 2007):

$$\chi^2 = \frac{1}{N} \sum_i^N \frac{(x_i - \mu_i)^2}{x_i}, \quad (6)$$

where x_i are the values of a polynomial fit to the asteroid spectrum and μ_i are the reflectance values for the meteorite spectrum. The meaning of this formula is that of a relative error at each wavelength (N being the number of wavelengths on which the comparison is made).

The third approach to curve fitting is based on the correlation coefficient

$$\rho_{X,M} = \frac{\text{cov}(X, M)}{\sigma_X \sigma_M}, \quad (7)$$

where $X = \{x_i\}$ is the spectrum of the asteroid and $M = \{\mu_i\}$ is the laboratory spectrum. The correlation coefficient detects linear dependences between two variables. If the variables are independent (i.e. the asteroid and laboratory spectra), then the correlation coefficient is zero. A unitary value for the correlation coefficient indicates that the variables are in a perfect linear relationship, though in this case we search for laboratory spectra that match the desired asteroid spectrum with the highest $\rho_{X,M}$.

Finally, we concluded that a good fitting can be achieved by combining the standard deviation method and correlation coefficient method. Thus, the fourth coefficient we propose is

$$\Phi_{\text{comb}} = \frac{\rho_{X,M}}{\Phi_{\text{std}}}, \quad (8)$$

where $\rho_{X,M}$ was defined in Eq. (7) and Φ_{std} was defined in Eq. (5). In this case, the laboratory spectra that match the asteroid spectrum are those with the highest value of Φ_{comb} .

5.3. Computing the space weathering effects

Our approach to computing space weathering effects applies the model proposed by Brunetto et al. (2006). On the basis of laboratory experiments, they concluded that a weathered spectrum can be obtained by multiplying the spectrum of the unaltered sample by an exponential function (see Eq. (9)) that depends on the precise parameter C_s .

By fitting the asteroid spectral curve with an exponential function using a least-square error algorithm, we can compute the C_s parameter

$$W(\lambda) = K \times \exp\left(\frac{C_s}{\lambda}\right) \quad (9)$$

Brunetto & Strazzulla (2005) demonstrated that ion-induced spectral reddening is related to the formation of displacements, with the C_s parameter being correlated with the number of displacements per cm^2 (named damage parameter – d). Brunetto et al. (2006) obtained an empirical relation between C_s and the number of displacements per cm^2

$$C_s = \alpha \times \ln(\beta \times d + 1), \quad (10)$$

where $\alpha = -0.33 \mu\text{m}$ and $\beta = 1.1 \times 10^{19} \text{ cm}^2$. M4AST applies Eq. (10) to compute the damage parameter d .

This model for the space weathering effects describes the effects of solar-wind ion irradiation. While this is not the only active weathering process, it seems to be the most efficient at 1 AU (Vernazza et al. 2009; Brunetto et al. 2006).

The removal of space weathering effects is made in M4AST by dividing the asteroid spectrum by $W(\lambda)$ at each wavelength.

5.4. Application of the Cloutis model

Cloutis et al. (1986) proposed a method for the mineralogical analysis of spectra showing absorption bands. We implemented an application to compute the spectral parameters defined by this method. The computation of all the parameters described in Sect. 4.2 is done for spectra that contains the V + NIR wavelength regions. If only the NIR region is given, then only the band minima can be computed.

The following steps are made: we first compute the minima and maxima of the spectrum. This is done by starting with the assumption that there is a maximum around $0.7 \mu\text{m}$ followed by a minimum around $1 \mu\text{m}$, then a maximum between 1.3 – $1.7 \mu\text{m}$ and a minimum around $2 \mu\text{m}$. The spectrum is fitted around these regions by a polynomial function. The order of the polynomial is selected to be between three to eight, in order to obtain the smallest least square residuals. The minima and the maxima are the points where the first derivative of the fitted polynomial functions is zero.

In the second step, using the wavelengths and the reflectance at the two maxima and at the end of the spectrum (around $2.5 \mu\text{m}$), we compute two linear continua, tangential to the spectral curve. The continuum part is removed by dividing the spectrum by the two tangential lines (in the corresponding regions). The band centers are computed following a method similar to that applied to the band minima, but after the removal of the continuum.

The last step consists in computing the two absorption-band areas. The first absorption band is located around $1 \mu\text{m}$ and between the first and second maxima. The second absorption band is located around $2 \mu\text{m}$, between the second maximum and the end of the spectrum. The area is computed using a simple integration method. This method consists in computing the area between two consecutive points in the spectrum defined by a trapezoid and summing all these small areas corresponding to the absorption band.

$$\frac{OPX}{OPX + OL} = 0.4187 \times \left(\frac{BII}{BI} + 0.125 \right). \quad (11)$$

The ratio of the areas of the second to the first absorption band ($BAR = \frac{BII}{BI}$) gives the relative abundance orthopyroxene vs. olivine presented in Eq. (11) (Fornasier et al. 2003).

6. Results and discussions

The functionality of M4AST is now exemplified by the analysis of three spectra available in the database that were previously discussed by Popescu et al. (2012), Binzel et al. (2009), and de León et al. (2011). Our selection here covers a wide variety of spectra: (9147) Kourakuen is a vestoid with deep absorption features, (99942) Apophis is an Sq type asteroid with moderate features, and (175706) 1996 FG3 is a primitive type with featureless spectra.

The discussion of the taxonomic type of each object is made with reference to both Fig. 2 for Bus-DeMeo taxonomy and Fig. 3 for G-mode taxonomies. Table 1 summarizes the comparison of asteroid spectra with spectra from the Relab database. The corresponding plots are given in Fig. 4.

6.1. Results

The spectrum of (9147) Kourakuen has the characteristics of a V-type asteroid. In Bus-DeMeo taxonomy, V-type asteroids are characterized by a very strong and very narrow $1 \mu\text{m}$ absorption and a strong $2 \mu\text{m}$ absorption feature (DeMeo et al. 2009). M4AST undoubtedly classify this spectrum as V-type. This agrees with the classification made via the MIT-SMASS online tool⁷. The next two matches (the programs always returns the first three matches) of Sv and Sr types have larger matching errors (Fig. 2(a)).

The solution given by all four methods for comparison with laboratory spectra shows that the spectrum of (9147) Kourakuen is almost identical to the spectrum of a sample from the Pavlovka meteorite (Fig. 4(a)), which is a howardite achondrite meteorite. The second best match corresponds to the spectrum of a man-made mixture of pyroxene hypersthene plagioclase bytownite ilmenite (Fig. 4(b)). This man-made mixture reproduces quite well the natural composition of volcanic rocks or melting rock of volcanic beds, and is consistent to the V-type mineralogical composition of asteroids. The majority of the laboratory spectra proposed by M4AST as good matches to this asteroid corresponds to Howardite-Eucrite-Diogenite (HED) achondrites, which are meteorites that come from asteroid (4) Vesta. This agrees with the classification of a V-type asteroid.

While the standard deviation measures the overall matching between the two spectra, the correlation coefficient find the spectra for which the spectral features positions and shapes are very close. In the case of spectrum of (9147) Kourakuen, a very high

⁷ <http://smass.mit.edu/busdemeoclass.html>

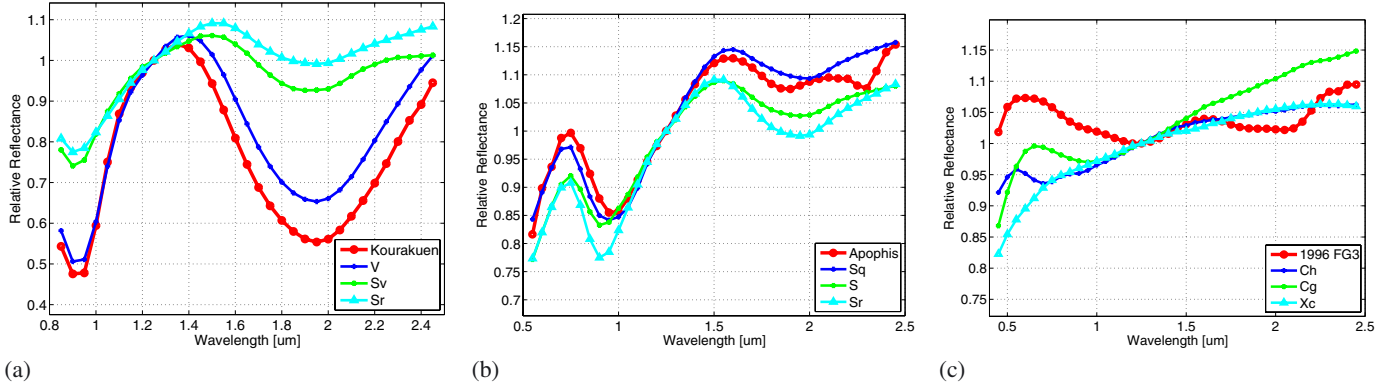


Fig. 2. Classification in Bus-DeMeo taxonomical system for: **a)** (9147) Kourakuen; **b)** (99 942) Apophis; and **c)** (175 706) 1996 FG3. All the spectra are normalized to 1.25 μm .

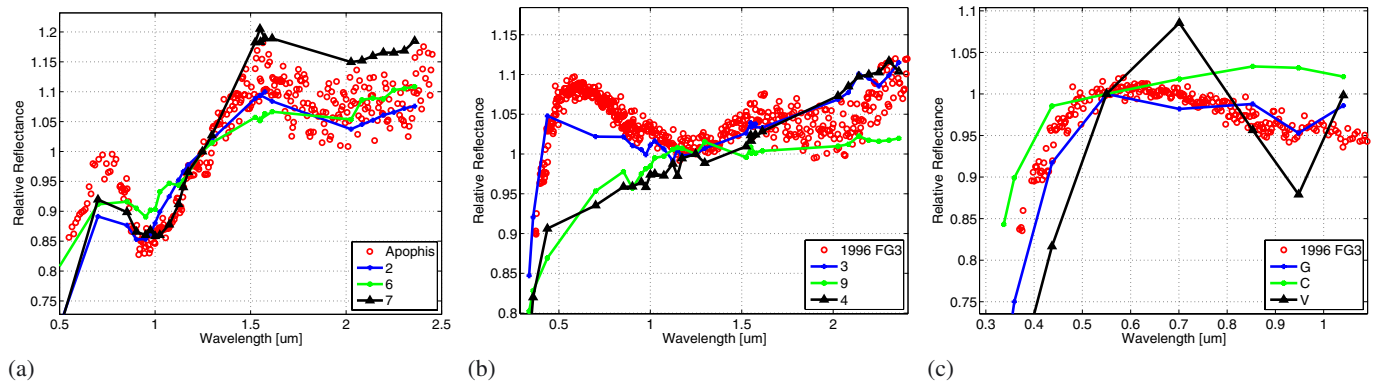


Fig. 3. Classification in the G-mode taxonomical system for: **a)** (99 942) Apophis using G13 taxonomy; **b)** (175 706) 1996 FG3 using G13 taxonomy; and **c)** (175 706) 1996 FG3 using G9 taxonomy. All the spectra are normalized either to 1.25 μm (left and central panel), or to 0.55 μm (c).

Table 1. Summary of the results obtained by matching the asteroids spectra with spectra from the Relab database.

Spectrum	Std. dev.	Corr. coef.	Meteorite/Sample	Sample ID	Type	Texture
(9147)	0.01884	0.99477	Pavlovka	MR-MJG-094	Achondrite(AHOW)	–
	0.02244	0.99207	Mixture	SC-EAC-039	Pyrox Hyper Plagi Bytow Ilmen	Particulate
(99 942)	0.01756	0.98013	Simulant	CM-CMP-001-B	Soil/Lunar	Particulate
	0.01970	0.98224	Hamlet	OC-TXH-002-C	OC-LL4	Particulate
(99 942) de-reddened	0.01539	0.96245	Cherokee Springs	TB-TJM-090	OC-LL6	Particulate
	0.01609	0.97272	Cat Mountain	MB-DTB-035-A	OC-L5	Particulate
(175 706)	0.01219	0.90546	Sete Lagoas	MH-JFB-021	OC-H4	Slab
	0.01504	0.85366	Murchison heated 1000 °C	MB-TXH-064-G	CC-CM2	Particulate

Notes. For each asteroid, we show the best two matches, obtained by measuring the standard deviation (std. dev.) and the correlation coefficient (corr. coef.).

correlation coefficient (more than 0.99) characterizes the first matching solutions (Table 1).

Since only the NIR part of the spectrum is available, we can only compute the band minima. The high signal to noise ratio of this spectrum ensures that there is a small error in computing the band minima. The first minimum is at $0.9217 \pm 0.0005 \mu\text{m}$ and the second minimum is at $1.9517 \pm 0.0062 \mu\text{m}$, which imply a band separation of 1.03 μm . The band separation provides a way of estimating the iron content. Cloutis et al. (1990) noted that the band separation is a linear function of the BII minimum for orthopyroxenes and that both parameters increase with the iron content. If we refer to the relation obtained by de Sanctis et al. (2011), the parameters that we found match their formula

$y = 0.801 * x - 0.536$, where y is the band separation and x is the BII minimum. These parameters corresponds to an iron content of around 40 wt%. However, the laboratory calibrations suggest that the correspondence is true for a number of low aluminum orthopyroxenes but invalid for mixtures of olivine, metal, and both ortho- and clino-pyroxenes (de Sanctis et al. 2011).

The second spectrum we consider to exemplify the M4AST routines is that of the potential hazardous asteroid (99 942) Apophis (Binzel et al. 2009). On the basis of this spectrum this asteroid was found to be an Sq type, and has a composition that closely resemble those of LL ordinary chondrite meteorites.

M4AST classifies this spectrum in the Bus-DeMeo taxonomy as an Sq-type (Fig. 2(b)). The next two types, S and Sr,

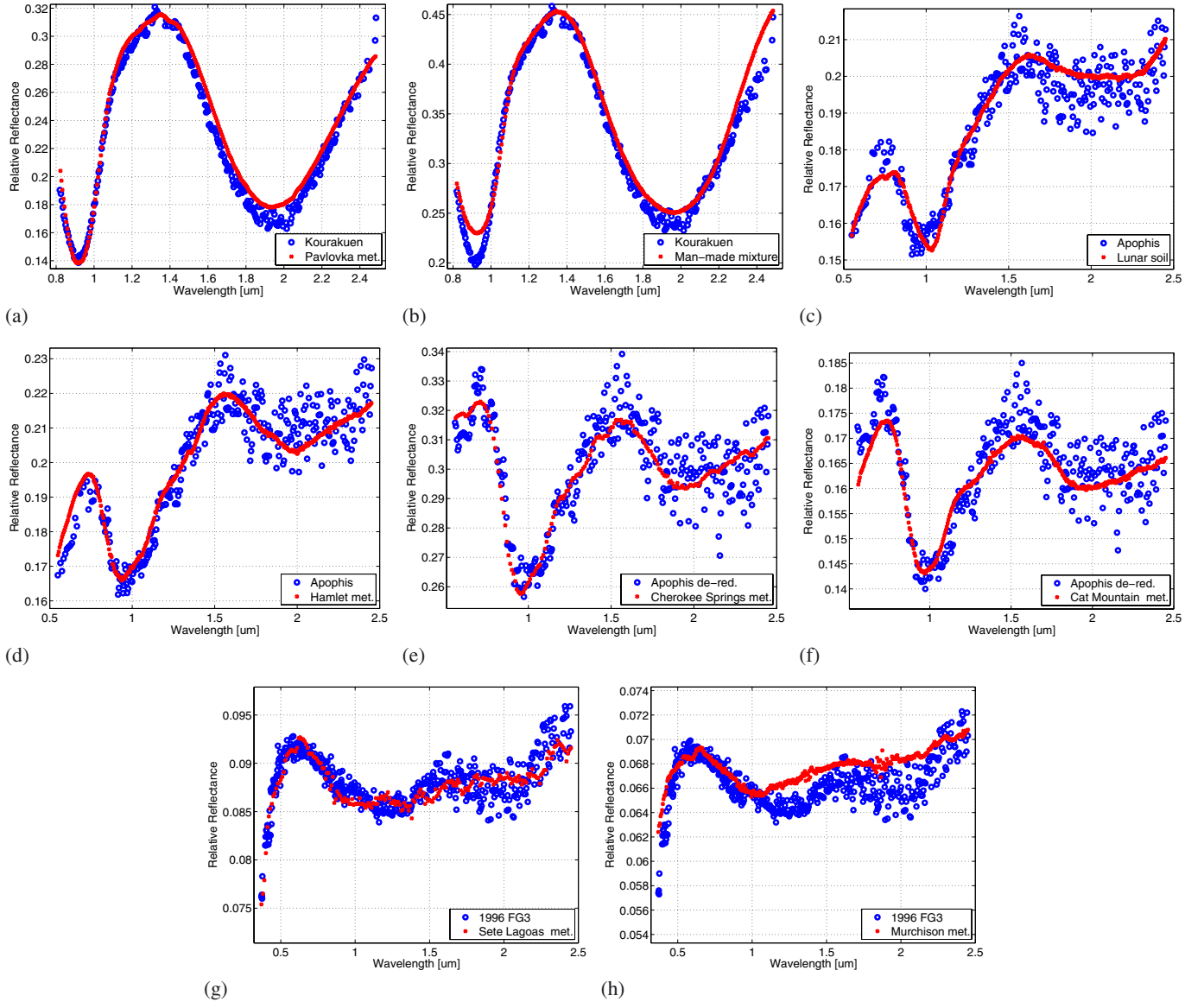


Fig. 4. Asteroid spectra and the best two matches derived from a comparison with laboratory spectra: **a)** spectrum of Kourakuen and the spectrum of a sample from Pavlovka; **b)** spectrum of Kourakuen and the spectrum of a mixture of pyroxene hypersthene plagioclase bytownite ilmenite; **c)** spectrum of Apophis and the spectrum of a simulant Lunar soil; **d)** spectrum of Apophis and the spectrum of a particulate sample from the Hamlet meteorite; **e)** de-reddened spectrum of Apophis and the spectrum of a particulate sample from the Cherokee Springs meteorite; **f)** de-reddened spectrum of Apophis and the spectrum of a particulate sample from the Cat Mountain meteorite; **g)** spectrum of 1996 FG3 and the spectrum of a sample from the meteorite Sete Lagoas; and **h)** spectrum of 1996 FG3 and the spectrum of a sample from the Murchison meteorite heated to 1000 °C.

are relatively good matches, but have larger errors. Applying the G13 taxonomy, M4AST classifies this asteroid as being in class 2 (Fig. 3(a)). Two other classes (namely 6 and 7) are relatively close in terms of g factor (Fig. 3, upper plot). Class 2 has the representative members (7) Iris and (11) Parthenope, which are S- and S-q type asteroids according to DeMeo et al. (2009). The classes 2, 6, and 7 are equivalent to the S profile.

Being an Sq type, for this asteroid spectrum we can apply the space weathering model proposed by Brunetto et al. (2006). Thus, fitting the spectrum with an exponential continuum we found $C_s = -0.196 \mu\text{m}$, corresponding to a moderate spectral reddening. The result obtained by Binzel et al. (2009) is $C_s = -0.17 \pm 0.01 \mu\text{m}$. This difference could be caused by the different method that they used: their “best fit was

performed as an integral part of the overall minimum RMS solution”. The C_s value gives the number of displacements per cm^2 , $d = 0.74 \times 10^{19}$ displacements/ cm^2 . We analyze both the original spectrum and the de-reddened spectrum.

Comparing the original spectrum of (99942) Apophis with all laboratory spectra from Relab, M4AST found matches with some ordinary chondrite meteorites (L and LL subtypes, and petrologic classes from 3 to 6) and some lunar soils (Figs. 4(c) and 4(d)). Referring to standard deviation and to correlation coefficient, the closest matches were those of particulate lunar soils and some spectra from the Hamlet meteorite which is particulate with grain sizes smaller than $500 \mu\text{m}$. The meteorite Hamlet is an ordinary chondrite, subtype LL4.

In the case of the de-reddened spectrum, the majority of solutions correspond to ordinary chondrite meteorites, of subtype

L and LL, with petrologic classes from 4 to 6. The best matches were those of the Cherokee Springs meteorite (an LL6 ordinary chondrite, Fig. 4(e)) and the Cat Mountain meteorite (an L5 ordinary chondrite, Fig. 4(e)). From spectral modeling of mixtures of olivine, orthopyroxene, and clinopyroxene, Binzel et al. (2009) correlate the spectrum of (99 942) Apophis with the spectra of LL meteorites. This results agrees with the spectral matching solutions found by M4AST.

No significant differences between the Cloutis model parameters computed for original and de-reddened spectrum are found. The application found the first band center at $0.9721 \pm 0.0143 \mu\text{m}$ ($0.9755 \pm 0.0144 \mu\text{m}$ for the de-reddened spectrum), the second band center at $1.8200 \pm 0.0679 \mu\text{m}$ ($1.8404 \pm 0.0591 \mu\text{m}$ for the de-reddened spectrum), and the band area ratio 0.4059 ± 0.0047 (0.3886 ± 0.0015 for the de-reddened spectrum). These parameters correspond to an ordinary chondrite with an $OPX/(OPX + OL)$ ratio of 0.222 (0.215 for the de-reddened spectrum). This ratio agrees with the compatibility relation between NEA and LL ordinary chondrites found by Vernazza et al. (2008), which is similarly consistent with the spectral matching we found.

This value means that the ordinary chondrite consist of 78% olivine, which is consistent with an LL ordinary chondrite. And this result agrees with the spectral matching.

The dark primitive asteroid (175 706) 1996 FG3 is the primary target of the ESA Marco Polo-R mission. Some papers were dedicated to this object, namely de León et al. (2011), Wolters et al. (2011), Rivkin et al. (2012), and Walsh et al. (2012). There are few spectra published in both V and NIR. In the M4AST database, we included the spectra from the MIT-UH-IRTF (MINUS) survey⁸ and the spectrum of de León et al. (2011).

On the basis of different spectra, the asteroid has been classified as belonging to primitive types (C, B, or X), but there is no consensus on its classification in the literature (de León et al. 2011; Walsh et al. 2012). In addition some spectral matchings have been noted with meteorites ranging from ordinary chondrite H-type to both CM2 and CV3 carbonaceous chondrite (de León et al. 2011; Rivkin et al. 2012).

To exemplify the applications of M4AST, we used the spectrum obtained on March 30, 2009 by MIT-UH-IRTF (MINUS). The classification in the Bus-DeMeo taxonomy returned the Ch, Cg, and Xc taxonomic types (Fig. 2(c)). The scores obtained for the classes Ch, Cg, Xc, C, and Cgh are very similar. This object has neither the absorption band centered at $0.7 \mu\text{m}$ typical of Ch-type, nor the redder spectral slope of Xk-types (de León et al. 2011). In addition, the slope in the NIR part of the spectrum, that is of Cg type does not corresponds to the spectrum of (175 706) 1996 FG3.

Classifying this spectrum of (175 706) 1996 FG3 using the G13 taxonomy, we obtain with high confidence ($g_s = -1.237$) the type corresponding to class 3. The other two types (classes 9 and 4) have greater g_s coefficients (Fig. 3(b)). Groups 3 and 4 are the equivalents for the C-type asteroids. As representative members of the class 3, there are (1) Ceres and (10) Hygiea, which are both primitive asteroids. The classification in the G9 taxonomy (Fig. 3(c)) confirms the classification as a primitive type, suggesting as the first options the classes G and C, while the third option (V) could be ignored because it has a larger g_s .

Considering these three classifications, the solution on which the applications of M4AST seems to converge is that the spectrum of (175 706) 1996 FG3 is of a Cg taxonomic type.

Comparing the spectrum of (175 706) 1996 FG3 to the laboratory spectra, we obtain a good match to a sample of the meteorite Sete Lagoas (Fig. 4(g)). Other matches are the spectrum of a sample from meteorite Murchison heated to 1000°C (Fig. 4(h)), the spectrum of a sample from the Dhofar 225 meteorite, and the spectrum of a sample from Ozona. This is puzzling, since both the Sete Lagoas and Ozona meteorites are ordinary chondrites (H4 and H6, respectively), and both Murchison and Dhofar 225 are carbonaceous chondrites. However, we note that the majority of matching solutions are spectra of carbonaceous chondrite meteorites (CM type). If additionally, we take into account the asteroid albedo⁹, then the spectrum of Dhofar 225 (sample ID: MA-LXM-078) and Murchison heated to 1000°C (sample ID: MB-TXH-064-G) seems to be the most probable analogs of this asteroid spectrum.

With the results of M4AST in agreement with those already published, we conclude that the routines of M4AST work correctly and their implementation is robust.

6.2. Discussions regarding misinterpretations of spectra

Applying the correct methods for interpreting asteroid spectra can reveal a lot of information about the physical properties of these objects. However, each method has its own limitations which in general are well-described in the corresponding paper, and using the methods beyond their limits may of course lead to incorrect results.

The first misinterpretation that may occur is related to space weathering. As Gaffey (2008) noted, “space weathering is commonly invoked to reconcile observational data to the incorrect expectation that ordinary chondrite assemblage are common in the asteroid belt”. While space weathering for the lunar samples has been well-documented using the samples returned from the Apollo missions, it has been observed that different models are required to interpret the space weathering processes that acted on different asteroid surfaces.

The model we applied for space weathering was based on laboratory experiments that consist in ion irradiation (Ar^+) of olivine and pyroxene powders. This model is suitable for asteroids that seems to consist of olivine and pyroxene, such as those from the S complex.

According to these experiments, the reddening in the infrared part of spectra due to solar-wind ion irradiation can be removed, by dividing the spectrum by an exponential function. However, there are several other effects that can modulate the spectra, such as either thermal influence (Rivkin et al. 2005) or the debated phase-angle effect (Veverka et al. 2000).

The second misinterpretation that may occur is related to the spectral matches with laboratory spectra (Gaffey 2008). Curve matching can provide clues to the nature of the asteroid surface composition. The efficiency of this method can be clearly observed in the case of asteroids that have strong spectral features, such as the vestoids. Misinterpretations can occur when the asteroid surface is modified by space weathering effects, while the meteorite can be modified by terrestrial influences.

The four methods we proposed take into account different characteristics of the spectra: spectral slope, band depths, and the various feature positions. In the context of taxonomic classification, albedo value, space-weathering effects, and similar solutions obtained from all four matching methods, we believe that

⁹ The geometric albedo was found as 0.039 ± 0.012 by Walsh et al. (2012).

⁸ <http://smass.mit.edu/minus.html>

spectral matches with laboratory spectra provide valuable constraints of the asteroid surface nature.

By applying the methods of M4AST, we observed that a good solution for interpreting the asteroid spectrum is found when all the methods converge to the same mineralogical interpretation. For example, when the spectrum of (99 942) Apophis was processed, despite the poor signal to noise ratio in the infrared part of its spectrum, we obtained the classification Sq in the Bus-DeMeo taxonomy and an analog of this class in the G13 taxonomy. We then found that the spectra of ordinary chondrite meteorites (L, LL subtypes) match this spectrum. These two results were confirmed and developed by applying the Cloutis model: the fraction of olivine-orthopyroxene is 22%, and the associated parameters are equivalent to those of an ordinary chondrite. This conclusion is in general valid for all the spectra we analyzed via M4AST.

7. Conclusions and perspectives

Spectroscopy plays a key role in determining the chemical composition and physical processes that took place and modified the surface of atmosphere-less bodies in the solar system. The development of telescopic instruments (such as SpeX on IRTF, NICS on TNG etc.) and the possibility to access them remotely has led to an increasing number of asteroid spectral measurements. In this context, the exploitation of spectral measurements becomes one of the important means of developing minor planet science. During the past few decades, several methods have been developed to analyze asteroid spectra in order to reveal the physical and chemical properties of these objects. These methods comprise taxonomic classifications, band analyses and comparative mineralogy.

In this paper, we have described M4AST (Modeling for Asteroids), which is a software project dedicated to asteroid spectra. It consists of an asteroid spectral database and a set of applications for analyzing the spectra. The M4AST spectral database has around 2700 asteroid spectra obtained from our observing program and different collaborations. The spectra from the database are in a standard format and are fully available for download.

The M4AST applications cover aspects related to taxonomy, curve matching with laboratory spectra, space weathering models, and diagnostic spectral parameters.

M4AST was conceived to be fully available via a web interface and can be used by the scientific community. We have presented the interfaces available to access this software tool and the algorithms behind each method used to perform the spectral analysis. The applications have been exemplified with three different types of spectra. The robustness of the routines has been demonstrated by the solutions found for the asteroid spectra of (9147) Kourakuen, a V-type asteroid, (99 942) Apophis an Sq asteroid, and (175 706) 1996 FG3 a Cg type asteroid and a target of *Marco Polo* – R mission. The results agree with and complement those previously published for these objects.

Future developments of this project will include increasing the number of spectra in the database, additional methods for analyzing the spectra (such as mineralogical charts – Birlan et al. 2011), and a more friendly interface.

Acknowledgements. The article is based on observations acquired with that InfraRed Telescope Facilities, as well as the CODAM remote facilities. We thank all the telescope operators for their contributions. This research utilizes

spectra acquired with the NASA RELAB facility at Brown University. The work of D. A. Nedelcu was supported by a grant of the Romanian National Authority for Scientific Research, CNCS – UEFISCDI, project number PN-II-RU-TE-2011-3-0163. We thank Julia De León for constructive and helpful suggestions.

References

- Barucci, M. A., Capria, M. T., Coradini, A., & Fulchignoni, M. 1987, *Icarus*, 72, 304
- Bell, J. F., Owensby, P. D., Hawke, B. R., & Gaffey, M. J. 1988, in *Lunar and Planetary Inst. Technical Report*, 19, 57
- Bevington, P. R., & Robinson, D. K. 1992, *Data Reduction and error analysis for the physical sciences* (McGraw-Hill, Inc.)
- Binzel, R. P., Rivkin, A. S., Thomas, C. A., et al. 2009, *Icarus*, 200, 480
- Birlan, M., & Popescu, M. 2011, in *EPSC-DPS Joint Meeting 2011*, 810
- Birlan, M., Barucci, M. A., & Fulchignoni, M. 1996, *A&A*, 305, 984
- Birlan, M., Barucci, M. A., Vernazza, P., et al. 2004, *New Astron.*, 9, 343
- Birlan, M., Vernazza, P., Fulchignoni, M., et al. 2006, *A&A*, 454, 677
- Birlan, M., Nedelcu, D. A., Descamps, P., et al. 2011, *MNRAS*, 415, 587
- Britt, D. T., Tholen, D. J., Bell, J. F., & Pieters, C. M. 1992, *Icarus*, 99, 153
- Brunetto, R., & Strazzulla, G. 2005, *Icarus*, 179, 265
- Brunetto, R., Vernazza, P., Marchi, S., et al. 2006, *Icarus*, 184, 327
- Bus, S. J., & Binzel, R. P. 2002a, *Icarus*, 158, 146
- Bus, S. J., & Binzel, R. P. 2002b, *Icarus*, 158, 106
- Chapman, C. R. 1996, *Meteor. Planet. Sci.*, 31, 699
- Chapman, C. R. 2004, *Ann. Rev. Earth Planet. Sci.*, 32, 539
- Chapman, C. R., Johnson, T. V., & McCord, T. B. 1971, *NASA Sp. Publ.*, 267, 51
- Cloutis, E. A., Gaffey, M. J., Jackowski, T. L., & Reed, K. L. 1986, *J. Geophys. Res.*, 91, 11641
- Cloutis, E. A., Gaffey, M. J., Smith, D. G. W., & Lambert, R. S. J. 1990, *J. Geophys. Res.*, 95, 8323
- de León, J., Licandro, J., Serra-Ricart, M., Pinilla-Alonso, N., & Campins, H. 2010, *A&A*, 517, A23
- de León, J., Mothé-Diniz, T., Licandro, J., Pinilla-Alonso, N., & Campins, H. 2011, *A&A*, 530, L12
- de Sanctis, M. C., Migliorini, A., Luzia Jasmin, F., et al. 2011, *A&A*, 533, A77
- DeMeo, F. E., Binzel, R. P., Slivan, S. M., & Bus, S. J. 2009, *Icarus*, 202, 160
- Fornasier, S., Barucci, M. A., Binzel, R. P., et al. 2003, *A&A*, 398, 327
- Fulchignoni, M., Birlan, M., & Antonietta Barucci, M. 2000, *Icarus*, 146, 204
- Gaffey, M. J. 2008, *LPI Contributions*, 1405, 8162
- Gaffey, M. J. 2010, *Icarus*, 209, 564
- Hapke, B. 2001, *J. Geophys. Res.*, 106, 10039
- Lazzarin, M., Marchi, S., Magrin, S., & Licandro, J. 2005, *MNRAS*, 359, 1575
- Lazzaro, D., Angeli, C. A., Carvano, J. M., et al. 2004, *Icarus*, 172, 179
- McCord, T. B., Adams, J. B., & Johnson, T. V. 1970, *Science*, 168, 1445
- McSween, H. Y. 1999, *Meteorites and their Parent Planets* (Knoxville: University of Tennessee)
- Nedelcu, D. A., Birlan, M., Vernazza, P., et al. 2007, *A&A*, 470, 1157
- Popescu, M., Birlan, M., Binzel, R., et al. 2011, *A&A*, 535, A15
- Popescu, M., Birlan, M., Gherase, R. M., et al. 2012, *UPB Scientific Bulletin, Series A*, in press
- Rivkin, A. S., Binzel, R. P., & Bus, S. J. 2005, *Icarus*, 175, 175
- Rivkin, A. S., Howell, E. S., DeMeo, F. E., et al. 2012, in *Lunar and Planetary Inst. Technical Report*, 43, 1537
- Sasaki, S., Nakamura, K., Hamabe, Y., Kurahashi, E., & Hiroi, T. 2001, *Nature*, 410, 555
- Tholen, D. J. 1984, *Ph.D. Thesis*, Arizona Univ., Tucson
- Tody, D., Dolensky, M., & McDowell, J. 2011, *Simple Spectral Access Version 1.1*
- Vernazza, P., Binzel, R. P., DeMeo, F. E., & Thomas, C. A. 2007, in *AAS/Division for Planetary Sciences Meeting Abstracts #39*, BAAS, 38, 476
- Vernazza, P., Binzel, R. P., Thomas, C. A., et al. 2008, *Nature*, 454, 858
- Vernazza, P., Binzel, R. P., Rossi, A., Fulchignoni, M., & Birlan, M. 2009, *Nature*, 458, 993
- Veverka, J., Robinson, M., Thomas, P., et al. 2000, *Science*, 289, 2088
- Walsh, K. J., Delbo', M., Mueller, M., Binzel, R. P., & DeMeo, F. E. 2012, *ApJ*, 748, 104
- Wolters, S. D., Rozitis, B., Duddy, S. R., et al. 2011, *MNRAS*, 418, 1246
- Xu, S., Binzel, R. P., Burbine, T. H., & Bus, S. J. 1995, *Icarus*, 115, 1
- Yamada, M., Sasaki, S., Fujiwara, A., et al. 1999, in *Lunar and Planetary Institute Science Conference Abstracts*, 30, 1566
- Zellner, B., Tholen, D. J., & Tedesco, E. F. 1985, *Icarus*, 61, 355

APPLICATIONS OF VISIBLE AND INFRARED SPECTROSCOPY TO ASTRONOMY

Marcel POPESCU¹, Mirel BIRLAN², Radu Mihai GHERASE³, Adrian Bruno SONKA⁴, Marian NAIMAN⁵, Constantin P. CRISTESCU⁶

Sunt descrise două aplicații ale spectroscopiei în studiul obiectelor de pe bolta cerească. Prelucrarea și analiza datelor pentru spectrele de emisie și spectrele de reflexie sunt exemplificate folosind observațiile la quasarul PG1634+706, respectiv observațiile la asteroidul (9147) Kourakuen.

Pentru quasarul PG1634+706 s-a obținut deplasarea Doppler spre roșu a liniilor spectrale utilizând o schemă simplă de telescop și spectrometru. Rezultatul este în concordanță cu valoarea acceptată în literatura de specialitate.

Spectrul în infraroșu apropiat obținut pentru asteroidul (9147) Kourakuen a permis clasificarea acestuia în tipul vestoizilor. Utilizând acest spectru a fost făcută o descriere a compoziției suprafeței acestui obiect. Soluția comparării cu spectrele meteoriților a scos în evidență potrivirea spectrală cu meteoriții HED.

We describe two applications of spectroscopy to study the properties of celestial bodies. Data reduction and data analysis for emission and reflection spectra in astronomy are outlined using the spectra acquired for the quasar PG1634+706 and the asteroid (9147) Kourakuen.

For the quasar PG1634+706 we obtained the Doppler redshift of the spectral lines using a basic design of a spectrometer and a telescope. Our result is in agreement with the one accepted in the literature.

The accurate near-infrared (NIR) spectrum obtained for the asteroid (9147) Kourakuen allows to classify this object as a vestoid. A description of the surface composition for this object was obtained using this spectrum. The comparison with meteorites spectra reveals a spectral matching with HED meteorites.

Keywords: spectroscopy, astronomy, asteroid, quasar

1. Introduction

Spectroscopy is one of the most powerful scientific tools for studying nature. The study of celestial bodies using spectroscopy connects astronomy with

¹ Ph.D. Student, Department of Physics, University POLITEHNICA of Bucharest, e-mail : mpopescu@imcce.fr;

² Researcher, IMCCE – Observatoire du Paris, Mirel.Birlan@imcce.fr

³ Member of Astroclub Bucharest, radu.gherases@gmail.com

⁴ Member of Astroclub Bucharest, sonka.adrian@gmail.com

⁵ Member of Astroclub Bucharest, Marian.Naiman@cchellenic.com

⁶ Professor, University POLITEHNICA of Bucharest, e-mail : cpcris@physics.pub.ro;

fundamental physics at atomic and molecular levels. The beginning of astrophysical spectroscopy could be traced back to early nineteenth century with the discovery of dark lines in the solar spectrum by W. H. Wollaston in 1802 and J. von Fraunhofer in 1815. The dark lines at discrete wavelengths arise from absorption of energy by atoms or ions in the solar atmosphere [1].

Due to atmosphere transparency, there are two spectral windows which allow the observation of celestial bodies: the visible to near-infrared region (Fig. 1), and the radio window. The X-rays and ultraviolet wavelengths are blocked due to absorption by ozone and oxygen, while the far infrared radiation is blocked mainly due to absorption by water and carbon dioxide [2].

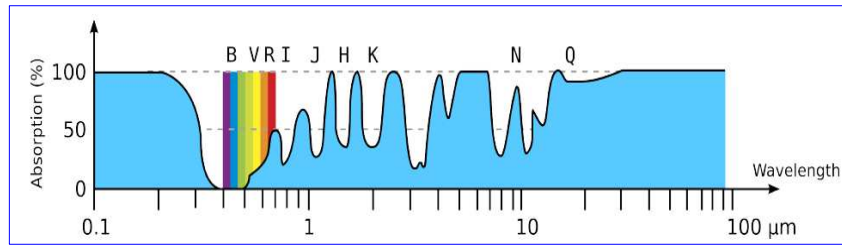


Fig. 1. Earth's atmospheric absorption as a function of wavelength (Adapted from [2])

In this article, we focus on the data reduction and data analysis for two types of spectra that we could obtain from celestial bodies: - the emission spectrum of a quasar and the reflection spectrum of an asteroid. Our observations were carried out in $0.4 - 0.7 \mu\text{m}$ and $0.8 - 2.5 \mu\text{m}$ spectral intervals.

For the emission spectroscopy, we attached a spectrometer to a telescope with the diameter of primary mirror of 200mm, with the purpose of studying the possibility to measure the redshift from quasars using this type of equipment. Thus, as application for the emission spectra, in this paper we describe the visible spectrum obtained on August 06, 2011, for PG1634+706 - a bright quasar with apparent magnitude ~ 14.7 , for which a large redshift was reported [3,4]. At this apparent magnitude, the observations with a Newtonian telescope, having a primary mirror with 200 mm diameter, are very challenging. With a robust method for data reduction we succeed to obtain a redshift ($z = 1.340$) similar with the one accepted in the scientific literature ($z = 1.337$). Both observing procedures and data reduction methods could serve as a basis for further systematic spectroscopic studies of celestial bodies using this relatively simple equipment.

In the case of reflectance spectroscopy we used the NASA InfraRed Telescope Facility (IRTF) - a 3.0 meter telescope located at the Mauna Kea Observatory, Hawaii. Reflectance spectroscopy is a remote sensing technique used to study the surfaces and atmospheres of solar system bodies. It provides

first-order information on the presence and amounts of certain ions, molecules, and minerals on the surface or in the atmosphere of the object. By looking at the changes in reflectance, the presence of absorption features can be identified. Localized dips in the spectrum indicate a particular material is absorbing light at that wavelength. From Mercury to the most distant dwarf planet, almost everything that is known about surface mineralogy has resulted from reflectance spectroscopy using ground-based telescopes [5, 6].

Our observation target for reflectance spectroscopy was the asteroid (9147) Kourakuen. Based on its colors in the visible, this asteroid was suspected to have a basaltic surface. We chose to observe the spectrum in the near-infrared (NIR) of this puzzling object from the main belt, having a favorable position and apparent magnitude (16.4) for observation with IRTF telescope on November 15, 2011.

The paper is organized as follow: in section two we present the observation methods giving also some details regarding the equipment we used. In section three we describe the data reduction and data analysis for the visible spectrum of PG1634+706. The steps for obtaining the spectrum of (9147) Kourakuen together with the analysis of the results are given in section four. The last section is dedicated to discussions and conclusions.

2. Acquiring spectra for celestial bodies

A simple way to obtain the spectra from celestial bodies is to use a prism or a transmission grating in front of a telescope objective. Depending on the equipment used, the sky quality at the observing moment and the data reduction procedures, the limiting magnitude could be pushed up to $V=15$ with a small telescope. On the other hand, a three meter telescope allows magnitudes up to $V=18$. These limiting magnitudes are valid for low resolution modes of the spectrograph.

Our first observations were carried out with telescopes having the diameter of principal mirror between 200-300 mm and a diffraction grating having 100 lines/mm. Since promising results were obtained both for stars and the quasar 3C273 we took the challenge to observe a quasar with an apparent magnitude $V=14.7$. For this run we used a *Celestron C8-NGT* telescope, which is a Newtonian type having the primary mirror of 200 mm and a focal length of 1000 mm, which means a focal ratio $f/5$. It is used on a *AS-GT (CG-5 GoTo)* equatorial mount allowing automated tracking of the objects. For image recording we used an *ATIK 314L+* CCD (charge coupled device) camera having 1.45 Megapixels (a matrix of 1391x1039), each pixel being a square - $6.45 \times 6.45 \mu\text{m}$ (chip size - $8.98 \times 6.71\text{mm}$). This camera has a resolution of 16 bits.

The spectrum was obtained using a *Star Analyser 100* - a high efficiency *100 lines/mm* transmission diffraction grating, blazed in the first order. It was mounted in a standard *1.25 inch* diameter threaded cell which is compatible with the telescope and CCD camera. A rough calibration of the system can be estimated according to the designer formula [7] adapted to our system (Eq. 1):

$$Dispersion_{estim}[nm/pixel] = \frac{6.45}{d[cm]} \quad (1)$$

where d is the distance between grating and CCD. Our optical design allows a resolution around $1.5nm$. A precise calibration was made using known lines identified in the spectrum of a bright star.

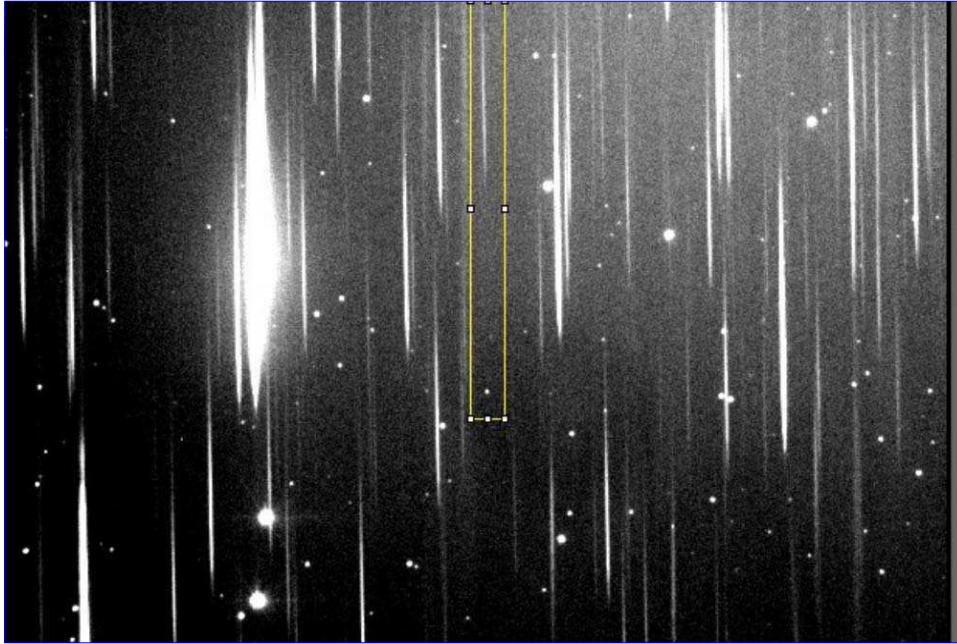


Fig. 2. Portion of the final image showing the field of quasar PG1634+706 (north is at bottom of the figure). The object and its spectrum are surrounded by a rectangle. In this image we distinguish the zero order (objects are dots) and the first order (light is dispersed)

The software used for data acquisition was Artemis Capture. The observations were carried out on 6 August 2011 in an area with low light pollution (Vălenii de Munte – Romania). The observational circumstances are given in Table 1. The final image (Fig. 2) consists in a stack of eighteen images with 90 seconds exposure time and three images with 60 seconds exposure time each, thus a 30 minutes total exposure time. Bias and flat field corrections were made using corresponding images taken at the beginning of the night.

Table 1

Observational circumstances of the selected objects: name of objects, moment of observation (UT), position of the objects (RA and DEC), visual magnitude (VMAG), airmass, and the integration time (ITIME) are presented.

Object	UT	RA[hrs]	DEC[°]	VMAG	Air mass	ITIME
PG1634+706	2011-08-05.089	16:34:29	+70:31:32	14.7	1.17	30 min
(9147) Kourakuen	2011-11-15.357	00:53:18	-04:36:21	16.4	1.14	32 min
HD4940	2011-11-15.375	00:51:17	-13:06:52	8.7	1.28	12 sec

In the last century the application of spectroscopy for astronomical objects has lead to the development of large ground-based observatories dedicated to this purpose. One of these is the NASA Infrared Telescope Facility (NASA IRTF) - a 3-meter telescope optimized for the infrared astronomy. SpeX, one of the instruments available to be used with this telescope, provides spectral resolutions of $R \sim 1000-2000$ across $0.8-2.4 \mu\text{m}$, $2.0-4.1 \mu\text{m}$, and $2.3-5.5 \mu\text{m}$, using prism cross-dispersers. Single order long slit modes are also available. A high throughput prism mode is provided for $0.8-2.5 \mu\text{m}$ spectroscopy at $R \sim 100$. It employs a 1024×1024 *Aladdin3 InSBb* CCD array for acquiring the spectra. Image acquisition could be made with a 512×512 *Alladin2 CCD InSb* array [8].

Two computers manage the instrument - namely GuideDog and BigDog, the first is dedicated for pointing and tracking the object and the second is used for spectrograph setup and image acquisition. Because the asteroid (9147) Kourakuen has an apparent motion of $0.16''/\text{min}$ a differential tracking was employed.

We observed (9147) Kourakuen in the $0.8-2.5 \mu\text{m}$ spectral region with the SpeX/IRTF instrument. The observations were performed remotely from the Centre d'Observation à Distance en Astronomie à Meudon (CODAM) [9, 10] on November 15, 2011. The moment of observation (given in universal time -UT), the position of the object, the visual magnitude, the airmass (optical path length through Earth's atmosphere for light from a celestial body) and the integration time are given in Table 1. The observations were carried out using the low resolution prism mode of the spectrograph. We used a $0.8 \times 15 \text{ arcsec}$ slit oriented north-south.

A solar-like standard star taken at similar airmass is required to correct for atmospheric effects and to remove the signature of the Sun's spectrum in order to have only the signature of the target surface. Two G2V solar analogs were observed, namely HD22361 and HD4940. We observed the last one (HD4940) since it was at favorable airmass (the differential airmass between the asteroid and this standard star was ~ 0.14) at the moment of observation. Three pairs of images having 2 seconds exposure time for each image were sufficient to obtain a good

SNR (signal to noise ratio), considering the 8.7 magnitude of the star. When choosing the analog solar we also considered that if the star is too bright will saturate the CCD, while a fainter star will require a too long integration time.

The spectra for the asteroid and the solar analog star were obtained alternatively at two separate locations along the slit (close to top and close to bottom) following the *nodding procedure* [11].

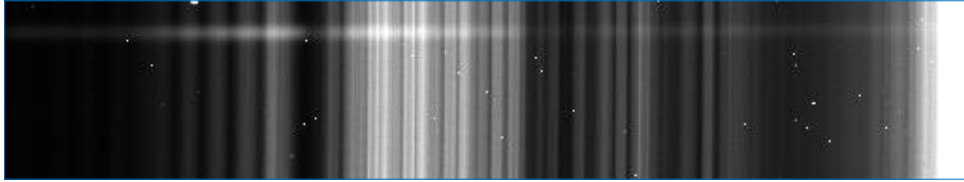


Fig. 3. Part of the image that contains the spectrum of (9147) Kourakuen. The horizontal trace represents the spectrum of the light reflected by the object.

Because the asteroid had an apparent magnitude of 16.4, eight pairs of images were taken with an exposure time of 2 minutes per image (Fig. 3). The spectrum of the object is the horizontal trace from the upper side of the image. The vertical stripes are the atmospheric lines caused by different transparency. The subtractions between adjacent images will partially remove the effect of the atmosphere (Fig. 4).

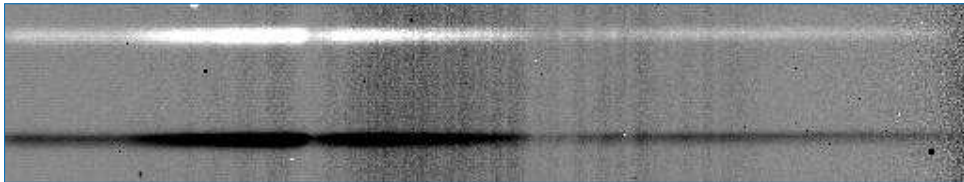


Fig. 4. Result obtained after the subtraction between two consecutive images. The white trace is the spectrum from the first image, and the dark trace (it appears black because the pixels have negative values after subtraction) is the spectrum from the second.

Preprocessing of the CCD images included bias and flat field correction. An averaged bias frame taken at the beginning of the night was used to perform bias subtraction. Flat field images were obtained using calibration lamps at the end of the night.

Our strategy was to look at objects as close to the zenith as possible, thus all observations were made at an airmass less than 1.3 (~50 deg altitude).

3. Data reduction and data analysis of emission spectra □ application to the quasar PG1634 + 706

Because for these observations we did not use a lamp for wavelength calibration, this was done by identifying the position of the known lines in the star spectra. In general stellar spectra share two dominant features: the continuum - emission at all wavelengths across their spectrum and discrete absorption lines corresponding to the elements which are present in the stellar atmosphere. Hydrogen is the most common gas in the atmosphere of stars, and thus its well known absorption lines from visible ($H\alpha$, $H\beta$, $H\gamma$) can be used for wavelength calibration. Since our image (Fig. 2) contains also the spectra of some stars an accurate calibration can be made using this procedure. The value of the resolution found is given in Eq. 2:

$$Dispersion[nm / pixel] = 1.480 \pm 0.008 \quad (2)$$

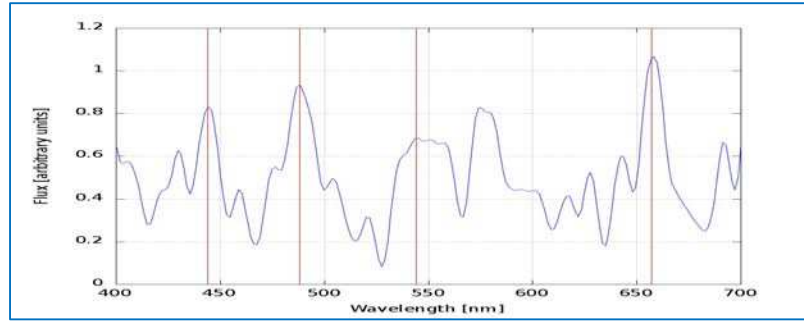


Fig. 5. PG1634 + 706 spectrum obtained after data reduction and continuum subtraction.

The preprocessing of this spectrum consists in noise reduction which was made by applying on the image a Gaussian filter with $\sigma = 2$ pixels. This filter replaces each pixel with a pixel of value proportional to a normal distribution computed over the current pixel and its neighbors [12].

The spectral profile contains a continuum part, which is the continuum emission part of the quasar modulated by the transfer function of the acquisition system (telescope, diffraction grating and CCD camera transfer functions). Continuum subtraction reduces the smoothly varying background to zero and essentially has the same effect as filtering out the long-period Fourier components of the spectra. Without continuum subtraction, the intensities of spectral lines are not clearly detectable [13]. The continuum was removed by dividing the spectrum with a fifth order polynomial curve fitting. The obtained result after data reduction and continuum subtraction is given in Fig. 5.

Quasars are objects with star-like appearance and strong radio emissions, their name being derived from *quasi-stellar radio sources*. The identification in

their spectra of the emission lines (example: hydrogen Balmer lines - $H\alpha$, $H\beta$, $H\gamma$) reveals that a large Doppler redshift exists for this type of objects. This redshift is defined as the ratio of the change in wavelength ($\Delta\lambda = \lambda_{obs} - \lambda_0$) to the non-shifted wavelength from a stationary source:

$$z = \frac{\Delta\lambda}{\lambda_0} = \sqrt{\frac{c+v}{c-v}} - 1 \quad (3)$$

where c is the speed of light and v is the recession speed of the object.

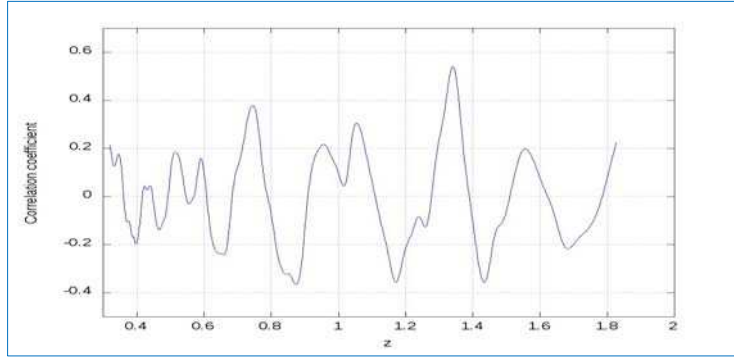


Fig 6. Correlation coefficient between quasar spectrum and the template spectrum shifted with different z .

The analysis of the obtained spectrum of the quasar PG1634+706 consists in redshift determination and application of Hubble law to determine the distance.

The most common technique [14] to determine the redshift is the cross-correlation of the observed spectrum with a template spectrum. The redshift is determined by the location of the largest peak in the cross-correlation functions. Several rest frame composite quasar spectra exists for the optical region like the one from article [15] obtained using data from Large Bright Quasar Survey (LBQS) and from article [16] based on Sloan Digital Sky Survey (SDSS). Thus for determining the redshift of our spectrum the following steps were taken: 1.) shift the template spectrum with a z varying from 0.4 to 1.8 using the step of 0.001. This is a reasonable assumption made after visual inspection of our data; 2.) at each step, the correlation coefficient between the quasar spectrum and the shifted template spectrum is computed (Fig. 6); 3.) choose the redshift corresponding to the best correlation coefficient found.

In this way, we obtained $z = 1.340$ corresponding to the peak value of the correlation coefficient equal with 0.5416. Our determination is at $\sim 3\sigma$ (where $\sigma = 0.1987$ is the standard deviation of the correlation coefficient values plotted in Fig. 6).

Considering the value found for the redshift - $z = 1.340$, the emission lines of known chemical elements could be identified in the spectrum of PG1634+706

(Table 2). Based on the emission line identification the accuracy of z determination can be ascertained: $z = 1.340 \pm 0.008$.

Table 2

Emission line identification in spectrum of PG1634 +706

Line	Rest-frame wavelength [nm]	λ shifted with $z=1.34$ [nm]	λ observed in quasar spectrum [nm]
C III]	190.6	446.0	444
Fe III	207.7	485.8	488
Fe II + CII]	232.6	544.3	544
Mg II	280.0	655.2	655

Edwin Hubble showed that there is a pattern in the speeds with which the galaxies are receding from us which implies that the Universe is expanding [15]. Observations that followed confirmed Hubble law:

$$v = H_0 \cdot d \quad (4)$$

where v is the radial velocity and d is the distance and H_0 is the Hubble constant. Recently, high-redshift measurements have been used to predict the value of H_0 [16, 17]:

$$H_0 = 70.3 \pm 1.3 \frac{km}{s \cdot Mpc} \quad (5)$$

Applying the equation (3), (4), (5) the speed of this object and the distance to it can be computed (Eq. 6).

$$v = c \cdot \frac{(z+1)^2 - 1}{(z+1)^2 + 1} = (2.073 \pm 0.018) \cdot 10^8 \frac{m}{s} \quad (6)$$

$$d = \frac{v}{H_0} = (9.644 \pm 0.16) \cdot 10^9 \text{ light years}$$

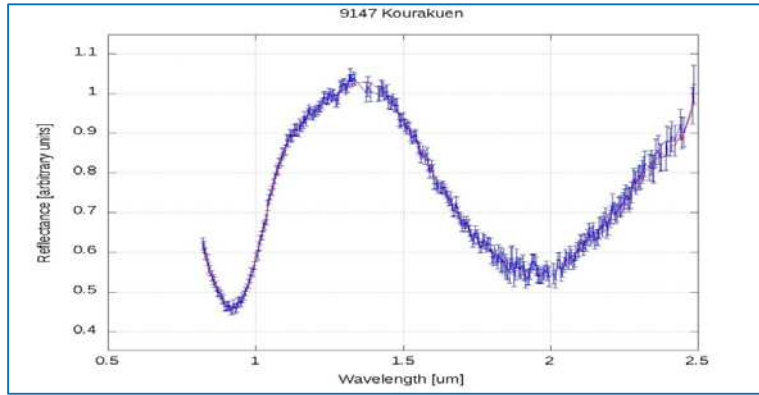
These results are in agreement with the value found by other studies of this bright quasar [3, 4, 31].

4. Data reduction and data analysis of reflection spectra □ application to 9147 Kourakuen

The observation of reflection spectra from a celestial object implies additional steps in both observing method and data reduction procedure. This is due to the fact that the light reflected from the surface of the body must be divided by a spectrum of a solar-like star to determine the reflectance relative to that of the original light source, the Sun. Thus, the data reduction process for the reflection spectra consist in three steps: 1) obtain the raw spectra for the object and the solar

analog, 2) obtain the wavelength calibration of the instrument using flat field images taken with calibration lamps and 3) compute normalized reflectance spectrum by dividing the asteroid spectrum by the solar analogue spectrum and performing a correction for Earth atmospheric lines [18, 19].

Fig 7. NIR spectrum of (9147) Kourakuen.



For the first two steps, the Image Reduction and Analysis Facility (IRAF) [20] was used in conjunction with some scripts that create the command files for a specific set of IRAF instructions. For the second step, specific IDL routines were used in order to diminish the influence of the telluric bands in our spectrum and to divide the obtained spectrum by the solar analog. The obtained result for (9147) Kourakuen is given in Fig. 7.

Basaltic *asteroids* are believed to derive from bodies whose interiors reached the melting temperature of silicate rocks and subsequently differentiated [21]. (4) Vesta was the first known asteroid presenting a basaltic crust. In the last years an increasingly large number of small asteroids with a similar surface composition have been discovered [22]. (9147) Kourakuen is a main belt asteroid with an estimated diameter of 5.1 Km. Having the semi-major axis $a = 2.19 AU$, eccentricity $e = 0.108$, and inclination $i = 6^\circ.892$, this object could not belong to Vesta family considering the dynamical criteria. However, its SDSS (Sloan Digital Sky Survey) colors [23] suggests a surface composition similar to (4) Vesta (a V-type object).

The first step in analyzing the reflecting spectrum for this object consists in finding the taxonomic type of the asteroid. Taxonomic types, although not usable to determine the mineralogical compositions of the objects, help constrain mineral species that may be present on the surface of the asteroid. We used two independent methods to establish the taxonomical class of this asteroid. In a first approach, spectral data of our asteroids were compared with Bus-DeMeo taxonomic classes [24] via the MIT-SMASS on-line tool. The second approach to taxonomic classification was a procedure using a χ^2 minimization method

accounting for the mean and standard-deviation values of the Bus-DeMeo taxonomic classes [18]. Both methods lead to the same result: this object is undoubtedly a V-type (Fig. 8.a). In the Bus-DeMeo taxonomy, V-type asteroids are characterized by very strong and very narrow 1-micron absorption and strong 2-micron absorption feature [24].

Putting the spectral data obtained from telescope observations, in relation to the laboratory measurements could reveal a lot of information related to the composition of the surface of these celestial bodies. Spectroscopy of different samples made in the laboratory provides the basis upon which compositional information about unexplored or unsampled planetary surfaces is derived from remotely obtained reflectance spectra. Such a comparison could be made based on a χ^2 coefficient [11]:

$$\chi^2 = \frac{1}{N_w} \sum_i^{N_w} \frac{(R_i - f(w_i))^2}{f(w_i)} \quad (7)$$

where R_i are the reflectances obtained in laboratory, $f(w_i)$ are the object normalized reflectances and N_w is the number of points.

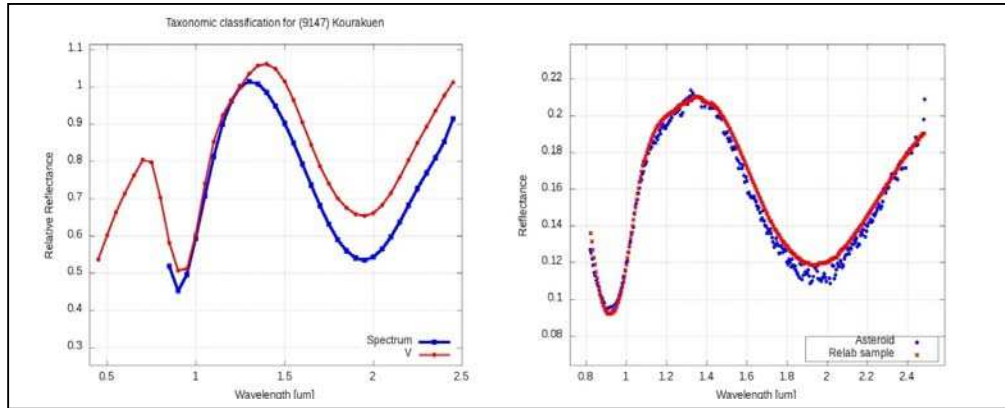


Fig 8.a) Taxonomic comparison between the polynomial fit of (9147) Kourakuen (blue) and the V-type class (red); b) Comparison between the spectrum of (9147) Kourakuen (blue) and the NIR spectrum of meteorite Pavlovka.

The Relab spectral database contains more than 15,000 spectra for different types of materials from meteorites to terrestrial rocks, man-made mixtures, and terrestrial and lunar soils [25]. We compared our spectrum with all the spectra from the Relab database, using a χ^2 minimization method and additionally, the correlation coefficient. The solution found with both methods was that the spectrum of (9147) Kourakuen is almost identical with the spectrum of Pavlovka meteorite (Fig. 8.b). The meteorite sample is of type achondrite howardite already studied so far [26, 27]. The bulk composition of the chondrules

from this meteorite contains SiO₂ (50.1%), MgO(23.7%), FeO(15%), Al₂O₃(6.2%), CaO(3.8%) [26].

Laboratory spectra similar to the spectrum of (9147) Kourakuen are those of the meteorites Roda (Achondrite Diogenite), Le Teilleul (Achondrite, Howardite) and Kapoeta (Basaltic HED Howardite). The first fifty solutions that matched our spectrum are HED (Howardite Eucrite Diogenite) meteorites. These are basaltic meteorites believed to result from large asteroids that melted to form a metallic core and basaltic magmas after the formation.

The absorption band parameters are diagnostic of the mineralogy present on the surface of the observed asteroids. The relationship between these spectral parameters and the mineralogy, particularly pyroxene and olivine, has been studied in various papers over the last years [28]. Most pyroxenes and the basaltic achondrites show a strong correlation between the position of band centers at 1 μm and 2 μm [28, 29, 30]. Thus, we computed the band minima and band centers (at 1 μm and 2 μm), defined as the wavelength position of the point of lowest reflectance before and after the removal of the continuum, respectively [28]. The computations were done using the standard procedures [31]. The results are given in Table 3.

Table 3

Band centers and band separation as deduced from Cloutis model.

BI center (μm)	BII center (μm)	Band separation [μm]
0.913 \pm 0.005	1.952 \pm 0.005	1.039 \pm 0.010

5. Discussions and conclusions

We described here two types of spectra of celestial bodies – the emission spectrum of a very far away object, the quasar PG1634 +706 and the reflection spectrum of a remnant object from the solar system formation, (9147) Kourakuen. The techniques for acquiring the spectra and the models used for data analysis are presented.

The two types of observations share common points in acquisition procedure, data reduction and data analysis methods. Conceptually the design of the acquisition system is the same: a telescope, a diffraction device (which could be a grating that works in transmission or reflection, or a prism) and the device to record the image of the spectrum – a charge coupled device (CCD). Also, extracting the spectrum from the image follows almost the same steps: the identification of the trace of the spectrum and getting pixel values, wavelength calibration, removing the Earth atmospheric influences in the spectrum. Data analysis includes the comparison between the spectra of celestial body with known spectra from the laboratory.

However the wide variety of results that can be obtained from analyzing the emission spectra and the reflection spectra from celestial bodies has lead to two separate domains of astronomy.

Because PG1634 +706 is a bright quasar, it has been studied in some papers like [3, 4, 31, 32]. Our observation for this object was at the limited magnitude for the type of equipment used. With a robust method, we succeed to extract the signal from noise and compute the redshift. Our determination of redshift $z = 1.340 \pm 0.008$, with a small telescope agrees with the value found after observation with large telescopes. The developed methods for observations and data reduction can be used as a starting point for spectroscopy of celestial bodies with small telescopes.

We obtained an accurate near-infrared spectrum of the asteroid (9147) Kourakuen. Based on this spectrum, a description of the surface composition was made. The comparisons with meteorites spectra revealed a spectral matching with HED type meteorites and in particular with the spectrum of Pavlovka meteorite. Using the Bus-DeMeo taxonomy, we classified this object as a V-type (taxonomic class describing asteroids with similar spectra as Vesta), which agrees to the type identified using a relatively more noisy spectrum by [22].

REFERENCES

- [1] *Anil K. Pradhan, Sultana N. Nahar*; Atomic Astrophysics and Spectroscopy; Cambridge University Press 2011;
- [2] *Bennoit Carry*; Etudes des proprietes physiques des asteroides par imagerie a haute resolution angulaire, Ph. D. Thesis; UNIVERSITE PARIS.DIDEROT (Paris 7), 29/09/2009
- [3] *Schmidt, M.; Green, R. F.*; Quasar evolution derived from the Palomar bright quasar survey and other complete quasar surveys; Astrophysical Journal, Part 1 (ISSN 0004-637X), vol. 269, June 15, 1983, p. 352-374.;06/1983
- [4] *Trevese, D.; et al.*; Line and continuum variability of two intermediate-redshift, high-luminosity quasars; Astronomy and Astrophysics, **Vol. 470**, Issue 2, August I 2007, pp.491-496
- [5] *Schelte John Bus*; Compositional structure in the asteroid belt: result of a spectroscopic survey; Ph. D. Thesis - MIT; 04/1999
- [6] *Francesca E. DeMeo*; La variation compositionnelle des petits corps a travers le systeme solaire; Ph. D. Thesis - Observatoire de Paris 16/06/2010
- [7] Star Analyser site: <http://www.patonhawksley.co.uk/staranalyser.html>
- [8] *Rayner, J. T.; et al* ; The Publications of the Astronomical Society of the Pacific, **Vol. 115**, Issue 805, pp. 362-382; 03/2003
- [9] *Birlan, M.; Barucci, A.; Thuillot, W.*; Solar system observations by remote observing technique: useful experience for robotic telescope strategies; Astronomische Nachrichten, **Vol.325**, Issue 6, p.571-573; 10/2004
- [10] *Birlan, M.; et al.*; Near infra-red spectroscopy of the asteroid 21 Lutetia. I. New results of long-term campaign; Astronomy and Astrophysics, **Vol. 454**, Issue 2, August I 2006, pp.677-681
- [11] *Dan Alin Nedelcu*; Modelisation Dynamique et spectroscopique des asteroides; Ph. D. Thesis - Observatoire de Paris; 23 09/2010;

- [12] Image J site: <http://imagejdocu.tudor.lu/>
- [13] *Fuqing Duan, Fuchao Wu*; Redshift Determination for Quasar Based on Similarity Measure; ICAPR 2005, LNCS 3686, pp. 529–537, 2005
- [14] *Tonry, J.; Davis, M.*; A survey of galaxy redshifts. I - Data reduction techniques; *Astronomical Journal*, **vol. 84**, Oct. 1979, p. 1511-1525; 10/1979
- [15] *Francis, Paul J.; et al.*; A high signal-to-noise ratio composite quasar spectrum; *Astrophysical Journal*, Part 1 (ISSN 0004-637X), **Vol. 373**, June 1, 1991, p. 465-470; 06/1991
- [16] *Vanden Berk, Daniel E.; et al.*; Composite Quasar Spectra from the Sloan Digital Sky Survey; *The Astronomical Journal*, **Vol. 122**, Issue 2, pp. 549-564; 08/2001
- [15] *Theo Koupeilis*; In quest of the Univers; 6th edition; Jones and Bartlett Publishers; 2011
- [16] *Komatsu, E.; et. al.*; Seven-year Wilkinson Microwave Anisotropy Probe (WMAP) Observations: Cosmological Interpretation; *The Astrophysical Journal Supplement*, **Vol.192**, Issue 2; 02/2011
- [17] *Riess, Adam G.; et al.*; A 3% Solution: Determination of the Hubble Constant with the Hubble Space Telescope and Wide Field Camera 3; *The Astrophysical Journal*, **Vol. 730**, Issue 2, article id. 119 (2011); 04/2011
- [18] *Popescu, M.; et al.*; Spectral properties of eight near-Earth asteroids; *Astronomy & Astrophysics*, **Vol. 535**, 11/2011
- [19] *Birlan, M.; Vernazza, P.; Nedelcu, D. A.*; Spectral properties of nine M-type asteroids; *Astronomy and Astrophysics*, **Vol. 475**, Issue 2, November IV 2007, pp.747-754
- [20] *Tody, Doug*; IRAF in the Nineties; *Astronomical Data Analysis Software and Systems II*, A.S.P. Conference Series, **Vol. 52**, 1993, p. 173.; 01/1993
- [21] *Gaffey, M. J.; et al.*; Mineralogy of Asteroids; *Asteroids III*, W. F. Bottke Jr., A. Cellino, P. Paolicchi, and R. P. Binzel (eds), University of Arizona Press, Tucson, p.183-204; 2002
- [22] *de Sanctis, M. C.; et al.*; Spectral and mineralogical characterization of inner main-belt V-type asteroids; *Astronomy & Astrophysics*, **Vol. 533**, 09/2011
- [23] *Nesvorný, David; et al.*; Thais, Fugitives from the Vesta family; *Icarus*, **Vol.193**, Issue 1, p. 85-95; 01/2008
- [24] *DeMeo, Francesca E.; Binzel et al.*; An extension of the Bus asteroid taxonomy into the near-infrared; *Icarus*, **Vol. 202**, Issue 1, p. 160-180.; 07/2009
- [25] Relab Spectral Database: <http://www.planetary.brown.edu/relab/>
- [26] *Olsen, Edward J.; et al.*; Chondrule-like objects and brown glasses in howardites; *Meteoritics* (ISSN 0026-1114), **vol. 25**, Sept. 1990, p. 187-194.; 09/1990
- [27] *Labotka, T. C.; Papike, J. J.*; Howardites - Samples of the regolith of the eucrite parent-body: Petrology of Frankfort, Pavlovka, Yurtuk, Malvern, and ALHA 77302; *Lunar and Planetary Science Conference*, 11th, Houston, TX, March 17-21, 1980, Proceedings. **Vol. 2.** (A82-22296 09-91) New York, Pergamon Press, 1980, p. 1103-1130.
- [28] *Cloutis, Edward A.; Gaffey, Michael J.*; Pyroxene spectroscopy revisited - Spectral-compositional correlations and relationship to geothermometry; *Journal of Geophysical Research*, **Vol. 96**, Dec. 25, 1991, p. 22,809-22,826
- [29] *Gaffey, M. J.; McCord, T. B.*; Asteroidal Surface Compositions; *Bulletin of the American Astronomical Society*, **Vol. 8**, p.459; 06/1976
- [30] *Adams, J. B.; McCord, T. B.*; The use of ground-based telescopes in determining the composition of the surfaces of solar system objects.; *Moon*, **Vol. 11**, p. 429 - 430; 12/1974
- [31] *Cloutis, Edward A.; et al.*; Calibrations of phase abundance, composition, and particle size distribution for olivine-orthopyroxene mixtures from reflectance spectra; *Journal of Geophysical Research*, **Vol. 91**, Oct. 1986, p. 11641-11653.

Spectral properties of (854) Frostia, (1333) Cevenola, and (3623) Chaplin^{*}

M. Birlan^{1†}, D.A. Nedelcu², P. Descamps¹, J. Berthier¹, F. Marchis³,
S. Merouane⁴, and M. Popescu¹

¹*Institut de Mécanique Céleste et de Calcul des Éphémérides (IMCCE),
Observatoire de Paris, 77 avenue Denfert-Rochereau, 75014 Paris Cedex, France*

²*Astronomical Institute of the Romanian Academy, 5 Cuștitul de Argint, RO-040557 Bucharest, Romania*

³*University of California at Berkeley, Dept. of Astronomy, 601 Campbell Hall, Berkeley, CA 94720, USA*

⁴*University Paris VII, Dept. of Physics, 75206 Paris Cedex, France*

17 March 2011

ABSTRACT

Near-infrared spectroscopy can play a key role for establishing the mineralogical composition and supporting other physical data obtained by complementary observational techniques such as adaptive optics, radar, and photometry. The objective of our survey was asteroids which present large variations in their lightcurves. We report observations for asteroids (854) Frostia, (1333) Cevenola, and (3623) Chaplin carried out in the 0.8–2.5 μ m spectral range using SpeX/IRTF in LowRes mode. The spectral modeling of these asteroids give new insights to these peculiar objects in the main-belt. (854) Frostia is a V-type asteroid, and its spectral properties are similar to those of basalts. The most probable mineralogical solution $Wo_8Fs_{43}En_{49}$ was calculated for Frostia. (1333) Cevenola was estimated to have an S_q spectral type, in agreement with its membership to the Eunomia family. (3623) Chaplin is an S-type asteroid, in agreement with the taxonomic type of the Koronis family.

Key words: asteroids, spectroscopy, mineralogical model

1 INTRODUCTION

The lightcurve of an asteroid is the display of the variation of its magnitude over time. The lightcurve is related to the rotation of an asteroid around an instantaneous axis. In other words, the lightcurve could be interpreted as an observable of the angular momentum for a given object. This variation is primarily due to the shape (French & Binzel 1989). The lightcurve could be also due to the albedo variation (Harris & Lupishko 1989) of the asteroids. The results of observations of lightcurves for asteroids are regularly synthesized in catalogs of lightcurves (for example Lagerkvist et al. (1987)).

Several asteroids exhibit large amplitude lightcurves, which remained unexplained until the last decade. Several explanations were proposed for these variations, starting with elongated shaped asteroids and including double and multiple systems of aggregates in a weak self-gravitational field (Cellino et al. 1985).

The number of known multiple systems among asteroids has increased significantly in recent years. In the past,

the binarity and multiplicity of asteroids was suggested by several authors (van Flandern et al. 1979) based on occultations of stars (for example in the articles of Binzel (1978)¹, and Donnison (1979)²) or photoelectric photometry (Tedesco 1979; Binzel & van Flandern 1979; Dunlap & Gehrels 1969). These observational facts were the origin of theoretical problems related to spin evolution and stability (Wijesinghe & Tedesco 1979; Zappala et al. 1980; Leone et al. 1984).

Several articles are based on observations using various techniques namely radar (Ostro et al. 2002, 2000; Magri et al. 2007), adaptive optics (Marchis et al. 2005), adaptive optics combined with lightcurve photometry (Descamps et al. 2007), and lightcurve photometry (Behrend et al. 2006; Pravec et al. 2002).

Analytical and numerical simulations of catastrophic collisions among small bodies, using several hypothesis, are published regularly by several teams (Durda et al. 2004;

¹ The article also presents historical facts of occultation of stars by asteroids.

² This satellite was not confirmed by direct imaging. (Storrs et al. 1999)

^{*} The article uses observations performed with SpeX/IRTF

[†] E-mail: Mirel.Birlan@imcce.fr

Dell'Oro & Cellino 2007; Holsapple & Michel 2008). This topic remains open despite an important acquisition of knowledge from laboratory experiments and numerical tests. In the framework of this paper the most important conclusion of these works is that elongated shapes, binarity or multiplicity could be explained for both large objects (≈ 100 km in size) and relatively small ones (kilometre-size asteroids). For instance, a *doublet system* is a binary system where both bodies are of nearly equal sizes. Their origin is not well understood, but several such systems have been reported (ex: (90) Antiope, (617) Patroclus, (69230) Hermes, 1998WW31). Theoretical studies concerning the movement of components around their center of mass can be validated with observational results (obtained for instance using adaptive optics); results of their dynamics will be constrained by the physical model which takes into account shape, bulk density, and internal properties of the components. Furthermore, the interaction between a dynamical and a physical model allows the derivation of the most probable configuration of the system (in terms of separation of components, orbital parameters, shapes and densities).

Spectroscopic measurements of asteroids contribute to the characterization of minerals at the surface. In the assumption of homogeneous bodies, this constrains the nature of tensile stress inside the object. The features of its spectrum constrains the mineralogical composition and implicitly the range of its density. By applying these considerations to the models, some physical parameters such as the macro-porosity or the *rubble pile* structures will be derived.

The article is focused on the spectroscopy of one binary system and two asteroids with large amplitude lightcurves. Near-Infrared (NIR) spectroscopic observations for the binary system of (854) Frostia are presented. Observations of (1333) Cevenola, and (3623) Chaplin, asteroids with large amplitude lightcurves are also presented. A detailed analysis of these spectra, and the models derived for each asteroid are then discussed.

2 THE OBSERVING PROTOCOL

The asteroids were observed in the $0.8\text{--}2.5\ \mu\text{m}$ spectral region by means of the instrument SpeX on the IRTF located on Mauna Kea, Hawaii. These observations were performed in remote mode from the Centre d'Observation à Distance en Astronomie à Meudon (CODAM), more than 12,000 km away from Hawaii, (Birlan et al. 2004, 2006) using the low resolution Prism mode ($R = 100$) of the spectrograph. We used a 0.8×15 arcsec slit oriented North-South. The spectra for the asteroid and the solar analog stars were obtained alternatively on two separate locations on the slit denoted A and B (the *nodding* procedure). The data reduction process consists of two main steps: 1) obtaining the raw spectra for the object and the solar analog and 2) computation of the normalized reflectance spectrum by dividing the asteroid spectrum by the solar analog spectrum and performing a correction for telluric lines.

For the first step, Image Reduction and Analysis Facility (IRAF <http://iraf.noao.edu>) was used. For the second step, after the wavelength calibration, specific IDL routines were also used in order to diminish the influence of telluric bands in our spectra (Rivkin et al. 2004). In order to publish

high confidence data, the raw images were also re-reduced via Spextool (Cushing et al. 2004) and specific MIDAS procedures, and the results were compared with the previous ones.

Our strategy was to observe all asteroids as close to the zenith as possible (circumstances of our targets are presented in Table 1). Thus, we managed to observe all targets with an airmass less than 1.25. No other correction for the differential refraction was considered. Each observed asteroid was preceded by observations of solar analogs in the vicinity of it (airmass differences between the asteroid and the standard less than 0.1). The seeing varied between 0.7–1.8 arcsec during the observing runs, and the humidity was in the 25% – 85% range.

In order to obtain a S/N in the 80–200 range, we needed 15 to 40 minutes of exposure time, depending on the asteroid magnitude, and counting both the effective exposure and CCD camera readout time. Circumstances of observations are presented in Table 2.

For the asteroid spectra, the solar analogs HD127913, G104-335, HD73708 were observed. For the computation of the final reflectance (ratio between the asteroid spectrum and the star spectrum) we took into account the similar dynamic regimes of the detector (Vacca et al. 2004; Rayner et al. 2003).

3 RESULTS

3.1 (854) Frostia

This asteroid was observed intensely in photometry (Behrend et al. 2006) by amateurs and professional astronomers³. The asteroid is a slow rotator with a synodic period of $37^h.728$. Its regular lightcurve with an amplitude of $0^m.33$ presents, for short periods of time, important attenuation, of about $0^m.7\text{--}0^m.8$. The large magnitude is very well explained by mutual eclipse/occultation events for an object with two components of comparable size. Based on a physical model of a double system, Behrend et al. (2006) calculated a bulk density of $750\text{--}1,020\text{ kg/m}^3$. They explain such a low density value by a possible C-type asteroid with a high macro-porosity of about 45 %.

Sloan Digital Sky Survey (SDSS) colors (Ivezić et al. (2001))⁴ of this object are reported. These data show large variations in color. It is important to note that the $v-i$ color is greater than the $v-z$ one⁵, which suggest the presence of absorption band around $1\ \mu\text{m}$.

Visible spectroscopy of Frostia was reported by Alvarez-Candal et al. (2006). These results are in agreement with SDSS colors and the authors classified this asteroid in the V-taxonomic class.

NIR spectrum of (854) Frostia (Fig 1) was obtained on March 13, 2007. The total integration time of 40 min allows an accurate spectrum with the S/N of 120. Following Bus-

³ http://obswww.unige.ch/~behrend/page_cou.html

⁴ <http://sbn.psi.edu/ferret/>

⁵ Sloan Digital Sky Survey was obtained using five broad band filters, namely u, g, r, i, z centered to 3,551, 4,686, 6,165, 7,481, and 8,931 Å respectively

Table 1. Circumstances of the observations are presented (date of observations with the fraction of the day for the beginning of the observation, number and name of the asteroid, semi-major axis, eccentricity, inclination, the apparent magnitude, phase angle, as well as heliocentric and geocentric distances).

Date (UT)	Asteroid	a (UA)	e	i(°)	V	Φ (°)	r (UA)	Δ (UA)
2007/03/13.48753	(854) Frostia	2.36823	0.17398	6.090	14.93	3.62	2.34843	1.36087
2007/03/12.54861	(1333) Cevenola	2.63584	0.13314	14.642	15.63	13.74	2.66963	1.82769
2007/03/13.57463	(1333) Cevenola	2.63584	0.13314	14.642	15.61	13.45	2.67108	1.82177
2007/03/12.37775	(3623) Chaplin	2.85048	0.08790	3.072	17.15	14.68	3.03656	2.30870
2007/03/13.26730	(3623) Chaplin	2.85048	0.08790	3.072	17.17	14.89	3.03710	2.31966

Table 2. Observation circumstances for each asteroid. The columns show the name of the asteroid, the mean JD value for each series, the individual time for each spectrum (Itime), the number of cycles, and the airmass at the mean JD of each series. The two columns present the standard star used for data reduction as well as its airmass during the observation.

Object	JD	Itime(s)	Cycles	Airmass	Standard	Airmass
(854) Frostia	2454172.98754	120	10	1.105	G104-335	1.070
(1333) Cevenola	2454172.04901	120	24	1.016	HD127913	1.055
(1333) Cevenola	2454173.07464	120	10	1.034	HD127913	1.031
(3623) Chaplin	2454171.87776	120	18	1.111	HD73708	1.085
(3623) Chaplin	2454172.76731	120	20	1.019	HD73708	1.018

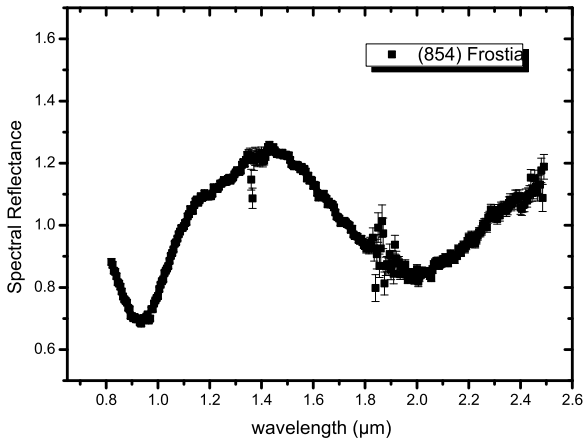


Figure 1. NIR spectrum of (854) Frostia with the error-bars is presented. The spectra is normalized to $1.25 \mu\text{m}$.

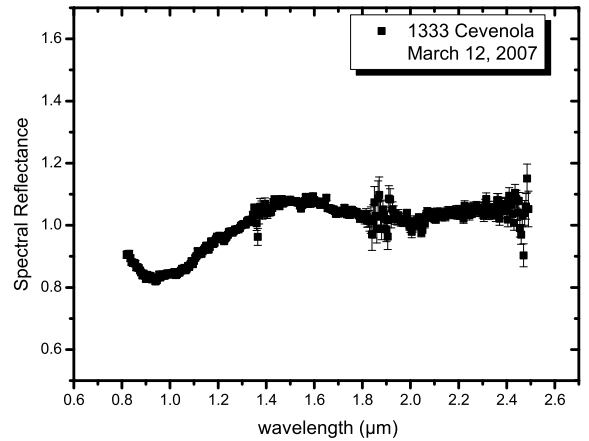


Figure 2. NIR spectrum of (1333) Cevenola obtained in March 12, 2007 with error-bars. The spectrum is normalized to $1.25 \mu\text{m}$.

DeMeo taxonomy, the NIR spectrum is typical of V-type asteroids (DeMeo et al. 2009)⁶.

3.2 (1333) Cevenola

Dynamically, (1333) Cevenola belongs to the Eunomia family (Zappala et al. 1995; Mothé-Diniz et al. 2005). Photometry of this asteroid shows a large amplitude of $0^m.97 \pm 0^m.03$ and a synodical period of $4^h.88 \pm 0^h.02$ (Warner 2002). The visible spectrum was reported by Lazzaro et al. (2004) in the framework of S^3OS^2 survey, and the analysis of spectral data places the asteroid into the S (S_q more precisely)

complex. The Eunomia family is actually dominated by objects displaying S -type spectra.

Two NIR spectra were obtained for this asteroid (Figs 2 and 3), on two consecutive nights, separated by 24 hours. The spectrum of March 12, 2007 is the result of the combination of individual spectra of 120 seconds each, for the total integration time of 1^h28^{min} . The second spectrum was obtained in March 13, 2007 for the total integration time of 40^{min} . Consequently, a S/N of 50 and 20 was estimated.

The NIR spectra are very similar. The consistency with the S_q classification (DeMeo et al. 2009) is confirmed either based on NIR data or the composite visible+NIR one.

⁶ <http://smass.mit.edu/busdemeoclass.html>

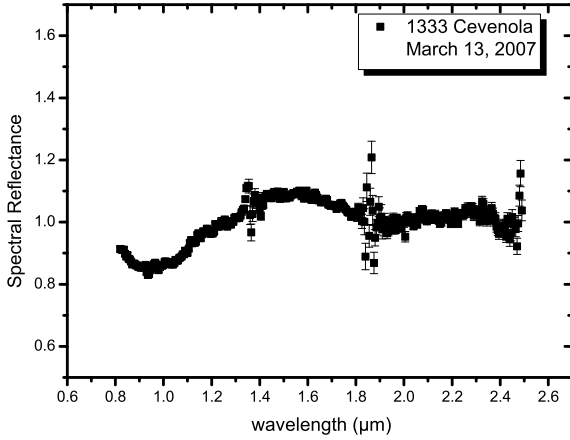


Figure 3. NIR spectrum of (1333) Cevenola obtained in March 13, 2007 with error-bars. The spectrum is normalized to 1.25 μm .

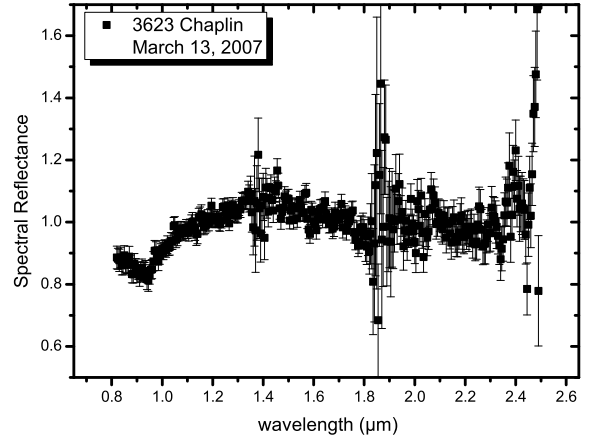


Figure 5. NIR spectrum of (3623) Chaplin obtained in March 13, 2007, with error-bars. The spectrum is normalized to 1.25 μm .

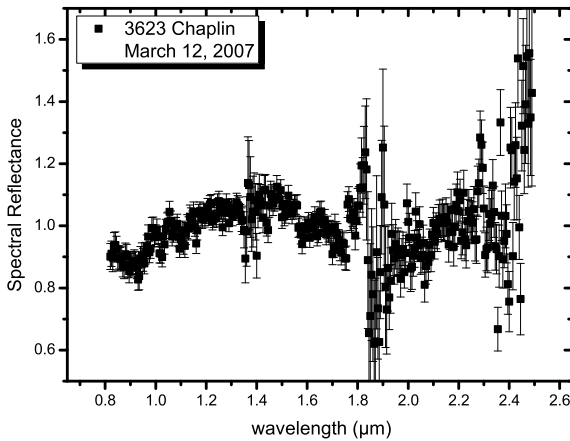


Figure 4. NIR spectrum of (3623) Chaplin obtained in March 12, 2007 with error-bars. The spectrum is normalized to 1.25 μm .

3.3 (3623) Chaplin

(3623) Chaplin belongs to the Koronis family (Zappala et al. 1995; Mothé-Diniz et al. 2005). The asteroid has the synodic period of $8.^h361 \pm 0.^h005$, and a large amplitude in its composite lightcurve estimated to $0.^m97 \pm 0.^m02$ (Birlan et al. 1996). There is no estimation for its pole coordinates.

Two NIR spectra of the asteroid, presented in Fig 4 and Fig 5 were obtained at a time interval of about 23 hours. The spectrum of March 12, 2007 is the result of combined individual spectra of 120 seconds each, for the total integration time of 72^{min} , while the the second spectrum (obtained in March 13, 2007) was obtained for the total integration time of 80^{min} . The S/N was estimated in the range of 15-20.

The NIR spectrum is typical among *S* complex asteroids (DeMeo et al. 2009), more precisely close to the *S_q* taxonomic subclass.

4 SPECTRAL MODELS AND MINERALOGICAL APPROACH

The three objects present absorption features around 1 and 2 μm , and the strength of absorption varies from one asteroid to another. The investigation was conducted using several techniques, namely the Modified Gaussian Model (Sunshine & Pieters 1993), and 2D mineralogical charts using χ^2 minimization of laboratory spectra.

4.1 MGM applied to spectra

The spectra were analyzed using the Modified Gaussian Model procedure (Sunshine & Pieters 1993). The procedure applied to high quality spectral data allows the quantitative characterization of absorption features, by simultaneous fitting multiple Gaussian-like absorption bands (Pieters & McFadden 1994). This condition is satisfied in our case for the spectra of Frostia and Cevenola, and in a relative way by the spectrum of Chaplin. The advantage of this method is the ability to quantitatively compare the asteroid spectra to certain minerals (Sunshine et al. 1990) by calculating individual bands centers, Full Width at Half Maximum, and strength. However, in the case of asteroid spectra, the results are physically relevant when the steps are carefully tested using laboratory measurements as standard (Canas et al. 2008). This method is appropriate for spectra revealing absorption features. The method is unable to solve, in terms of mineralogical solution, the continuum of analyzed spectra.

The MGM approach was initially used in free parameter mode, by considering the best fit obtained with a minimum number of absorption bands, in an *a priori* assumption of mineralogical compounds. In a second step, depending on minerals, the parameters of the continuum were fixed as well as the parameters of some individual absorption bands. We used the constraints obtained by Sunshine & Pieters (1998) for the olivine while the pyroxene was constrained by the results published by Cloutis & Gaffey (1991a). The MGM analysis was performed for Cevenola by taking advantage of

Table 3. Modified Gaussian Model applied to (854) Frostia and (1333) Cevenola. The best fit of this tool is summarized as follows: number of bands, the center of the band, the Full Width at Half Maximum value, the absorption strength, and the slope of the continuum.

Asteroid	Number of Bands	Center of Band (μm)	FWHM (μm)	Strength (log reflectance)	Continuum slope
(854) Frostia	5	0.922	0.162	-0.359	-5.10 E-05
		1.032	0.202	-0.173	
		1.248	0.150	-0.064	
		1.933	0.522	-0.414	
		2.330	0.546	-0.223	
(1333) Cevenola	6	0.482	0.278	-0.196	-7.12 E-06
		0.851	0.239	-0.100	
		0.916	0.184	-0.099	
		1.045	0.177	-0.118	
		1.220	0.459	-0.097	
		2.041	0.570	-0.130	

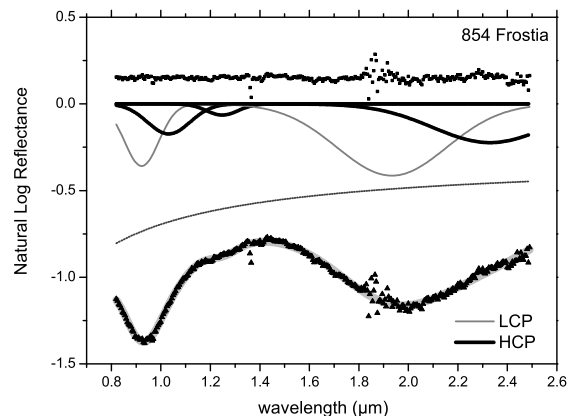
previous work done by Sunshine et al. (2004) on the S-type asteroids. The non-uniqueness of mineralogical solution obtained from spectral modeling justifies the omission of minor components. The major part of the best mineralogical solutions from the literature (for the same sample) are reliable in a limit of few percent. Even at this level of confidence, the mineralogy is not unique. Thus, our approach is justified.

A mineralogical solution was obtained for (854) Frostia using five absorption bands (Fig 6). This model shows that spectral features indicate the presence of both Low-Ca-Pyroxene(LCP) and High-Ca-Pyroxene(HCP). The presence of HCP is required for the spectral fit at wavelengths larger than $2.1 \mu\text{m}$. This band over $2.1 \mu\text{m}$ is a specific behavior of type B pyroxene, with bands attributable to crystal field transitions in ferrous iron located in the M2 crystallographic site (Cloutis & Gaffey 1991b). For the spectral profile around $1.25 \mu\text{m}$, the presence of plagioclase such as feldspar may be plausible. We note that the presence of absorption bands for olivine in the MGM analysis is not necessary for the fit of telescopic data.

The composite spectrum contained the visible data from S^3OS^2 program and our NIR data for (1333) Cevenola obtained in March 12, 2007 was also investigated using 6 absorption bands. In the model we used three absorption bands for the olivine in the $1 \mu\text{m}$ region (Sunshine & Pieters 1998). The band at $2.05 \mu\text{m}$ is recovered by only one pyroxene band with a good fit. Finally the fit was obtained by fixing the continuum and the width of absorption bands for the olivine. The model (Fig 7) is relatively good within a limit of 1.6%. Finally, the band at $1 \mu\text{m}$ is reproduced by four bands superimposed, implying the presence of both olivine and pyroxenes.

4.2 χ^2 best fit with RELAB data

Spectral properties of minerals in a intimate mixture combine in a non-additive, generally unique manner (Singer 1981). In the case of pyroxenes, this non-linearity was presented also by Cloutis & Gaffey (1991a). However, no other analytical law or approach by polynomial function was proposed until now for modelling real spectra. Thus, we propose the approach of three component minerals linearly mixed

**Figure 6.** MGM modeling of NIR data of (854) Frostia using five absorption bands of Low-Ca-pyroxene (LCP) and High-Ca-pyroxene(HCP). This figure presents, from the bottom to the top, the observational data superimposed to the MGM fit, the continuum, the individual absorption bands, and the errors between the model and the observational data. These plots are offset for clarity.

as a possible/probable solution to find families of minerals which are the best matches for our telescopic data.

The spectra were investigated with three component mixtures. This is the first time when mineralogical χ^2 residual space is plotted for asteroids. The initial components used for the mixtures are real laboratory spectra from the RELAB database ⁷.

In order to have a homogeneous data-set, the end-members were selected from the spectra obtained in the $0.3 - 2.6 \mu\text{m}$ wavelength range using the bidirectional visual and infrared spectrometer (BD-VNIR) within the Planetary Geology and Geophysics programme (PGG). The olivine

⁷ <http://www.planetary.brown.edu/relab>

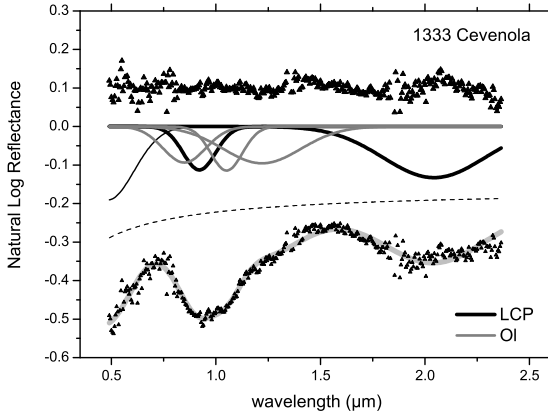


Figure 7. MGM modeling of VNIR data of (1333) Cevenola. The presence of both olivine (OI) and pyroxene (LCP) minerals are necessary for this fit. The individual absorption bands are drawn in black for LCP and gray for the olivine.

(OI), orthopyroxene (OPx) and clinopyroxene (CPx)⁸ sets that were identified contain 44, 33 and 55 spectra respectively. The olivine set includes synthetic spectra that span the $\text{Fa}_0\text{Fo}_{100}$ - $\text{Fa}_{100}\text{Fo}_0$ domain in 5-10 mol% increments (Dyar et al. 2009) while the members of orthopyroxene set sample the range $\text{En}_0\text{Fs}_{100}$ - $\text{En}_{100}\text{Fs}_0$ (Klima et al. 2007). The clinopyroxene spectra represents minerals with different Wo, En, Fs content. The wide variety of minerals included in the three above sets make them suitable for generating synthetic mixtures spectra.

The high resolution, high S/N RELAB spectra were fitted using a cubic B-spline function with 25 fitting coefficients. For the asteroids spectra, in order to avoid the overfitting, the number of coefficients was reduced to 12. In both cases it was confirmed by visual inspection that the interpolating functions approximate well the overall shape of the spectra.

For each possible combination of olivine, ortho- and clinopyroxene, synthetic spectra were generated from b-splined end-members spectra using a linear mixture by varying the end-member's concentration in 0.5% increment (step). Each of the obtained spectra were compared to spline smoothed spectra of (854) Frostia, (1333) Cevenola, and (3623) Chaplin. The χ^2 calculations were performed following the formula:

$$\chi^2 = \frac{1}{N_w} \sum_{i=1}^{N_w} \frac{(R_i - f(w_i))^2}{f(w_i)} \quad (1)$$

where N_w is the number of R_i reflectance values at w_i wavelength, and $f(w_i)$ the reflectance value of the geometric mixture obtained from laboratory spectra (i.e. additive contribution of individual component).

The concentration for each of the components will span the range between 0 and 100%, and the sum of the mixture

is 100%. The best mixture identified by the above χ^2 -test is further refined in 0.1% concentrations step this time with fixed end-members.

The χ^2 minimization will allow the derivation of a map of possible/plausible models. This method allows the plot of 2D mineralogical charts, an interesting tool for visualize the best mineralogical solutions.

Two dimensional charts derived from the χ^2 fit are presented in Figure 8, Figure 9, and Figure 10 for (854) Frostia (1333) Cevenola, and (3623) Chaplin respectively. These charts plot olivine on the X axis, and $\text{OPx}/(\text{CPx}+\text{OPx})$ on the Y axis. The color code indicates the concordance of the model to the observational data, the blue color representing the best fit. The white regions of the 2D charts are an indicator of the limit where the χ^2 minimization fails.

The best fit mixture for (854) Frostia was obtained using (OI, OPx, CPx) = (0, c1dl14, c1dl07) with following ratios (0%, 33.5%, 66.5%), while for the asteroid (1333) Cevenola the best fit was obtained using (OI, OPx, CPx) = (cgpo84, c1dl01, c1dl12) with ratios (25%, 67.5%, 7.5%).

In the case of (3623) Chaplin the closest analogue was the mixture (0, c1dl01, c1dl08) with ratios (0%, 96.5%, 3.5%).

The inferred mineralogical solutions explain well the asteroids spectra. However, giving the inherent complications of curve matching procedure as the χ^2 -test Gaffey et al. (2002) a family of mineralogical solutions could fit our spectroscopic data.

5 DISCUSSION

The binarity of (854) Frostia is supported by photometric data (Behrend et al. 2006). Unfortunately, no physical ephemerides of Frostia are not known to have a precise timing of possible mutual phenomena of this system. Nevertheless there is little chance for a geometry allowing mutual phenomena at the time of our observations. The spectrum likely represents this object globally, thus being a first attempt in the characterization of the asteroid's mineralogy.

The spectrum of (854) Frostia (Fig 1) reveals large and deep absorption bands around 1 and 2 microns. This spectrum, similar to the asteroid (4) Vesta, allows the classification of (854) Frostia in the V type taxonomic class. Based on spectroscopic behavior and dynamical consideration from the main-belt through the resonances 3:1 and ν_6 resonances (Binzel & Xu 1993), Vesta and the vestoids are supposed to be at the origin of Howardite-Eucrite-Diogenite meteorites. The structure of HED meteorites is very close to mafic materials. Thus, the parent body of HED meteorites are supposed to have experienced volcanism and metamorphism in the process of formation during the early solar system. The parent body of Vesta and vestoids underwent accretion, total melting, fractionation, and differentiation during the first few million of years of solar system formation (Keil 2002).

(854) Frostia was not included in the family of (4) Vesta by Zappala et al. (1995). The location of (854) Frostia inside the Main-Belt is very similar to that of Vesta family in semi-major axis and inclination and may justify its membership to the same clan. Frostia's eccentricity of 0.17 is slightly over the greater boundary (of 0.12) of Vesta family. This case is not particular while other V-type asteroids were already

⁸ structures of orthorhombic and monoclinic crystals of pyroxenes

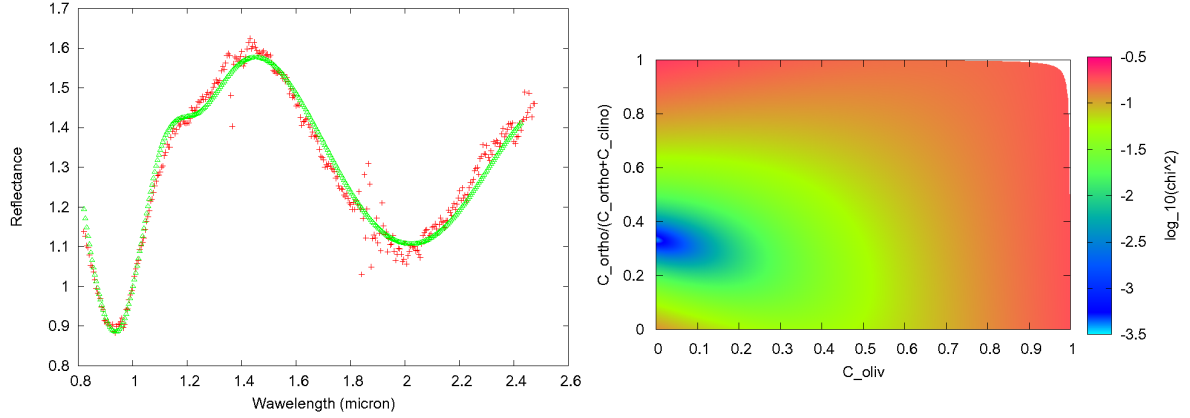


Figure 8. Two dimension chart of concentration for the asteroid (854) Frostia using olivine, orthopyroxene, and clinopyroxene from RELAB is presented in the right side of the figure. The best fit mixture for (854) Frostia using (Ol, OPx, CPx) = (0, c1dl14, c1dl07) with ratios (0%, 33.5%, 66.5%) is presented in the left side in the figure.

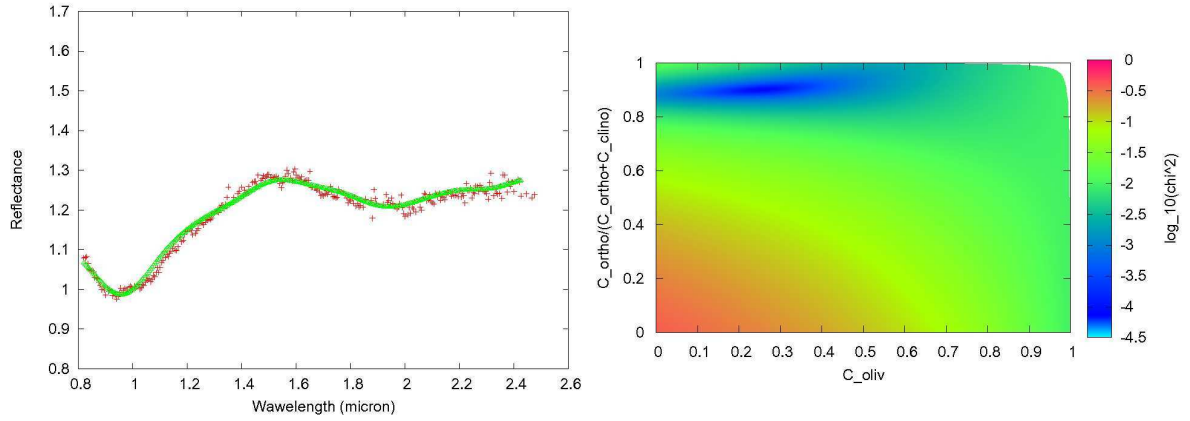


Figure 9. Two dimension chart of concentration for the asteroid (1333) Cevenola using olivine, orthopyroxene, and clinopyroxene from RELAB is presented in the right side of the figure. The best mineralogical model for (1333) Cevenola using (Ol, OPx, CPx) = (cgpo84, c1dl01, c1dl12) and the ratios (25%, 67.5%, 7.5%) is presented in the left side of the figure.

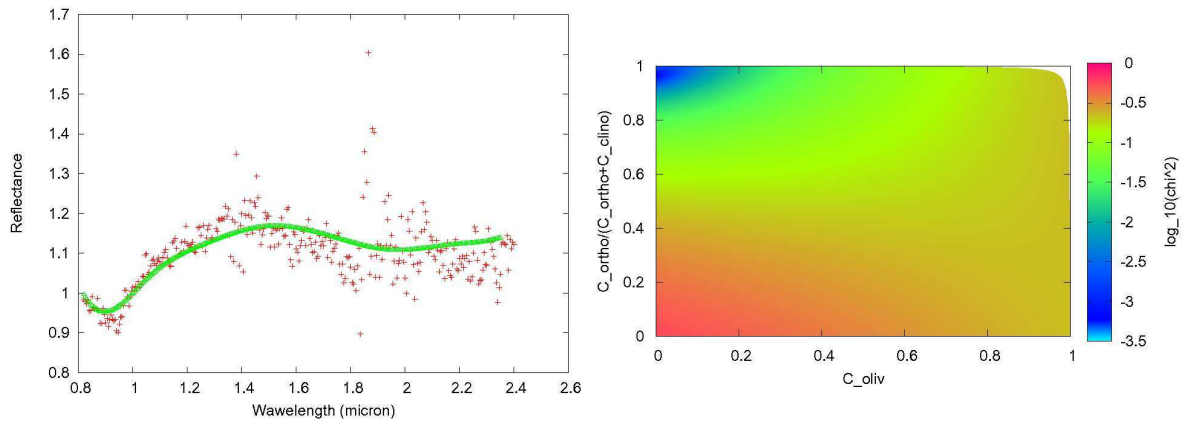


Figure 10. Two dimension chart of concentration for the asteroid (3623) Chaplin using olivine, orthopyroxene, and clinopyroxene from RELAB. The best mineralogical mixture using (Ol, OPx, CPx) = (0, c1dl01, c1dl08) with ratios (0%, 96.5%, 3.5%) is presented in the left of the figure.

reported in the inner part of the Main Belt, relatively close to the Vesta family (Duffard et al. 2004).

The V-type asteroids are objects with reflectance spectra similar to the asteroid (4) Vesta and to HED meteorites. Vesta is considered as *the smallest terrestrial planet* (Keil 2002) and is a differentiated object with a basaltic crust and exposed mantle material (Gaffey 1997) that survived almost intact during the solar system history. Objects smaller in size than Vesta (commonly called 'vestoids') present spectral properties similar to this asteroid. Partly the vestoids are identified as fragments of Vesta, a result of a catastrophic collision who excavated material from the crust and the mantle (Binzel & Xu 1993) of Vesta. Vesta's density was derived from the estimation of its mass (Hilton 2002) and shape (Thomas et al. 1997). The computed values of the bulk density span the range 3,000–4,300 kg/m^3 (Birlan 2000). This interval is supported also by models of internal structure of large differentiated bodies. Ruzicka et al. (1997) calculated the density of silicate fraction in Vesta-like asteroids, assuming an average value of the bulk density of 3,540 kg/m^3 . They conclude that Vesta could be modeled with an eucritic/diogenitic crust and an olivine mantle for a metallic core between zero and 25% of the total mass of the asteroid. In this case, the density of the crust could not be less than 3,000 kg/m^3 .

In the assumption of (854) Frostia as a fragment of Vesta's crust, a value of its density around 3,000 kg/m^3 seems to be reasonable. The value calculated by Behrend et al. (2006) (around 1,000 kg/m^3) is very difficult to explain even if we assume unrealistic porosities of 75% in a rubble-pile structure. In fact, large porosities for small fragments of large differentiated bodies are not realistic while the self-gravitation tendency is to decrease the volume of empty space inside the object. Behrend et al. (2006) inferred a C-type asteroid by analogy with the asteroid (90) Antiope. It is difficult to reconcile the C and V taxonomic classes while the objects experienced different temperatures in their history.

Descamps (2010) published recently a refined study of binary systems by accounting inhomogeneous bodies with ellipsoidal shapes. This model allows the simultaneous fit of grain density and the bulk porosity. The author calculated a grain density of $(2,790 \pm 380) \text{kg/m}^3$ in agreement to the one of Vesta-like asteroids, correlated to a bulk porosity of 63% ($\approx 55\%$ of macroscopic porosity + $\approx 8\%$ of microporosity).

The mineralogy of (854) Frostia could be refined by taking into account the precise position of the band centres at 1 and 2 μm . To estimate the minima of these absorption features, we removed the continuum by considering a linear function for each one. The continuum for the Band I was estimated using the reflectances at 0.7 and 1.43 μm , while for the Band II the continuum was estimated using the reflectances at 1.43 and 2.49 μm respectively. While our spectrum do not contains the reflectance at 0.7 μm , this value was estimated by polynomial extrapolation. The reflectance at 0.7 μm usually represents the lower limit of the 1 μm absorption feature for the V-types asteroids (Duffard et al. 2004; Vernazza et al. 2005). The continuum was then extracted from the spectrum in each corresponding region. The band centre was then computed using a 6-th order polynomial function. We found that the Band I minimum is located at $0.931 \pm 0.004 \mu\text{m}$, while the Band II minimum is

located at $1.976 \pm 0.004 \mu\text{m}$. In the case of Band I we calculated the thermal correction using the formulas 2 and 4 from Burbine et al. (2009). This value is of 0.002 μm , within the value of the errorbar for Band I centre, thus we can neglect its influence. The positions of Band I and Band II centres are relatively similar to that obtained for the asteroid (1459) Magnya (Hardersen et al. 2004). If we place these values for Frostia in the context of the pyroxene studies of Adams (1974) and Cloutis & Gaffey (1991a) we conclude a dominant presence of orthopyroxene on the asteroids' surfaces. The position of the bands place the asteroid between the Eucrite and Diogenite regions (see Fig 6 from Hardersen et al. (2004)). These results are partially confirmed by our Figure 8, that presents a large dominance of orthopyroxene.

The spectrum of (854) Frostia presents an inflexion near 1.2 μm which is an indication of the presence of feldspar in the basaltic achondrite materials. The mineralogical composition using the pyroxene calibration (Gaffey et al. 2002) suggests the formula $\text{Wo}_{85}\text{Fs}_{43}\text{En}_{49}$ (with a 4% of uncertainty for wollastonite and ferrosilite). This composition is, within the error-bars, similar to that of (4) Vesta and (1459) Magnya, and similar to that of the asteroid (3269) De Sanctis (Duffard et al. 2004).

Another important mineralogical parameter which was investigated for (854) Frostia was the band area ratio (BAR). This is the result of the ratio between Band I and Band II. Band I area was calculated as the area between the continuum defined by the correspondent reflectances at 0.7 and 1.4 μm and the spectrum. Band II area was calculated as the area between the continuum defined by the correspondent reflectances at 1.4 and 2.43 μm and the spectrum. The reflectance value at 0.7 μm was estimated by linear extrapolation. Depending on the range that this value could span, the estimation for the area of Band I could differ by up to 5%. This extrapolation of our spectrum is also in agreement with the visible spectrum of Alvarez-Candal et al. (2006). The procedure of computation for the BAR value was prior tested and validated using two spectra of V-type asteroids (4) Vesta and (1459) Magnya (R. Binzel, Personal communication). The calculated BAR for (854) Frostia was 1.57 ± 0.08 , in agreement with the basaltic achondrite minerals (Gaffey et al. 1993).

V-type asteroids are mainly located in the population represented by the Vesta family, and is considered to be the reservoir of HED meteorites. However, basaltic asteroids, not yet considered members of Vesta family, are also located in the vicinity of the family (Florczak et al. 2002; Duffard et al. 2004). Data on V-type asteroids such as (1459) Magnya are reported at different semi-major axis (Lazzaro et al. 2000; Roig & Gil-Hutton 2006; Duffard & Roig 2009) and in the NEA population (Binzel et al. 2002). This picture of V-type asteroids supports the hypothesis of formation of several objects with basaltic crust in the Main-Belt. The plot of Band I center versus BAR exhibits a diversity among V-type asteroids much larger than the one obtained for basaltic achondrite meteorites. This extension of BAR range may be explained by reconsidering the physics and mineralogy of asteroid surfaces.

The asteroid (1333) Cevenola is a member of Eunomia family, counting more than 430 objects (Zappala et al. 1995). 44 members of this family (including Cevenola) were studied spectroscopically in the visible region by Lazzaro et al.

(1999). 41 of them were classified as S-type objects, while three asteroids exhibit flat spectra and were considered as interlopers. If we consider this sample in the frame of the Bus-DeMeo taxonomy (DeMeo et al. 2009), only three objects are re-observed in the near-infrared region. A robust conclusion about this family cannot be drawn in the Bus-DeMeo taxonomic system, however we can speculate on a S_q taxonomic type for the three objects considering the VNIR data.

The MGM analysis (Figure 7) strongly indicate that the presence of both olivine and pyroxene are necessary for reproducing the observational data of (1333) Cevenola. The mineralogical solution corresponds to fayalitic material with the molar percentage equal to 20 ± 5 (Sunshine et al. 2007) and the width of these absorption bands span the same range as in presented in Sunshine & Pieters (1998). However, the strength ratio between the M1 and M2 olivine crystals is different from the calibration values proposed by Sunshine et al. (2007). This imply that mineralogies with fayalitic-forsteritic components need to be completed with other components. Recently Isaacson & Pieters (2010) proposes a mineralogical solution of surfaces of Mars rich in olivine, by considering the spectral influence of chromites. The effect of chromite in olivine minerals is observed in the reduced reflectance and in the absorption feature beyond $1.5 \mu\text{m}$. A similar mineralogical solution together with solutions obtained from different olivine varieties (dunite, peridot, chrysolite, wadsleyite) need future analysis.

The family of mineralogical solutions computed by the χ^2 composition map (Figure 9) for (1333) Cevenola is also composed by the mixture of orthopyroxene and olivine (the horizontal dark-blue region in the figure). The olivine is less constrained ranging from 0% to 60%. This region is completed by the blue part of the map for high olivine percentages. In this case, the family of mineralogical solutions is less constrained than that obtained for (854) Frostia.

Following DeMeo et al. (2009) the S_q asteroids "present a wide $1\mu\text{m}$ absorption band with evidence of a feature near $1.3 \mu\text{m}$ like the Q-type, except the $1\mu\text{m}$ feature is more shallow" for this class. (1333) Cevenola is similar to the S-IV mineralogical subtype (Gaffey et al. 1993). Following Gaffey et al. (1993) this subclass is characterized by assemblages of olivine-orthopyroxene which could represent assemblages similar either to the undifferentiated ordinary chondrites or to the unmelted silicate portions of primitive achondrites.

(3623) Chaplin is a member of the Koronis family. The NIR spectrum spans the same characteristics with the S-type complex, which is the taxonomic class of the Koronis family. We extrapolate its thermal albedo to the one of the S-class of 0.198 ± 0.067 (Fulchignoni et al. 2000). The mineralogical map obtained in section 4.2 (dark blue region in the mineralogical map) shows a best fit for families of mineralogical solutions dominated by orthopyroxene with clinopyroxenes and olivine as minor constituents.

(1333) Cevenola and (3623) Chaplin were observed over two consecutive nights in order to detect spectral variations in their spectra. Their correspondent spectra has the same profile, which is interpreted as a homogeneity of the surfaces of each object.

6 CONCLUSIONS

0.8-2.5 μm spectral data were obtained and analyzed for the Main-Belt asteroids (854) Frostia, (1333) Cevenola, and (3623) Chaplin. This NIR spectral interval is covered for the first time for our targets, chosen among the asteroids with large amplitudes in their lightcurves, which were observed previously photometrically. Detailed mineralogical analysis using Modified Gaussian Model was performed for our objects. Newly instruments such are 2D spectral charts by a χ^2 fit of mineralogical assemblages was performed for (854) Frostia and (1333) Cevenola.

The asteroid (854) Frostia was classified as V-type, for which the density and the spectral properties are incompatible with the previous findings on density. Spectral properties of this object are similar to those of basalts. We calculated the mineralogical solution $Wo_8Fs_{43}En_{49}$, with an error of 4% in wollastonite and ferrosilite, for Frostia.

(1333) Cevenola is a member of Eunomia family and belongs to the S_q taxonomic type. The mineralogical maps were constructed for the first time for (854) Frostia and (1333) Cevenola, using as end-members the available laboratory data for the olivine, ortho- and clinopyroxenes.

Finally, (3623) Chaplin belongs to the S-type taxonomic complex, which characterize the members of the Koronis family. Its mineralogy corresponds to minerals with olivine and pyroxene content.

7 ACKNOWLEDGEMENTS

The article is based on observations acquired with InfraRed Telescope Facilities as well as the CODAM remote facilities. We thank all the telescope operators for their contribution. This research utilizes spectra acquired with the NASA RELAB facility at Brown University. The authors thank to Francesca DeMeo and Rick Binzel for careful reading and pertinent remarks. The work of D.A.N was partially supported by the Romanian National Authority for Scientific Research (ANCS) under the project POSCCE-A2-O2.1.2-2009-2/651. We thank the anonymous referee for useful remarks.

REFERENCES

- Adams J. B., 1974, J. Geophys. Res., 79, 4829
- Alvarez-Candal A., Duffard R., Lazzaro D., Michtchenko T., 2006, A&A, 459, 969
- Behrend R., Bernasconi L., Roy R., Klotz A., Colas F., Antonini P., Aoun R., Augustesen K., Barbotin E., Berger N., Berrouachdi H., Brochard E., Cazenave A., Cavadore C., Coloma J., Cotrez V. a., 2006, A&A, 446, 1177
- Binzel R. P., 1978, Minor Planet Bulletin, 6, 18
- Binzel R. P., Lupishko D., di Martino M., Whiteley R. J., Hahn G. J., 2002, Asteroids III, pp 255–271
- Binzel R. P., van Flandern T. C., 1979, Science, 203, 903
- Binzel R. P., Xu S., 1993, Science, 260, 186
- Birlan M., 2000, Earth Moon and Planets, 88, 1
- Birlan M., Barucci M. A., Angeli C. A., Doressoundiram A., de Sanctis M. C., 1996, Planet. Space Sci., 44, 555

- Birlan M., Barucci M. A., Vernazza P., Fulchignoni M., Binzel R. P., Bus S. J., Belskaya I., Fornasier S., 2004, *New Astronomy*, 9, 343
- Birlan M., Vernazza P., Fulchignoni M., Barucci M. A., Descamps P., Binzel R. P., Bus S. J., 2006, *A&A*, 454, 677
- Burbine T. H., Buchanan P. C., Dolkar T., Binzel R. P., 2009, *Meteoritics and Planetary Science*, 44, 1331
- Canas L., Duffard R., Seixas T., 2008, *Earth Moon and Planets*, 102, 543
- Cellino A., Pannunzio R., Zappala V., Farinella P., Paolicchi P., 1985, *A&A*, 144, 355
- Cloutis E. A., Gaffey M. J., 1991a, *J. Geophys. Res.*, 96, 22809
- Cloutis E. A., Gaffey M. J., 1991b, *Earth Moon and Planets*, 53, 11
- Cushing M. C., Vacca W. D., Rayner J. T., 2004, *Planet. Space Sci.*, 116, 362
- Dell'Oro A., Cellino A., 2007, *MNRAS*, 380, 399
- DeMeo F. E., Binzel R. P., Slivan S. M., Bus S. J., 2009, *Icarus*, 202, 160
- Descamps P., 2010, *Icarus*, 207, 758
- Descamps P., Marchis F., Michalowski T., Vachier F., Colas F., Berthier J., Assafin M., Dunckel P. B. a., 2007, *Icarus*, 187, 482
- Donnison J. R., 1979, *MNRAS*, 186, 35P
- Duffard R., Lazzaro D., Licandro J., de Sanctis M. C., Capria M. T., Carvano J. M., 2004, *Icarus*, 171, 120
- Duffard R., Roig F., 2009, *Planet. Space Sci.*, 57, 229
- Dunlap J. L., Gehrels T., 1969, *AJ*, 74, 796
- Durda D. D., Bottke W. F., Enke B. L., Merline W. J., Asphaug E., Richardson D. C., Leinhardt Z. M., 2004, *Icarus*, 170, 243
- Dyar M., Sklute E., Menzies O., Bland P., Lindsley D., Glotch T., Lane M., Schaefer M., Wopenka B., Klima R., Bishop J., Hiroi T., Pieters C., Sunshine J., 2009, *American Mineralogist*, 94, 883
- Florczak M., Lazzaro D., Duffard R., 2002, *Icarus*, 159, 178
- French L. M., Binzel R. P., 1989, in R. P. Binzel, T. Gehrels, & M. S. Matthews ed., *Asteroids II CCD photometry of asteroids*. pp 54–65
- Fulchignoni M., Birlan M., Antonietta Barucci M., 2000, *Icarus*, 146, 204
- Gaffey M. J., 1997, *Icarus*, 127, 130
- Gaffey M. J., Burbine T. H., Piatek J. L., Reed K. L., Chaky D. A., Bell J. F., Brown R. H., 1993, *Icarus*, 106, 573
- Gaffey M. J., Cloutis E. A., Kelley M. S., Reed K. L., 2002, *Asteroids III*, pp 183–204
- Hardersen P. S., Gaffey M. J., Abell P. A., 2004, *Icarus*, 167, 170
- Harris A. W., Lupishko D. F., 1989, in R. P. Binzel, T. Gehrels, & M. S. Matthews ed., *Asteroids II Photometric lightcurve observations and reduction techniques*. pp 39–53
- Hilton J. L., 2002, *Asteroids III*, pp 103–112
- Holsapple K. A., Michel P., 2008, *Icarus*, 193, 283
- Isaacson P. J., Pieters C. M., 2010, *Icarus*, 210, 8
- Ivezić Ž., Tabachnik S., Rafikov R., Lupton R. H., Quinn T., Hammegren M., Eyer L., Chu J., Armstrong J. C., Fan X., Finlator K. a., 2001, *AJ*, 122, 2749
- Keil K., 2002, *Asteroids III*, pp 573–584
- Klima R. L., Pieters C. M., Dyar M. D., 2007, *Meteoritics and Planetary Science*, 42, 235
- Lagerkvist C., Barucci M. A., Capria M. T., Fulchignoni M., Guerriero L., Perozzi E., Zappala V., 1987, *Asteroid photometric catalogue*.
- Lazzaro D., Angeli C. A., Carvano J. M., Mothé-Diniz T., Duffard R., Florczak M., 2004, *Icarus*, 172, 179
- Lazzaro D., Michtchenko T., Carvano J. M., Binzel R. P., Bus S. J., Burbine T. H., Mothé-Diniz T., Florczak M., Angeli C. A., Harris A. W., 2000, *Science*, 288, 2033
- Lazzaro D., Mothé-Diniz T., Carvano J. M., Angeli C. A., Betzler A. S., Florczak M., Cellino A., Di Martino M., Doressoundiram A., Barucci M. A., Dotto E., Bendjoya P., 1999, *Icarus*, 142, 445
- Leone G., Paolicchi P., Farinella P., Zappala V., 1984, *A&A*, 140, 265
- Magri C., Nolan M. C., Ostro S. J., Giorgini J. D., 2007, *Icarus*, 186, 126
- Marchis F., Descamps P., Hestroffer D., Berthier J., 2005, *Nature*, 436, 822
- Mothé-Diniz T., Roig F., Carvano J. M., 2005, *Icarus*, 174, 54
- Ostro S. J., Hudson R. S., Benner L. A. M., Giorgini J. D., Magri C., Margot J. L., Nolan M. C., 2002, *Asteroids III*, pp 151–168
- Ostro S. J., Hudson R. S., Nolan M. C., Margot J.-L., Scheeres D. J., Campbell D. B., Magri C., Giorgini J. D., Yeomans D. K., 2000, *Science*, 288, 836
- Pieters C. M., McFadden L. A., 1994, *Annual Review of Earth and Planetary Sciences*, 22, 457
- Pravec P., Šarounová L., Hicks M. D., Rabinowitz D. L., Wolf M., Scheirich P., Krugly Y. N., 2002, *Icarus*, 158, 276
- Rayner J. T., Toomey D. W., Onaka P. M., Denault A. J., Stahlberger W. E., Vacca W. D., Cushing M. C., Wang S., 2003, *PASP*, 115, 362
- Rivkin A. S., Binzel R. P., Sunshine J., Bus S. J., Burbine T. H., Saxena A., 2004, *Icarus*, 172, 408
- Roig F., Gil-Hutton R., 2006, *Icarus*, 183, 411
- Ruzicka A., Snyder G. A., Taylor L. A., 1997, *Meteoritics and Planetary Science*, 32, 825
- Singer R. B., 1981, *J. Geophys. Res.*, 86, 7967
- Storrs A., Weiss B., Zellner B., Burleson W., Sichert R., Wells E., Kowal C., Tholen D., 1999, *Icarus*, 137, 260
- Sunshine J. M., Bus S. J., Corrigan C. M., McCoy T. J., Burbine T. H., 2007, *Meteoritics and Planetary Science*, 42, 155
- Sunshine J. M., Bus S. J., McCoy T. J., Burbine T. H., Corrigan C. M., Binzel R. P., 2004, *Meteoritics and Planetary Science*, 39, 1343
- Sunshine J. M., Pieters C. M., 1993, *J. Geophys. Res.*, 98, 9075
- Sunshine J. M., Pieters C. M., 1998, *J. Geophys. Res.*, 103, 13675
- Sunshine J. M., Pieters C. M., Pratt S. F., 1990, *J. Geophys. Res.*, 95, 6955
- Tedesco E. F., 1979, *Science*, 203, 905
- Thomas P. C., Binzel R. P., Gaffey M. J., Zellner B. H., Storrs A. D., Wells E., 1997, *Icarus*, 128, 88
- Vacca W. D., Cushing M. C., Rayner J. T., 2004, *PASP*, 116, 352
- van Flandern T. C., Tedesco E. F., Binzel R. P., 1979, *Satellites of asteroids. Asteroids*, pp 443–465

- Vernazza P., Mothé-Diniz T., Barucci M. A., Birlan M.,
Carvano J. M., Strazzulla G., Fulchignoni M., Migliorini
A., 2005, *A&A*, 436, 1113
Warner B. D., 2002, *Minor Planet Bulletin*, 29, 74
Wijesinghe M. P., Tedesco E. F., 1979, *Icarus*, 40, 383
Zappala V., Bendjoya P., Cellino A., Farinella P., Froeschle
C., 1995, *Icarus*, 116, 291
Zappala V., Scaltriti F., Farinella P., Paolicchi P., 1980,
Moon and Planets, 22, 153